NASA CR-165,635

NASA Contractor Report 165635

NASA-CR-165635
19830022135

Advanced Composite Aileron for L-1011 Transport Aircraft Design and Analysis

C.F. Griffin and L.D. Fogg

Lockheed Corporation
Lockheed-California Company
Post Office Box 551
Burbank, California 91520

E.G. Dunning

NF02192

Avco Aerostructure Division
Post Office Box 210
Nashville, Tennessee 37202

CONTRACT NAS1-15069
APRIL 1981

MAY 1961

NASA

National Aeronautics and
Space Administration

Langley Research Center
Hampton, Virginia 23665

FEDP REMOVED PER NASA LARC
LTR DTD 7-15-83, S/J.G. ROSS

SAM
7-27-83

This Page Intentionally Left Blank

FOREWORD

N81- 7434274

This Page Intentionally Left Blank

TABLE OF CONTENTS

This Page Intentionally Left Blank

LIST OF ILLUSTRATIONS

LIST OF ILLUSTRATIONS (Continued)

LIST OF ILLUSTRATIONS (Continued)

LIST OF ILLUSTRATIONS (Continued)

This Page Intentionally Left Blank

LIST OF TABLES

LIST OF TABLES (Continued)

ADVANCED COMPOSITE AILERON
FOR L-1011 TRANSPORT AIRCRAFT

DESIGN AND ANALYSIS

C.F. Griffin, L.D. Fogg, E.G. Dunning

SUMMARY

During Task I of the Advanced Composite Aileron (ACA) program, design trade-off studies and materials screening tests were conducted leading to the selection of the configuration and materials for the composite aileron. The activities documented in this report are associated with Task II of the program. These activities include: design and analysis, material verification, process development and concept verification.

The composite aileron design is a multi-rib configuration with single piece upper and lower covers mechanically fastened to the substructure. Covers, front spar and ribs are fabricated with graphite/epoxy tape or fabric composite material. The design has a weight savings of 23 percent compared to the aluminum aileron. The composite aileron has 50 percent fewer fasteners and parts than the metal aileron and is predicted to be cost competitive.

Structural integrity of the composite aileron was verified by structural analysis and an extensive test program. Static, failsafe, and vibration analyses have been conducted on the composite aileron using finite element models and specialized computer programs for composite material laminates. The fundamental behavior of the composite materials used in the aileron was determined by coupon tests for a variety of environmental conditions. Critical details of the design were interrogated by static and fatigue tests on full-scale subcomponents and subassemblies of the aileron.

Tooling concepts and manufacturing processes were developed for the various components within the composite aileron. The fact that the processes result in spars, ribs, and covers with satisfactory structural behavior was established by a series of process development and verification tests using production tooling. Drilling and machining techniques were also developed which result in high quality parts.

INTRODUCTION

The broad objective of NASA's Aircraft Energy Efficiency (ACEE) Composite Structures Program is to accelerate the use of composite materials in aircraft structures by developing technology for early introduction of structures made of these materials into commercial transport aircraft. This program, one of several which are collectively aimed toward accomplishing this broad

objective, has the specific goal to demonstrate the weight and cost/saving potential of secondary structures constructed of advanced composite materials. The secondary structure selected for the program is the inboard aileron of the Lockheed L-1011 transport aircraft.

The scope of this program is to design, fabricate, qualify, and certificate a composite inboard aileron; to test selected subcomponents to verify the design; to fabricate and test two ground test articles; to fabricate and install ten shipsets of inboard ailerons; and to gather flight service data on the ten shipsets of composite ailerons.

The Lockheed-California Company is teamed with Aerostructures Division of Avco Corporation. Lockheed designed the aileron; conducted the materials, concept verification, and ground tests; and will evaluate in-flight service experience. Avco developed manufacturing processes, fabricated test specimens, and fabricated the ground test and flight articles.

As shown on the master schedule, figure 1, the program is being conducted in six nonsequential tasks. Task I, Engineering Development, and Task II, Design and Analysis, are the portions of the program wherein the composite aileron design was formulated and subcomponents fabricated and tested to verify design concepts and fabrication procedures. During Task III, Manufacturing Development, and Task IV, Ground Test and Flight Checkout, production quality manufacturing tools were constructed, and two full-scale ailerons were fabricated and tested. A production run of five shipsets were fabricated during Task V, Aileron Manufacture, to provide manufacturing and cost information. In Task VI, Flight Service, inspection and maintenance data will be gathered on the five shipsets of ailerons to assess their potential for economical operation in routine service. The work performed during this program is intended to provide the data required to make a production commitment.

This report describes work accomplished during Task II.
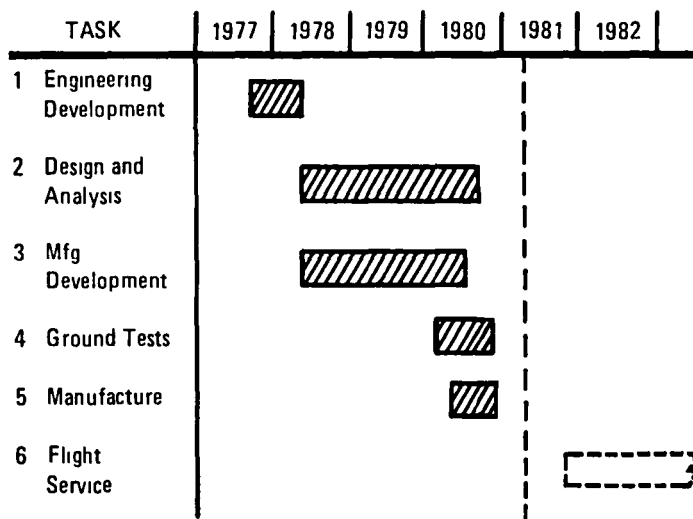
Figure 1. - Master schedule.

2

SYMBOLS

Basic Symbols

A	– area
a	– length dimension
b	– width dimension
E	– modulus
F	– stress
G	– shear modulus
h	– height dimension
K	– general coefficient
M.S.	– margin of safety
N	– force component (stress resultant) or number of items
P	– load
p	– pressure
t	– thickness
α	– coefficient of thermal expansion
γ	– shear strain
ε	– strain
ν	– Poisson's ratio
ρ	– density

Subscripts

B	– B' basis
BRU	– bearing ultimate
ET	– environmental/notched
L T	– laminae natural orthogonal coordinate axes
N	– normalized
PL	– proportional limit
X, Y	– laminate coordinate axes
1, 2	– primary, secondary

Superscripts

c	– compression
t	– tension

MEASUREMENT VALUES

All measurement values in this technical report are expressed in the
International System of Units and customary units. Customary units were
used for the principal measurements and calculations.

1. COMPONENT DEFINITION

1.1 Detailed Design

1.1.1 <u>Aileron general description</u>. - The inboard aileron is located
on the wing trailing edge between the outboard and inboard trailing edge
flaps and is directly behind the engine, as shown in figure 2. It is
supported from the wing at two hinge points and is actuated by three hydrau-
lic actuators. Basic dimensions of the inboard aileron are shown in fig-
ure 3. It is basically a wedge-shaped, one-cell box, thinning slightly from
root to tip. The planform is trapezoidal, with parallel leading and trailing
edges.

1.1.2 <u>Structural configuration - metal aileron</u>. - The inboard aileron
is a single-cell box beam with added trailing-edge shrouds and end fairings.
An illustration of the current aluminum inboard aileron is shown in figure 4.

The box consists of a front beam, rear beam, and upper and lower skins,
joined by hinge ribs and airload ribs. The front beam consists of a web
with lightening holes and extruded caps. Attached to the web are formers
supporting the shrouds, which consists of two aluminum clad sheets bonded
together.

The rear beam is an 'I' section extrusion with lightening holes in the
web. Upper and lower skins are clad aluminum sheets with bonded doublers
and are attached to the rib caps with rivets on the upper surface and screws
on the lower surface.

Joining the front and rear beams are 18 ribs at about 178 mm (7 in)
pitch, most of which are airload ribs. These are of channel extrusion truss
construction. The two main actuator ribs are of cap and corrugated web
construction, with fittings at the front beam to accommodate hinge and actu-
ator loads, and with titanium straps splicing the upper rib caps and skin to
the front beam cap.
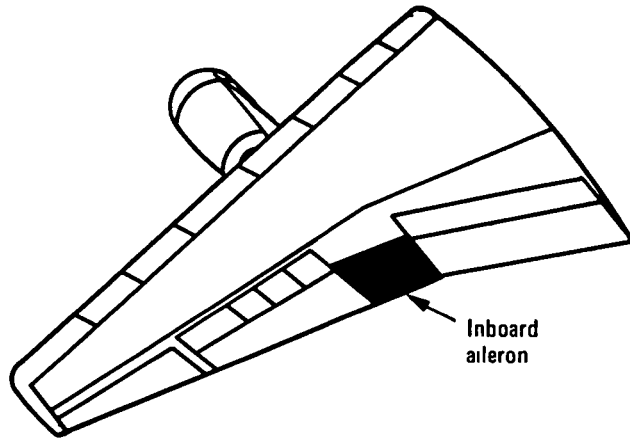
Figure 2. - Inboard aileron location on L-1011 wing.
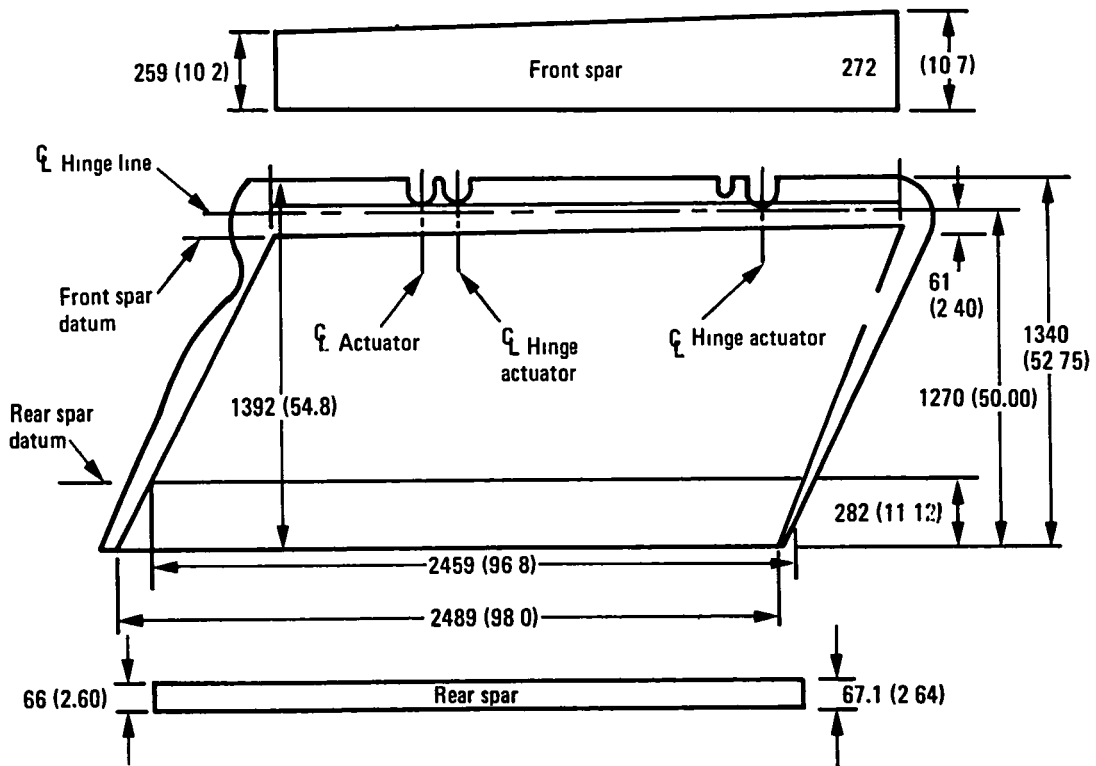
Figure 3. - Inboard aileron dimensions (All dimensions shown in mm (in)
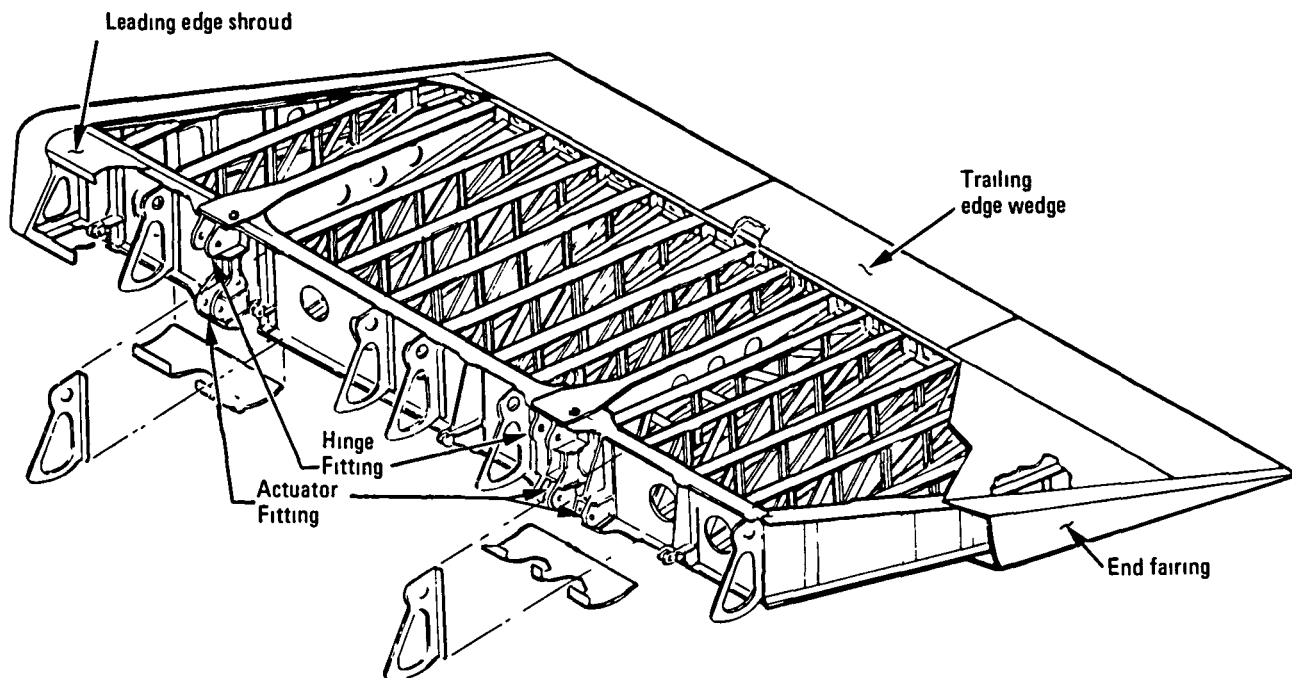
Figure 4. – Current aluminum aileron.

The trailing-edge wedge is a sandwich construction and is attached to the rear beam in three discontinuous sections with screws. The end fairings are of beaded fiberglass construction, attached to the close-out rib caps with screws.

The aileron support fittings are aluminum two-piece forgings, joined by Hi-Tigue fasteners. The hinge bearing housings are separate split fittings bolted to the aileron support fittings.

1.1.3 Structural configuration – composite aileron. – The selected design (see reference 1) for the advanced composite aileron is a multirib configuration with single-piece upper and lower covers mechanically fastened to the substructure. Covers and front spar of the aileron are fabricated with graphite/epoxy unidirectional tape. Graphite/epoxy bidirectional fabric is used for construction of the ribs. The rear spar is fabricated from 7075-T6 clad aluminum alloy sheet. A schematic of the aileron assembly is shown in figure 5.

The upper surface, ribs, and spars are permanently fastened with Triwing titanium screws and stainless steel Hi-Lok collars. The removable lower surface, trailing edge wedge, leading edge shroud, and end fairings are attached with the same type of screws but with stainless steel nut plates attached to the substructure with stainless steel cherry rivets.

6

Leading edge
shroud aluminum

Back-up fittings
aluminum

End fairings
fiberglass

Trailing edge
wedge kevlar
and nomex core

Covers
graphite/epoxy
tape and
syntactic core

Hinge/actuator
fittings aluminum
forgings

Front spar
graphite/epoxy
tape

Ribs
graphite/epoxy
fabric
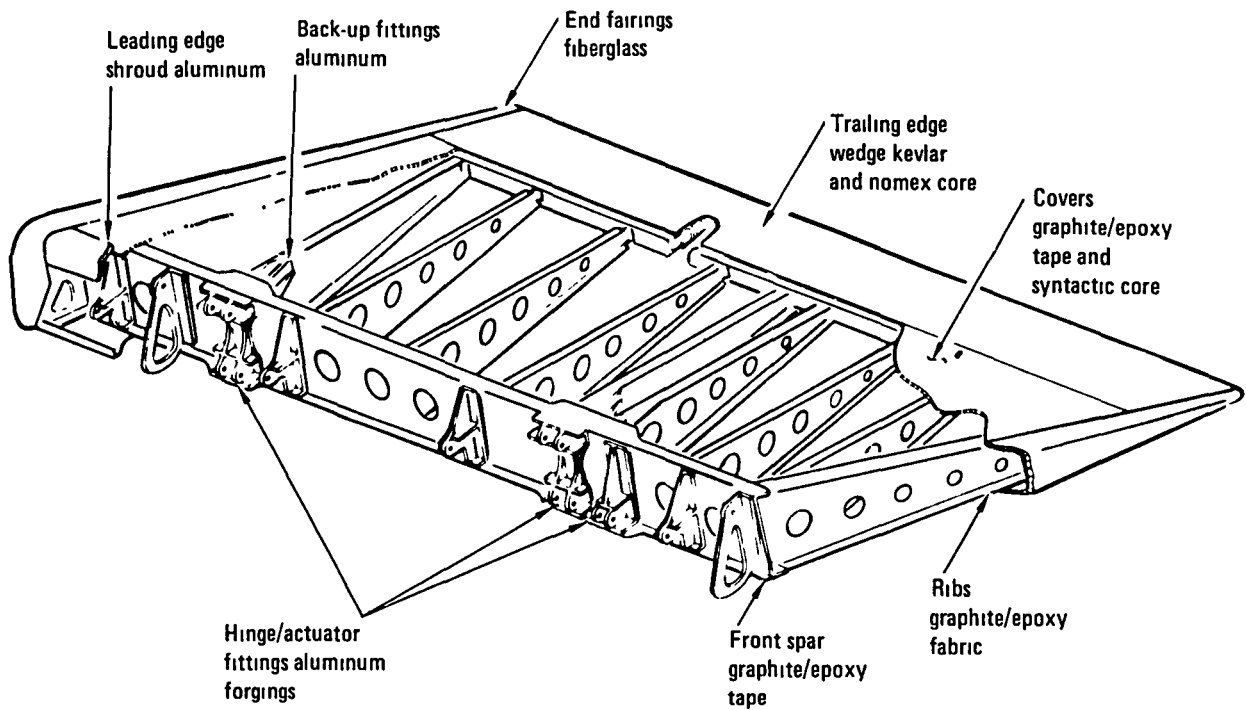
Figure 5. - Advanced composite aileron.

To preclude galvanic corrosion, aluminum parts are anodized, primed with epoxy and then given a urethane topcoat. Graphite/epoxy parts in contact with aluminum parts are also painted with a urethane topcoat. Faying surface sealant is used at the interface of all aluminum and composite parts. After assembly the aileron is primed and painted. No protection is provided against swept-stroke lightning.

Thermal expansion differences between the graphite/epoxy aileron and the aluminum wing were calculated over the operating temperature range. This analysis indicated a net movement of the hinge supports of 1.5 mm (0.059 in) over the temperature range of 297K (75°F) to 219.3K (-65°F). The outboard hinge reacts spanwise loading, and the inboard hinge has a clearance of 2.54 mm (0.10 in) on each side of the bearing. In order to retain the same clearance as on the metal aileron, the inboard hinge fittings are being counterbored approximately 1.52 mm (0.060 in) on the interior lugs.

Several of the subassemblies that are currently being used on the metal aileron have been incorporated into the composite aileron design. These include the aluminum hinge/actuator fittings, the aluminum leading edge shroud, the Kevlar 49/epoxy trailing edge wedge and the fiberglass/epoxy end fairings. The aileron assembly is shown in figure 6 without the lower cover, shroud or end fairings installed.

7
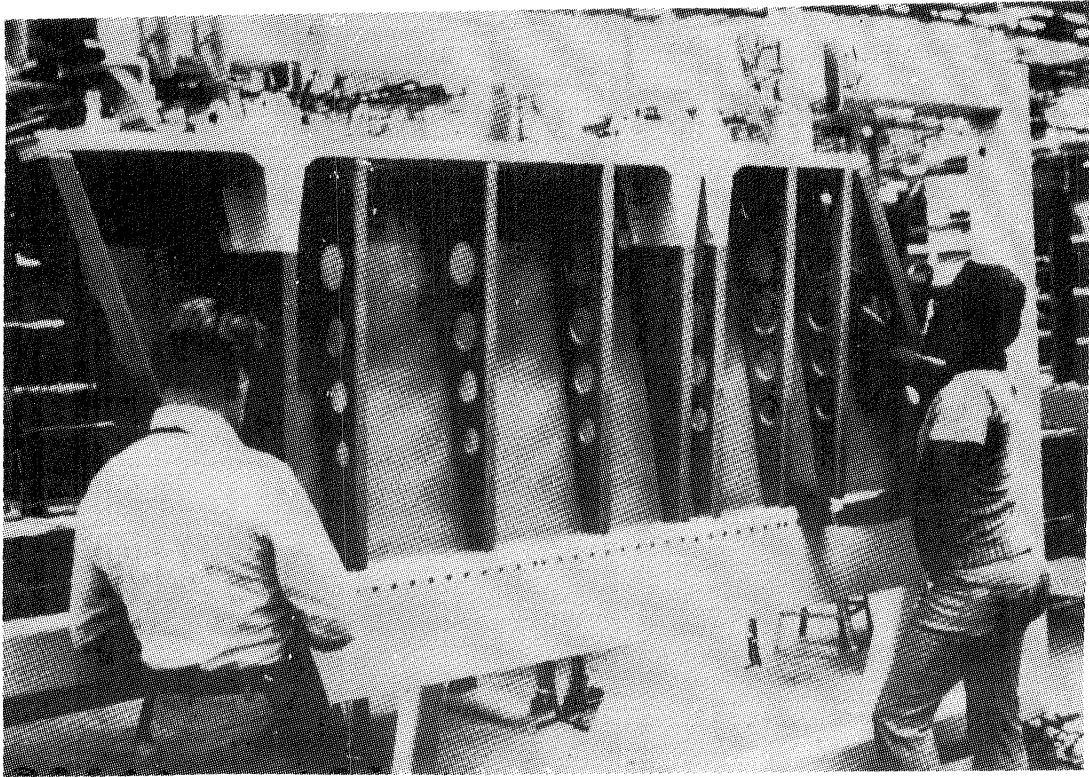
Figure 6. - Aileron assembly.

Covers – The cover configuration, shown in figure 7, is a syntactic core sandwich consisting of three plies of graphite/epoxy unidirectional tape 0.19 mm/ply (0.0075 in/ply) on each side of a 0.953 mm (0.0375 in) syntactic epoxy core. The orientation of the tape is ($45^{o}/0^{o}/135^{o}$) with the 0° ply in the spanwise direction.

In the vicinity of the main ribs and at the ends of the aileron the syntactic core in the covers is replaced with five plies of graphite/epoxy tape to provide additional chordwise stiffness and act as an additional load path for the rib caps. The ($95^{o}/85^{o}/90^{o}/85^{o}/95^{o}$) orientation of this five ply internal reinforcement was selected rather than 90°s to prevent microcracking of the laminate due to curing stresses. Inner surface doublers are cocured with the basic cover over the ribs and spars to assist in load transfer between covers and substructure and to provide the thickness buildup necessary for countersunk fasteners. These doublers consist of three plies of tape, ($45^{o}/90^{o}/135^{o}$), which are then covered with one ply of fabric. At the leading edge of the cover additional inner surface doublers are cocured to the basic cover to function as part of the front spar cap. This arrangement enhances the failsafety of the design by proving an alternate load path for spanwise bending loads.

8
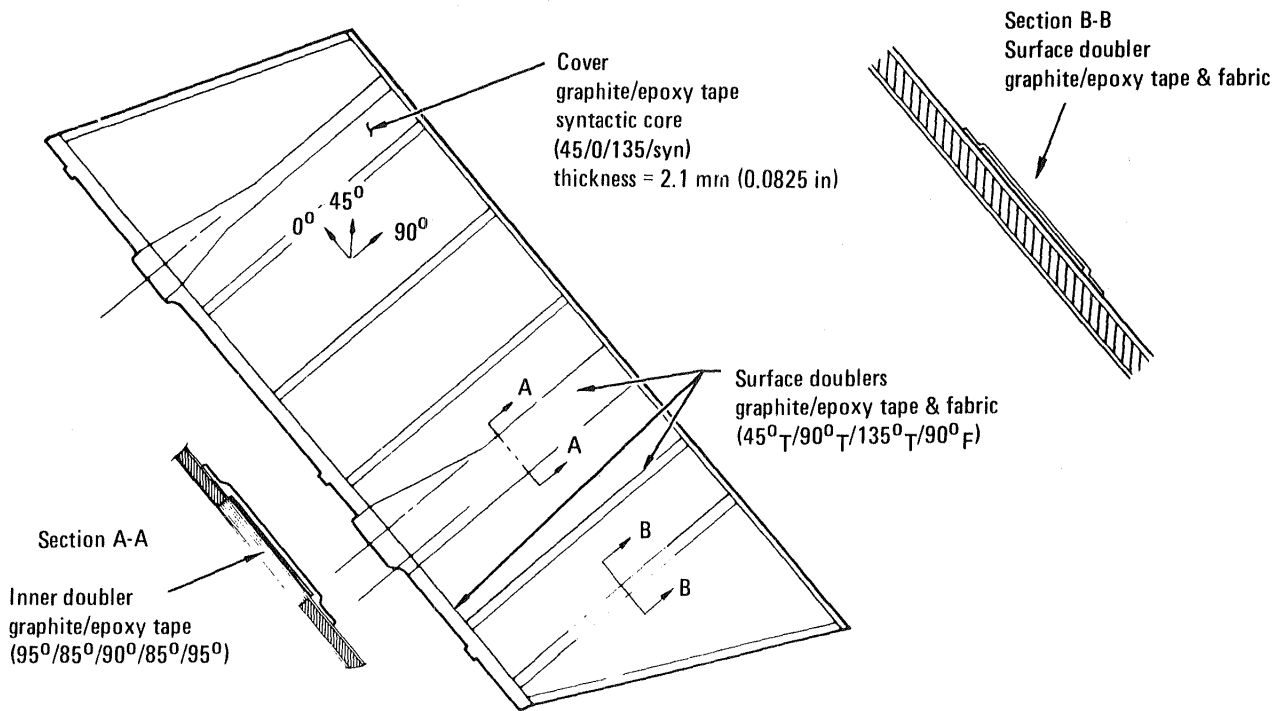
Figure 7. - Aileron cover configuration.

Front spar - The front spar, shown in figure 8, is a constant thickness channel section constructed of ten plies of unidirectional graphite/epoxy tape laid up at $(45°/0°/135°/90°/0°)_s$ where the 0° direction is spanwise. Note that the flange width of the spar caps is increased locally at the main
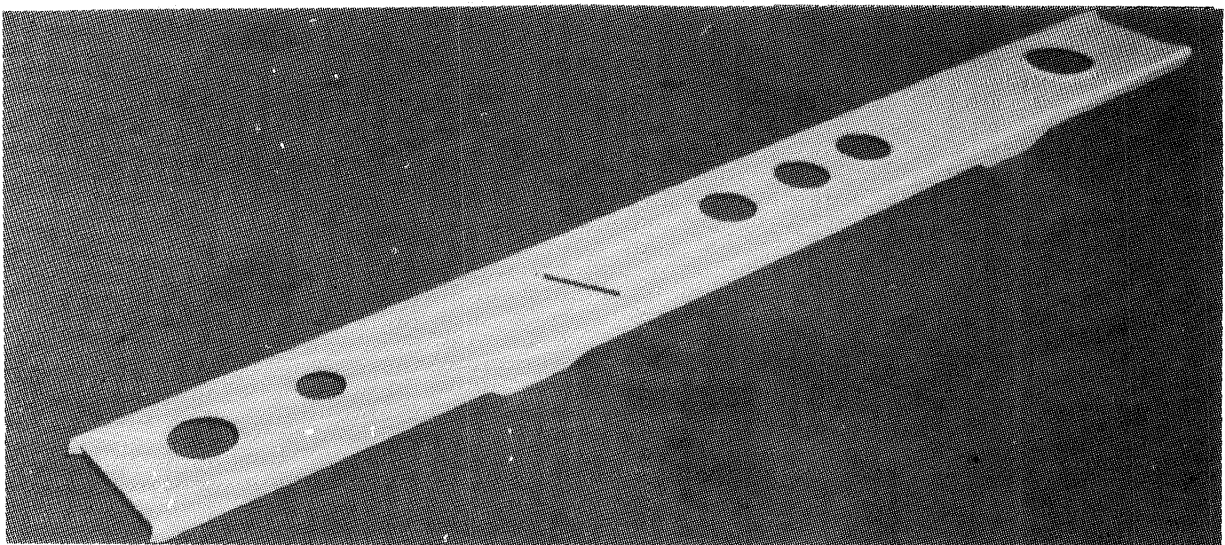
Figure 8. - Front spar.

rib locations to provide mounting surfaces for the main ribs and rib backup fittings. Flanged holes are provided in the spar web for access for inspection purposes.

Front spar bending moments are shared by both the spar cap and the leading edge of the cover which has local doublers at the main rib-front spar intersections. This design approach yields a very efficient fail-safe design. The ribs, hinge/actuator fittings, and leading edge shroud supports act as stiffeners on the spar shear web; thus, no additional stiffening elements are necessary.

Rear Spar - The rear spar is a constant thickness 1.02 mm (0.040 in) channel section fabricated of 7075-T6 clad aluminum. It has aft facing flanges to which both the covers and training edge wedge are attached. Aluminum was selected for this component because utilization of composites would be too costly for the small amount of weight saved.

Main Ribs - The main ribs are located at each of the three hinge/actuator fitting locations to transfer concentrated loads from the fittings to the aileron covers and spar. Aileron hinge/actuator fittings attach to the forward face of the front spar web, and the rib to spar joint is completed by means of aluminum backup fittings which attach to either side of the ribs as shown in figure 9.
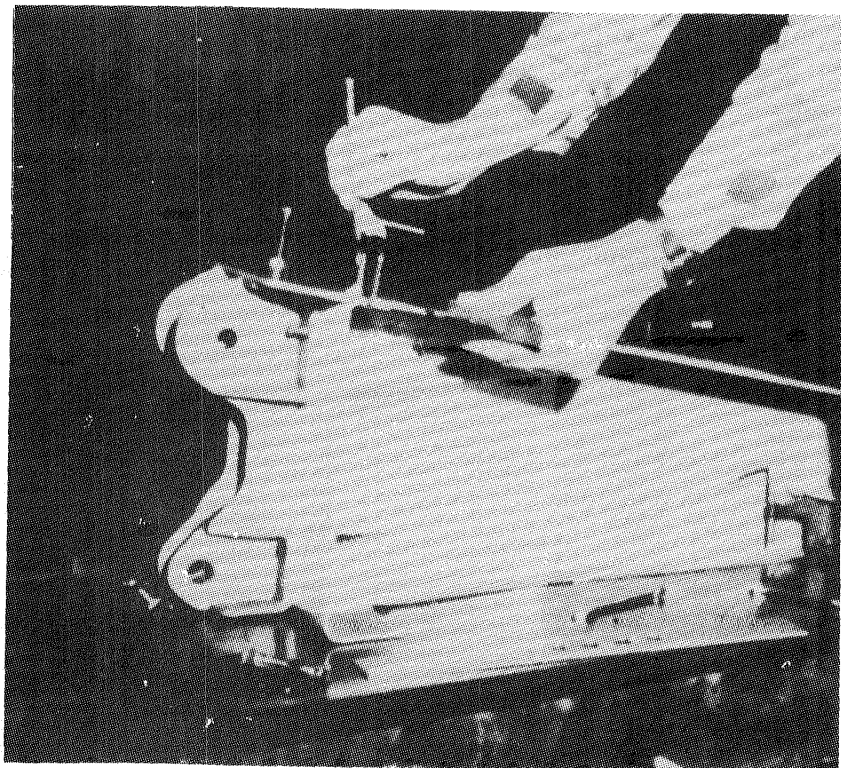
Figure 9. - Main rib hinge/actuator fitting assembly.

The main ribs are a channel section configuration constructed with four plies of graphite/epoxy bidirectional fabric 0.36 mm/ply (0.014 in/ply) oriented at $(45°/90°_2/45°)$ where $0°$ is the lengthwise direction of the rib. Five plies of graphite/epoxy tape are added to the rib caps to increase the stiffness and strength of the ribs. As with the inner doublers in the cover these five plies are oriented at $(5°/-5°/0°/-5°/5°)$ instead of all $0°$ to inhibit microcracking.

Intermediate and End Ribs - In addition to the three main ribs, the aileron has five intermediate ribs and two closeout ribs which support the covers and react the air pressure loads. Intermediate and closeout ribs are constant thickness channel sections consisting of five plies of graphite/ epoxy bidirectional fabric oriented at $(45°/90°/135°/90°/45°)$ where the $0°$ is again the lengthwise direction of the rib. Each rib contains five flanged lightening holes. As shown in figure 10, the ribs are flanged on all four sides to eliminate the necessity of using separate clips to attach the ribs to the spars and covers.

1.2 Weight

The weight statement for the composite aileron is presented in table 1. The average of the actual weights of the first four articles is 48.9 kg (107.8 lb, which is a saving of 22.9 percent compared to the current indicated weight of an all-aluminum baseline. Total composite material used is 31.3 kg (69.0 lb).

When the Advanced Composite Aileron Program was initiated in September of 1977 the metal aileron had an aluminum trailing edge wedge. As a result of a previous design study on the development of composite ailerons, which was funded by NASA (reference 2), the weight savings benefits of employing
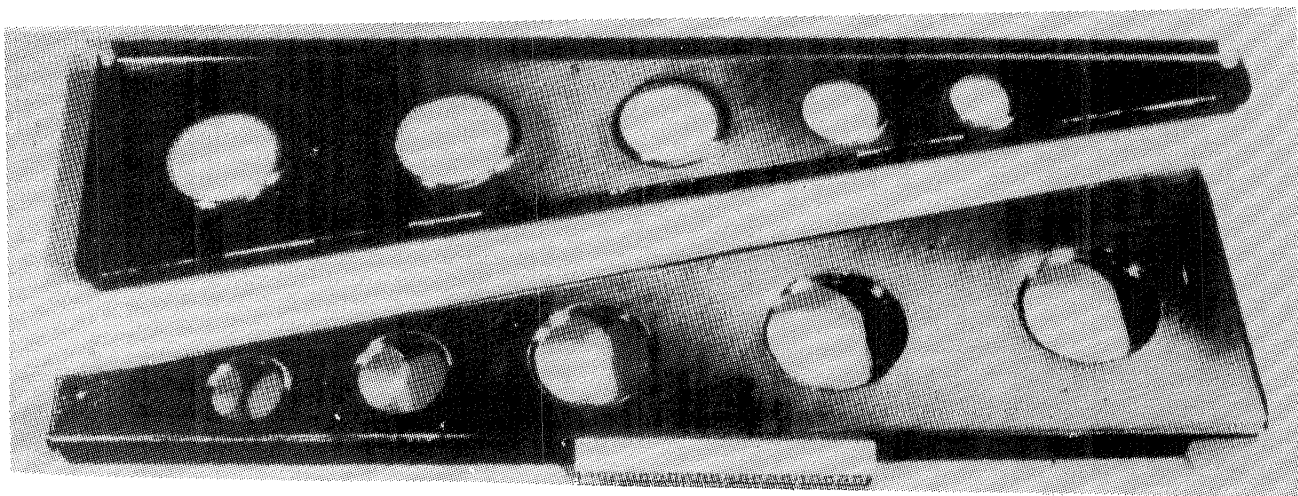
Figure 10. - Intermediate ribs.

TABLE 1. — WEIGHT STATEMENT (SI UNITS)

Item	Baseline Aluminum Aileron	Current Aluminum Aileron	Composite Aileron	
			Indicated Weight	Composite Material Weight
Covers — kg	17 8	17.8	15 0	15 0
Spars — kg	11.4	11 4	9 1	2 2
Ribs — kg	17.7	17 7	10 0	5.7
Fairings and Shrouds — kg	7 3	7 3	8 4	3 0
T E. Wedge Assy — kg	5 7	2.7	3 2	3 0
Assembly Hardware —kg	1 9	1.9	0 6	—
Protective Finish — kg	1 5	1.5	1.4	—
Manufacturing Variation — kg	---	---	1 0	1 0
Total Aileron — kg	63 4	60 5	48 9 △	31 3
Weight Saving — kg/unit	---	3 0	14 6	---
Weight Saved — %	---	4 7	22 9	---
% Composite Material	5 8	10 6	---	64 0

△ Weight Basis   Average actual weight of first 4 ailerons

TABLE 1A. — WEIGHT STATEMENT (CUSTOMARY UNITS)

Item	Baseline Aluminum Aileron	Current Production Aileron	Composite Design	
			Indicated Weight	Composite Material Weight
Covers — lb	39 3	39.3	33 2	33 2
Spars — lb	25 2	25 2	20.0	4 8
Ribs — lb	39 0	39 0	22.0	11 5
Fairing and Shrouds — lb	16 2	16 2	18 6	10 5
T E. Wedge Assy — lb	12 6	6 0	7 1	6 7
Assembly Hardware — lb	4 2	4 2	1 4	---
Protective Finish — lb	3.4	3 4	3 2	—
Manufacturing Variation — lb	---	---	2 3	2 3
Total Aileron — lb	139 9	133 3	107 8 △	79 0
Weight Saving — lb/unit	---	6.6	32.1	---
Weight Saved — %	---	4 7	22 9	---
% Composite Material	5 8	10 6	---	64 0

△ Weight Basis   Average actual weight of first 4 ailerons

Kevlar 49 for construction of the trailing edge wedge were identified. Subsequently trailing edges fabricated with Kevlar 49 were incorporated into the aluminum aileron design and production initiated in 1978. For clarification, the weight breakdown of both the current production metal aileron and the baseline metal aileron have been presented in table 1.

1.3 Analysis

The specific criteria used for the design and analysis of the advanced composite aileron are given in reference 1. In summary, it is required that the composite aileron be a direct replacement for the metal aileron without equipment modification, operating restrictions, or decrease in performance; and it must have equivalent torsional stiffness and withstand the same static and acoustic loading environment as the metal aileron.

1.3.1 <u>Finite element model.</u> - Based on the selected design concept a NASA Structural Analysis (NASTRAN) three-dimensional finite element model of the aileron was developed. The model was used to determine internal loads, deflections, and structural influence coefficients. The Lockheed-developed anisotropic quadrilateral membrane element, a linear stress function element, was used to model the surfaces and webs.

The general layout of the model is shown in figure 11. The models for the actuator and hinges are shown in figure 12. Auxiliary stations at model stations 1100, 1300, 1700, 2000, 2300 do not include rib panels, or rib caps. They have been included in the model to provide additional detail for the stress pattern in the surfaces. The model has 701 degrees of freedom and consists of 632 elements: 211 rods, 106 bars, and 315 membrane elements.

1.3.2 <u>Preliminary design material properties.</u> - The preliminary design material properties used in the NASTRAN model and for preliminary analysis purposes for T300/5208 graphite-epoxy tape are shown in table 2. Preliminary design properties used for the graphite/epoxy fabric, summarized in table 3, are based on tests conducted on HMF 330C (T300/934; 24 x 23 8HS) by Lockheed Missiles and Space Company (LMSC). They are normalized to 65 percent fiber volume and 0.33 mm/ply (13 mils/ply) based upon LMSC tests which showed this to represent the minimum product of thickness and stiffness.

Final design analysis was based on material properties developed from material and concept verification test results discussed in section 3.

Figure 11. – Composite aileron finite element model.
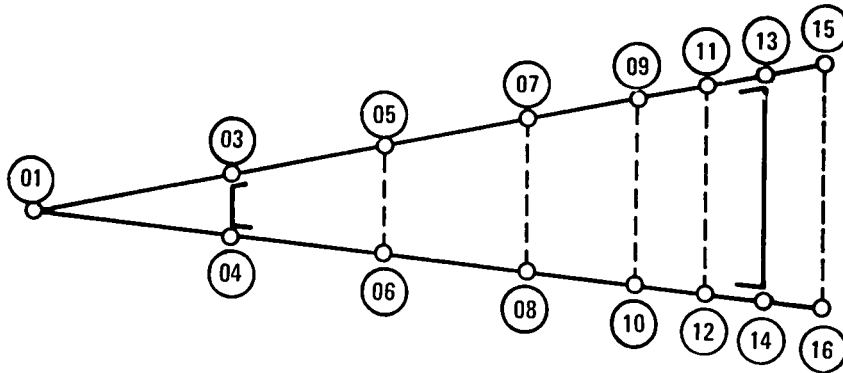
Typical section at hinge + actuator ribs at model stations 1200 and 1800

SPC1

Spoint
1891

Actuator Station

17   Upper
     extreme

18

19

20

21   Lower
     extreme

Spoint
1891

SPC 1
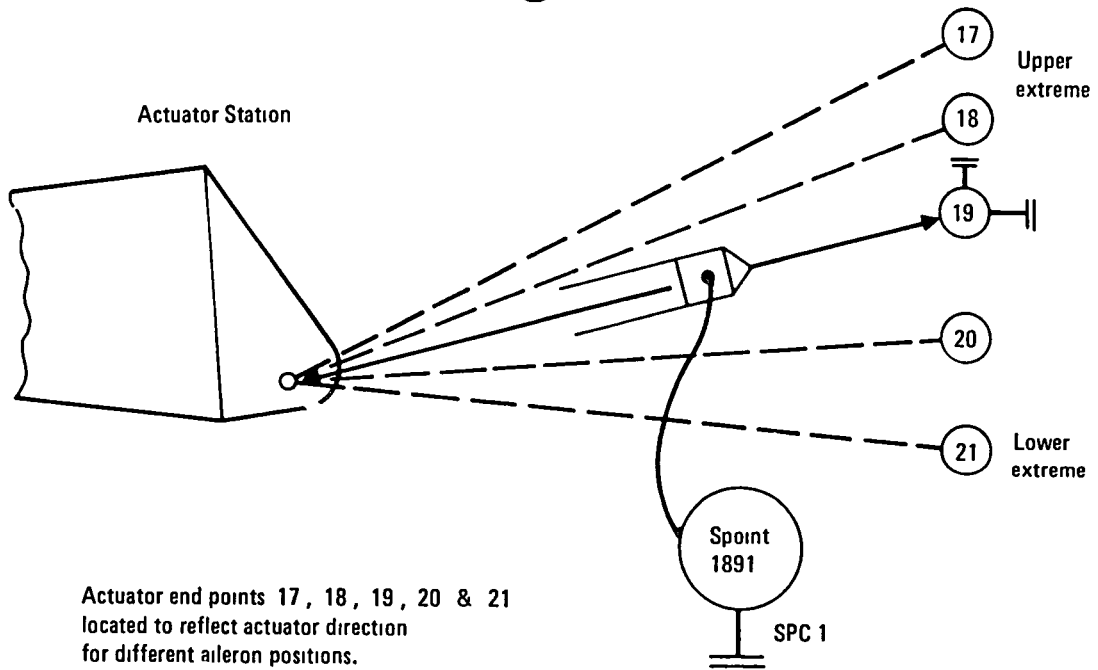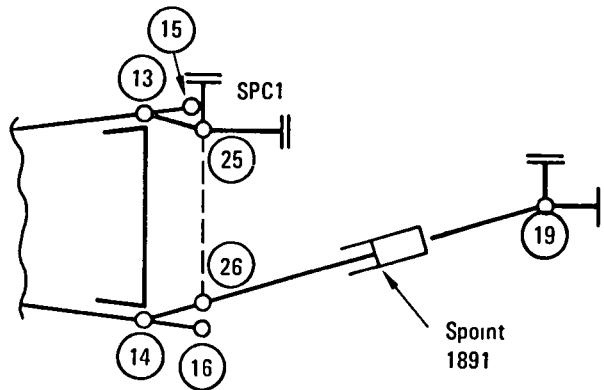
Actuator end points 17, 18, 19, 20 & 21
located to reflect actuator direction
for different aileron positions.

Figure 12. – Modeling of actuator and hinge support stations.

15

TABLE 2. - PRELIMINARY DESIGN PROPERTIES FOR T300/5208 GRAPHITE/EPOXY TAPE

	Direction, Type of Property	SI Units	RTD Average	Customary Units	RTD Average
Extensional Moduli	L, Initial Tensile	GPa	96 1	Msi	21 60
	L, Initial Compres	GPa	82 7	Msi	18 60
	L, Second Tensile	GPa	96 1	Msi	21 60
	L, Second Compres	GPa	64 1	Msi	14 40
	T, Initial Tensile	GPa	7 1	Msi	1 60
	T, Initial Compres	GPa	6 9	Msi	1 56
	T, Second Tensile	GPa	7 1	Msi	1 60
	T, Second Compres	GPa	6 3	Msi	1 42
Shear Mod	LT, Initial Shear	GPa	3 6	Msi	0 80
	LT, Second Shear	GPa	1 3	Msi	0 30
	LT, Major Poisson	–	0 30		0 30
Therm Exp	L, Coef of Exp.	10^6 mm/mm/K	0 34	10^{-6} in/in/F	0 19
	T, Coef of Exp		25 7		14 3
Auxiliary Data	Fiber Volume	%	62 67	%	62 67
	Density	g/m^3	1 606	lbs/in^3	0 058
	Ply Thickness	mm	0 127	in	0 005

1.3.3 Design loads. - The ultimate design loads used for the ACA are the same as those used for the design of the metal aileron. The loads are conservatively based on the pressure relief valve setting for the hydraulic actuator, and the resultant hinge moments at five aileron positions were determined. The chordwise pressure distribution on the aileron in the faired, or 0°, position is parabolic, and for the deflected aileron it is triangular with 75 percent to the upper surface and 25 percent to the lower surface.

Ultimate design loads are shown in table 4. Pressures are constant in the spanwise direction. The maximum pressures are shown and are designated by U (upper surface) and L (lower surface). The NASTRAN program automatically distributes the loads from these pressures to the panel points. The design hinge-moment (M) and normal load (P) for the aileron are also shown. The model loads-check verified these hinge-moments and normal loads with +6 percent.

16

TABLE 3. - PRELIMINARY DESIGN PROPERTIES FOR GRAPHITE/EPOXY FABRIC[1]

Property	SI Units	RTD Average	Customary Units	RTD Average
Tension				
E_w	GPa	76 5	msi	11 1
E_f	GPa	71 7	msi	10 4
Compression				
E_w	GPa	65 5	msi	9 5
E_f	GPa	61 4	msi	8 9
Shear				
G	GPa	6 9	msi	1 00
Other				
ν		0 09		0 09
α_w	mm/mm/K	29×10^{-6}	in/in/°F	$1 6 \times 10^{-6}$
α_f	mm/mm/K	36×10^{-6}	in/in/°F	2.0×10^{-6}
ρ	g/m^3	1 55	lb/in^3	0 056
t	mm	0 33	in	0 013

(1) Based on Lockheed Missile and Space Company data HMF 330C (T300/934; 24 x 23/8HS)
    Normalized to 65% fiber volume

Subscripts w-warp direction, f-fill direction

1.3.4 <u>Internal loads analysis</u>. - The NASTRAN finite element model was analyzed for five basic applied load conditions. The finite element model stress fields for various subcomponents of the composite aileron were plotted and analyzed. Maximum internal loads from the NASTRAN model are summarized on figures 13 through 16 for typical aileron composite parts. Besides the maximum load, the critical condition number is shown for each element. The panel loads shown are the average of the loads at each panel point.

1.3.5 <u>Stability analysis</u>. - One of the more buckling prone regions on the covers is the area between the I.A.S. 78.087 rib and the I.A.S. 92.087 rib. The region was analyzed with a finite element buckling analysis program using the distributed loads (N_x, N_y, and N_{xy}) from the NASTRAN finite element model. This analysis predicts local instability of the cover at 20.3 percent of design ultimate load. Local instability of the cover in this region at 20.3 percent of ultimate load is acceptable for several reasons. First, the actual flight loads are such that buckling will occur infrequently in the aircraft's lifetime, since the ultimate load has been conservatively established as 1.5 times the maximum actuator output. Second, industry testing has indicated that repeated buckling of flat panels does not significantly degrade their structural integrity.

TABLE 4. - AILERON DESIGN ULTIMATE LOADS
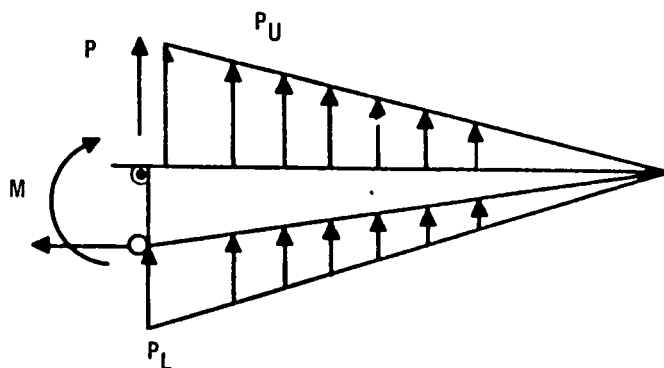
Condition number	1	2	3	4	5
Aileron angle, degrees	−20	−12	0*	+12	+20
SI Units					
M, hinge moment kN−m	30 68	32 04	−27 12	−31.73	−30 68
P, hinge shear kN	−73 4	−75 6	48 0	75 2	72 5
P_U kPa	−34 2	−35 4	21 7*	35 1	33 9
P_L kPa	−11 4	−11 8	−8.07*	11 7	11 3
Customary Units					
M, hinge moment 1000 in-lb	271.5	283 5	−240	−280 8	−271 5
P, hinge shear 1000 lb	−16 5	−17 0	10 8	16.9	16.3
P_U psi	−4.96	−5.13	3 14*	5 09	4 92
P_L psi	1.65	1.71	1.17*	1 70	1 64

*Parabolic pressure distribution

The remaining regions of both the upper and lower covers between ribs were analyzed in a similar manner. This analysis resulted in the eigenvalues shown in table 5. A further analysis was performed which indicated that the predominant cause of buckling was the N_x load component. This analysis was confirmed by an examination of the eigenvector pattern which showed only a very slight skew due to the shear loads.

Figure 13. – Upper surface load map (SI Units).

Key

Condition of maximum shear load (see table 4)

N_x
N_y lb/in
N_{xy}

Maximum shear load with corresponding N_x and N_y

View looking down

y
x

| 132 68 | Front spar | 107 098 | 102 698 | | 78 087 | | 57 087 | | 36 627 |

③ 24 0 −27 | ③ −71 −16 −15 | ③ −162 −22 −79 | ④ −322 −43 −166 | ⑤ −348 −129 −661 | ② −425 184 −339 | ④ −300 −98 246 | ⑤ −120 −28 24 | ① 109 20 101 | ① 114 −38 195 | ② 129 62 201 | ③ −72 −44 33 | ① 61 6 9

③ −45 11 19 | ③ −94 −24 −52 | ④ −204 −65 −142 | ④ −247 −107 −193 | ⑤ −149 −95 −560 | ② 212 90 −294 | ④ −203 −144 254 | ⑤ −154 −49 61 | ① 137 31 88 | ② 93 52 184 | ② 67 60 191 | ③ −19 −44 32 | ⑤ −25 −9 24

③ −62 18 −41 | ④ −116 −18 −96 | ④ −153 −83 −180 | ④ −154 −141 −185 | ⑤ −89 −143 −368 | ④ −61 −250 187 | ② 161 156 −195 | ④ −158 −61 77 | ③ −89 −36 −49 | ② 61 48 132 | ② 25 74 127 | ⑤ 3 −63 24 | ④ 12 3 44

② 67 −56 67 | ② 98 34 133 | ④ −93 −72 −168 | ④ −72 −123 −150 | ④ −7 −94 −144 | ② 20 179 −48 | ④ −69 −125 94 | ④ −109 −53 74 | ⑤ −67 −22 13 | ③ −18 −45 −41 | ③ 17 −53 −34 | ⑤ 39 −27 14 | ② −32 −22 −46

③ −53 9 −56 | ② 45 3 76 | ② 44 4 140 | ② 49 36 146 | ② 57 61 116 | ③ −59 −52 −51 | ③ −46 −72 −20 | ④ −33 −53 33 | ④ −30 −26 66 | ② 34 16 −53 | ① 27 20 −45 | ② 25 24 −53 | ② 4 6 −20

Rear spar

Figure 13A. − Upper surface load map (Customary Units).

Key

Load condition (see table 4)

Upper cap

| ○ | P N | Maximum tension load |
| ○ | −P N | Maximum compression load |

Web

| ○ | N_x N_y N_{xy} kN/m | Maximum shear load with corresponding N_x and N_y |

Lower cap

| ○ | P N | Maximum tension load |
| ○ | −P N | Maximum compression load |

X

Y

Inboard

View looking aft

36 627   57 087   78 087   102 698   107 098   128 825

Upper cap

| ② 1512 | ② 5186 | ② 6828 | ② 3981 | ① 2429 | ① 5213 | ① 12464 | ① 25772 | ① 21199 | ② 9423 | ② 5649 | ② 1788 | ② 107 |
| ④ −1552 | ④ −5151 | ④ −6721 | ④ −3843 | ④ −1548 | ④ −3118 | ④ −9314 | ④ −19491 | ④ −18201 | ④ −9652 | ④ −5871 | ④ −1895 | ⑤ −178 |

Web

| ② 18 0.2 −25.6 | ② −21.2 −4.7 −30.6 | ⑤ 0.2 2.1 −23.1 | ⑤ 0.4 0.7 −21.5 | ① −0.4 3.0 −14.2 | ① −1.4 7.7 −42.0 | ① 10.3 13.1 −66.5 | ① −63.9 −7.7 −70.0 | ① −81.4 −9.5 164.4 | ② −0.9 10.5 52.7 | ② −0.5 −6.7 50.4 | ② 0.0 −2.8 32.0 | ④ 0.2 0.4 −15.6 |

| ④ 1668 | ④ 4724 | ④ 5622 | ④ 3180 | ④ 1103 | ④ 2073 | ④ 7682 | ④ 15719 | ④ 18290 | ④ 15266 | ④ 6485 | ④ 2091 | ⑤ 182 |
| ② −1672 | ② −4439 | ② −5391 | ② −3425 | ① −2055 | ① −4248 | ① −11111 | ① −21057 | ② −19980 | ② −14398 | ② −6303 | ② −2002 | ② −125 |

Lower cap

Figure 14. – Front spar load map (SI Units).

Key

Load condition (see table 4)

Upper cap

| ○ | P | lb | Maximun tension load |
| ○ | −P | lb | Maximum compression load |

x

Inboard ← → y

Web

| ○ | N_x N_y lb/in N_{xy} | Maximum shear load with corresponding N_x and N_y |

Lower cap

| ○ | P | lb | Maximum tension load |
| ○ | −P | lb | Maximum compression load |

View looking aft

36 627   57 087   78 087   102 698 107.098   128 825

Upper cap

| ② | 340 | ② | 1166 | ② 1535 | ②895 | ① | 546 | ① | 1172 | ① | 2802 | ① 5794 | ① 4766 | ② 2051 | ② | 1270 | ② | 402 | ②24 |
| ④ | 349 | ④ | 1158 | ④ 1511 | ④864 | ④ | 348 | ④ | 701 | ④ | 2094 | ④ 4382 | ④ -4092 | ④ 2170 | ④ | 1320 | ② | -426 | ⑤-40 |

Web

| ② 10 1 146 | ② 121 27 175 | ⑤ 1 12 132 | ⑤ 2 4 123 | ① 2 17 81 | ① 8 44 240 | ① 59 75 380 | ① 365 44 400 | ① 465 54 939 | ② 5 60 301 | ② 3 38 288 | ② 0 16 183 | ④ 1 2 89 |

Lower cap

| ④ | 375 | ④ | 1062 | ④ 1264 | ④715 | ④ | 248 | ④ | 466 | ④ | 1727 | ④ 3534 | ④ 4112 | ④ 3432 | ④ | 1458 | ④ | 470 | ⑤41 |
| ② | 376 | ② | 998 | ② 1212 | ②770 | ① | 462 | ① | 955 | ① | 2498 | ① 4734 | ② -4492 | ② 3237 | ② | 1417 | ② | -450 | ② 28 |

Figure 14A. - Front spar load map (Customary Units).

Figure 15. — IAS 102.698 main rib load map (SI Units).

Key

Load condition (see table 4)

Upper cap

	P	lb	Maximum tension load
	−P	lb	Maximum compression load

Web

○	
N_x N_y N_{xy}	lb/in

Maximum shear load with corresponding N_x and N_y

Lower cap

	P	lb	Maximum tension load
	−P	lb	Maximum compression load

Rear spar

Front spar

View looking outboard

Figure 15A. I.A.S. 102.698 main rib load map (Customary Units)

Key

Load condition (see table 4)

Upper cap

| ○ | P | N | Maximum tension load |
| ○ | −P | N | Maximum compression load |

x

y

Web

| ○ | | |
| N_x N_y N_{xy} | kN/m | Maximum shear load with corresponding N_x and N_y |

Lower cap

| ○ | P | N | Maximum tension load |
| ○ | −P | N | Maximum compression load |

④ 298
① −436

④ 387
① −480

④ 378
② −423

④ 240
② −249

②

②

4
−187

②
③

②

②

②

−2.6
−2 8
−22.8

−1.9
−4.7
−19.6

−1.8
−3 3
−16.3

−1 4
−1.8
−11.6

4 0
1.1
5 3

③

Rear spar

Front spar

| ② | 160 | ② | 507 | ② | 725 | ① | 752 | ① | 552 |
| ④ | −142 | ④ | −498 | ④ | −681 | ④ | −658 | ④ | −387 |

View looking outboard

Figure 16. — IAS 78.087 intermediate rib load map (SI Units).

Key

Load condition (see table 4)

Upper
cap

| ○ | P | lb | Maximum tension load |
| ○ | −P | lb | Maximum compression load |

Web

N_x
N_y lb/in
N_{xy}

Maximum shear load
with corresponding N_x and N_y

Lower
cap

| ○ | P | lb | Maximum tension load |
| ○ | −P | lb | Maximum compression load |

View looking outboard

Rear
spar

Front
spar

Figure 16A. − I.A.S. 78.087 intermediate rib load map (Customary Units).

TABLE 5. - STABILITY ANALYSIS EIGENVALUES*

Station	Upper	Condition**	Lower	Condition**
64 1 – 78.1	0 366	4	0.321	1, 2
78.1 – 92.1	0.235	4	0.203	1, 2
92 1 – 102.7	0 441	4	0 395	1, 2
107 1 – 117.4	0.401	4	0 540	1, 2
117.4 – 126 2	0 779	4	0 842	1, 2

*Eigenvalue represents fraction of ultimate load at which buckling initiates
**See table 4

Since the development of a buckle reduces the effective stiffness of the buckled surface, the postbuckled internal load distribution differs from that in the unbuckled state. To evaluate this load redistribution, the NASTRAN finite element model was rerun using stiffness effectiveness factors for the buckled surfaces. The objective was to obtain a surface load distribution approximating that at ultimate load and to determine the resultant load changes in the spars and ribs.

Some tests have shown that after buckling, shear stiffness is only slightly reduced. The effective skin width at the rib caps enables the skin to carry chordwise load beyond initial buckling. The spanwise load in the skin is shared with the spar caps, and the spanwise stiffness is most affected by buckling. Consequently, the following effectiveness factors were used as an estimate:

$$ETA_x \quad \text{(SPANWISE)} \quad = \text{eigenvalue}/2$$

$$ETA_y \quad \text{(CHORDWISE)} \quad = \text{eigenvalue}$$

$$ETA_{xy} \quad \text{(SHEAR)} \quad = 1.0$$

Load conditions 1 and 2 were run with the above effectiveness factors for the lower surface. The eigenvalue was estimated as 0.6 for the surface outboard of IAS 126.2. The resultant lower surface loads were slightly increased in the most highly loaded region of the cover. The lower spar cap load increased 28 percent, and the maximum spar web shear flow increased 6 percent. With these increases the resultant strains are less than the allowable strains.

Since some investigators have indicated shear stiffness reductions for buckled panels as high as 40 percent, additional runs were made including $ETA_{xy} = 0.6$ for the buckled panels. However, the internal loads distribution was only slightly different than those with an assumed eigenvalue of 1.0.

27

A comparison between the resultant cover loads and the buckling analysis led to the conclusion that the results are a satisfactory approximation of the internal load distribution at ultimate load with the covers buckled.

The loads on the front spar with the cover buckled were then used for a finite element buckling analysis of the front spar web. The loads included shear, in-plane bending, and crushing. Initial buckling of the web is predicted at 57 percent of design ultimate load between IAS 92 and 98. The major contributor to web buckling is the in-plane bending loads. The section of the spar web between IAS 64 and IAS 78, which contains a reinforced access hole, was analyzed for combined shear and bending. This analysis indicated a 14 percent margin of safety against initial buckling.

The fatigue loading spectrum was reviewed, and the maximum hinge load occurring once per lifetime (36,000 flights) was a mean hinge moment of -678 N-m (-6,000 in-lb) and a variable moment of ±10169 N-M (±90,000 in-lb) (roll maneuver). This is 34 percent of the ultimate load for condition 4 (critical for buckling in the upper surface), and it is 30 percent of the ultimate load for conditon 2 (critical for buckling in the lower surface). Considering these loads and those for the next lower spectrum level -678, ±7909 N-m, (-6,000, ±70,000 in-lb), the upper and lower surfaces between IAS 78.1 and 92.1 will buckle only 10 times in a lifetime. Ground testing of the composite aileron has demonstrated that repeated buckling of the elements of the aileron did not degrade their structural integrity.

1.3.6 <u>Point stress analysis</u>. - The results of the NASTRAN internal loads analysis were surveyed to determine critical internal loads. The most critical regions of each major subcomponent were subject to a detailed analysis to determine ply-level strains. The combined internal loads from the finite element model were input together with the ply properties and stacking sequences for the laminates into a laminate margin-of-safety analysis program. The quadrilateral elements were analyzed at each nodal point as well as in the center. The maximum ply-level strains are summarized on table 6 where the load conditions are indicated. The maximum strains occur in the ±45 plies of the spar web between the IAS 102.7 and 107.1 hinge/actuator fittings. When the covers buckle the front spar carries a higher proportion of load, and this is reflected in the strains shown. The notched allowable fiber direction strains for tape and fabric are shown. These values are from the data presented in section 3. Comparison with these values shows the aileron is not strain (or strength) critical.

The covers are designed to give the aileron box a torsional stiffness of at least 0.86 MN-m^2 (300 x 10^6 lb-in^2). The computed stiffness is 1.06 MN-m^2 (369 x 10^6 lb-in^2) including the effect of access holes in the spars.

TABLE 6. — AILERON PLY-LEVEL STRAIN SUMMARY

Component	Material	Station	Load Condition (See table 4)	L, Fiber Direction Strain 10^{-6} mm/mm (in/in)		T Transverse Direction Strain 10^{-6} mm/mm (in/in)		Shear Strain 10^{-6} mm/mm (in/in)
				Tension	Compression	Tension	Compression	
Upper Cover	Tape	98 8	1.2	1800		1800		
		102.7	4.5		-2000		-2000	3200
Lower Cover	Tape	98.8	4	1100		1100		
		102.7	1		-1400		-1400	1900
Front Spar Cap	Tape	98 8	1	1180*				
		92.1	1		-1280*			
Web		102.7	1	2800	-3700	2800	-3700	5200
Rear Spar Cap	Alum	98 8	2,4	348	-377			
102.7 Rib Cap	Tape/ Fabric	102 7	2,4	1645	-1709			
Web	Fabric		1,3 2,4	1200	-1900	1700	-1800	3200
78.1 Rib Cap	Fabric	78 1	4		-209			
			1	232				
Tape Allowable Strain (See Table 21)				4750	-4000	4750	-4000	8000
Fabric Allowable Strain (See Table 21)				3900	-4000	4750	-4000	8200

*With Postbuckled Lower Surface

1.3.7 Fail-safe analysis. - The ACA was analyzed for all five of the loading conditions using loads equal to two-thirds of the design ultimate loads shown on table 4 for each of the following fail-safe conditions:

- One actuator out

- A 305 mm (12-inch) cut in the upper cover at IAS 102.7

- The upper cap of the IAS 102.7 hinge/actuator rib severed

- The upper cap of the front spar at IAS 102.7 severed

- The front spar web at IAS 102.7 completely cut.

For each fail-safe condition, the upper and lower covers, the front and rear spars, and the IAS 102.7 and 78.1 ribs were mapped for maximum loads. These, in turn, were surveyed to determine which fail-safe condition was most critical for each component based upon those regions with the highest strains. The upper cover and front spar have the highest loads with the 102.7 rib cap failed. The lower cover, rear spar, and IAS 102.7 and 78.1 ribs have the highest loads with the upper cover cut. Load maps were prepared and compared with those for intact structure. These comparisons showed that the internal loads for the damaged conditions were less than those for ultimate loading for the undamaged aileron. The NASTRAN finite element model was modified to analyze the case in which the front spar web at IAS 102.7 was failed. In this case shear is carried by differential bending in the caps. Accordingly, they were modeled by bar elements.

As a result of this fail-safe analysis, and the internal load comparisons discussed, it is concluded that none of the failed conditions result in internal loads greater than those ultimate loads used to design the components.

1.3.8 Flutter/vibration analysis. - Analyses were performed to determine the vibration characteristics of the ACA using NASTRAN. The results of these analyses were compared with known vibration characteristics of the basic L-1011-1 metal inboard aileron to provide an indication as to whether the ACA stiffness characteristics were satisfactory.

The vibration analysis are based on a finite element structural model in which the aileron is constrained at the hinge supports and actuators, and which has the capability of varying actuation stiffness. The aileron is divided into 54 mass elements which are transformed onto 34 structurel degrees of freedom. With an actuation stiffness representative of the actual system, the resulting vibration characteristics of the first two modes of the composite aileron are shown on table 7 along with a comparison of the

30

TABLE 7. – ACA VIBRATION FREQUENCIES TRIMMED
POSITION, HINGE FLEXIBILITY INCLUDED

Mode	ACA Analysis	Metal Aileron Test
1 Rotation	23 49 Hz	23.11 Hz
2 Torsion	44.48 Hz	38.6 Hz

corresponding first two modes of the metal aileron as measured on L-1011
S/N 1001. The first mode is a rotation mode about the hinge-line and shows
good frequency and mode shape agreement between analysis and test. The second
mode is a spanwise torsion mode and shows good agreement in mode shape, but
with the analysis frequency being higher than the measured second mode for the
metal aileron. In an additional investigation, the effect of reduced stiff-
nesses due to buckling of the cover during worst-case flight maneuvers indi-
cated a negligible reduction in vibration frequencies.

The results from these analyses indicate that the ACA stiffness levels
and distribution are comparable to those of the metal aileron.

1.4 Maintenance and Repair

In order to develop, establish, and verify maintenance and repair
requirements and procedures, tests were conducted on coupons and subcomponents
to determine the mechanical property effects of defects and damage caused
during processing, assembly and service. The principal defects and damage
considered were voids and impact damage. Several types of repairs were also
evaluated by coupon tests for each type of defect or damage investigated.
In addition, lightning strike tests were conducted on a full-size section of
the aileron assembly to evaluate their effects on the fail-safe character-
istics of the aileron.

1.4.1 Effect of voids and delaminations. – Voids, delaminations, or
porosity can be caused by a discrepancy during processing or foreign materials
inadvertently cured into the laminate. Nondestructive inspection of parts
after they are cured is utilized to identify the size and number of defects
present within the laminate. Accept/reject criteria have been established
for the types of laminates used within the aileron. These criteria allow
ultrasonic indications typical of voids to be no larger than 1.61 cm^2 (0.25
in^2).

Static and fatigue tests were conducted on typical laminates used within
the composite aileron to determine the effect of voids on mechanical strength.
The test coupon used for the cover laminate and the intermediate rib laminate is
shown in figure 17. A void was created by inserting a teflon coated stain-
less steel shim 0.038 mm (0.0015 in) thick into the laminate prior to cure.
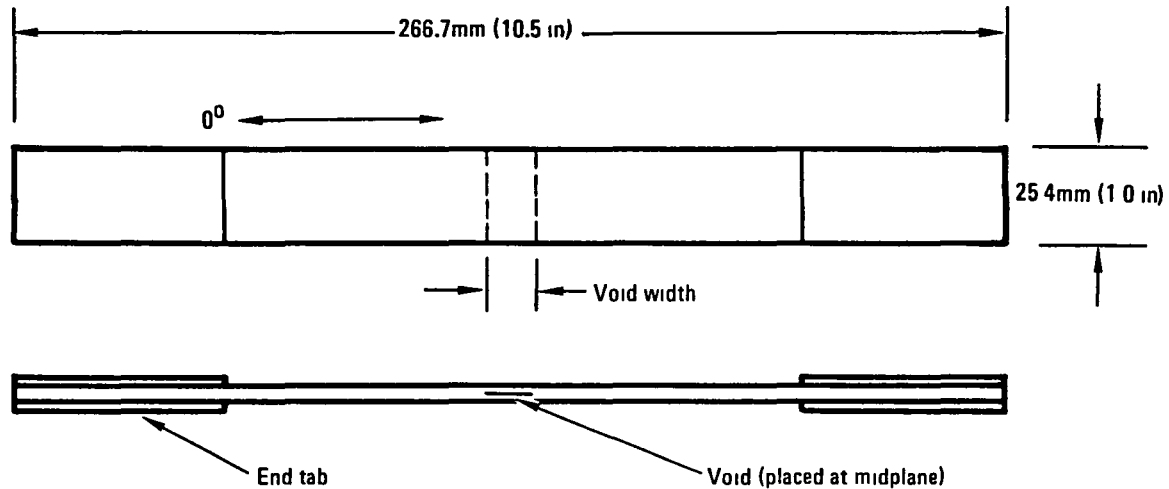
Figure 17. - Cover and intermediate rib laminates - void tolerance coupon.

After the laminate was cured and coupons machined, the shim was removed. This specimen configuration results in a conservative estimate of the effects of a void on a laminate since two edges of the delamination are free. This would not be the case for a void occurring in the center of a panel. Static specimens were tested in compression. To prevent instability the coupon was sandwiched between steel plates during load application.

A similar loading arrangement was used for coupons containing 6.45 cm^2 (1.0 in^2) voids which were tested in fatigue. Two lifetimes (660,000 cycles) of spectrum fatigue were applied to the coupons prior to residual strength testing. No damage growth was detected in any of the coupons which were fatigue tested. Residual strength tests indicated no change in strength due to the fatigue loading.

Results of cover laminate void tolerance tests are presented in table 8. Also shown for comparison are data for notched and unnotched coupons which did not contain voids. Note that the 12.7 mm (0.5 in) wide void test is twice the size allowed in the ultrasonic inspection criteria. As the data presented indicate, for fully supported compression coupons the effect of the void is approximately equal to the strength reduction due to a 4.76 mm (3/16 in) diameter open hole. All of the specimens containing a defect failed a stress levels in excess of the 126.9 MPa (18.4 ksi) compressive design allowable for the cover laminate. Note that the laminate allowable includes the syntactic epoxy which was assumed to have no inplane load carrying capability.

32

TABLE 8. – COVER LAMINATE – VOID TOLERANCE

Laminate $(45^0_T/0^0_T/-45^0_T/\text{SYNTACTIC}/-45^0_T/0^0_T/45^0_T)$; T = Tape

Nominal Thickness. 2.10 mm (0 0825 in)

Void Size		Notch	Test Condition	No of Coupons	Average Compression Strength ④	
cm²	in²				MPa	ksi
None		None	RTD ①	2	289.7	42.0
None		4 76 mm (3/16 in) dia hole	RTD	4	220.7	32.0
3 22	0 5	None	RTD	3	253 8	36 8
None		None	219 3K (-65°F) D ②	4	317.3	46 0
3 22	0 5	None	219 3K (-65°F) D	3	275 9	40 0
None		None	355 4K (180°F) W ③	5	246 9	35 8
None		4 76 mm (3/16 in) dia hole	355 4K (180°F) W	10	198 6	28.8
3 22	0 5	None	355 4K (180°F) W	3	186 9	27.1
6 45	1 0	None	355 4K (180°F) W	3	206.2	29 9
6 45	1 0	None	355 4K (180°F) W	3	207.6	30 1 ⑤

① Room temperature dry

② Dry – as received

③ Wet – approximately 1% moisture by weight

④ Design allowable for this laminate = 126 9 MPa (18 4 ksi)

⑤ 2 Lifetimes cyclic environment/load

A summary of the compression test data for the intermediate rib laminate with voids is reported in table 9. For comparison, the unnotched and notched laminate data for coupons without voids are also presented. As was determined from the cover laminate tests, the effect of the 12.7 mm (0.5 in) wide void on compressive strength is not as severe as the effect of a 4.76 mm (3/16 in) diameter open hole.

The effects of voids on the main rib cap was determined using a specimen which contained a 4.76 mm (3/16-in) diameter hole and an artificial void. The specimen configuration, shown in figure 18, has a 12.7 mm (0.5 in) wide void across one-half of the width of the coupon in the vicinity of a hole. As with the previously described coupons containing voids the defect was created by inserting a teflon coated shim in the laminate prior to cure and then removing while the coupon was being machined.

Results of compression tests conducted on the rib cap coupons are presented in table 10. For comparison purposes test data for unnotched coupons and coupons with just the 4.76 mm (3/16-in) diameter hole are also tabulated. All of the data indicate the effect of the void is minimal.

TABLE 9. – INTERMEDIATE RIB LAMINATE – VOID TOLERANCE

Laminate. $(45^0_F/0^0_F/135^0_F/0^0_F/45^0_F)$, F = Fabric

Nominal Thickness. 1.78 mm (0.070 in)

Void Size		Notch	Test Condition	No of Coupons	Average Compression Strength ④	
cm²	in²				MPa	ksi
None		None	RTD ①	27	466.9	67 7
None		4.76 mm (3/16 in) dia. hole	RTD	5	292.4	42 4
3.22	0 5	None	RTD	3	300.7	43.6
None		None	219 3K (-65°F) D ②	5	446.9	64.8
None		4.76 mm (3/16 in) dia hole	219 3K (-65°F) D	8	342.1	49 6
3.22	0 5	None	219 3K (-65°F) D	3	335.2	48 6
None		None	355 4K (180°F) W ③	5	337.9	49 0
None		4 76 mm (3/16 in) dia hole	355 4K (180°F) W	8	244.9	35 5
3.22	0.5	None	355 4K (180°F) W	3	280 0	40 6

① Room temperature dry
② Dry – as received
③ Wet – approximately 1% moisture by weight
④ Design allowable for this laminate = 153 8 MPa (22 3 ksi) (see figure 46)
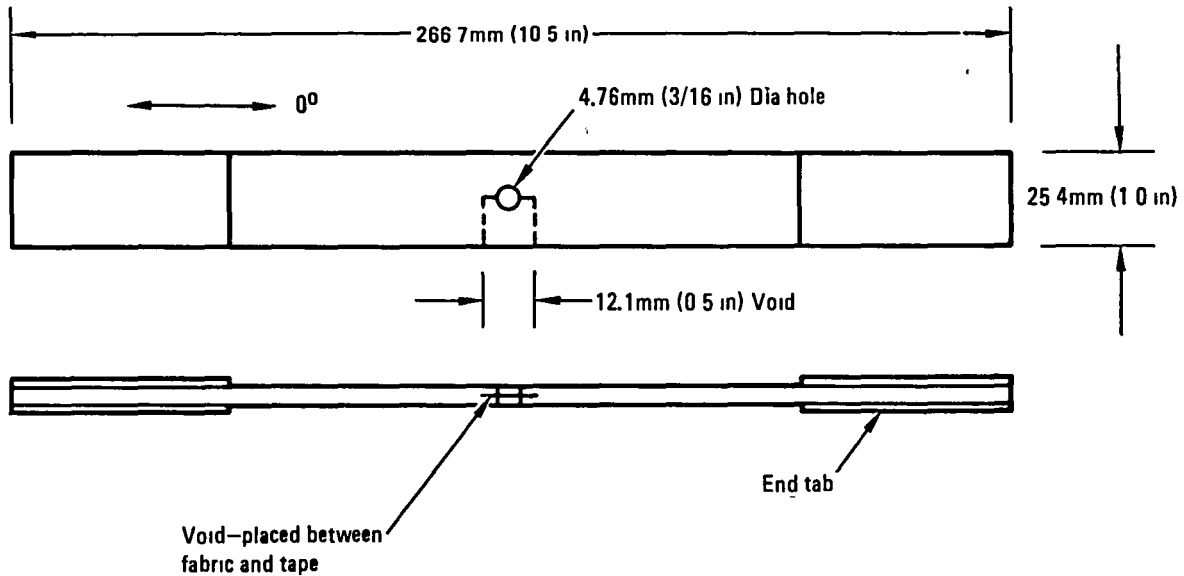
Figure 18. – Main rib cap – void tolerance coupon.

TABLE 10. – MAIN RIB CAP – VOID TOLERANCE

Laminate. $(45^\circ F/90^\circ F/0^\circ 5T/90^\circ F/45^\circ F)$, T = Tape, F = Fabric

Nominal Thickness. 2.37 mm (0.0935 in)

Void Size		Notch	Test Condition	No. of Coupons	Average Compression Strength ④	
cm²	in²				MPa	ksi
None		None	RTD ①	5	810.5	117.5
None		4.76 mm (3/16 in) dia notch	RTD	5	480.0	69.6
3 22	0.5	None	RTD	3	453 9	65 8
None		None	219 3K (-65°F) D ②	4	813 2	117.9
3 22	0 5	None	219 3K (-65°F) D	3	478 0	69.3
None		None	355 4K (180°F) W ③	5	678.0	98 3
3 22	0.5	None	355 4K (180°F) W	3	362 8	52 6

① Room temperature dry

② Dry – as received

③ Wet – approximately 1% moisture by weight

④ Design allowable for this laminate = 303 5 MPa (44 0 ksi) (Calculated with hybrid laminate analysis)

Further investigations were conducted into the effects of typical manu-facturing defects on the compression strength of a portion of the aileron cover which contains both internal and external doublers. The specimens were machined out of a cover panel which had been rejected due to ultrasonic indications. The defective areas extended almost all the way across the coupon. Photo-micrographic examinations of the defective areas revealed that the ultrasonic indication was due to extensive porosity.

Two types of tests were conducted on the coupons containing defects, 25.4 mm (1.0 in) wide coupons with steel plates on both sides of the coupon to prevent buckling, and 76.2 mm (3 in) wide coupons with the coupon edges supported with a dovetail arrangement which extended 9.5 mm (0.375 in) into the specimen edge.

Test results for the coupons containing defects are presented in table 11 and compared to results on good quality coupons. Note that the failure strength of the defective coupons is a function of the support technique utilized. The 25.4 mm (1 in) wide coupons with full support have a higher strength because the delamination failure mode is prevented by the support plates. For coupons containing defects the full support test for static loading in compression a strength decrease of approximately 28 per-cent was measured for the 76.2 mm (3 in) wide coupons of the laminate con-figuration and type of defect investigated. The 76.2 mm (3 in) wide

TABLE 11. – COVER DOUBLER REGION – DEFECT TOLERANCE

Laminate. $(45^{\circ}_T/90^{\circ}_T/-45^{\circ}_T/5^{\circ}_T/-5^{\circ}_T/0^{\circ}_T/-5^{\circ}_T/+5^{\circ}_T/-45^{\circ}_T/90^{\circ}_T/45^{\circ}_T/45^{\circ}_T/0^{\circ}_T/-45^{\circ}_T/0^{\circ}_F)$; T = Tape, F = Fabric

Nominal Thickness: 3 02 mm (0.119 in),

Specimen Size mm (in)	Support Condition	Test Condition	No. of Coupons	Average Compression Strength	
				MPa	ksi
25.4 (1.0)x 266.7 (10.5)	Full	RTD – unnotched	5	511 8	74 2
25.4 (1.0)x 266.7 (10.5)	Full	355 4K (180°F) W – 4.76 mm (3/16 in) dia hole	20	397.3	57.6
25 4 (1 0) x 266.7 (10 5)	Full	RTD – contains defects	2	444 2	64 4
76 2 (3.0) x 355 6 (14.0)	Edge	RTD – contains defects	2	369.7	53.6

coupon support technique allowed local instability of the plies in the defective region and consequently a lower strength was measured. However, testing coupons with damage or defects all the way across the cross section of the coupon may result in an overly conservative estimate of the defect effect due to finite width effects.

1.4.2 Effects of impact damage. – The composite aileron is subject to impact damage during fabrication and assembly and in service. Primary damage threats identified for the aileron include tool drops and hailstone damage. Hailstones cannot strike the aileron during flight since it is protected by the wing, thus the primary hailstone threat to the aileron is while the aircraft is parked. For this condition hailstone impingement is assumed perpendicular to the aileron surface.

To determine the susceptibility of the aileron to impact damage a variety of impact tests were conducted using blunt object impactors to simulate tool drops and hailstones. Impact test data for the aileron cover are presented in figure 19. For those tests the structure was impacted and then ultrasonically inspected to determine the extent of damage. The data are plotted for impacts on the cover at a distance equidistant between two ribs. Impact energies in excess of 2.7 Joules (2 ft-lb) are required to cause any damage to the cover; this is approximately equivalent to a 25.4 mm (1.0 in) diameter hailstone striking the aileron at terminal velocity. The hailstone impact criteria established for the composite aileron specified no damage at 0.54 Joules (0.4 ft-lb) from a 17.8 mm (0.7 in) diameter hailstone at terminal velocity, thus the structure far exceeds the requirements.
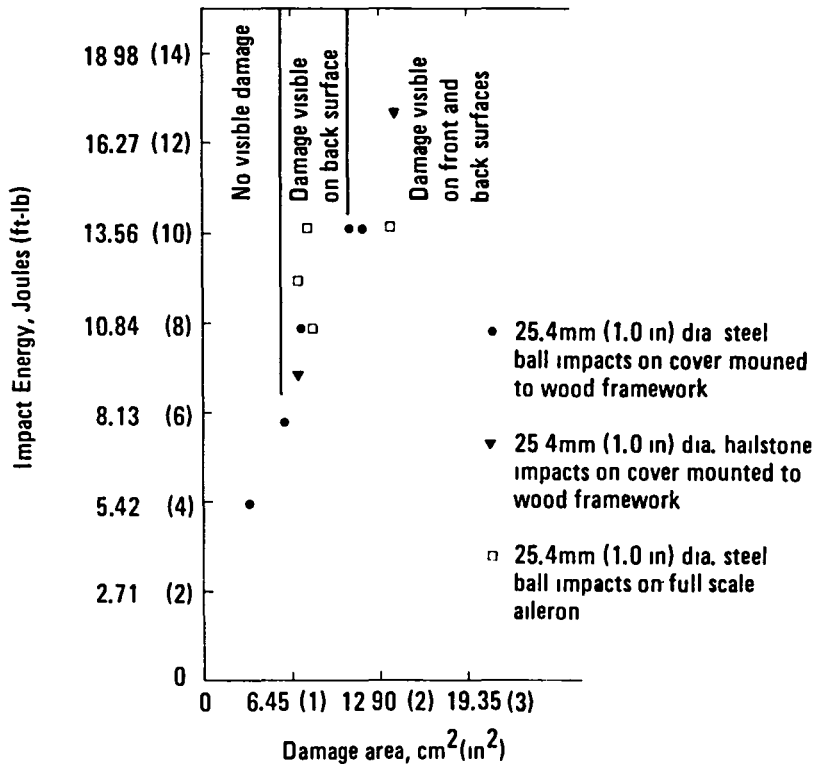
Figure 19. – Aileron cover impact tests.

The effect of impact damage on the mechanical properties of typical aileron laminates was determined by impacting test panels with a 25.4 mm (1.0 in) diameter steel impactor and then conducting static and fatigue tests. A summary of the test results is presented in table 12. For comparison purposes the data for undamaged laminates and laminates containing an open hole are also presented. The data indicate that for tension loading or inplane shear loading, impact damage of the sizes tested had little or no effect on strength. Impact damage caused a significant decrease in compression strength. The nonvisible damage caused a strength degradation of 52 percent. The larger, visible, impact damage caused a strength reduction of 67 percent. However, for this test the damage extended from one edge of the antibuckling guides across the specimen width to the other edge. Due to finite width effects, the static test data from the coupons containing large impact damage are suspect.

TABLE 12. — IMPACT DAMAGE EFFECTS ON COVER LAMINATE (SI UNITS)

Laminate: $(45^\circ_T/0^\circ_T/-45^\circ_T/SYNTACTIC/-45^\circ_T/0^\circ_T/45^\circ_T)$; T = Tape

Nominal Thickness: 2.10 mm

Type of Test	Coupon Size mm	Impact Damage Size cm^2	Notch	Test Condition	No. of Coupons	Average Strength MPa
Tension	25.4 x 266 7	None	None	RTD ①	5	315.2
Tension	25.4 x 266 7	None	4 76 mm dia.	RTD	30	193 8
Tension	203.2 x 609 6	1.48 – NV ⑦	None	RTD	3	260 0
Tension	203.2 x 609 6	3 93 – V ⑦	None	RTD	3	259.3
Tension	25 4 x 266 7	None	None	219 3 K D ②	5	319.4
Tension	25 4 x 266 7	None	4 76 mm	219 3 K D	8	175.2
Tension	203 2 x 609 6	1.48 – NV	None	219 3 K D	3	243 5
Tension	203.2 x 609.6	3 93 – V	None	219 3 K D	3	247.6
Tension	25 4 x 266 7	None	None	355.4 K W ③	5	370 4
Tension	25.4 x 266.7	None	4.76 mm dia	355 4 K W	10	220 0
Tension	203.2 x 609 6	1 48 – NV	None	355 4 K W	3	264.9
Tension	203.2 x 609 6	3.93 – V	None	355 4 K W	3	265 6
Inplane Shear	304 8 x 304.8	None	None	RTD	3	100.7
Inplane Shear	304 8 x 304 8	10 39 - V	None	RTD	3	103 4
Compression	76 2 x 355.6 ④	None	None	RTD	3	271.1
Compression	25 4 x 266.7 ④	None	4 76 mm dia	RTD	4	220.7
Compression	76.2 x 355.6 ⑤	1 87 – NV	None	RTD	3	131 0
Compression	76.2 x 355.6 ⑤	8 52 – V	None	RTD	3	93.1
Compression	76 2 x 355 6 ⑤	8.52 – V	None	RTD	3	89 7 ⑥

Notes

① RTD — Room temperature dry
② D — Dry, as received
③ W — Wet, approx. 1% moisture by weight
④ Fully supported coupon
⑤ Coupon supported on edges only
⑥ Residual strength after 1 lifetime of spectrum fatigue
⑦ NV — nonvisible damage, V — visible damage

38

TABLE 12A. – IMPACT DAMAGE EFFECTS ON COVER LAMINATE (CUSTOMARY UNITS)

Laminate: $(45^{\circ}_T/0^{\circ}_T/-45^{\circ}_T/SYNTACTIC/-45^{\circ}_T/0^{\circ}_T/45^{\circ}_T)$; T = Tape

Nominal Thickness: 0 0825 in

Type of Test	Coupon Size in	Impact Damage Size in^2	Notch	Test Condition	No. of Coupons	Average Strength ksi
Tension	1 x 10 5	None	None	RTD ①	5	45 7
Tension	1 x 10 5	None	3/16 inch dia	RTD	30	28 1
Tension	8 x 24	0 23 – NV ⑦	None	RTD	3	37 7
Tension	8 x 24	0 61 – V ⑦	None	RTD	3	37.6
Tension	1 x 10.5	None	None	-65°F D ②	5	46 3
Tension	1 x 10.5	None	3/16 inch dia	-65°F D	8	25.4
Tension	8 x 24	0 23 – NV	None	-65°F D	3	35 3
Tension	8 x 24	0 61 – V	None	-65°F D	3	35 9
Tension	1 x 10 5	None	None	180°F W ③	5	53.7
Tension	1 x 10 5	None	3/16 inch dia	180°F W	10	31 9
Tension	8 x 24	0 23 – NV	None	180°F W	3	38 4
Tension	8 x 24	0 61 – V	None	180°F W	3	38 5
Inplane Shear	12 x 12	None	None	RTD	3	14 6
Inplane Shear	12 x 12	1.61 – V	None	RTD	3	15 0
Compression	3 x 14 ④	None	None	RTD	3	39 3
Compression	1 x 10.5 ④	None	3/16 inch dia	RTD	4	32 0
Compression	3 x 14 ⑤	0 29 – NV	None	RTD	3	19 0
Compression	3 x 14 ⑤	1.32 – V	None	RTD	3	13 5
Compression	3 x 14 ⑤	1.32 – V	None	RTD	3	13 0 ⑥

Notes

① RTD – Room temperature dry

② D – Dry, as received

③ W – Wet, approx. 1% moisture by weight

④ Fully supported coupon

⑤ Coupon supported on edges only

⑥ Residual strength after 1 lifetime of spectrum fatigue

⑦ NV – nonvisible damage, V – visible damage

1.4.3 _Repair_. - Three types of repairs have been evaluated for the composite aileron: a bolted repair, a bonded repair, and a resin injection repair. Representative aileron subcomponent laminates were fabricated, damaged, and then repaired using the above techniques. Static tests were conducted on the repaired laminates and the results compared to undamaged and damaged strengths.

The bolted repair, shown in figure 20 is suitable for either flush repairs of the aileron (as shown in figure 20) or external repairs. This repair consists of an aluminum sheet bolted to the composite structure with titanium fasteners and stainless steel nuts. Both the aluminum and graphite/epoxy pieces are painted and faying surface sealant used to prevent galvanic corrosion.

A bonded repair was designed, primarily for repair of damage incurred during fabrication and assembly. This repair, shown in figure 21 is accomplished by securing graphite/epoxy unidirectional tape to both sides of the damaged composite laminate. A layer of film adhesive is placed between the patch and laminate to assure adequate bondline adhesive.

Delamination damage could occur in the structure either due to a processing error or due to foreign object impact. An effective repair technique for this type of damage was determined to be a resin injection repair. Small holes are drilled into the damaged laminate and a low viscosity epoxy resin is injected into the damaged area via the small holes.

A summary of the test data for the various types of repairs is presented in table 13. In all cases the repairs returned the strength of the laminate to a level which exceeded the design allowable strength.

1.4.4 _Aileron assembly lightning strike tests_. - To verify the tolerance of the aileron assembly to lightning a full-scale section of the composite inboard aileron was subjected to both direct and swept stroke lightning tests. The composite aileron is in the Zone 2 swept stroke area of the wing. Four tests were conducted to determine the effect of swept stroke lightning on the structure. In addition, two direct strike tests, which are not required for certification, each of which had a magnitude of about 200,000 amperes, were conducted to determine the response of the structure to a high current strike.

The swept stroke tests simulated an initial strike to a forward part of the wing which is swept onto the aileron where a high current restrike occurs. The high current restrike had a magnitude of about 100,000 amperes.

Rout out cover

Filler
2024 T3
aluminum

NAS 5202
HL 94 LP 5
Installed
with sealant

Cover

2024 T3
Aluminum

Faying
surface
sealant

Typ section

4D Typ

2D Typ

4D Typ

2D Typ
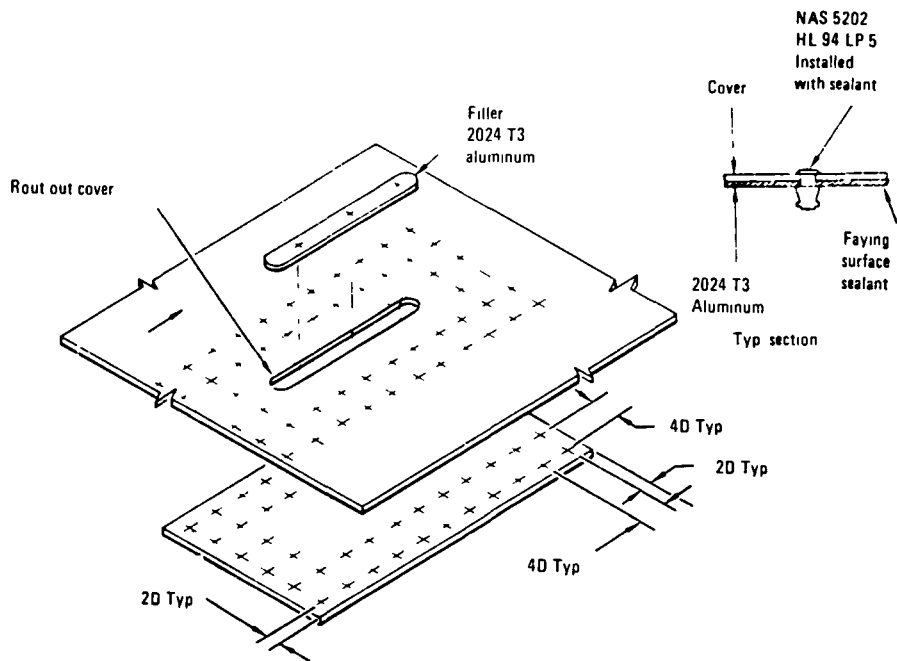
Figure 20. - Typical bolted repair for cover.

₵ Sym

0°

Rout out
damage
area

Cover laminate

Potting
Compound

6 4mm (0 25 in) Typ

90°
135°
45° 0°

Film
adhesive

0°
135° 45° 0°
90°

12 7mm (0 50 in) Typ

Typ section
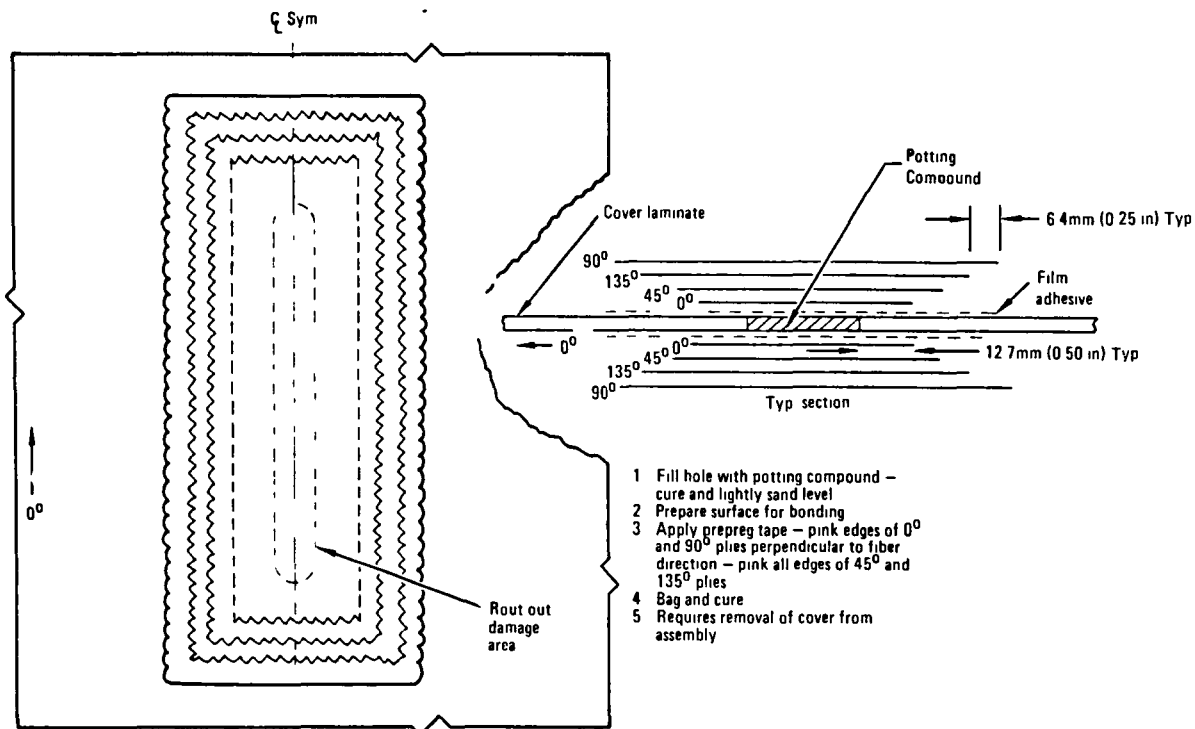
1 Fill hole with potting compound –
   cure and lightly sand level
2 Prepare surface for bonding
3 Apply prepreg tape – pink edges of 0°
   and 90° plies perpendicular to fiber
   direction – pink all edges of 45° and
   135° plies
4 Bag and cure
5 Requires removal of cover from
   assembly

Figure 21. - Typical bonded repair for cover.

41

TABLE 13. – COVER LAMINATE REPAIRS (SI UNITS)

Laminate· $(45^o{}_T/0^o{}_T/-45^o{}_T/SYNTACTIC/-45^o{}_T/0^o{}_T/45^o{}_T)$; T = Tape

Nominal Thickness 2.10 mm

Type of Test	Coupon Size mm	Defect Size & Type mm	Type of Repair	Test Condition	No of Coupons	Average Strength MPa
Tension	25 4 x 266 7	None	None	219 3K D ①	5	319.4
Tension	25.4 x 266 7	4.76 mm dia hole	None	219 3K D	8	175 2
Tension	203 x 609 6	38 1 mm dia. hole	Bonded	219 3K D	3	258.6
Tension	203 x 609.6	38.1 mm dia. hole	Bolted	219 3K D	3	175.2
Inplane Shear	305 x 305	None	None	RTD ②	3	100.7
Inplane Shear	305 x 305	15 7 x 95 slot	None	RTD	1	62.7
Inplane Shear	305 x 305	15 7 x 95 slot	Bolted	RTD	1	99 3
Inplane Shear	305 x 305	12.7 x 114 slot	Bonded	RTD	1	126 2
Compression	76.2 x 356	None	None	RTD	3	271.1 ③
Compression	76.2 x 356	8.52 cm^2 impact	None	RTD	3	93.1 ④
Compression	76 2 x 356	8 52 cm^2 impact	Resin Injection ⑤	RTD	3	218 6 ④

TABLE 13A. – COVER LAMINATE REPAIRS (CUSTOMARY UNITS)

Laminate· $(45^o{}_T/0^o{}_T/-45^o{}_T/SYNTACTIC/-45^o{}_T/0^o{}_T/45^o{}_T)$, T = Tape

Nominal Thickness. 0.0825 inch

Type of Test	Coupon Size in	Defect Size & Type in	Type of Repair	Test Condition	No. of Coupons	Average Strength ksi
Tension	1 x 10.5	None	None	-65°F D ①	5	46 3
Tension	1 x 10.5	3/16 in dia hole	None	-65°F D	8	25 4
Tension	8 x 24	1-1/2 in dia hole	Bonded	-65°F D	3	37.5
Tension	8 x 24	1-1/2 in dia hole	Bolted	-65°F D	3	25.4
Inplane Shear	12 x 12	None	None	RTD ②	3	14.6
Inplane Shear	12 x 12	0.62 x 3 74 slot	None	RTD	1	9 1
Inplane Shear	12 x 12	0 62 x 3 74 slot	Bolted	RTD	1	14 4
Inplane Shear	12 x 12	0 50 x 4 50 slot	Bonded	RTD	1	18 3
Compression	3 x 14	None	None	RTD	3	39 3 ③
Compression	3 x 14	1 32 sq in impact	None	RTD	3	13 5 ④
Compression	3 x 14	1.32 sq in impact	Resin Injection ⑤	RTD	3	31 7 ④

Notes for Tables 13 and 13A

① D – dry (as received)
② Room temperature dry
③ Fully supported coupon
④ Coupon supported on edges only
⑤ Injected with CG-1034 epoxy

42

Upon completion of the lightning tests the covers were removed from the assembly and a complete visual and ultrasonic inspection made of the covers and substructure. The results of these inspections are reported in the following paragraphs.

The outer cover surface of the aileron which was subjected to the lightning strikes is shown in Figure 22. Also shown is the type of strike that caused the damage. A summary of the lightning strike damage measurements for each strike is given in table 14. Note that three of the strikes resulted in penetration of the cover: the center panel direct strike, and the swept strokes at the center of the panel and at an intermediate rib. The penetration for the swept stroke damage was just large enough to push a pencil through the cover.

Figure 23 shows a closeup view of the damage due to a swept stroke at the center of a panel. The ultrasonic 'C' scan of this region is shown in figure 24. The outer ply of the cover laminate which is oriented at 45 degrees to the spanwise direction of the aileron has been delaminated and torn off for a distance of approximately 381 mm (15 in). Damage to the remainder of the laminate is centralized about the strike location. In this area the cover has been punctured and most of the resin vaporized for an area of approximately 3.23 cm^2 (0.5 square in). The total area of the delamination for this strike was calculated to be 198.7 cm^2 (30.8 square in).

The swept stroke at the main rib, shown in figure 25, resulted in much less damage to the cover than did the strike at the center of the panel. Note that in this region of the cover the syntactic core is replaced by a graphite/epoxy internal doubler. A photograph of the ultrasonic 'C' scan inspection of the cover is shown in figure 26. The calculated delamination area is 111.6 cm^2 (17.3 square in). No penetration occurred for this strike; however, back-surface damage was evident. Ultrasonic inspection of the substructure revealed that the main rib cap was delaminated over an area of approximately 17.4 cm^2 (2.7 square in). This delamination was evident by visual inspection of several of the fastener holes.

A fail-safe analysis has been conducted of the composite aileron with assumed damage equal to or greater than that obtained from the swept stroke lightning tests. This analysis indicated that for limit load the damaged aileron strains were less than those for ultimate load applied to an un-damaged aileron. Verification of the fail-safe characteristics of the aileron
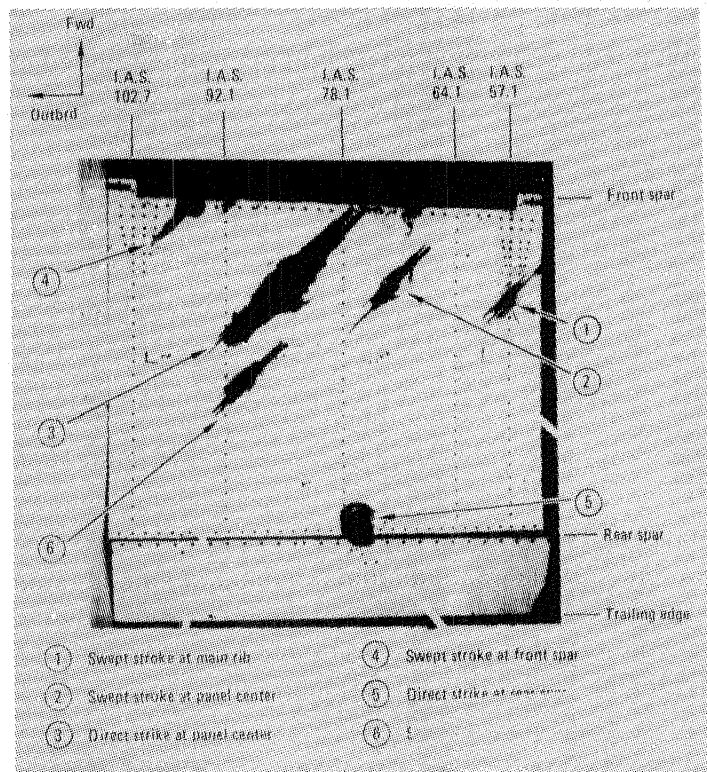
Figure 22. - Exterior of composite aileron after lightning strike tests.

TABLE 14. - SUMMARY OF LIGHTNING STRIKE DAMAGE MEASUREMENTS

Location*	Type of Strike	Approximate Size of Damage mm (in)	Area of Delamination Damage cm^2 (in^2)	Cover Penetration	Substructure Damage
I.A.S. 57.1 Main Rib	Swept	267 (10.5 x 41 (1.6)	111.6 (17.3)	No	17.4 cm^2 (2.7 in^2) delamination of main rib cap
Panel Center @ I.A.S. 71	Swept	376 (14.8) x 76 (3.0)	198.7 (30.8)	Yes	No
Panel Center @ I.A.S. 85	Direct	495 (19.5) x 104 (4.1)	490.0 (76.0)	Yes	No
Front Spar @ I.A.S. 100	Swept	190 (7.5) x 33 (1.3)	53.5 (8.3)	No	19.4 cm^2 (3.0 in^2) delamination of spar cap
Rear Spar @ I.A.S.75	Direct	127 (5.0) x 117 (4.6)	116.8 (18.1)	No	One fastener hole enlarged
I.A.S. 92.1 Rib	Swept	305 (12) x 61 (2.4)	184.5 (28.6)	Yes	6.5 cm^2 (1.0 in^2) delamination of rib cap

*I.A.S. = Inboard Aileron Station
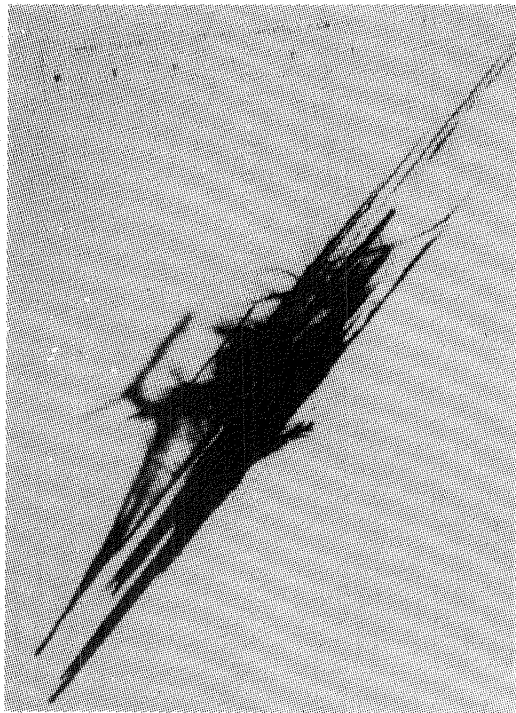
Figure 23. – External damage from swept stroke
at center of panel.
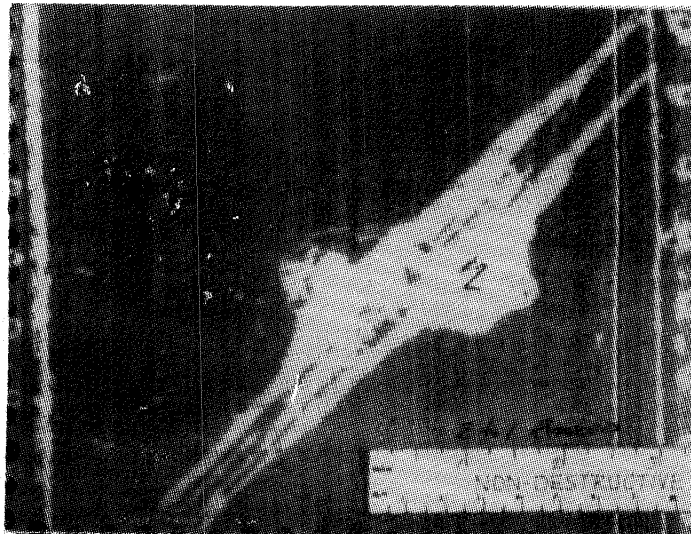
Figure 24. – Cover delamination damage due to swept stroke
at center of panel.
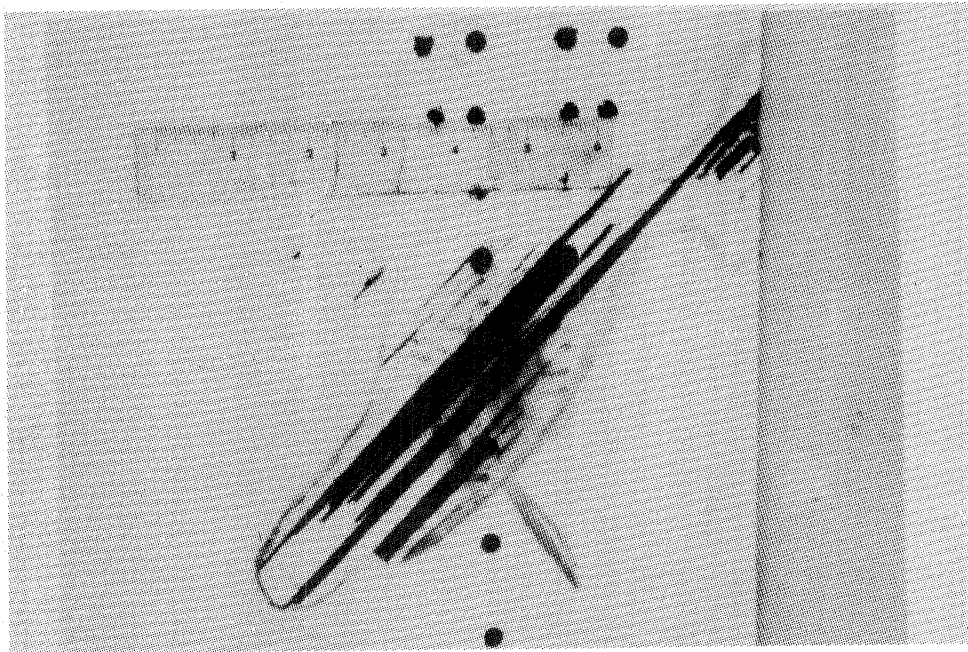
Figure 25. – External damage from swept stroke at main rib location.

Figure 26. – Cover delamination damage due to swept stroke at main rib location.

was made by statically testing the second ground test article with damage which simulates that due to swept stroke lightning.

2. MATERIAL VERIFICATION

The primary material systems used in the composite inboard aileron are Thornel 300/Narmco 5208 graphite/epoxy unidirectional tape (0.19mm (0.0075 in./ply) and bidirectional fabric (0.35mm (0.014 in./ply). Mechanical and physical property data of these materials required for the aileron design and analysis have been determined. Both tape and fabric material characterization programs were conducted to obtain lamina properties of strength, strain, and modulus for tension, compression, and inplane shear loading. In addition, tensile, compressive, inplane shear, and bearing properties were determined for laminate configurations representative of various aileron components. These tests were conducted on unnotched and notched coupons exposed to a variety of environmental conditions.

2.1 Design Allowables Approach

Statistical analysis of the data has led to the formulation of 'B' basis design allowables. 'B' basis design allowables are those mechanical properties that are expected to be equaled or exceeded by at least 90 percent of the population of values, with a confidence of 95 percent. For the unidirectional tape, the 0.19mm (0.0075 in/ply) data derived in this program have been combined with data for 0.13mm (0.0050 in/ply) tape from the Advanced Composite Vertical Fin Program, contract NAS1-14000 to formulate design allowables.

The basic approach for determination of design allowables is illustrated in figure 27. Average lamina data are used in a laminate property prediction program to predict the unnotched room temperature dry strength. This unnotched prediction is reduced by factors to account for notches, impact damage, and environmental conditions to arrive at a design allowable strength for a particular laminate.

2.2 Test Program Summary

Tests were conducted on 0°, 90°, and $\pm 45^{\circ}$ laminates to formulate ply level properties. These properties are the basis of analytical predictions of laminate properties. Crossplied laminates were tested with and without notches at various environmental conditions. These data were utlized to verify analytical predictions of laminate strength and stiffness, and to establish factors to account for notch and environmental effects.

The notch size used for the laminate tests was a 4.76mm (3/16 in) diameter hole. This notch size was selected since most of the fasteners used for assembly of the aileron are 4.76mm (3/16 in) diameter or smaller.

Ply Level Tests

0°	tens	RTD
90°	&	219K (-65°F)
$\pm45^\circ$	comp	355K (180°F)

→ Normalized bilinear stress - strain data → Laminate computer program

Laminate tests

tens	RTD	Notched
comp	219K (-65°F)	and
shear	355K (180°F)	unnotched

→ Verify program predictions - modify ply data if required →

Calculate

'B' Basis scatter factors - K_B

notched/environmental factors - K_{ET}

→ Notched Design Allowables

$$F_x^t = F_{x\ RTDU}^t \times K_{ET} \times K_B$$

Figure 27. - Design allowables approach.

Laminate tests were conducted at temperatures ranging from 219.3K (-65°F) to 355.4K (180°F). Analysis of the thermal environment of the aileron led to the selection of these temperatures as the most extreme conditions. Graphite/epoxy materials absorb moisture when exposed to humid environments. This absorbed moisture reduces the mechanical properties of the composite, particularly for tests conducted at elevated temperatures. To account for the detrimental effect of moisture on laminate properties some of the test coupons were moisture conditioned to a weight gain of 1 percent which is 67 percent of the moisture saturation level in T300/5208 graphite/epoxy composites. This extreme condition was selected based on an analysis of L-1011 environmental exposures for a large variety of route structures.

Test data for the tension, compression, and inplane shear tests conducted on tape, fabric, and hybrid laminates are summarized in Appendix A. The data summarized include the strength, modulus, failure strain and the normalized values of strength and modulus. Normalization of the data is based on thickness ratios, where the nominal thickness for tape is 0.19mm (7.5 mils/ply) and the thickness for fabric is 0.356mm (14 mils/ply). Note that while the nominal thickness of the fabric differs slightly from that used for the preliminary design properties (table 3) the resultant ply properties are not significantly different. The configurations of the coupons used for the design data tests are reported in Appendix B.

Testing of the syntactic epoxy included physical and mechanical properties of syntactic sheet specimens. The syntactic epoxy used is 0.95 mm (0.0375 in) thick. Six layers were stacked to make the cured syntactic sheet. This makes a cured sheet sufficiently thick to be readily machined and handled.

48

The most significant test data obtained from the syntactic sheet are the tensile tests which are run on dogbone type specimens. A summary of the cured syntactic sheet properties is presented in table 15. Tests were also run on graphite/syntactic sandwich test panels representative of the end application. These specimens incorporate the T300/5208 graphite tape prepreg which is cocured with the syntactic epoxy as the core material. Interlaminar tensile and short-beam shear were the principal mechanical tests run on the sandwich specimens. The test values show that syntactic epoxy used as core material provides an order of magnitude improvement in compression and shear properties over conventional honeycomb. A summary of these test data is shown in table 16.

2.3 Statistical Analysis of Test Data

Statistical analysis of the test data was performed to determine "B" allowables for the family 0°, ±45°, 90° laminates. The "B" values must be applicable for various environment conditions as well as various combinations of 0°, ±45°, 90° laminates. It is impractical to conduct tests for each laminate used in the structure for various environment conditions to determine the "B" values. This would involve a minimum of thirty specimens for each laminate, each environment and each material property. Therefore, a limited number of laminates covering the range of 0°, ±45°, 90° laminates used in the structure were tested. The test results were related to predicted strength, so that "B" allowable values could be calculated for laminate conditions that were not tested.

Figure 28 shows a flow chart of some of the statistical analyses performed and the results obtained. A laminate analysis program was used to predict the unnotched strength of the composite laminates. An evaluation of the unnotched predicted strength and the mean notched strength test data was made to determine the appropriate reduction factors. Evaluation was also made of the coefficient of variation obtained from each test group and the fit of normal, log normal and Weibull probability distribution functions to data sets with 20 or more specimens. Based on the above evaluations, the "B" allowables were established for tension and compression strength of tape and fabric composites.

Since it is impractical to conduct tests for all laminates, properties and environmental conditions, the allowables must be related to the analytical predictions. Sufficient tests are conducted to cover the range of laminates and test conditions that are applicable to the structure. It is assumed that each test group represents a sample from the population for which the allowable is being derived. The tests cover a range of laminates, environmental conditions and batches of material.

For establishing the "B" allowable, the data can be pooled by relating the test strength to the predicted strength as shown in figure 29. If there is perfect correlation between predicted strength and test strength the test data would fall on the line with a slope of 1.0. Based on the analysis of the data, the scatter is proportional to the strength, i.e., the coefficient

TABLE 15. - SYNTACTIC EPOXY CURED (ADX 819) SYNTACTIC SHEET PROPERTIES

Properties	Test Results Average	
Density	609 kg/m^3	0 022 lb/in^3
Thickness	5 45 mm	0 216 in
Moisture wt gain*	8 5%	8 5%
Flatwise compressive strength at 297K (75°F)	60 016 MPa	8701 psi
Flatwise compressive strength at 219K (-65°F)	71.928 MPa	10428 psi
Flatwise compressive strength at 355K (180°F)	54 684 MPa	7928 psi
Flatwise compressive strength at 355K (180°F) wet	29 025 MPa	4208 psi
Tensile strength 297K (75°F)	23 500 MPa	3407 psi
Tensile strength at 219K (-65°F)	18 230 MPa	2643 psi
Tensile strength at 355K (180°F)	18 465 MPa	2677 psi
Tensile strength at 355K (180°F) wet	11.643 MPa	1688 psi
Tensile ult strain at 297K (75°F)	0 0093	0 0093
Tensile ult strain at 219K (-65°F)	0 0073	0 0073
Tensile ult strain at 355K (180°F)	0 0077	0 0077
Tensile ult strain at 355K (180°F) wet	0 0071	0 0071

*19 days at 339K (150°F), 95-100% relative humidity

TABLE 16. - SYNTACTIC EPOXY (ADX 819) GRAPHITE/SYNTACTIC SANDWICH PROPERTIES

Properties	Test Results Average	
Density	6 96 kg/m^3	0 035 lb/in^3
Thickness	3 07 mm	0 121 in.
Moisture wt gain*	2 7%	2.7%
Interlaminar tensile strength at 297K (75°F)	12.190 MPa	1768 psi
Interlaminar tensile strength at 219K (-65°F)	11.273 MPa	1635 psi
Interlaminar tensile strength at 355K (180°F)	7.695 MPa	1116 psi
Interlaminar tensile strength at 355K (180°F) wet	13 285 MPa	1926 psi
Short beam shear strength at 297K (75°F)	15 230 MPa	2208 psi
Short beam shear strength at 219K (-65°F)	17.299 MPa	2508 psi
Short beam shear strength at 355K (180°F)	17 637 MPa	2557 psi
Short beam shear strength at 355K (180°F) wet	17.044 MPa	2472 psi

*19 days at 339K (150°F), 95-100% relative humidity

TEST DATA   ANALYSIS   RESULTS

Strength and Modulus data for 0°, $\pm 45^o$ and 90° laminates and failure strain data for cross plied laminates

Hybrid computer prediction program

Predicted unnotched strength and modulus

Notched and unnotched strength data for laminates tested under various environmental conditions

Evaluate ratio of test/predicted mean notched strength for various environmental conditions to determine K_{ET}

Probability distribution of test/predicted notched mean strength and K_{ET} factors

Evaluate coefficient of variation

Probability distribution of coefficient of variation

Evaluate probability distribution of individual test groups

Probability distribution of composite strength data

"B" strength allowables for various environmental conditions

Figure 28. — Flow diagram of analysis of test data to obtain mean and "B" values for 0°, $\pm 45^o$, 90° family of laminates.

51
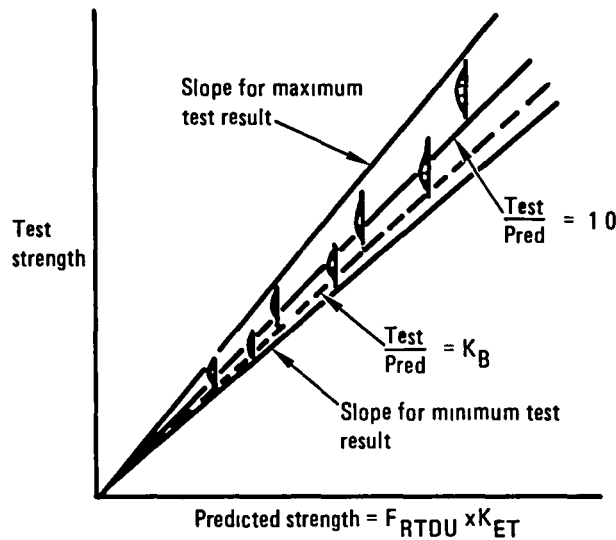
Figure 29. — Schematic showing the relation of the "B" allowable factor, K_B, to test and predicted strength values.

of variation is the same for all test groups. Therefore, the data are distributed within a scatterband represented by the slope of lines through the minimum and maximum test results. The data can be pooled by considering that each test result gives an independent assessment of the relation between the test strength and predicted strength.

For establishing "B" allowables the individual results must be considered. The "B" value for the slope, K_B, is the value that is equal or exceeded by 90 percent of the population with a 95 percent confidence. If the probability distribution of values is known or can be determined, then the K_B value can be determined using the appropriate statistical analysis procedure. However, rather than perform an analysis of the probability distribution of individual values of (Test/Pred), a nonparametric statistical analysis procedure for an unknown distribution was used.

The nonparametric procedure ranks the values of (Test/Pred) from the lowest to the highest, including all data points. The K_B value is then determined by counting down to the rth calculated value which is a function of the total number of test data points. A summary of these calculated values are given in table 17. The notched "B" allowable can be determined from the predicted strength using the following equation:

$$F_B = F_{RTDU} \times K_{ET} \times K_B$$

52

TABLE 17. – DETERMINATION OF K_B FACTORS ASSUMING DISTRIBUTION FUNCTION IS UNKNOWN

Rank Order r	Test/Predicted Ratios ①			
	Tape Tension N = 158	Tape Compression N = 76	Fabric Tension N = 263	Fabric Compression N = 65
1	903	821	849	.801
2	939	920	850	.875
3	958	924	850	901
4	962	940	856	921
5	965	947	903	
6	974		905	
7	975		953	
8	983		954	
9	987		964	
10	987		966	
11	988		968	
12			971	
13			972	
14			974	
15	.		976	
16			985	
17			987	
18			992	
19			998	
20			1 015	

①Non parametric K_B value is just above the line based on Table 9 6 4 2 in MIL-HDBK-5C, VOl 2

where F_{RTDU} = predicted unnotched room temperature dry strength

K_{ET} = notch/environmental factor given in table 18

K_B = 0.99 tape tension, 0.94 tape compression, 1.0 fabric tension and 0.90 fabric compression

2.4 Graphite/Epoxy Design Allowables

2.4.1 Ply-level design data. – Laminate analysis methods for strength, stiffness and stability prediction require the orthotropic properties of a

TABLE 18. – NOTCH/ENVIRONMENTAL AND STATISTICAL SCATTER FACTORS

Material	Loading	K_{ET} Condition			K_B
		219K (-65°F) Dry	RT Dry	355K (180°F) Wet	
Tape	Tension	49	.52	.59	99
	Compression	84	.71	.68	.94
Fabric	Tension	46	.52	.54	1.00
	Compression	77	72	.53	.90

single ply of the material. Laminate tests were conducted on $0°$, $90°$ and $\pm45°$ laminates to obtain the·lamina data. This information was then modified, based on the correlation of predictions to average laminate data, so that the predicted strength was less than the average measured strength for a laminate. The resulting ply-level properties are presented in table 19. Note that the tape properties apply to both the 0.127mm (5 mil/ply) and 0.19mm (7.5 mil/ply) tape.

2.4.2 Laminate design allowables. – The ply-level data presented in table 19 were utilized in a laminate strength prediction computer program to determine the laminate property carpet plots for the $0°/\pm45°/90°$ family. Carpet plots for tape and fabric rocm temperature dry, unnotched tension and compression strengths are presented in figures 30 through 33. The failure criterion used for predicting strength was the maximum strain criterion. For laminates with fibers in the direction of loading, failure was assumed when laminate strain exceeded the ply-level $0°$ failure strain. For laminates which contained only $\pm45°/90°$ plies and which are loaded in tension in the $0°$ direction, failure was conservatively assumed to occur when the $90°$ tensile failure strain was exceeded. When the $\pm45°/90°$ laminates were loaded in compression, failure was conservatively assumed to occur when the shear strain in the $\pm45°$ plies exceeded the ply-level yield shear strain.

TABLE 19. PLY LEVEL PROPERTY DATA FOR LAMINATE ANALYSIS, RTD AVERAGE

Property	Units	Tape	Fabric	Units	Tape	Fabric
E_{L1}^t	GPa	141	67 6	10^6 psi	20 5	9 80
E_{L1}^c	GPa	128	60 3	10^6 psi	18 5	8 74
E_{L2}^t	GPa	141	67 6	10^6 psi	20.5	9 80
E_{L2}^c	GPa	99	51 8	10^6 psi	14 3	7.52
E_{T1}^t	GPa	11 5	64 8	10^6 psi	1 67	9 40
E_{T1}^c	GPa	11.3	75 9	10^6 psi	1 64	8 40
E_{T2}^t	GPa	11 5	64 8	10^6 psi	1 67	9 40
E_{T2}^c	GPa	9 8	51 9	10^6 psi	1 42	7 53
G_{LT1}	GPa	6 0	5 0	10^6 psi	87	73
G_{LT2}	GPa	1 8	1 6	10^6 psi	26	23
LT	-	0 30	0 53	--	30	053
a_L	10^{-6} mm/mm/K	0 43	2 58	10^{-6} in/in/°F	24	1 5
a_T	10^{-6} mm/mm/K	29 2	3 96	10^{-6} in/in/°F	16 2	2 2
ϵ_{L1}^t	10^{-6} mm/mm	9800	8490	10^{-6} in/in	9800	8490
ϵ_{T1}^t	10^{-6} mm/mm	5000	7440	10^{-6} in/in	5000	7440
ϵ_{L2}^t	10^{-6} mm/mm	9800	8490	10^{-6} in/in	9800	8490
ϵ_{T2}^t	10^{-6} mm/mm	5000	7440	10^{-6} in/in	5000	7440
ϵ_{L1}^c	10^{-6} mm/mm	6200	5300	10^{-6} in/in	6200	5300
ϵ_{T1}^c	10^{-6} mm/mm	9900	5300	10^{-6} in/in	9900	5300
ϵ_{L2}^c	10^{-6} mm/mm	11200	10100	10^{-6} in/in	11200	10100
ϵ_{T2}^c	10^{-6} mm/mm	18400	9350	10^{-6} in/in	18400	9350
γ_{LT1}	10^{-6} mm/mm	10300	12780	10^{-6} in/in	10300	12780
γ_{LT2}	10^{-6} mm/mm	27500	32820	10^{-6} in/in	27500	32820
t	mm	0 127/0 191	0 356	in.	0050/ 0075	.0140
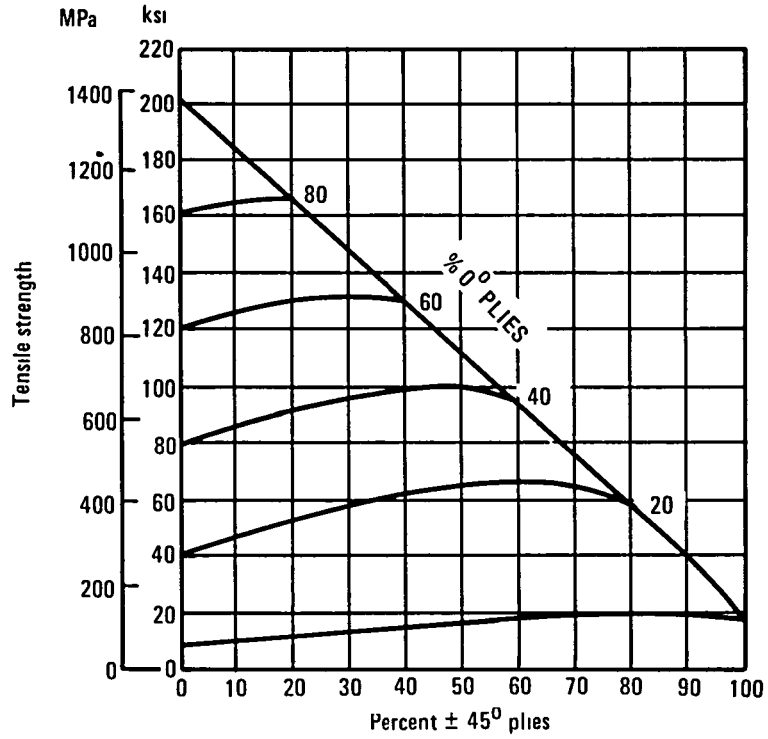
Figure 30. - Tape tension strength predictions - room
temperature dry, unnotched.
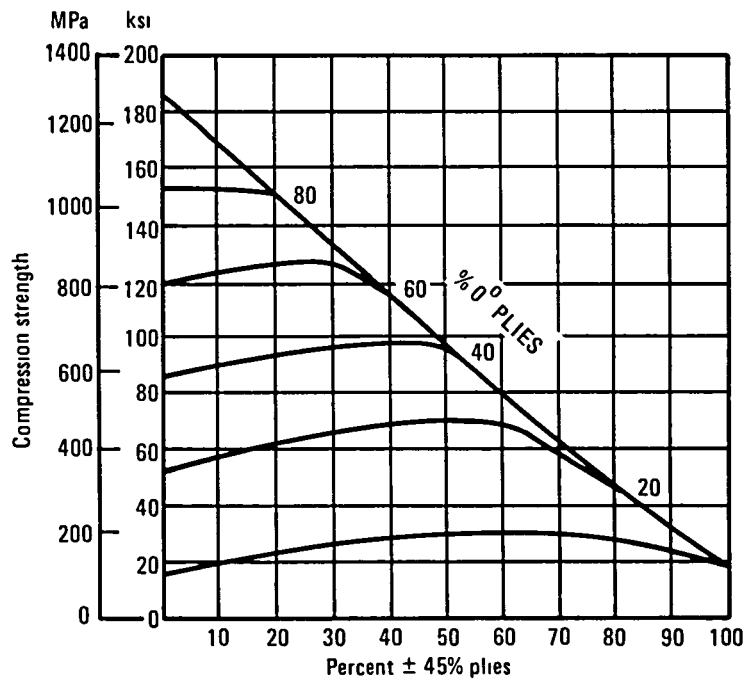
Figure 31. - Tape compression strength predictions - room
temperature dry, unnotched

56
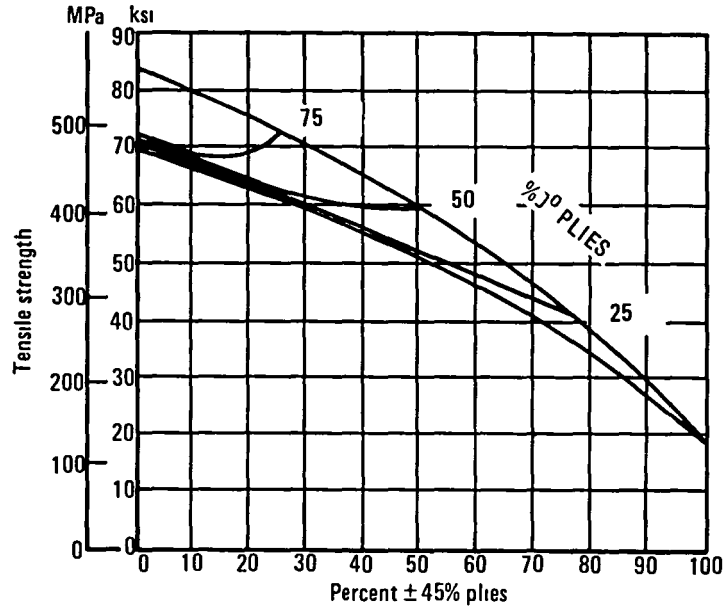
Figure 32. - Fabric tension strength predictions - room
temperature dry, unnotched.
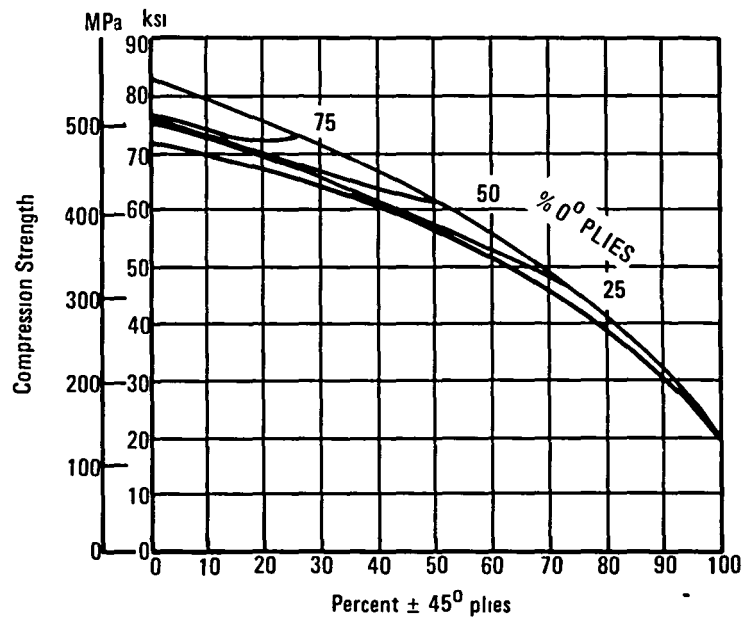
Figure 33. - Fabric compression strength predictions - room
temperature dry, unnotched.

The equation presented earlier was used to determine the allowable strength of a laminate for tension or compression loading. The values of K_{ET} and K_B are tabulated in table 18. Using these values, the $0°$ ply-level failures strains have been computed and are presented in table 20.

TABLE 20. - $0°$ PLY LEVEL FAILURE STRAINS FOR NOTCHED LAMINATES

Material	Loading	Failure Strain (10^{-6})		
		Condition		
		219K (-65°F) Dry	RT Dry	355K (180°F) Wet
Tape	Tension	4750	5050	5720
	Compression	8460	6870	6500
Fabric	Tension	3900	4420	4590
	Compression	6740	6240	4500

Note that the notched design allowables are based on notched strength where the notch is a 4.76mm (3/16 in) diameter hole. For a structure having holes greater than 4.76mm (3/16 in) diameter the tensile strength must be further reduced to account for the greater notch size. The curve presented in figure 34 should be used for this purpose. If the structure has a larger diameter hole than 4.76mm (3/16 in), then an additional factor, K_T, should be used to modify K_{ET}. This modification should be accomplished as follows:

$$K_{ET} \text{ large dia holes} = K_{ET} \times \frac{K_T \text{ for large dia}}{K_T \text{ for } 0.476 \text{ cm } (3/16 \text{ in}) \text{ dia}}$$

Advanced composite structures are vulnerable to impact damage. Coupon test data have indicated that impact damage which is not visible may seriously degrade the compressive strength of a laminate. Following the layup and cure of a composite part a nondestructive inspection is conducted. Generally, no additional nondestructive inspections are made while the structure is being assembled or while it is in service unless visual inspections indicate the existence of damage. Impact damage could occur to a composite structure during subassembly, assembly, or in service and not be detected.

Compression tests have been conducted on coupons containing both non-visible and visible impact damage. Some of these data are summarized in figure 35. Note that the failure strain for nonvisible impact damage is generally lower than previously reported for a laminate containing a 3/16 inch diameter hole. Thus to account for the effect of nonvisible impact damage on the compressive strength of a laminate, a maximum strain of 4000 micro mm/mm (in/in) will be used for all environmental conditions for both tape and fabric laminates.

58
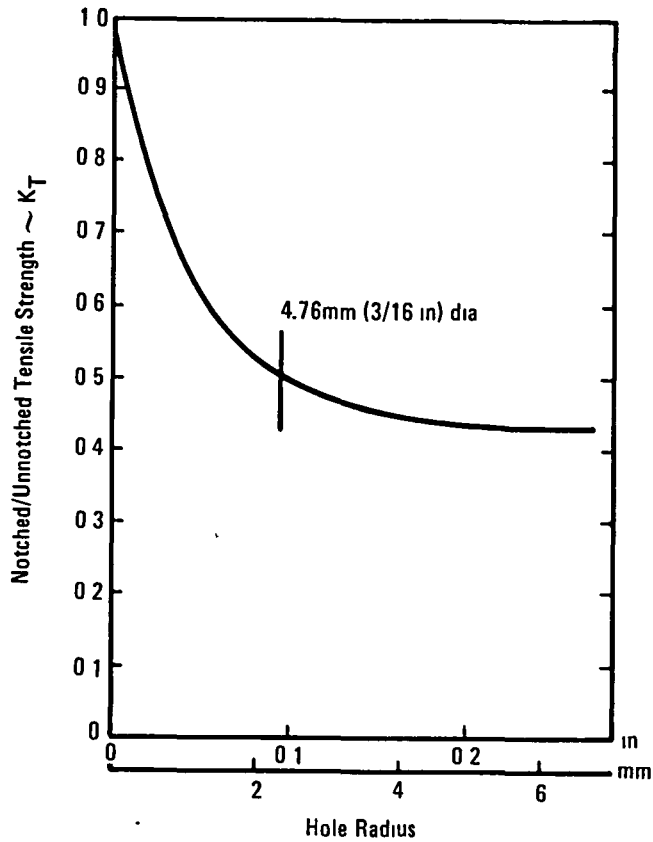
Figure 34. – Hole radius effects on tensile strength.
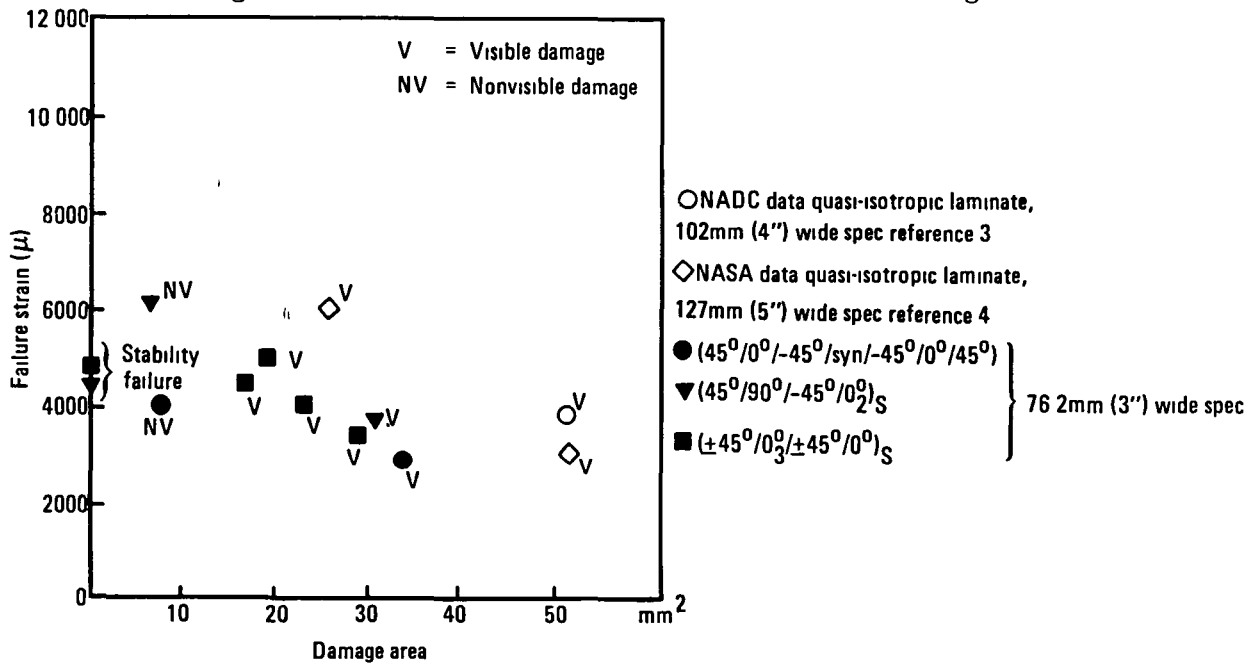
Figure 35. – Compression impact data.

For the aileron program the design allowables used for analysis reflect the worst environmental condition in combination with a 4.76mm (3/16 in) diameter notch (greater if required) or nonvisible impact damage. These allowables are conservatively used for all loading conditions irrespective of associated environmental conditions.

The allowable lamina level strains in the direction of the fiber for tape and fabric are shown in table 21. The carpet plots for tape and fabric graphite/epoxy based on lamina level strains are presented in figures 36 through 49. Note that these curves reflect the worst environmental condition in combination with a 4.76mm (3/16 in) notch for tension and assumed impact damage for compression. For shear loading or combined loading the strain allowables are to be used in the laminate strength computer program to predict an allowable strength.

TABLE 21. - ALLOWABLE LAMINA STRAINS

Material	0° Loading	Allowable Strain 10⁻⁶ mm/mm (in/in)
Tape	Tension	4750*
	Compression	-4000
Fabric	Tension	3900*
	Compression	-4000

4 76mm (*3/16 in) diameter notch or less

2.5 Bearing Strength and Push-Through Strength

The bearing tests are summarized in table 22. Tests included cylindrical bolt bearing (figures 50 and 51) and countersunk screw bearing (figure 52). The test specimens had an edge distance ratio of 5.3 to assure bearing failures rather than shear-out failures. The countersunk single lap shear bearing specimen was attached to an aluminum extruded channel to minimize the rotation of fastener and specimen due to the eccentric load for single shear. To prevent fastener failure a 1517 MP$_a$ (220 ksi) heat treated screw was used. The 4.76mm (3/16 in) diameter fasteners were installed with standard torques of 2.82N-m-3.39N-m (25-30 in-lb).

Tests were conducted for tape laminates, fabric laminates, and tape laminates cocured to a syntactic core for various combinations of 0°, ±45°, 90° plies. Tests included room temperature dry, 219K (-65°F) dry and 356K (180°F) wet environmental conditions which cover the extreme conditions applicable for the L-1011 aileron.

Table 22 gives the mean ultimate bearing strength for each test group along with the standard deviation. The bearing strength was determined from the ultimate load recorded during test divided by the nominal bearing area.

60
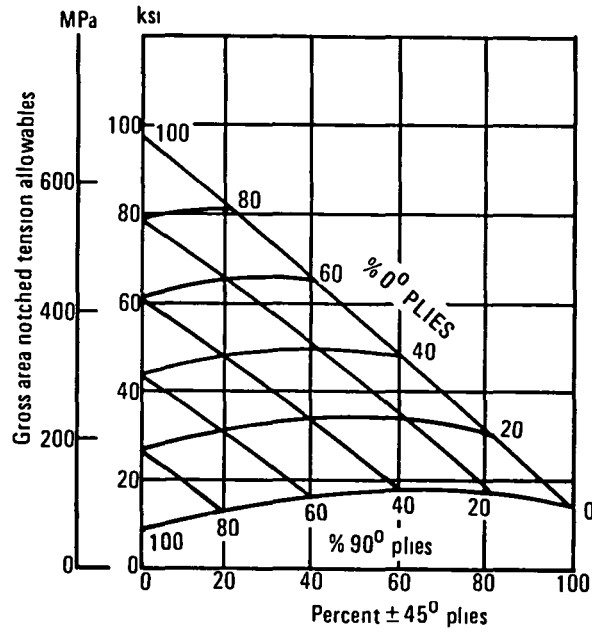
Figure 36. – T300/5208 unidirectional tape tensile strength
design allowables, notched.
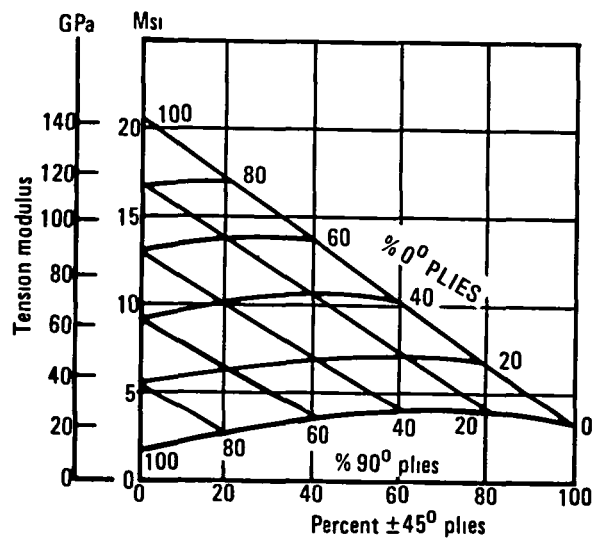
Figure 37. – T300/5208 unidirectional tape tensile modulus.
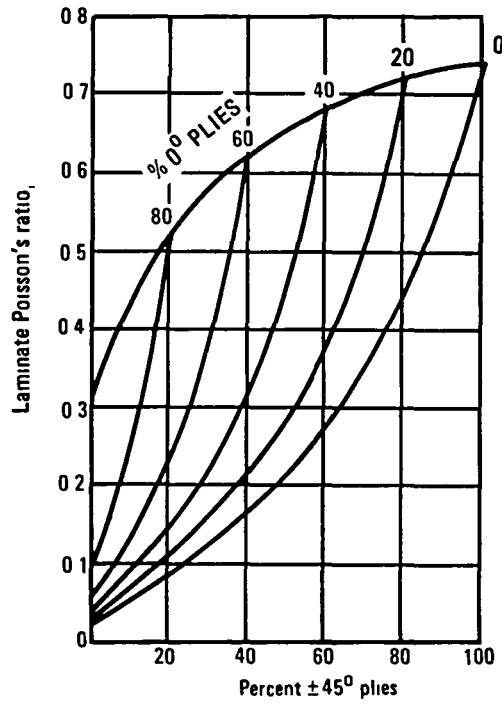
Figure 38. - T300/5208 unidirectional tape Poission's ratio.
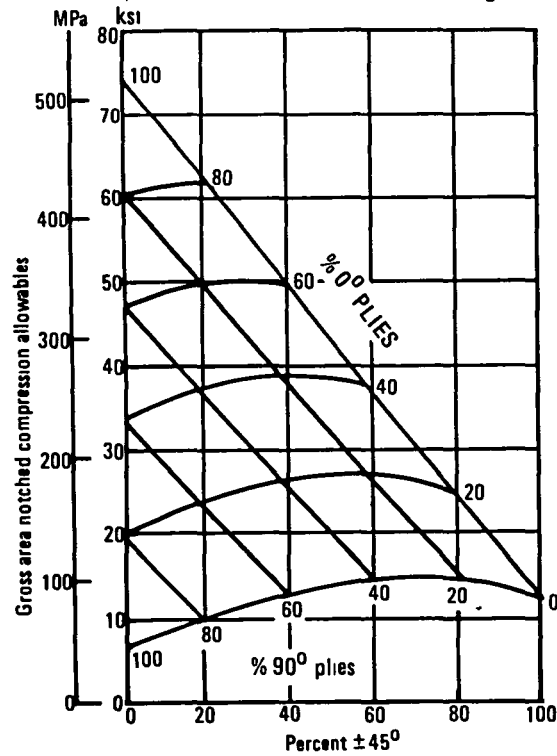
Figure 39. - T300/5208 unidirectional tape compression
strength design allowables, impacted
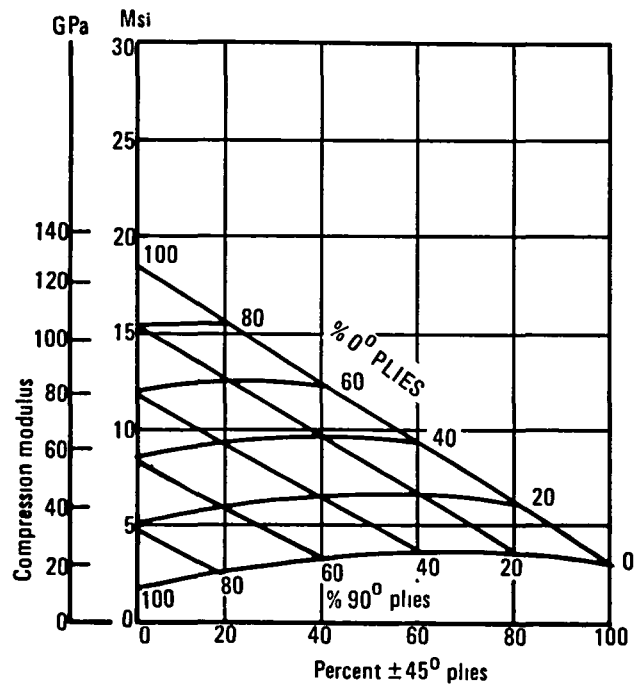
Figure 40. - T300/5208 unidirectional tape compression modulus.
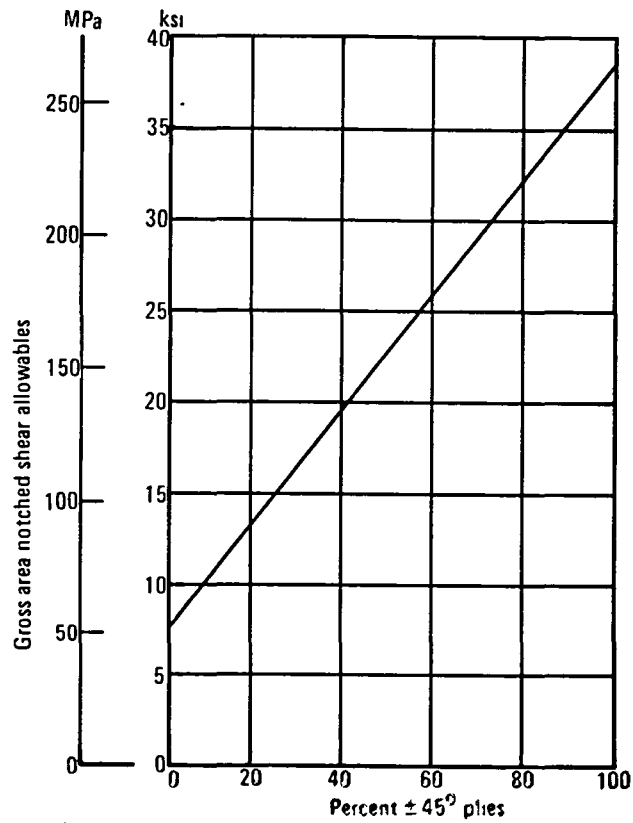
Figure 41. - T300/5208 unidirectional tape inplane shear
strength design allowables

63
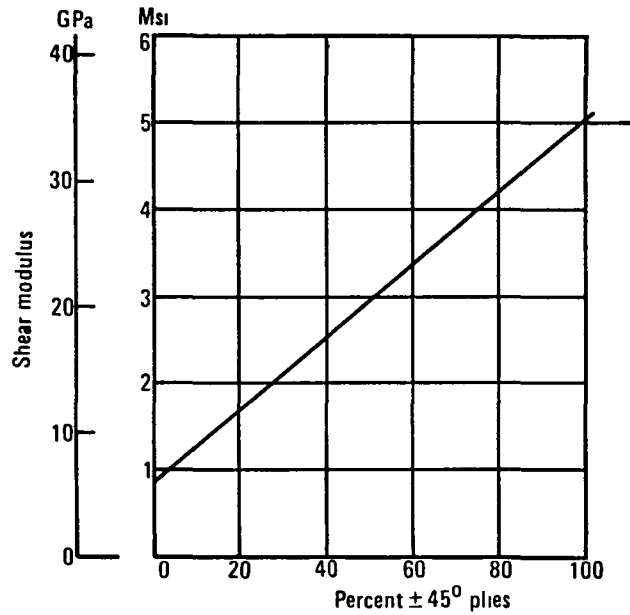
Figure 42. - T300/5208 unidirectional tape inplane shear modulus.
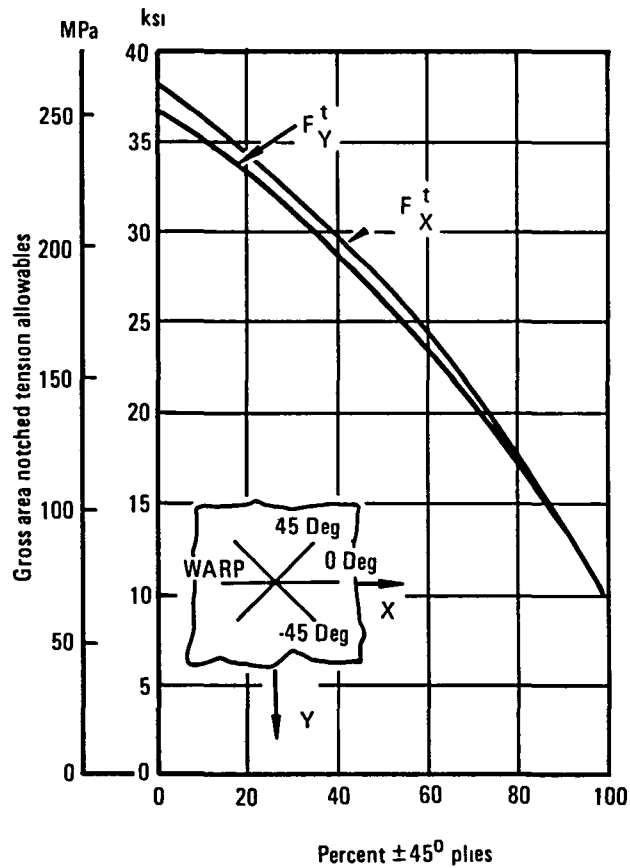
Figure 43. - T300/5208 bidirectional fabric tensile strength
design allowables, notched.

64
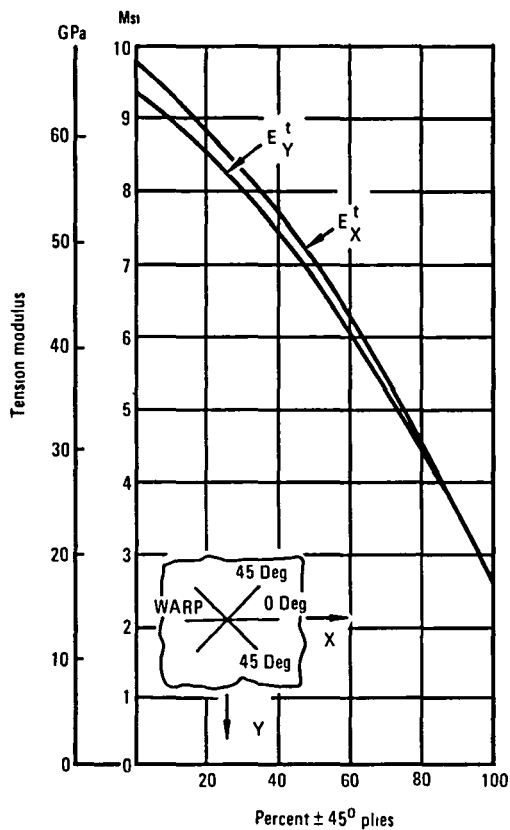
Figure 44. - T300/5208 bidirectional fabric tensile modulus.
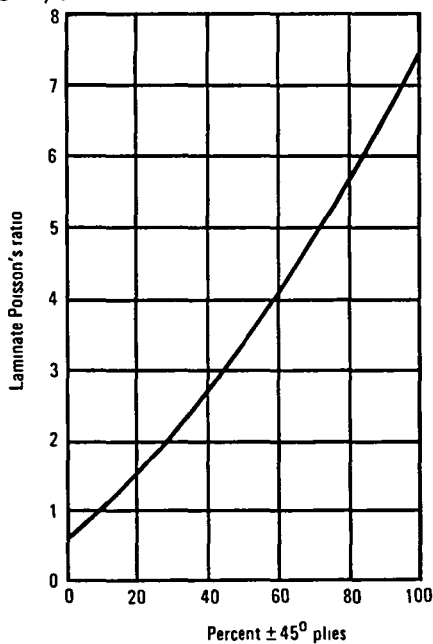
Figure 45. - T300/5208 bidirectional fabric Poisson's ratio
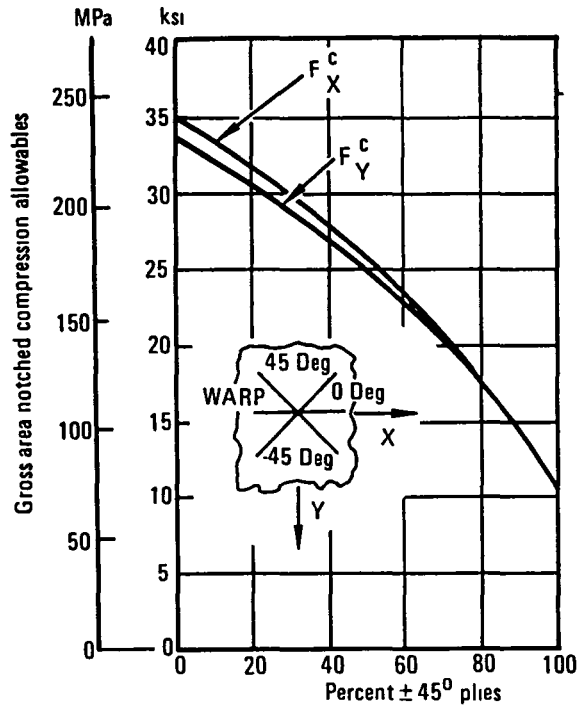
Figure 46. - T300/5208 bidirectional fabric compression strength
design allowables, impacted.
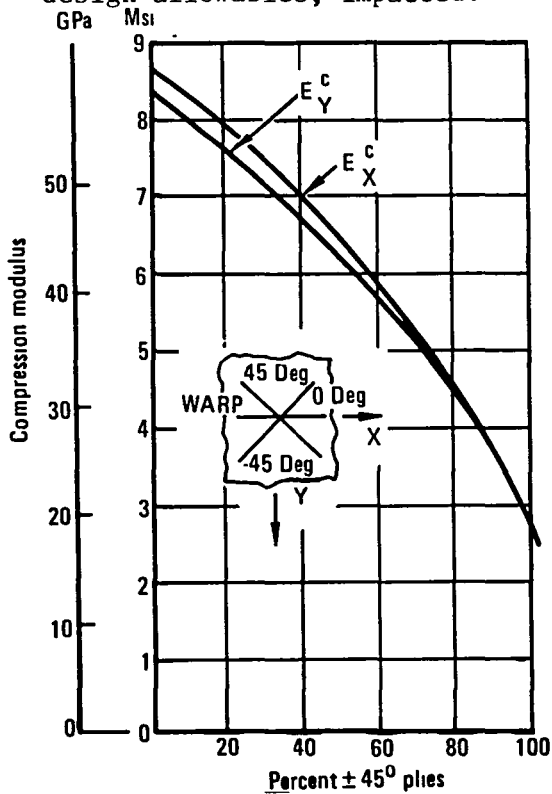
Figure 47. - T300/5208 bidirectional fabric compression modulus.
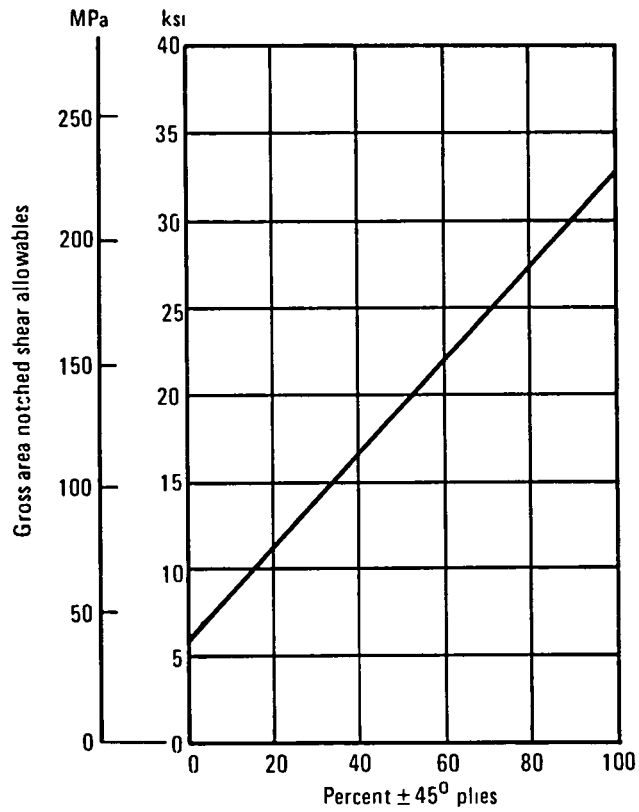
Figure 48. - T300/5208 bidirectional fabric inplane shear
strength design allowables.
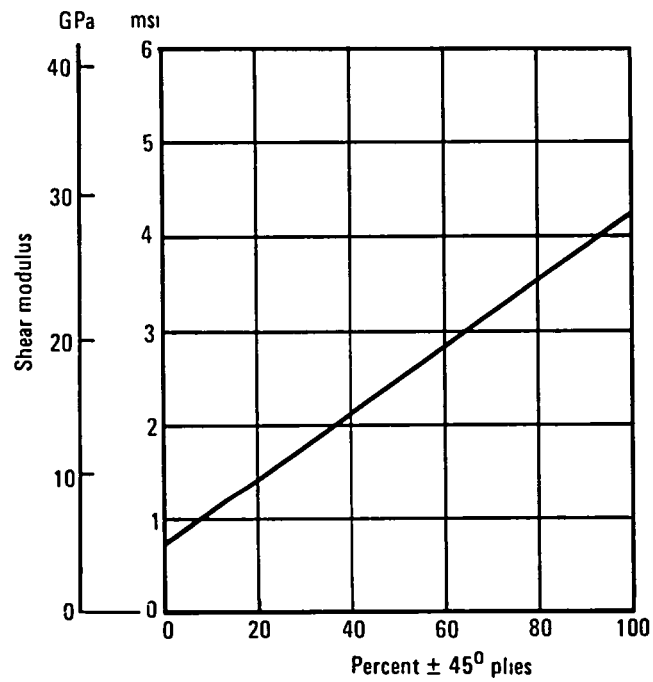
Figure 49. - T300/5208 bidirectional fabric inplane shear modulus.

TABLE 22. – SUMMARY OF BEARING TEST DATA FOR GRAPHITE/EPOXY LAMINATES

Percent 0°/±45°/90°	Thickness		⑤ Type	Condition	No. of Tests	Load Direction	Mean Ultimate Bearing Stress		Standard Deviation		$\frac{P_{PL}}{P_{BRU}}$ ④	Comments
	mm	in					MPa	ksi	MPa	ksi		
0/50/50	3 175	123	DB	RTD	5	90°	934	135 4	60 7	8 81	0 69	0.13 mm (5 Mil) Tape Laminates
0/50/50	3 150	126	SB	RTD	5	90°	650	94 3	24.3	3.53	0 68	
0/90/10	2 642	104	DB	RTD	5	90°	1163	168 7	38 1	5 53	0.67	0.13 mm (5 Mil) Tape Laminates
0/90/10	2 616	103	SB	RTD	5	90°	820	118 9	29 0	4 20	0 79	
25/50/25	2 134	084	DB	RTD	5	0°	1129	163 8	34 0	4 93	0 79	0 13 mm (5 Mil) Tape Laminates
25/50/25	2 134	084	SB	RTD	5	0°	849	121 1	43.4	6 29	0 83	
56/44/0	1 648	183	DB	RTD	5	0°.	1049	152 1	14.1	2 05	0 71	0 13 mm (5 Mil) Tape Laminates
56/44/0	4 597	181	SB	RTD	5	0°	651	94 4	40 3	5 84	0 75	
50/50/0	3 100	122	DL	RTD	5	0°	1149	166 6	30 3	4 39	0.74	0 13 mm (5 Mil) Tape Laminates
50/50/0	3 100	122	SB	RTD	5	0°	848	123 0	24 4	3 54	0 72	
50/50/0	3 100	122	DL	RTD	3	0°	1216	176 3	73 6	10 68	0 79	① 0.13 mm (5 Mil) Tape Laminates
50/50/0	3 073	121	DL	RTD	3	0°	1203	174 5	29 9	4 34	0 73	② 0 13 mm (5 Mil) Tape Laminates
40/40/20	2 159	085	DB	RTD	4	0°	994	144 1	22 3	3 23	0 68	0.19 mm (7 5 Mil) Tape Laminates
40/40/20	2 083	082	DB	355K (180°F) Wet	3	0°	856	124 1	5 7	0 83	0 72	
40/40/20	2 070	085	DB	219K (-65°F) Dry	3	0°	1473	213 6	28 6	4 15	0 68	
40/60/0	1 956	077	DB	RTD	3	0°	868	125 9	14 3	2 07	0 70	Fabric Laminates
40/60/0	1 956	077	DB	355K (180°F) Wet	3	0°	796	115 5	8 7	1 26	0 83	
40/60/0	1 956	077	DB	219K (-65°F) Dry	3	0°	1063	154 2	53 0	7 69	0 76	
33/67/0 ③	1 219	048	DB	RTD	3	0°	1051	152 4	44 2	6 41	0 70	3 Plies of 0.19 mm (7.5 Mil) Tape on Each Side of Syntactic Core
33/67/0	1 219	048	DB	355K (180°F) Wet	3	0°	858	124 5	79 9	11 59	0 75	
33/66/0	1 219	048	DB	219K (-65°F) Dry	3	0°	1334	193 5	126 5	18 35	0 76	

① Bearing Holes drilled at 4° angle
② Bearing Holes drilled w/o back-up
③ Thickness does not include 0.95 mm (.0375 in) syntactic core
④ Proportional limit load divided by bearing ultimate load
⑤ DB = Fig 50, SB = Fig 52, DL = Fig 51

143
(5 63)

25.4
(1 00)

57
(2.25)

4.0
(5/32 in) rivets

16 (0 63)

4 0 (1.56)

9.5 (0.38)

Double lap shear
coupon

32 (1 25)

1 3
(0 50)

4 76 (3/16 in) HLT 318 bolt and collar
(1100 MPa (160 ksi) material)

4 Sheets of 3 2 (0 125) aluminum

Dimensions in mm (in)
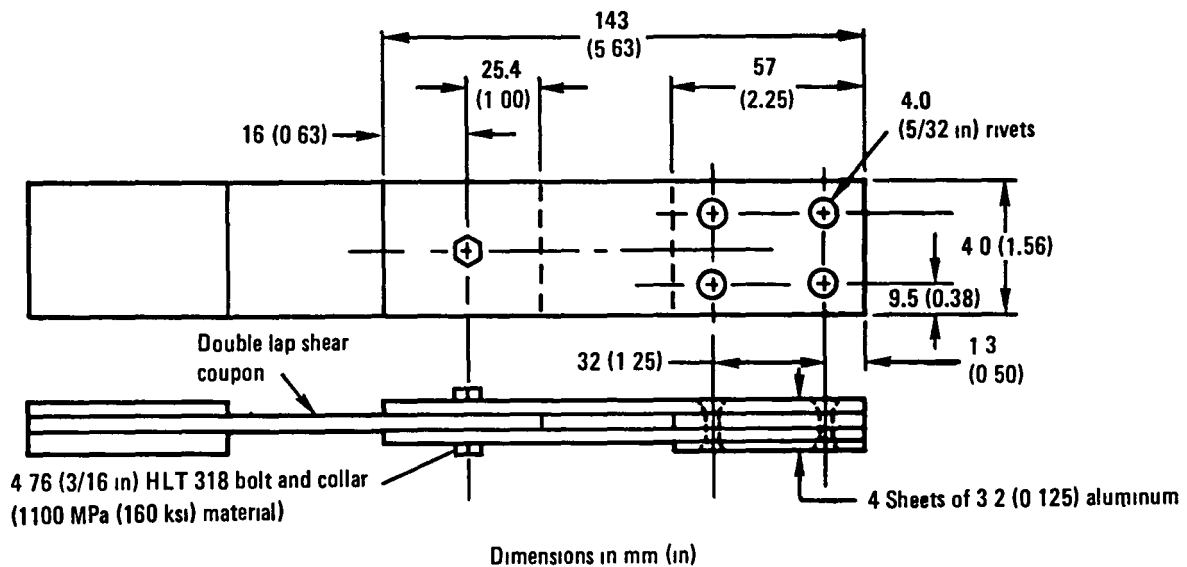
Figure 50. - Double lap cylindrical shear bearing specimen - single bolt.

The proportional limit load was determined from the autographic load-deflection curves for each specimen and divided by the ultimate load to obtain the (P_{PL}/P_{BRU}) ratios given in table 22. The proportional limit load is the maximum load that can be applied without causing permanent deformation in the bearing area of the composite material. In all cases, the proportional limit load was at least 2/3 of the ultimate bearing load.

The effect of manufacturing errors on the cylindrical bearing strength was evaluated for a hole drilled slightly oversize 5.05 - 5.13 mm (0.199 - 0.202 in) at an angle of 0.07 radians (4 degrees) off the perpendicular to the load direction and for a hand drilled hole without using a backup for a (50/50/0 percent) tape laminate. The results indicate no detrimental effect of the manufacturing errors on the bearing ultimate strength.

Push-through tests were conducted to evaluate the effect of fastener head configuration on out-of-plane load capacity of typical composite joints. The test technique, shown in figure 53, measures the load required to push the fastener head through the composite material. The test results are summarized in table 23. The aileron cover tests showed that loads obtained from push-through tests were equivalent to the loads obtained from pull-through tests; so only push-through data are reported here.
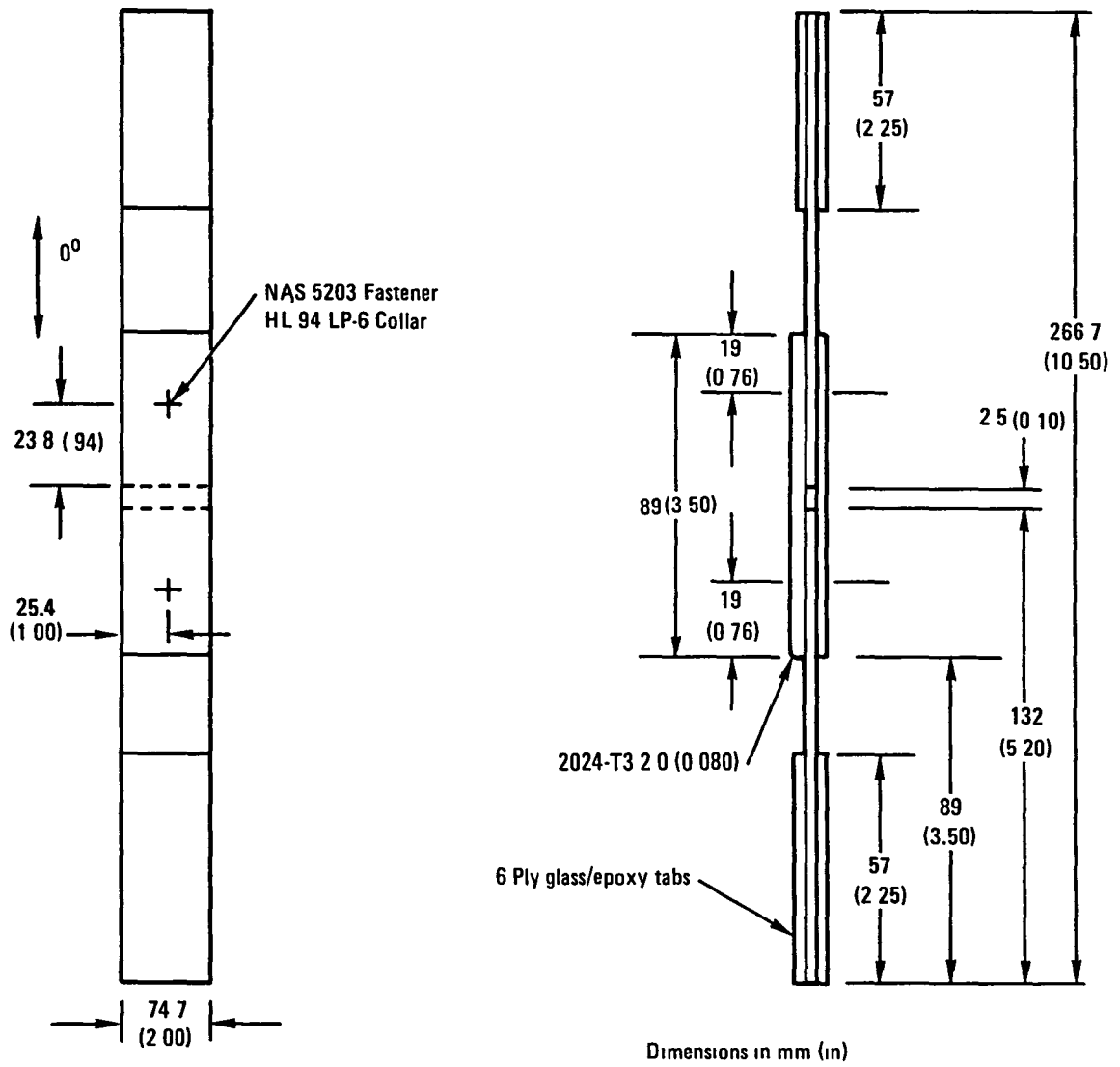
Figure 51. – Double lap cylindrical shear bearing specimen.

25 4
(1 00)

Aluminum extruded
channel

Single lap shear
coupon

Aluminum test
fixture

4.76mm (3/16 in) HLT 349 Fastener and collar
(1517 MPa (220 ksi) material)
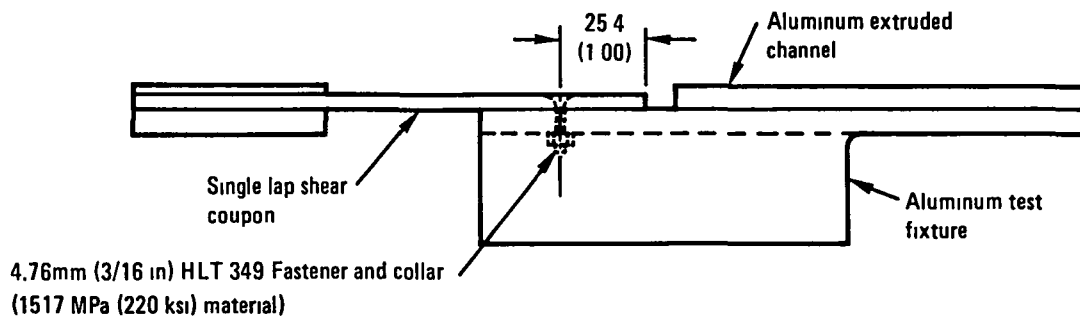
Figure 52. – Single lap screw shear bearing specimen.
(all dimensions in mm (in))

Composite
laminate

Push
rod

Edge
support
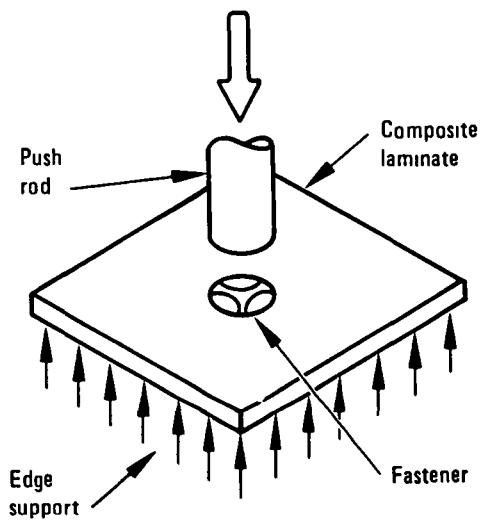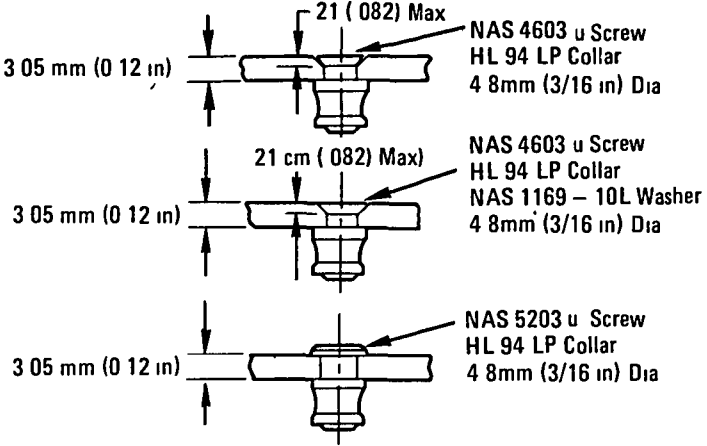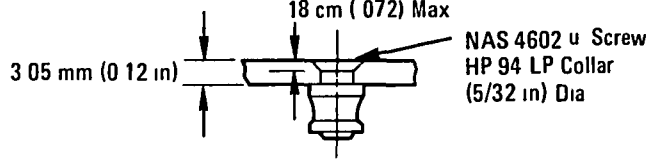
Fastener

Figure 53. – Push-thru specimen.

TABLE 23. – FASTENER PUSH–THRU TEST RESULTS

Type of Material	Type of Fastener	Load Deflection Characteristics	Initial Failure Load		Final Failure Load	
			N	(LB)	N	(LB)
Thornel 300/5208 Quasi-Isotropic Graphite/Epoxy Laminate $(0^0/45^0/90^0/-45^0)$ 3S	3 05 mm (0 12 in) — 21 (082) Max — NAS 4603 u Screw / HL 94 LP Collar / 4 8mm (3/16 in) Dia		2456 3311 2670	(552) (744) (600)	4486 4558 3791	(1008) (1049) (852)
			2812	(632) Ave	4316	(970) Ave
	3 05 mm (0 12 in) — 21 cm (082) Max) — NAS 4603 u Screw / HL 94 LP Collar / NAS 1169 – 10L Washer / 4 8mm (3/16 in) Dia	Figure 54a	5171 5999 4935	(1162) (1348) (1109)	6995 7102 6813	(1572) (1596) (1531)
			5367	(1206) Ave	6959	(1566) Ave
	3 05 mm (0 12 in) — NAS 5203 u Screw / HL 94 LP Collar / 4 8mm (3/16 in) Dia		4379 5287 5767	(984) (1188) (1296)	6065 6141 6141	(1363) (1380) (1380)
			5114	(1156) Ave	6114	(1374) Ave
Cover at Aileron Rib $(45^0_T\ 0^0_T\ 135^0_T$ SYN $135^0_T\ 0^0_T\ 45^0_{2T}\ 90^0_T$ $135^0_T\ 90^0_F)$ T300/5208 Graphite/Epoxy	3 05 mm (0 12 in) — 18 cm (072) Max — NAS 4602 u Screw / HP 94 LP Collar / (5/32 in) Dia	Figure 54b	1868 1841 1886 1944	(420) (414) (424) (437)	1815 1788 1859 1753	(408) (402) (418) (394)
			1886	(424) Ave	1806	(406) Ave

Three types of 4.76 mm (3/16 in) diameter fastener configurations (countersunk screw, pan head screw and countersunk screw with a dimpled washer) were investigated for push-through strength of the solid laminate material. Only the 3.97 mm (5/32 in) diameter countersunk screw configuration was tested for the aileron cover material. For each specimen, the fastener and collar was installed with sufficient torque to shear off the external wrenching portion of the collar.

The push-through specimens were tested statically to failure at a deflection rate of 1.4 mm/minute (0.050 in/minute). The load-deflection characteristics of each specimen was similar. Typical load-deflection curves are shown in figure 54.

The load deflection curves for the solid laminates exhibited a bimodal failure characteristic, as shown in figure 54(a). The initial failure was a localized crushing of the laminate under the head of the laminate followed by a final shear-out failure of the composite material around the periphery of the fastener head. The average value of the initial failure was from 65 percent to 84 percent of the final failure as shown in table 23. The combination of a countersunk fastener with a dimpled washer yielded the greatest push-through capability.

For the aileron cover material, the initial failure load was higher than the final failure load as shown in table 23 and figure 54(b). The initial failure was again due to localized crushing of the material and the final failure, a shear tear-out failure. However, the shear tear-out failure exhibited a lower strength than the initial crushing failure. This is due to the presence of the syntactic core. The countersunk depth extends through the 3 outer plies and into the syntactic core. Therefore, the outer plies plus the syntactic core ($\sim$ 1.52 mm (0.060 in.) thickness) cannot be counted on to contribute much to the shear tear-out strength.

a) Laminate tests   b) Cover tests
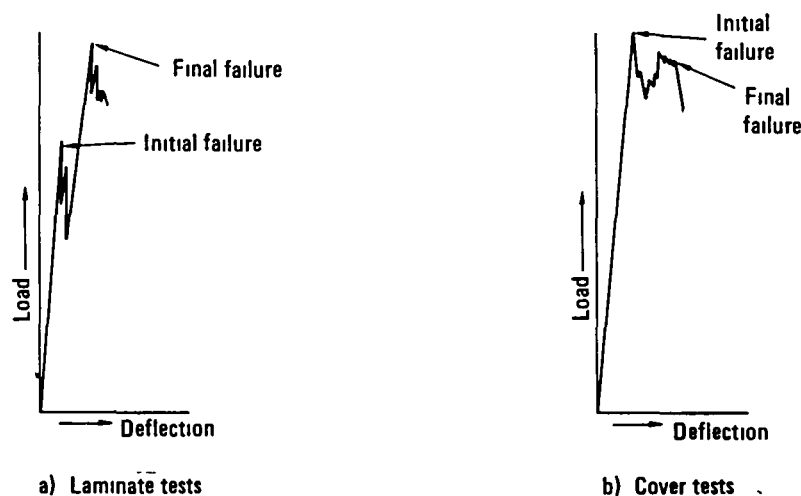
Figure 54. - Load deflection behavior for push-through tests.

3. PROCESS DEVELOPMENT AND PROCESS VERIFICATION

The Avco effort in Task II consisted of developing the manufacturing processes necessary to produce the composite parts required for the fabrication of the advanced composite inboard aileron for the L-1011 aircraft and the fabrication of the concept verification specimens and test assemblies.

The major emphasis in developing the processes and tooling for this program was low cost manufacturing. This effort included making as many of the processing elements as possible common for each type of component; i.e., covers, ribs and spars. The prime processing elements evaluated were cure cycle, damming, and bleeding and breathing. Prior to the initiation of process development, a tool evaluation program was conducted for determining the basic tool concept (male or female) for cure of the channel shaped members. In addition, it was necessary to develop a production oriented drilling and countersink system for graphite which would facilitate the assembly of the aileron. An integral part of this task was to develop procedures for shop and field type repairs. The flow chart of figure 55 outlines the effort expended in the development requirements for this program.

3.1 Tool Development

In conjunction with the initial process development effort, it was necessary to evaluate male and female tooling concepts to determine the most effective tool for flanged parts. In order to accomplish this task, one male and one female cure tool was fabricated to evaluate the following layups:

1. Intermediate and closeout rib, 5 ply graphite fabric

2. Main rib, 4 ply graphite fabric with a 5 ply graphite tape internal doubler in the flanges

3. Spar, 10 ply graphite tape

Effectiveness of the tools was evaluated for dimensional stability, tool cost, part manufacturing and cost, and physical and mechanical property stability. To evaluate the dimensional repeatability of the cured parts, a check fixture was fabricated to measure the outside dimensions. This fixture is shown in figure 56. Fifteen (15) layups were made on the male tool, and eleven (11) on the female tool. A summary of the dimensional data of these parts is shown in table 24. The data shown summarize the dimensional variation on all parts, taken at seventeen (17) locations on each part.
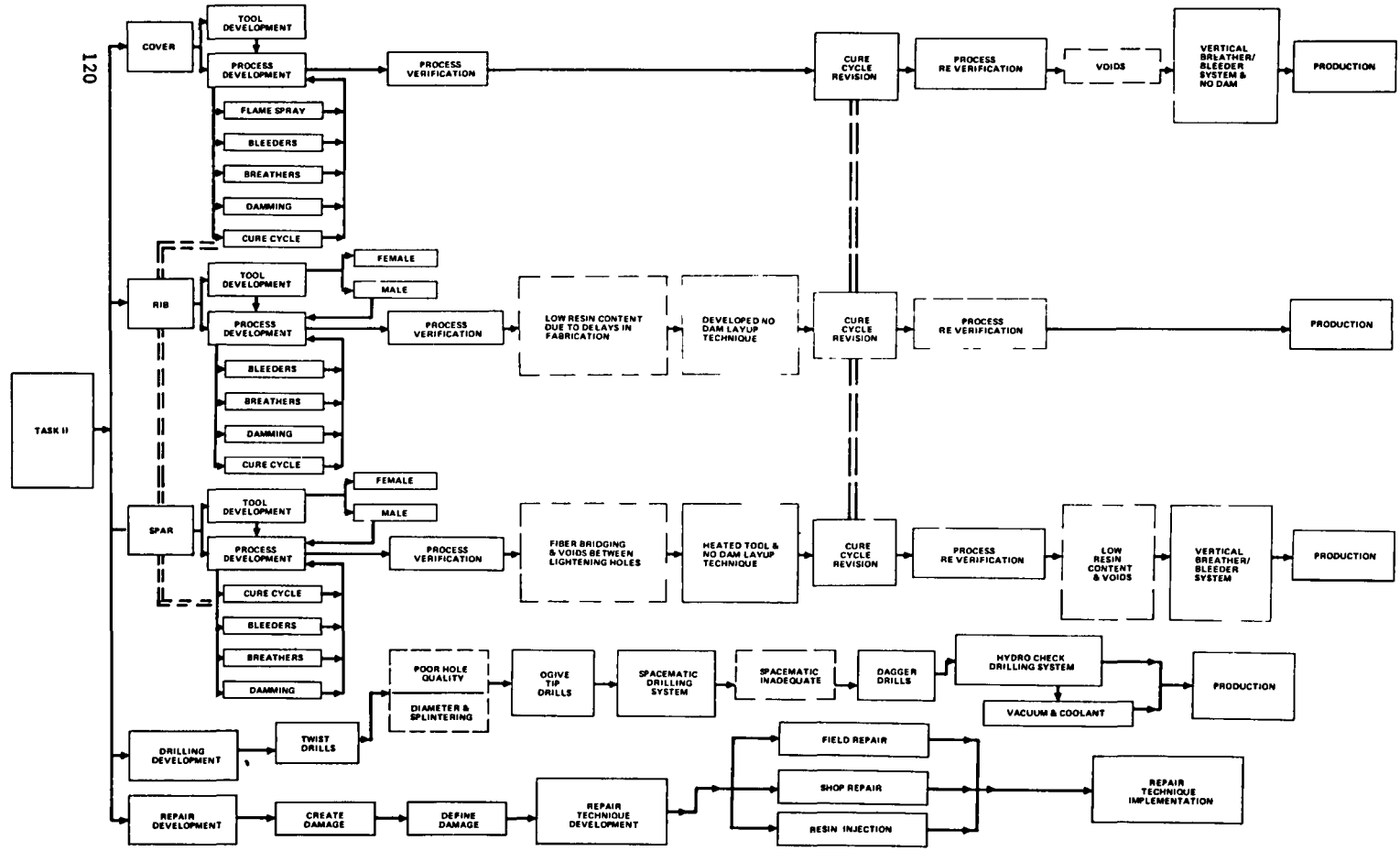
Figure 55. – Task II Process development requirements – flow chart.

Figure 56. - Rib dimensional check fixture.

TABLE 24. - SUMMARY OF DIMENSIONAL DATA FOR MALE
AND FEMALE TOOL CURED COMPONENTS

Material Configuration	Part Configuration	Cure Tool	No. Tested	External Size Variance mm (in)	Flange Thick. Variance mm (in)	Flange Angle Closed
5 Plies Fabric (F) $(45^0/90^0/135^0/90^0/45^0)$	Intermediate Rib	Male	6	0.356 (0.014)	0.254 (0.010)	2^0
		Female	4	0.762 (0.030)	0.051 (0.002)	2^0
4 Plies Fabric plus 5 Plies Tape (T) - Cap $(45^0{}_F/90^0{}_F/0^0{}_{5T}/90^0{}_F/45^0{}_F)$	Main Rib	Male	5	0.483 (0.019)	0.229 (0.009)	2^0
		Female	4	1.524 (0.060)	0.152 (0.006)	2^0
10 Plies Tape $(45^0/0^0/135^0/0^0/90^0)_S$	Front Spar	Male	4	0.406 (0.016)	0.330 (0.013)	1^0
		Female	3	0.203 (0.008)	0.381 (0.015)	1^0

76

The layup procedure for fabricating these parts was as follows:

Male tool layup procedure:

1. Using a shop knife, trim the graphite plies in a flat pattern to a template.

2. Layup on the form block/cure tool, hand form the flanges and flanged lightening holes during layup.

3. Bag and cure part.

Female tool layup procedure:

1. Using a shop knife, trim the graphite plies in a flat pattern to a template.

2. Layup on the elastomeric rubber form block, hand form the flanges and flanged lightening holes during layup.

3. Place form block and layup in female tool and assemble sides of tool.

4. Bag and cure part.

The tooling requirements using the male tool concept consist of a trim template and a one-piece layup/cure block. The female tool concept requires a trim template, a elastromeric rubber form block, and a multipart cure tool. It is readily recognized that tool cost for the male tool concept is less than for the female tool.

Layup cost for the parts made on the male tool is less than the female tool parts since tool cleanup is less for a one-piece tool, and the tool does not require disassembly and reassembly for each part made.

During tool evaluation, difficulty was experienced in maintaining the seals on the female tool which resulted in excessive resin bleeding from the part during cure. This inconsistency resulted in unacceptable resin content variations which would require additional costly tool development.

Analysis of the detail data summarized in table 32 showed that the male tools produce intermediate and closeout ribs, main ribs, and spars of the required dimensional consistency. This, coupled with the lower tooling and layup cost when using male tools, resulted in the decision to use male tools for all channel shaped parts.

3.2 Process Development

In developing the manufacturing processes, it was necessary to evaluate independently the bleeder/breather, cure cycle and damming for each part and material configuration. The graphite fabric prepreg had a resin content of 41 ± 3%. The graphite tape prepreg had a resin content of 34 ±3%. The developed processes required that the properties of the cured composite details meet the requirements of table 25. While this is not considered a no-bleed system, it was lower in resin content than most systems in use when this program was initiated, since the cured fabric components have a nominal of 9% resin removed and the graphite tape has a nominal of 5% resin removed during cure. The major problem that had to be overcome during the process development was to permit the breathing off of the entrapped air and volatiles while controlling the flow of the low viscosity resin during cure.

3.3 Cover Development

The process options for development of the cover consisted of prebleed or normal bleed.

The prebleed investigation was necessary since the cover design required a syntactic sandwich which might have an aluminum flame spray on one surface. Since it is more economical to cocure the flame spray with the sandwich panel, and since the flame spray prevented any bleeding during the cure operation,

TABLE 25. – PHYSICAL AND MECHANICAL PROPERTY REQUIREMENTS
FOR ACA COMPOSITE PARTS

Part Identity	Specimen Location	Resin Content %	Void Content %	Thickness mm (in)	Short Beam Shear — MPa (psi)	
					RT, Dry	355 4K(180°F), Wet**
Cover	Basic*	26 - 32	1 0 Max.	1.918-2 319 (0 0755-0 0913)	20 68 (3,000)	20.68 (3,000)
	Doubler	26 - 32	1.0 Max	2 797-3 338 (0 1101-0.1314)	34 47 (5,000)	34 47 (5,000)
Spar	Web & Cap	26 - 32	1 0 Max	1.778-2.108 (0 070-0 083)	48.26 (7,000)	41.37 (6,000)
Intermediate & Closeout Rib	Web & Cap	29 - 35	1 0 Max	1 537-1.943 (0 0605-0 0765)	51 71 (7,500)	41 37 (6,000)
Main Rib	Web	29 - 35	1.0 Max.	1 229-1.554 (0.0484-0.0612)	41 37 (6,000)	41 37 (6,000)
	Cap	28 - 34	1.0 Max	2 118-2 609 (0 0834-0.1027)	41 37 (6,000)	37.92 (5,500)

*Basic cover sandwich
**2 hour water boil

prebleed of the graphite epoxy tape was investigated. It was determined during this effort that using the low resin content (34% ±3%) prepreg tape and the minimum bleed cycle obtainable, resulted in excessive and erratic bleed. Results of tests on these cover prebled panels are shown in table 26.

Other cover panels were prepared without prebleed, but with cocured flame spray and flame spray after curing. Both methods resulted in good resin content and short beam shear properties. Test results of these panels are shown in table 27.

TABLE 26. - PREBLEED COVER PANELS TEST DATA

Specimen No	Laminate Configuration	Prepreg Resin %	Prebleed Resin %	Cured Resin %	Short Beam Shear		Flame Spray
					MPa	psi	
C-4 1-1	Basic Cover 3T/SYN/3T	32 3	26 7	26 99	–	–	Before Cure
C-4.1-2	Basic Cover 3T/SYN/3T	32.3	25 4	23 79	19 77	2,867	Before Cure
C-4.1-3	Basic Cover 3T/SYN/3T	32.3	25 9	25 47	18 17	2,635	Before Cure

TABLE 27. - COCURED BASIC COVER PANELS TEST DATA

Specimen No	Prepreg Resin %	Bagging Method	Cured Resin %	Short Beam Shear MPa (psi)	Thickness mm (in)	Flame Spray
C-4 1-4	32 3	A,B,G,C, G,B,E,F	27 97 (T) 27.91 (B)	23.10 (3351)	2 159/2 311 (0 085/0 091)	After Cure
C-4 1-5	32.3	A,B,G,C, G,B,E,F	29 55 (T) 27 72 (B)	22 41 (3250)	2.184/2 337 (0 086/0 092)	After Cure
C-4 1-6	32 3	A,B,G,C, G B E F	28 43 (T) 28 50 (B)	22 45 (3256)	2 057/2 286 (0 081/0 090)	After Cure
C-4.1-7	32.3	A,J,H,C, G,B,E,F	35 15 (T)* 32 35 (B)*	23.08 (3347)	2.388/2.464 (0 094/0 097)	Before Cure
C-4 1-8	32.3	A,J,H,C, G,B,E,F	31.69 (T) 30 02 (B)	22.71 (3294)	2.362/2.464 (0 093/0 097)	Before Cure

LEGEND
A Tool
B. Tedlar (Solid)
C. Graphite Composite
E. 1-Ply Bleeder (Lease Zero P2)
F. Vacuum Bag

G. Peel Ply
H 1-Ply Fiberglass 120
J Flame Spray

(T) Tool Side
(B) Bag Side

*Data inaccurate due to glass and flamespray in layup

79

The flame spray was applied to these panels prior to cure or after cure. Both methods of flame spray application gave good results from an appearance, adherence, and surface finish standpoint.

The aileron cover design has integral doublers which for economic reasons it is desirable to be cocured with the panels. During layup of the above panels, the doublers were added. These doublers 3-ply (45°/0°/135°) and 5 ply (0°) were cocured with the panels and exhibited minimal washout. Caul sheets were not used; however, the bleeder (Lease Zero P-2) was manually compressed at the edge of the doublers which resulted in washout control.

During this phase of the development, it was determined that aluminum flame spray would not be required on the covers for lightning protection; as a result, the development for flame sprayed cover panels was discontinued.

Two cover panels were laid up with a bleeder/breather arrangement shown in figure 57 with care taken to maintain a good vacuum path between the peel ply layers, the bleeder (Lease Zero P-2), the glass breather and the vacuum source. The cure cycle used during this effort is shown in figure 58.

The results of the resin and void content checks for the panels are shown in table 28. As a result of the good resin and low void content exhibited by these panels, it was decied to fabricate the process verification test panels.

Two process verification covers (one upper and one lower) were laid up in accordance with figure 57 and cured using the cure cycle shown in figure 58. The physical and mechanical properties of these covers and process control coupons are shown in table 29. In addition, table 29 shows the properties of the process control coupon for the concept verification test cover. It should be noted that the values shown are an average of a minimum of three specimens cut from different areas of the cover. The data indicate that the resin content of the cover typically is approximately 2% higher than the process control coupon. This is attributed to more resin edge bleed on the process control coupon since the periphery is much larger proportionally to the enclosed area. It should be noted that all specimens were well within the specification requirements.

As a result of excessive porosity in some parts during the production of the ribs and spars, the cure cycle was revised to be more tolerant of the production environment. Concurrent with this development, Lockheed conducted computer analysis of the cure cycle on viscosity and percent gel. From these data, it was determined that it was likely that with the current cure cycle, the autoclave pressure could be applied after the resin had passed the 80% gel point. If this were to happen, the incident of voids would be greatly increased. Investigation of a revised cure cycle was conducted which increased the dwell time and added pressure earlier during the dwell portion of the cure cycle. Figure 59 defines this revised cure cycle which is more tolerant of such variables as heatup rates, moisture in the prepreg and temperature differentials between parts in the same autoclave load. As a result of this

80

Composite cover
layup

Corprene dam

Fiberglass cloth

Bag sealer

Nylon vacuum bag

Airweave FR (2 plies)

Tedlar (Solid)

Bleeder — zero P-2

Tedlar (slit at corners)

Peel ply (2 plies)

Tedlar (solid)

Peel ply (2 plies)

Tool
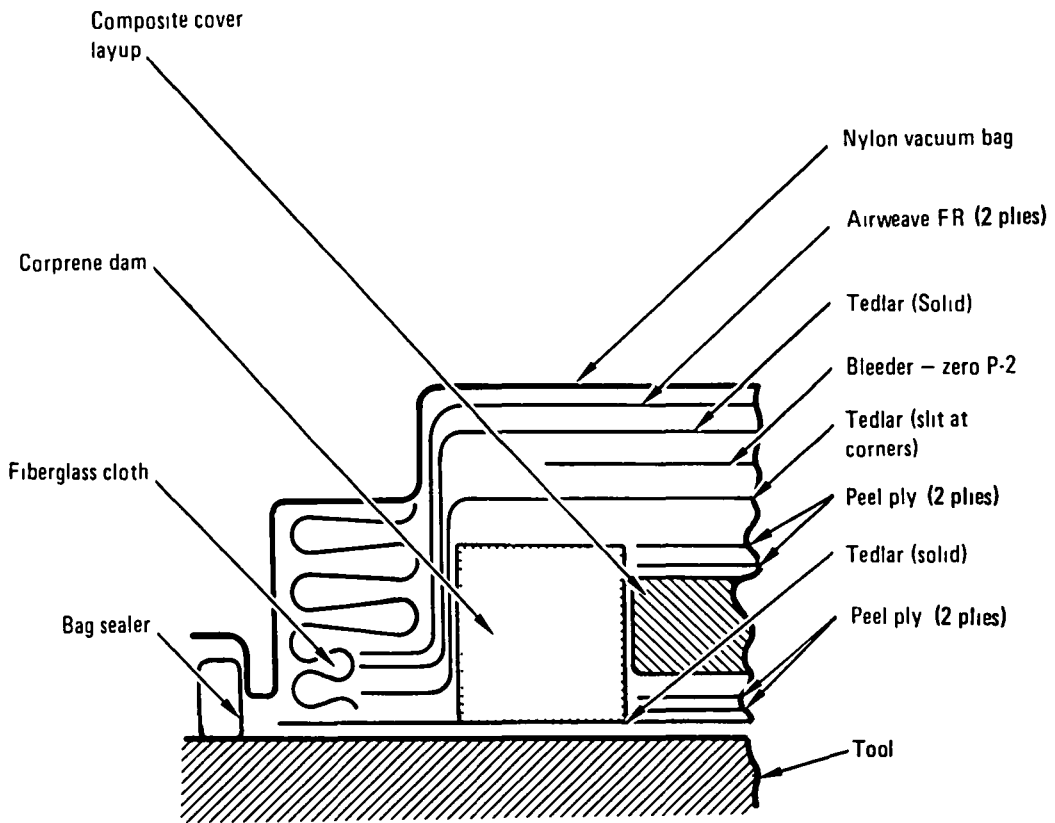
Figure 57. - Process development cover layup.

10 MPa
+
533 mm Hg

(15 psi)
+
(21 in Hg)

59 — .69 MPa

(85 — 100 psi)

Temperature
K (°F)

477 6
(400)

422 0
(300)

366 5
(200)

310 9
(100)

Heat rise rate
83 — 94 K/min
(1 5 — 3 5°F/min)

0   1   2   3   4   5   6   7

Time — hours
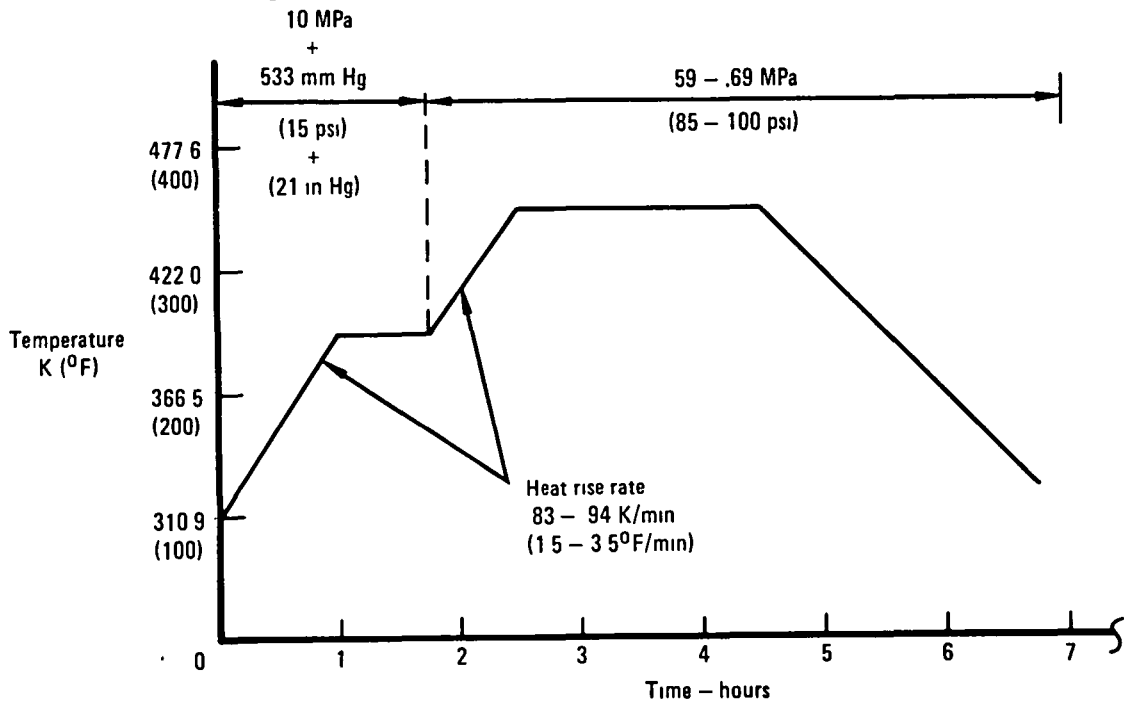
Figure 58. - Initial cure cycle.

TABLE 28. – COVER PANEL PROCESS DEVELOPMENT DATA

Specimen No	Location	Resin Content %		Void Content %	
		C-4 1-10	C-4 1-11	C-4 1-10	C-4 1-11
1B	Bag Side of Syntactic	28 68	26 91	0 47	0 28
1B ..	In Basic Cover Configuration	28 47	27 08	0 66	0 29
3B	3T/Syn/3T	28 45	27 20	0 53	0 27
1T	Tool Side of Syntactic	28 74	27 52	0 33	0 22
2T .	In Basic Cover Configuration	28 44	27 59	0 44	0 06
3T	3T/Syn/3T	28 92	27 60	0 51	-0 06
4	5-Ply Tape Internal Doubler +	27 90	27 41	0 38	-0 05
5 .	6-Ply Tape Basic Cover +	27 98	27 56	0 37	0 03
6	3-Ply Tape External Doubler	28 24	27.78	0 35	-0 05
7	6-Ply Tape Less Syntactic	28 58	26 56	0 33	0 45
8 .	6-Ply Tape Less Syntactic	29 41	27 01	0 60	0 56
9	6-Ply Tape Less Syntactic	28 54	26 74	0 34	0 39
10	24 Plies Tape	27 42	26 34	0 49	0 55
11 .	Consisting of 6-Ply Basic +	27 52	26 33	0 47	0 59
12	5-Ply Internal Doubler + 13 Ply External Doubler	26 72	26 44	0 48	0 56

change, reverification of the cover process was required. Table 30 shows the resin content and thickness measurements for this reverification of the covers. The specimen locations for these data are shown in figure 60.

During the fabrication of the first five ship sets of aileron parts, excessive voids and porosity appeared in the cured covers. As a result, it was necessary to continue development to effect a process that was more forgiving for uncontrollable perturbations in a production environment. The nondestructive inspection (NDI) results showed the voids to be primarily located in the syntactic and the graphite/syntactic faying surface. It was surmised that the primary voids were caused by either, or both, of the following conditions: 1) the inability of the lateral bleed system to remove all air and volatiles, and 2) possible bridging of the bleeder system at the edges of the external doublers. To improve the overall breathing capability of the cover, it was decided to go to a vertical bleed system. The vertical bleed system is one which allows the volatiles to breath up through a barrier film prior to the lateral flow to the vacuum source. In implementing this system, several bleeder/breather materials and arrangements were investigated as defined by table 31. A detail schematic of the chosen bleeder/breather system (the last item of table 31) is shown in figure 61. The result of this development is a forgiving system in a production environment.

82

TABLE 29. – COVER PROCESS VERIFICATION TEST DATA

Part Identity	Specimen Location	Resin Content %	Void Content %	Thickness mm (in)	Short Beam Shear — MPa (psi)	
					RT, Dry	355 4K(180°F), Wet*
1618001-103PC S/N 1	Basic	27 25 (B) 27 36 (T)	-0 75 (B) -0 81 (T)	2 002 (0 0788)	33 21 (4,817)	25 71 (3,729)
	Doubler	26 02	0 39	2 714 (0 1069)	50 97 (7,393)	56 99 (8,258)
1618001-103 S/N 1	Basic	28 92 (B) 28 96 (T)	0 38 (B) 0 34 (T)	2 056 (0 0810)	31.14 (4,517)	27 30 (3,959)
	Doubler	28 76	0 78	2 799 (0 1102)	49 77 (7,219)	52 32 (7,588)
1618001-103PC S/N 2	Basic	29 37 (B) 29 01 (T)	0 47 (B) 0 45 (T)	2 083 (0 0820)	24 84 (3,603)	19 53 (2,833)
	Doubler	28 21	0 57	2 758 (0 1086)	58 08 (8,424)	49 80 (7,223)
1618001-103 S/N 2	Basic	28 16 (B) 28 25 (T)	-1 07 (B) -1 05 (T)	2 070 (0 0815)	28 52 (4,136)	30 06 (4,360)
	Doubler	28 00	0 06	2 731 (0 1075)	49 51 (7,181)	42 42 (6,153)
1618002-103PC S/N 1	Basic	27 01 (B) 27 21 (T)	0 31 (B) 0 56 (T)	2 113 (0 0832)	22 05 (3,198)	N/A
	Doubler	26 32	0 43	2 649 (0 1043)	40 03 (5,806)	N/A
1618002-103 S/N 1	Basic	29 10 (B) 29 01 (T)	-0 13 (B) -0 21 (T)	2 120 (0 0835)	20 48 (2,971)	21 58 (3,130)
	Doubler	28 25	0 40	(0 1097)	(6,426)	(8,442)
1618002-103PC S/N 2	Basic	28 49 (B) 28 65 (T)	0 70 (B) 0 57 (T)	2 090 (0 0823)	25 33 (3,674)	23 39 (3,393)
	Doubler	28 26	0 78	2 746 (0 1081)	38 86 (5,636)	40 71 (5,905)
1618002-103 S/N 2	Basic	30 01 (B) 28 51 (T)	-0 33 (B) -0 19 (T)	2 073 (0 0816)	29 98 (4,348)	29 11 (4,222)
	Doubler	28 59	-0 62	2 774 (0 1092)	57 82 (8,386)	54 30 (7,875)

LEGEND   1618001-103 — Upper Cover
1618002-103 — Lower Cover

PC — Denotes Process Control Coupon — Preply, Layup, Bag, Cure Simultaneous with Full Size Part

(B) Bag Side
(T) Tool Side
 * 2 hour water boil

10 MPa
+
533 mm Hg

59 MPa
+
533 mm Hg

69 MPa

(15 psi)
+
(21 in Hg)

(85 psi)
+
(21 in Hg)

(100 psi)

Temperature K (°F)

(Based on leading thermo couple)

477 6 (400)

422 0 (300)

366 5 (200)

310 9 (100)

0

Heat rise rate
83 – 1 94 K/min
(1 5 – 3 5°F/min)

Time – Hours
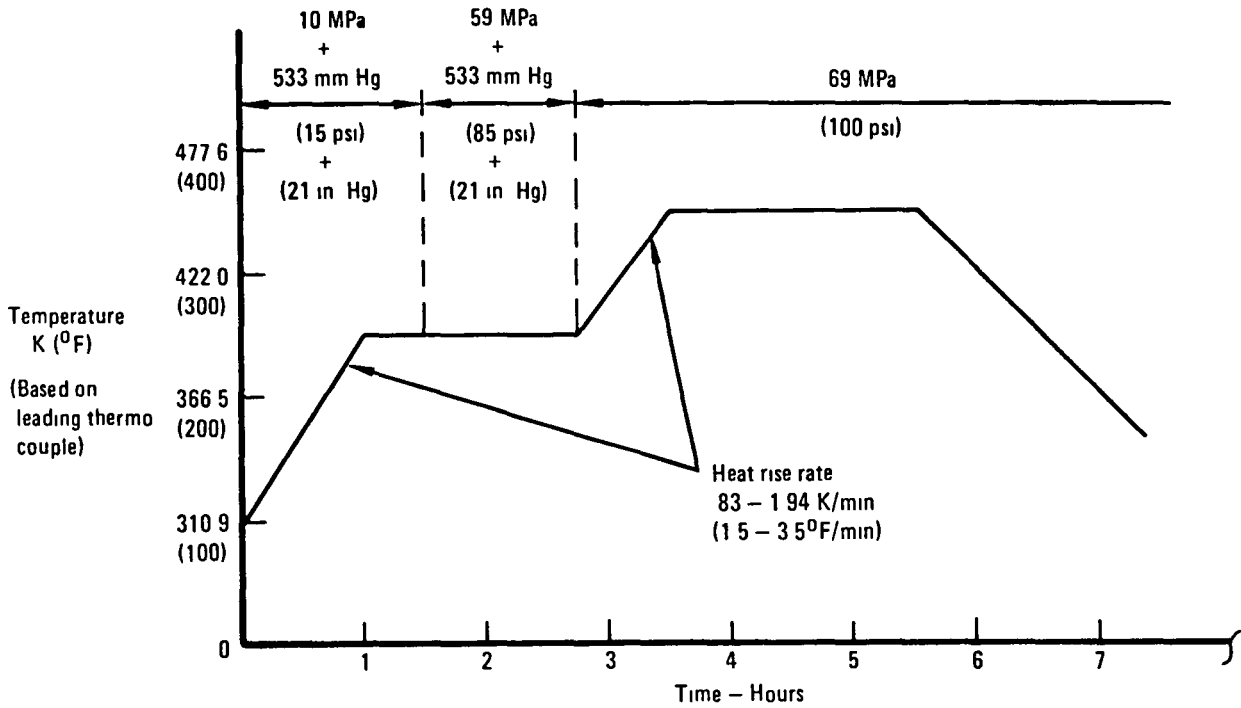
Figure 59. – Revised cure cycle.

TABLE 30. – COVER PROCESS RE-VERIFICATION TEST DATA
(RESULTING FROM CURE CYCLE REVISION)

Laminate Configuration	TEST AREA*						
	Resin Content %						
	1	2	3	4	5	6	7
Basic							
Bag Side	30 43	30 70	30 36				
Tool Side	30 52	30 75	31 01				
Doubler				30 22	30 37	30 51	27 95

Laminate Configuration	TEST AREA*						
	Thickness — mm (in)						
	1	2	3	4	5	6	7
Basic							
Bag Side	2 134 2 210 (0 084 0 087)	2 108 2 210 (0 083 0 087)	2 135 2 235 (0 084 0 088)				
Tool Side				3 073 3 277 (0 121 0 129)	3 099 3 277 (0 122-0 129)	3 124 3 226 (0 123 0 127)	
Doubler							4 724-4 826 (0 186 0 190)

*(See Figure 60 for Location)

Cover

Spar

Ribs
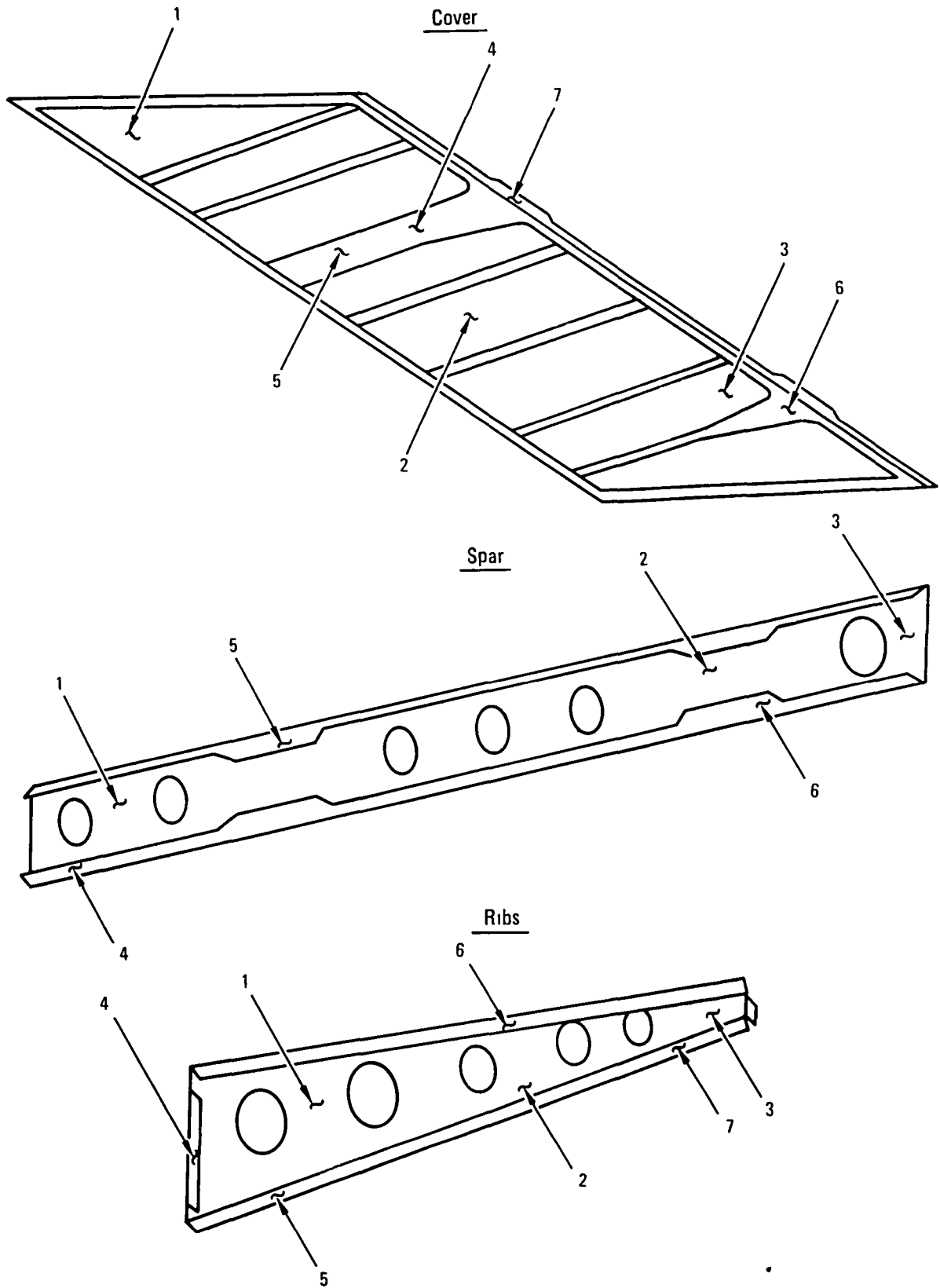
Figure 60. – Specimen location for process verification testing.

TABLE 31. – COVER VERTICAL BREATHER/BLEEDER SYSTEM DEVELOPMENT

Quantity Tested	Tool Side Breather	Bag Side Breather	Cured Resin Content %	Ultrasonic Results	Conclusion
1	2 Ply Armalon	Composite Armalon A4000P3 Armalon Solid Tedlar Airweave SS FR Bag	25 5/26	Generally Good Not Repeatable	Better Breathing required to assure consistency
3	Composite Peel Ply A4000P3 Armalon Solid Tedlar Tool	Composite Peel Ply (on Bias) A4000P3 Armalon (on Bias) Solid Tedlar Bag	24/26 5	No Voids	The low resin content indicated that high bleed removed volatiles It was necessary to reduce the resin flow
2	Armalon	Composite Armalon or Peel Ply (Bias) A4000P3 Armalon (Bias) A4000P3 Airweave SS FR Bag	26/26 5	No Voids	Control of resin flow desired to obtain nominal specification requirement for resin content
2	Armalon	Composite A4000P3 Peel Ply (Bias) A4000P4 2-Ply Armalon (Bias) Bag	26 5/27 5	No Voids	Resin content improved, however, still below nominal
2	Armalon	Composite Armalon A4000P3 Armalon A400P4 Airweave SS FR Bag	28/29	Occasional minor voids Minor porosity	Resin content improved, however, still below nominal
1	Armalon	Composite Armalon A4000P4 Armalon A4000P4 Airweave SS FR Bag	30/31	Voids	Not enough resin flow and vertical breather path too restricted to remove voids
6*	Armalon	Composite Armalon A4000P3 Armalon A4000P4 Airweave SS FR Bag	29/31 5	Occasional minor voids	Removal of dam and requirements for no wrinkles in bag at edges resulted in optimum parts

NOTE   All the above panels, except the ones identified (*), used a Corprene dam

A400GP4 — 0 051mm   A4000P3 — 0 051mm
(2 mil)   (2 mil)

Nylon vacuum bag   Airweave SS FR   Armalon (bias cut)   Armalon (bias cut)

Bag sealer

Fiberglass cloth   Tool   Tedlar (Solid)   Armalon   Composite cover
(tie to vacuum source)   layup
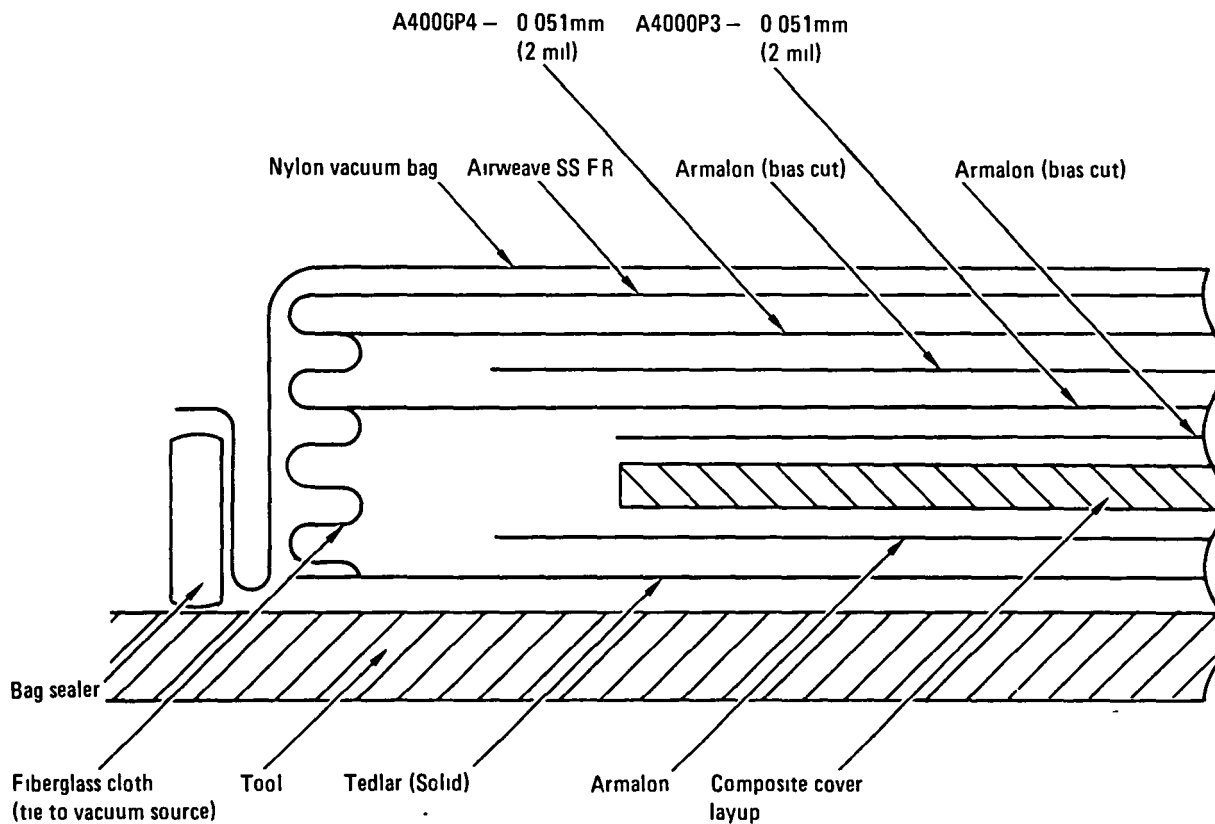
Figure 61. – Vertical bleeder/breather cover layup.

3.4 Rib Development

On completion of the tooling development and selection of the male
tooling concept, development of the process for fabrication of ribs was initi-
ated. Using data derived during the tool development phase as a starting
point for layup and bagging systems, twenty perturbations were evaluated.
This development incorporated in the following parameters:

1. Cure cycle – see figures 58 and 59.

2. Bleeder/breather – peel ply (plain), peel ply (release coated),
    Armalon, bleeder (Lease Zero P2), Airweave "A":, fiber glass cloth.

3. Barrier film – Tedlar (solid), Tedlar (slit at corners) A-4000P3.

4. Damming materials – Corprene, AIRDAM I.

87

During the rib development, the major problem encountered was control of resin flow resulting in low resin content in the rib. To control this flow, variations in the use of the above materials included such items as inverting the tool during cure, tucking the bleeder/breathers under the dam, and doubling the breather material over the dam. The net result of this development was the layup sequence shown in figure 62. Parts were fabricated using this layup and the cure cycle shown in figure 58, and the properties for the main and intermediate ribs process development and verification specimens were obtained as shown in tables 32 and 33, respectively. It should be noted that the values reported are an average of a minimum of three specimens.

The process verification data for the ribs show that the process control coupons are near the minimum (above and below) allowable tolerance in resin content while all the specimens from the parts are above minimum tolerance but near the low side. The cause of this variation was the effect of edge bleed, since the ratio of the periphery to the area is greater on the process control coupon than on the part. It was determined that the flange thickness was a good check of the resin content. Using this criterion for acceptance, it was decided to proceed with the fabrication of the ground test articles.
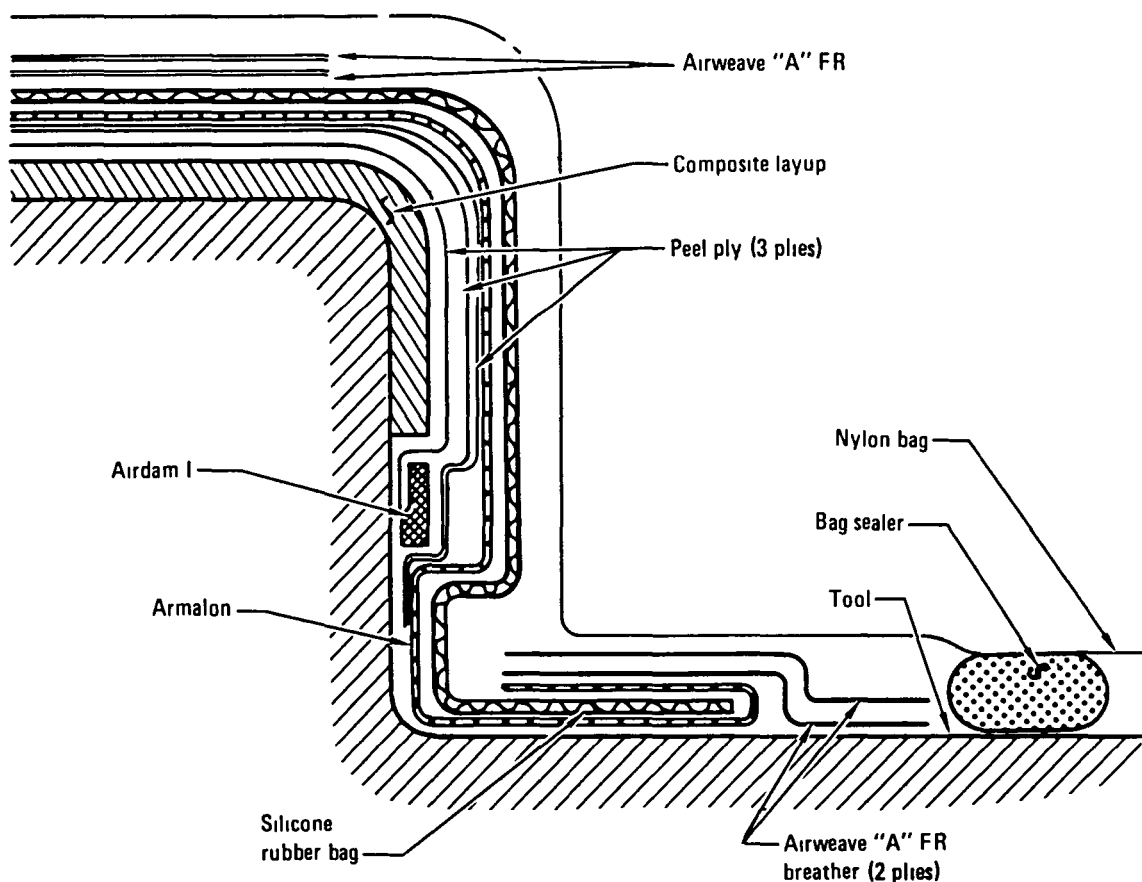
Figure 62. - Process development rib layup.

TABLE 32. – MAIN RIB PROCESS DEVELOPMENT AND VERIFICATION TEST DATA

Part Identity	Specimen Location	Resin Content %	Void Content %	Thickness mm (in)	Short Beam Shear — MPa (psi)	
					RT, Dry	355.4K(180°F), Wet*
R-4 1-5 2	Web	32 89	0 76	1 449 (0 0571)	55 00 (7,977)	51 37 (7,451)
	Cap	29 09	0 73	2 352 (0 0926)	65 32 (9,474)	43 09 (6,250)
1617988-105PC S/N 1	Web	29 42	0 91	1 384 (0 0545)	68 94 (9,999)	51 96 (7,536)
	Cap	26 69	0 84	2 169 (0 0854)	48 06 (6,970)	42 75 (6,201)
1617988-105 S/N 1	Web	32 13	1 03	1 483 (0 0584)	69 51 (10,081)	54 66 (7,928)
	Cap	28 64	0 94	2 410 (0 0949)	78 35 (11,364)	58 30 (8,456)
1617992-105PC S/N 2	Web	30 71	0 73	1 392 (0 0548)	67.50 (9,790)	54 10 (7,846)
	Cap	27 87	0 25	2 261 (0 0890)	84 03 (12,187)	72 11 (10,459)
1617992-105 S/N 2	Web	33 64	1 28	1 440 (0 0567)	65 96 (9,566)	56 73 (8,228)
	Cap	28 70	0 80	2 367 (0 0932)	79 12 (11,475)	67 89 (9,847)
1617993-105PC S/N 1	Web	30 40	0 53	1 453 (0 0572)	63 25 (9,174)	50 27 (7,291)
	Cap	27 56	0 70	2 177 (0 0857)	87 94 (12,754)	43 04 (6,243)
1617993-105 S/N 1	Web	32 85	0 86	1 476 (0 0581)	74 06 (10,741)	84 48 (12,252)
	Cap	29 73	0 90	2 388 (0 0940)	55.24 (8,012)	52 82 (7,661)

NOTE PC – Denotes Process Control Sample – Preply, Layup, Bag, Cure Simultaneous with Full Size Part
  * 2 hour water boil

TABLE 33. – INTERMEDIATE AND CLOSEOUT RIB PROCESS DEVELOPMENT
AND VERIFICATION TEST DATA

Part Identity	Specimen Location	Resin Content %	Void Content %	Thickness mm (in)	Short Beam Shear — MPa (psi)	
					RT, Dry	355 4K(180°F), Wet*
R-4 1-50	Web	31 85	0 04	1 801 (0 0709)	73 99 (10,587)	51 57 (7,480)
	Cap	31 57	0 32	1 786 (0 0703)	67 12 (9,735)	52 79 (7,656)
1617986-105PC S/N 1	Web	30 30	1 07	1 819 (0 0716)	76 08 (11,035)	53 26 (7,725)
	Cap	28 69	1 62	1 781 (0 0701)	70 02 (10,156)	54 38 (7,887)
1617986-105PC S/N 1	Web	32 12	-0 09	1 814 (0 0714)	67 36 (9,770)	52 32 (7,588)
	Cap	31 42	-0 11	1 798 (0 0708)	67 84 (9,840)	51 51 (7,471)
1617987-105PC S/N 1	Web	29 22	0 34	1 737 (0 0684)	70 22 (10,184)	52 23 (7,575)
	Cap	28 38	0 31	1 735 (0 0683)	70 66 (10,249)	52.91 (7,674)
1617987-105 S/N 1	Web	32 00	-0 06	1 831 (0 0721)	69 38 (10,063)	51 21 (7,428)
	Cap	32 08	0 19	1 808 (0 0712)	66 50 (9,645)	55 76 (8,088)
1617989-105PC S/N 1	Web	28 82	0 55	1 727 (0 0680)	63 24 (9,172)	46 57 (6,754)
	Cap	28 53	0 21	1 727 (0 0680)	62 56 (9,074)	48 44 (7,025)
1617989-105 S/N 1	Web	31 12	0 51	1 834 (0 0722)	70 00 (10,152)	54 15 (7,854)
	Cap	29 80	0 48	1 811 (0 0713)	73 86 (10,713)	52 39 (7,599)
1617990-105PC S/N 3	Web	27 58	0 23	1 615 (0 0636)	68 00 (9,862)	53 88 (7,814)
	Cap	27 45	0 42	1 623 (0 0639)	69.11 (10,024)	55 88 (8,105)
1617990-105 S/N 3	Web	29 58	0 61	1 671 (0 0658)	59 07 (8,568)	54 21 (7,863)
	Cap	29 00	0 64	1 648 (0 0649)	58 76 (8,522)	49 26 (7,144)
1617991-105PC S/N 1	Web	29 65	0 84	1.717 (0 0676)	66 27 (9,611)	53 12 (7,705)
	Cap	28 79	0 85	1 679 (0 0661)	61 74 (8,954)	48 28 (7,002)
1617991-105 S/N 1	Web	30 52	0 79	1 770 (0 0697)	63 72 (9,242)	51 71 (7,500)
	Cap	29 75	0 85	1 735 (0 0683)	63 28 (9,178)	52 91 (7,674)

TABLE 33. – INTERMEDIATE AND CLOSEOUT RIB PROCESS DEVELOPMENT AND VERIFICATION TEST DATA (Cont'd)

Part Identity	Specimen Location	Resin Content %	Void Content %	Thickness mm (in)	Short Beam Shear — MPa (psi)	
					RT, Dry	355 4K(180°F), Wet*
1617994-105PC S/N 1	Web	29 48	0 41	1 872 (0 0737)	69 75 (10,116)	52 17 (7,567)
	Cap	27 73	0 36	1 775 (0 0699)	65 46 (9,494)	55 81 (8,094)
1617994-105 S/N 1	Web	30 54	0 69	1 763 (0 0694)	73 21 (10,618)	49 71 (7,210)
	Cap	30 22	0 80	1 748 (0 0688)	66.50 (9,645)	49 64 (7,199)
1617995-105PC S/N 1	Web	29 46	0 24	1 768 (0 0696)	70 20 (10,182)	54 97 (7,972)
	Cap	27 61	0 16	1 778 (0 0700)	68 26 (9,900)	55 43 (8,040)
1617995-105 S/N 1	Web	32 66	-0 44	1 819 (0 0716)	71 78 (10,411)	53 06 (7,696)
	Cap	30 97	0 42	1.781 (0 0701)	70 02 (10,155)	50 51- (7,326)

NOTE PC – Denoted Process Control Sample – Preply, Layup, Bag, Cure Simultaneous with Full Size Part
      * 2 hour water boil

During fabrication of the first ribs for the ground test article in a production environment, the resin content of the ribs process control coupons continued to be on or below the low side of the allowable tolerance. Investigation of the cause of this discrepancy revealed that the only change in the procedure was the increase in time between layup and bagging. It was determined that during this time, the prepreg layup was relaxing and the rib caps were pulling away from the tool and edge dam. When the layup was pulled down by the vacuum bag, the breather and the bleeder material did not return to its original location which provided a path for the resin to flow over the resin dam. The following solutions were evaluated to eliminate this problem:

1. Better coordination between layup and bagging personnel to assure prompt bagging. Note: In a production environment, 100 percent assurance would be difficult.

2. Develop the necessary tooling to hold the composite after layup prior to bagging.

3. Develop an integral bag tool seal that would permit application of the vacuum bag by the layup personnel.

4. Modify the resin damming technique so that it will not be dependent on time between layup and bagging.

The effect of these solutions were evaluated (see table 34) in regard to cost and schedule impact.

The fourth method was chosen because it would result in a reduction in cost by decreasing the cost of expendable production material and layup labor, without an increase in tooling cost.

The new damming technique investigated consisted of utilizing the rubber bag as a dam directly against the tool surface. This system requires that the bleeding be accomplished from the composite surface. A fiber glass string was laid around the periphery of the rib cap, and tied to the vacuum source with 10 equally spaced fiber strings to provide a breather path for the volatiles and any entrapped air. It was found that the silicone rubber bag did a good job of controlling the edge bleed and the strings provided ample breather path to control the void content. Several specimens were prepared using different surface bleeding systems; the results of these are shown in table 35.

In an effort to further reduce the layup cost, it was decided to run the breather string across the composite layup instead of around the periphery. The string was applied between the CW1850 Mochburg paper and the silicone rubber bag. This method produced comparable results to that shown in table 35, however, a mark off of about 0.102 mm (0.004 in) was found in the surface of the composite rib. While this mark off is not desirable, it was found to be acceptable in the graphite fabric parts.

Refinements were also made to the layup of the ribs that affect the bleeding and breathing of the curing resin. Figure 63 defines the rib layup using no separate damming material. The main difference in this layup is the porous Armalon breathing strips which now overlap the flanges approximately 12.7 mm (0.50 in) instead of completely spanning the layup.

TABLE 34. – EVALUATION OF CORRECTIVE ACTION TO RESIN CONTENT VARIATIONS

Action to Correct Resin Content Variation	Labor Cost	Tooling Cost	Material Cost	Schedule Impact
1	Increase	No Change	No Change	None
2	Slight Increase	Increase	No Change	Yes
3	Decrease	Increase	Decrease	Yes
4	Decrease	No Change	Decrease	Minimal

TABLE 35. – EFFECT OF VARIOUS SURFACE BLEEDERS ON PHYSICAL PROPERTIES

Specimen No	Surface Bleed System	Thickness mm (in)	Cured Resin Content %	Resin Removed During Cure %	Void %
4.1-60	3-peel ply	1 549/1 575 (0 061/0 062)	35 01	5 99	-0 02
4 1-61	1-peel ply + 1-120 glass (white)	1 537 (0 0605)	34 56	6 44	-0 15
4 1-62	1-peel ply + 1-120 (pink)	1 600/1 613 (0 063/0 0635)	36 12	4 88	0 10
4 1-63	1-peel ply + 1-Airweave FR	1 537/1 549 (0 0605/0 061)	33 94	7 06	0 08
4 1-64	1-peel ply + 2 FR	1 382/1 405 (0 0544/0 0553)	30 19	8 81	0 56
4 1-65	1-peel ply + 1-CW1850 Mochburg	1 440/1 448 (0 0567/0 0570)	31 92	7 08	0 41
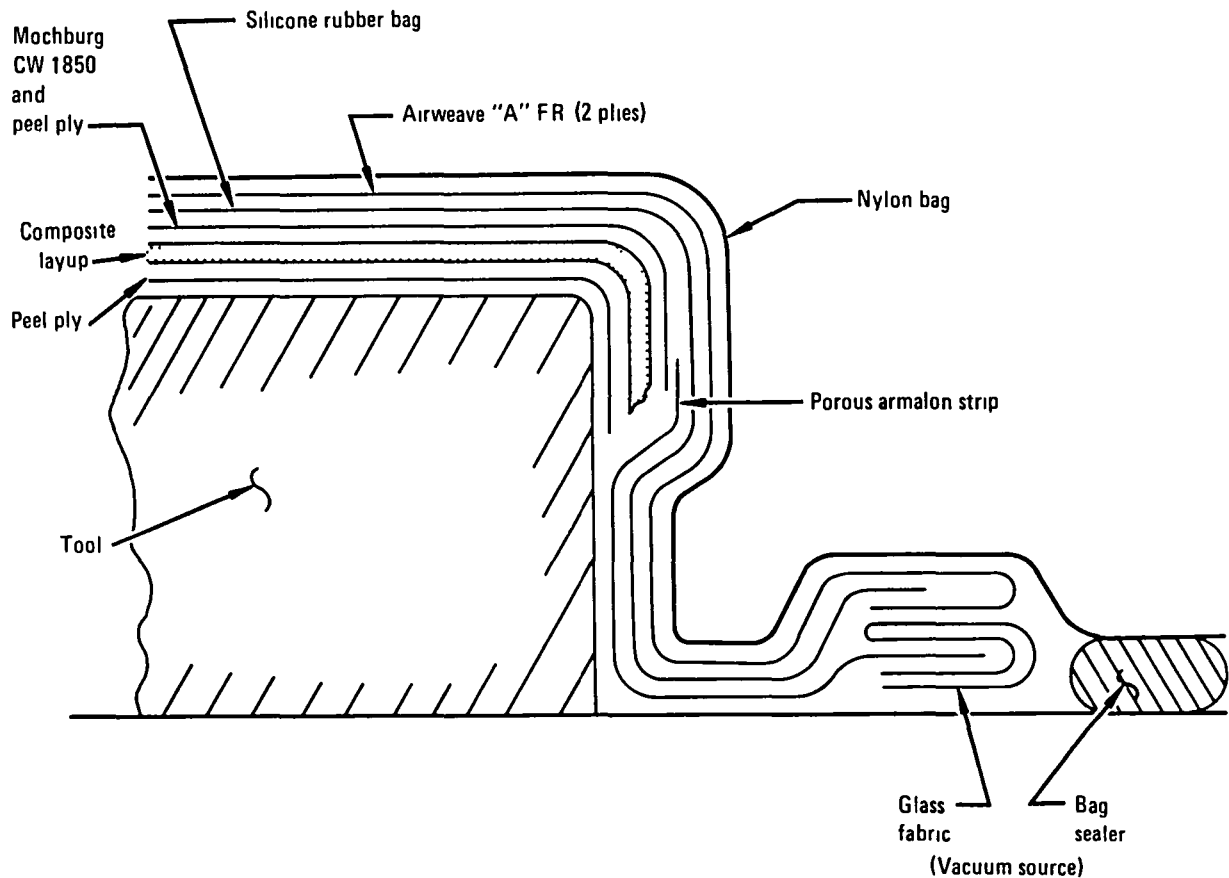
Figure 63. - Damless technique rib layup.

The benefits realized from this layup technique are:

1. Lower cost due to a decrease in labor and expendable production material because no damming material is required.

2. Lower cost because the flange edges are cured to a net dimension and any subsequent trimming operations are eliminated.

3. Less stringent scheduling requirements between layup, bagging and curing operations.

As a result of the above process refinements, additional process verification test articles were fabricated and tested. These specimens showed improved control of resin, voids and porosity content. Maps showing the specimen location within the part are shown in figure 60. The resin content and thickness measurements of these specimen are shown in table 36.

TABLE 36. - RIB PROCESS RE-VERIFICATION TEST DATA
(RESULTING FROM CURE CYCLE REVISION)

Specimen Identity	TEST AREA*						
	Resin Content %						
	1	2	3	4	5	6	7
Intermediate Rib							
Web	33 23	33 56	33 53				
Cap				32.92	32 61	33 12	33 03
Main Rib							
Web	32 86	32 96	32 40	32 74			
Cap					29 86	30 51	30 24

Specimen Identity	TEST AREA*						
	Thickness — mm (in)						
	1	2	3	4	5	6	7
Intermediate Rib							
Web	1 727 1 803 (0 068-0 071)	1 753 1 803 (0 069-0 071)	1 753 1 803 (0 069-0 071)				
Cap				1 753 1 829 (0 069-0 072)	1 753 1 829 (0 069-0 072)	1 753 1 829 (0 069-0 072)	1 753 1 829 (06069-0 072)
Main Rib							
Web	1 422 1 448 (0 056-0 057)	1 397 1 524 (0 055-0 060)	1 422 1 448 (0 055-0 060)	1 397 1 448 (0 055-0 067)			
Cap					2 311 2 388 (0 091-0 094)	2 312 2 337 (0 091-0 092)	2 311 2 388 (0 091 0 094)

*See Figure 60 for Location

94

3.5 Spar Development

The spar development was conducted in a parallel effort to the rib. In fact, initial development was accomplished on a rib tool. This was considered acceptable since both the spar and rib are basic channel shapes. The spar, however, utilized 10 plies of graphite tape with a prepreg resin content of 34 ±3 percent and required a finished product resin content of 29 ±3 percent. Since the spar required approximately half the amount of resin to be removed as the rib during cure, less surface bleed absorption was required. The same bleeder/breather materials and cure cycle were evaluated for the spar layup as defined previously for the rib. The result of nineteen (19) perturbations of the spar layup was the derivation of the system shown in figure 64. Properties of the process development and verification spars fabricated using this layup and the cure cycle shown in figure 58 are reported in table 37.
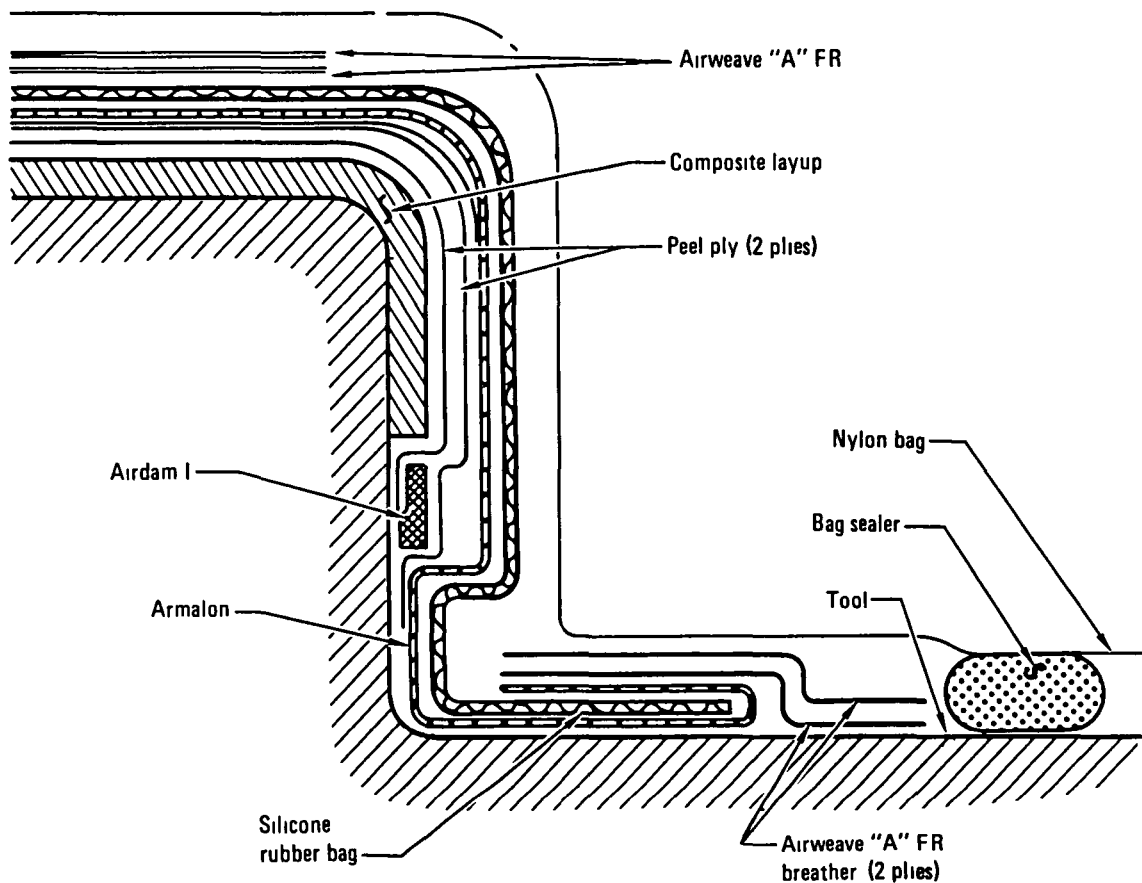
Figure 64. - Process development spar layup.

TABLE 37. - SPAR PROCESS DEVELOPMENT AND VERIFICATION TEST DATA

Part Identity	Specimen Location	Resin Content %	Void Content %	Thickness mm (in)	Short Beam Shear — MPa (psi)	
					RT, Dry	355 4K(180°F), Wet*
S-4 1-40	Web	32 01	0 38	2 098 (0 0826)	59 36 (7,140)	40 85 (5,925)
	Cap	30 99	0 36	2 103 (0 0828)	53 74 (7,794)	51 64 (7,490)
1617984-105PC S/N 1	Web	28 57	0 69	1 983 (0 0781)	56 66 (8,218)	47 55 (6,897)
	Cap	28 07	0.51	1 953 (0 0769)	60 92 (8,835)	51 17 (7,422)
1617984-105 S/N 1	Web	29 35	0 69	2 027 (0 0798)	66 90 (9,703)	48 04 (6,968)
	Cap	26 77	0 82	1 976 (0 0778)	66 71 (9,676)	49 26 (7,145)
1617984-105PC S/N 2	Web	28 87	0 56	1 996 (0 0786)	56 28 (8,162)	59 16 (8,581)
	Cap	26 00	0 43	2 035 (0 0801)	52 46 (7,608)	

NOTE PC — Denotes Process Control Sample — Preply, Layup, Bag, Cure Simultaneous with Full Size Part
    * 2 hour water boil

During fabrication of the ground test article spars, wrinkles became prevalent in the web between the access holes. It was determined that by heating the layup tool prior to layup, the prepreg resin would soften and allow the preplied tape to be more formable around the flanges, thus minimizing the tendency of the fibers to wrinkle. When the tool was heated, the cured composite part tool surface appeared to have a resin starved finish, however, the resin and void content was 30.84% and .03% respectively. Additional runs were made using various breather materials between the tool and the composite to eliminate this dry appearing condition. All these specimens were good in resin and void content varying from 27.07% to 29.98% content and .09% to .63% void content.

It was decided that the "dry" appearing condition of the tool surface was caused by the resin sealing to the warm tool surface which prevented the entrapped air and/or volatiles from being pulled off. It is also possible that the cure cycle does not allow sufficient time for the air or volatiles to be forced out due to the high resin viscosity when the pressure is applied.

The spar process redevelopment was conducted concurrently with the rib process redevelopment. Mark-off of the breather string on the spar surface was more critical than on the ribs because the spar is laid up with graphite tape as opposed to the ribs which are laid up with graphite fabric. In an effort to eliminate this mark-off, the following alternatives to glass string were tried:

96

1. A 25.4 mm (1.0 in) wide integral tab (spaced about every 305 mm) (12.0 in) to the surface peel ply which was tied to the vacuum source.

2. A 25.4 mm (1.0 in) wide integral tab (spaced about every 305 mm) (12.0 in) to the surface Armalon which was tied to the vacuum source.

3. A 25.4 mm (1.0 in) wide strip of Armalon across the top of the layup which was tied to the vacuum source.

On the spar specimens prepared, each of these methods gave satisfactory results. A derivation of the third method in which the strip overlapped the flange approximately 12.7 mm (0.50 in) was selected, since the porous armalon did not tend to load up as much as the peel ply. A schematic of this bleeding system is shown in figure 65. The process was reverified using this layup
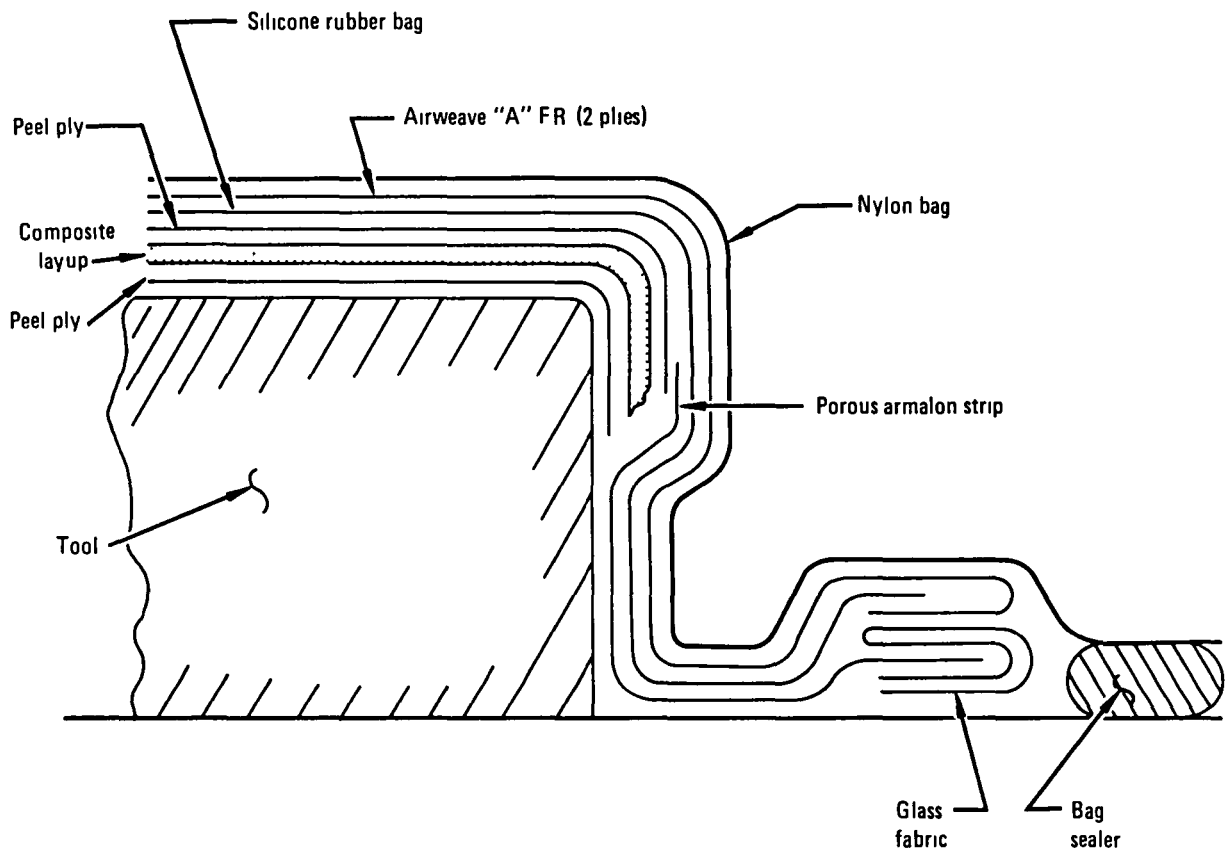
Figure 65. - Damless technique spar layup.

and the cure cycle of figure 58. The resin content thickness measurements of reverification parts are reported in table 38. The specimen locations for these data are shown in figure 60.

It was noted that as the temperature and humidity of the layup room approached the maximum allowed by process specification, voids were detected in the web of the spars. In an effort to vary the bleeder system to remove the voids, the cured resin content was decreased. An evaluation was made of the lateral bleeding capabilities of peel ply and Armalon using a test setup as shown schematically in figure 66. This evaluation consisted of applying the vacuum and measuring the time to draw a vacuum to the other side of the breather material. From these tests, it was determined that the Armalon had approximately twice the breathing capability as the peel ply. This was true even when the test was conducted at elevated temperature. However, since both breathers tended to block off at the dwell temperature of the cure cycle, it was decided to investigate a vertical breathe system layup.

To be effective, the vertical breather/bleeder system had to pass air and volatiles up to the time of resin gel, however, the resin flow must be controlled to maintain the required resin content of the composite. Based on the data derived from the cover vertical breather/bleeder development,

TABLE 38. – SPAR PROCESS RE-VERIFICATION TEST DATA
(RESULTING FROM CURE CYCLE REVISION)

Specimen Identity	TEST AREA*					
	Resin Content %					
	1	2	3	4	5	6
Web	30 72	30 18	30 23			
Cap				28 94	29 91	29 67

Specimen Identity	TEST AREA*					
	Thickness – mm (in)					
	1	2	3	4	5	6
Web	1 982 2 032 (0 078-0 080)	1 905 2 032 (0 075 0 080)	1 930 1 981 (0 076-0 078)			
Cap				1 905 1 981 (0 075 0 078)	1 880 1 981 (0 074-0 078)	1 905 2 007 (0 075 0 079)

*See Figure 60 for location
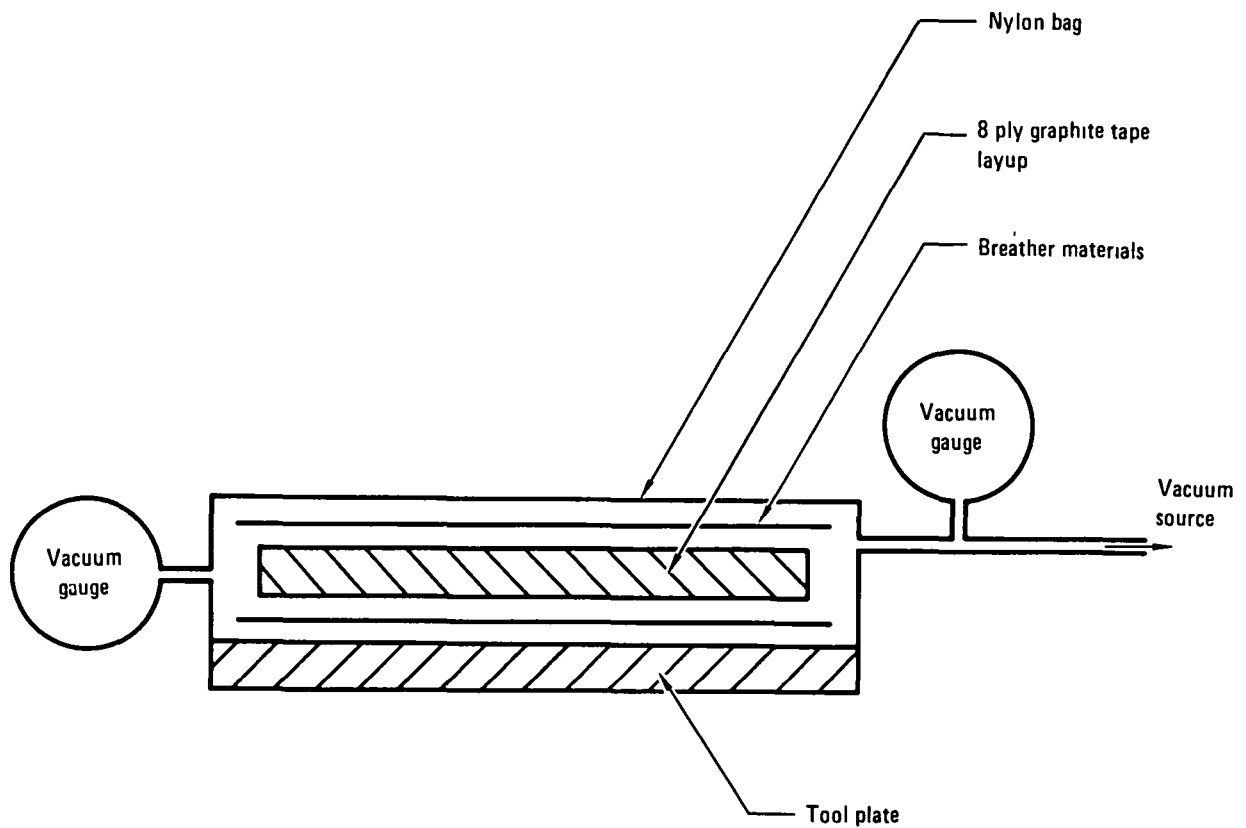
Figure 66. – Schematic lateral breathe test.

several systems, as (shown in table 39,) were evaluated for the spar using
the cure cycle of figure 59. From these data, it was determined that the
third system gave the best results. Figure 67 defines this vertical breather/
bleeder layup system. Spar production is continuing using this system and
cure cycle.

3.6 Drilling Development

The initial drilling development was begun in the laboratory environ-
ment. Preliminary tests employed standard twist drills (HSS, Cobalt
and Carbide) with varying rake angles. Primary methods of drilling were by

TABLE 39. - SPAR VERTICAL BREATHE/BLEED SYSTEM DEVELOPMENT

Quantity Tested	Tool Side Breather	Bag Side Breather	Cured Resin Content %	Ultrasonic Results	Conclusion
1	Peel Ply Armalon Strips (Tied to Vacuum)	Composite Peel Ply A4000P4 2-Ply Armalon tied to Vacuum Silicone Rubber Bag Airweave SS FR Bag	26 5-27 5	Minor Porosity & Voids	Peel Ply appears to take too much Resin and may block off before all Volatiles can be withdrawn Resin content below nominal
2	Armalon	Composite Armalon A4000P4 2-Ply Armalon tied to Vacuum Silicone Rubber Bag Airweave SS FR Bag	27 - 29	Generally Good but not 100% Repeatable	Resin Content improved Breather Path may be restricted somewhat to consistently eliminate all voids
1	Armalon (Tied to Bag Side Breather)	Composite Armalon (tied to Tool Side Breather) A4000P4 (EOP + 6 35 mm (0 25 in) 2-Ply Armalon (EOP + 12 7 mm (0 50 in) and Continuous Strips tied to Vacuum — See Fig A12) Silicone Rubber Bag Airweave SS FR Bag	28 - 30 5	Some Voids and Porosity	Resin Content is Acceptable Some minor perturbations will be implemented to provide acceptable parts, concerning voids

drill press, Bridgeport and standard air powered hand held drill motors with various spindle speeds and feed rates. Best results were obtained with a setup of 2700 RPM and 0.038 mm (0.0015 in) per revolution feed rate. Surveys made during the initial development also revealed that good quality holes were being drilled using carbide drills sharpened with an ogive tip configuration. The utilization of bushings, backup materials, lubricants/coolants (water spray mist, Shell Dromus "B", Freon and TFE Coat), and vacuum systems were evaluated. Results of these preliminary tests are reported in table 40.

100
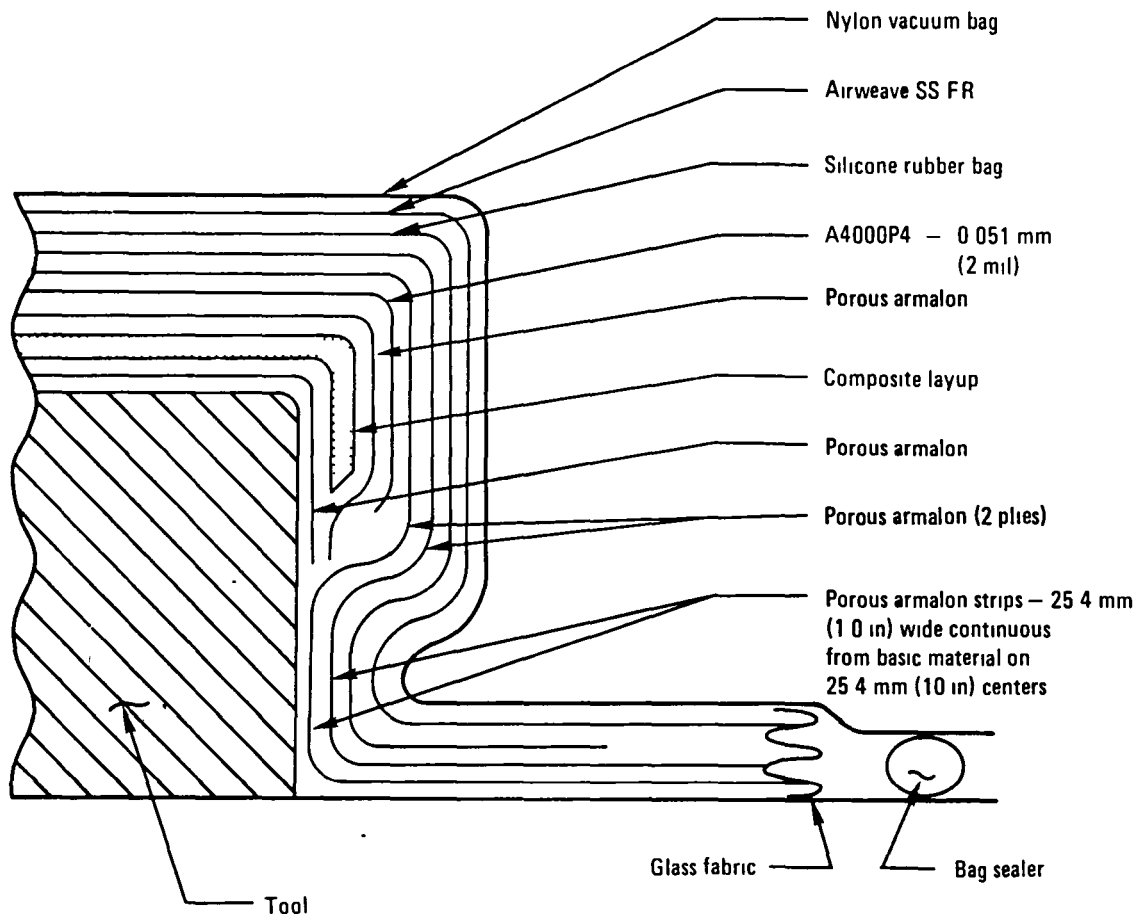
Figure 67. – Vertical breather/bleeder spar layup.

TABLE 40. – INITIAL DRILLING DEVELOPMENT TEST DATA

Drill Type	No Backup	Solid Backup Clamped	Pilot Holes With Backup	Front Piece and Backup Clamped*	Aluminum Tape Backup	Lead In Bushing, Aluminum Tape and Backup
Drill Rake Angle						
18 - 20°	U	U	U	U	U	U
22 - 24°	U	U	U	5S	U	5S
26 - 28°	U	U	U	U	U	U
Ogive Tip	U	U	U	U	U	U

LEGEND U – Unsatisfactory holes
        5S – Satisfactory holes, 5 holes per drill bit

*On assembly fixture, this presents problems for location of holes

101

Using the above methods, the number of holes that could be drilled before bit resharpening was unsatisfactory and also the necessary requirements for hole quality as well as the tolerances for hole diameter, angularity and perpendicularity were not being met.

Further evaluation of the drilling problems led to the use of the Spacematic automatic drilling system which has a spindle speed of 9000 RPM. The Spacematic with the ogive tip drill at a feed rate of 0.005 mm (0.0002 in) per revolution proved to be a most satisfactory drilling method in the laboratory, with up to two hundred (200) acceptable holes being drilled before bit resharpening. However, the production assembly fixtures were examined and it was apparent that there would be certain situations necessitating hand drilling or excessive and costly tooling modifications would have to be incorporated to accommodate the Spacematic system. Also, in the limited production use of the Spacematic system at that time, the system was not proving to be entirely satisfactory, since the locking pin did not always lock into place and a material backup was required.

The major problem associated with hand drilling was splintering of the fibers on the drill exit side of the graphite tape parts due to the "punch-through effect." This problem was solved by adapting a hydraulic check cylinder, which is designed to attach between the drill motor and drill bit. This unit allows a controlled feed rate of the drill bit by metering the flow of hydraulic fluid within the cylinder. The drill motor used with the hydraulic check unit had a spindle speed of 2500 RPM. This system is shown in figure 68. Initial tests with this system employed the ogive tip carbide drill. Results were promising; however, a survey of composite machining equipment manufacturers revealed that a dagger type solid carbide drill manufactured by Metal Removal Co., Chicago, Illinois, provided good results. The dagger drill is shown in figure 69. Two 6.35 mm (0.250 in) dagger drills were obtained, and utilizing the hydraulic check system, development was continued. Preliminary testing proved that hole quality and drill bit life was improved with the use of lubrication which acts both as a flush and coolant.

As a result of difficulties experienced in controlling proper hole location during the assembly development effort, it was decided that the foot of the hydraulic check attachment be adapted to incorporate a bushing to help stabilize the drill bit. Since coolant and vacuum removal of shavings was necessary, the foot was made to allow coolant to be fed to the drill point via a ported bushing and vacuum attachments were added. The lubricant used was Shell Dromus "B", which is water soluble and mixes at a ratio of 25:1 (water to lubricant). The coolant lubricant is fed through a pressurized tank and a standard wet or dry shop vacuum is used to evacuate shavings, dust and excess coolant.

The drilling system with dagger drills produced satisfactory results for joints which included graphite tape and fabric and graphite/aluminum stackups when the aluminum did not exceed 2.54 mm (0.10 in) thick. The dagger drill did not perform adequately for graphite/aluminum stackups where the aluminum
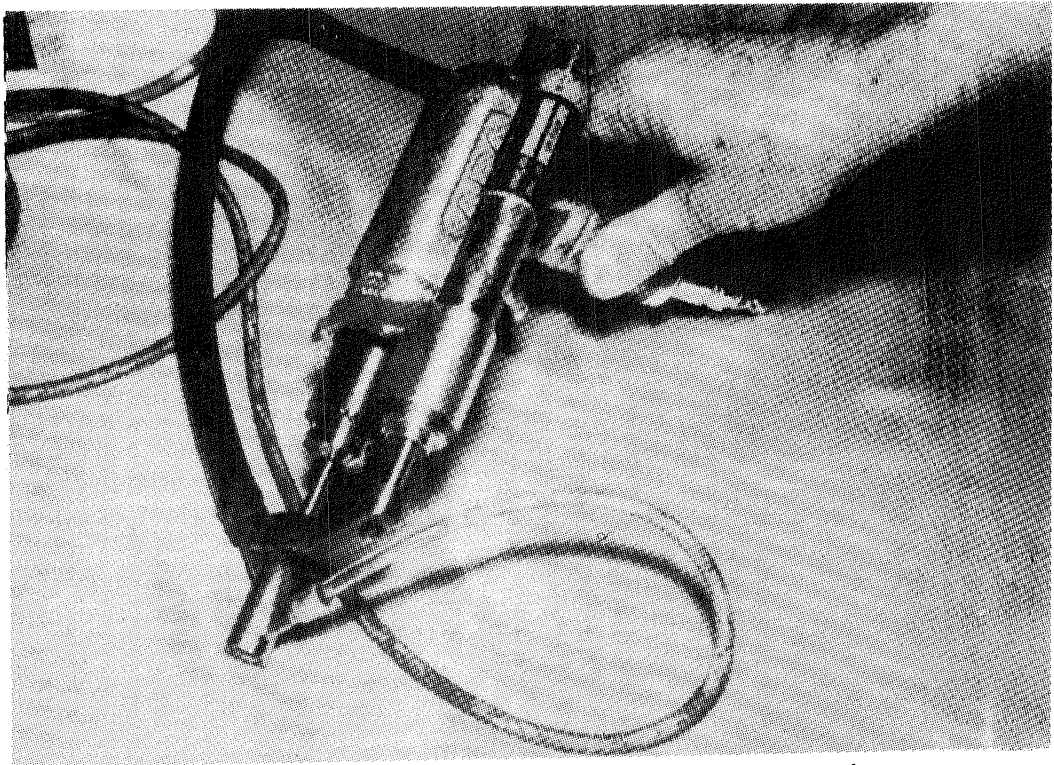
Figure 68. - Closeup of the hydraulic check attachment.
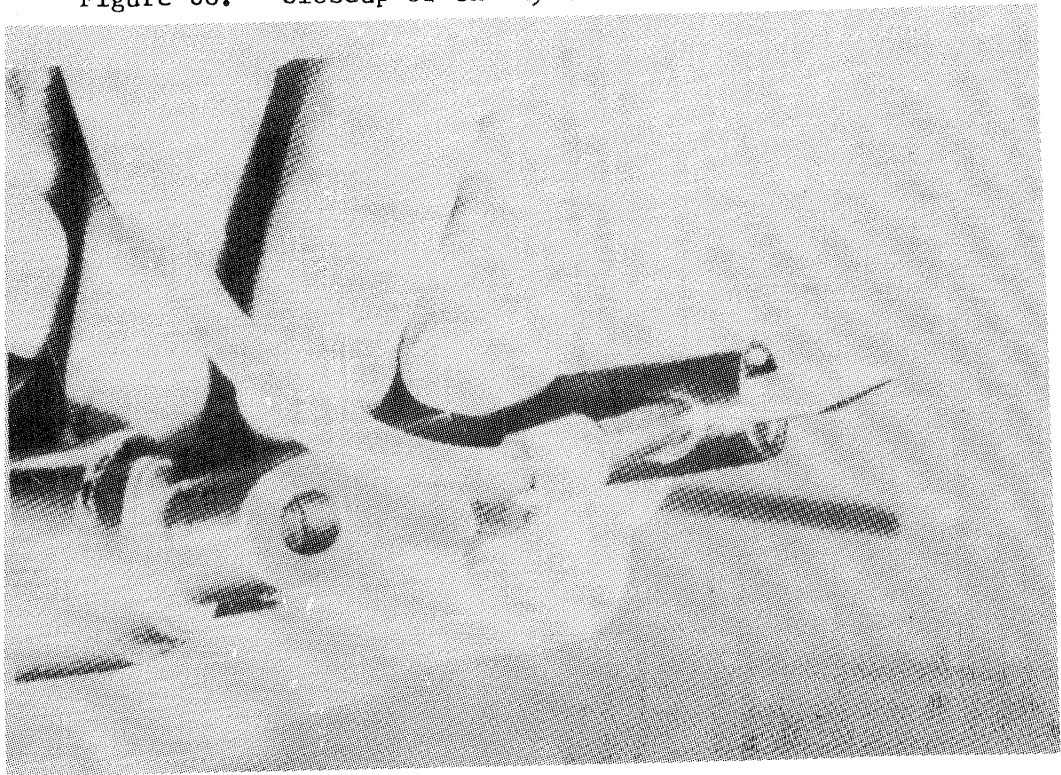
Figure 69. - Dagger drill.

103

is 6.35 mm (0.250 in) thick. These holes were tapered with the drill entrance being up to 0.254 mm (0.010 in) larger than the exit. More development tests determined that a Metal Removal Co. Standard Series 225 carbide twist drill would produce acceptable holes in this particular stackup. Hole quality was further enhanced by drilling accompanied by a subsequent reaming operation with a carbide straight flute reamer. Using the same basic system with a foot designed for the setup to accept a standard micro stop attachment, it was determined that an Everede Tool Co. countersink tool with replaceable carbide cutter would produce goood quality countersinks in the graphite material. It should be noted that it is necessary for the countersink cutter to be rotating prior to contact with the graphite to eliminate splintering. Other modifications to the drill foot were made to allow slip renewable bushings to accommodate the production effort in that different diameter drills can be used in any of the drill motor setups. Dagger drills with integral countersink cutters for standard Winslow drill motors have been proofed for use in drilling nutplate rivets. The schematic shown in Figure 70 depicts the system developed for drilling and countersinking holes in graphite epoxy parts.

3.7 Repair Development

This phase of development was directed at the investigation of damage and defects and associated repairs which could occur during processing, machining, assembly and service of the composite aileron. The investigation concluded that the most prevalent defects would be delaminations, interlaminar voids,
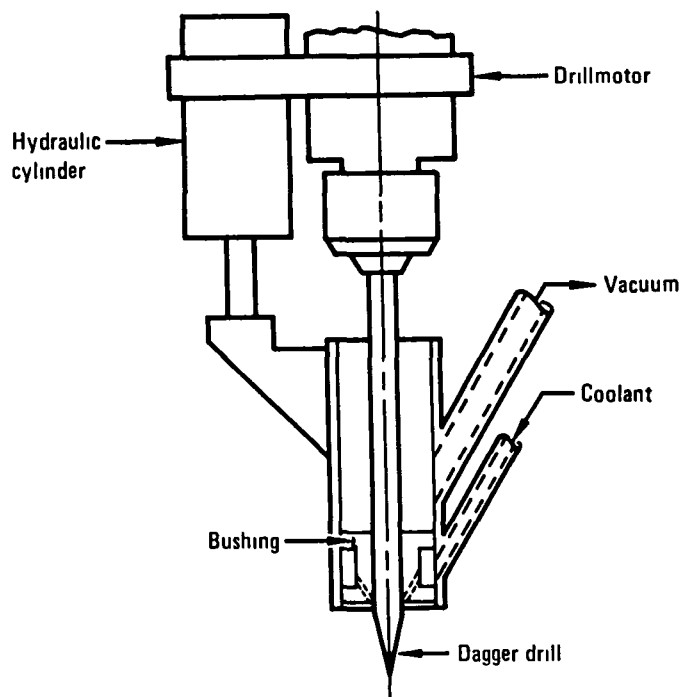
Figure 70. - Drill and countersink system schematic.

104

misdrilled holes and foreign object damage, primarily impact damage. The major effort of the development was directed at: 1) creating known defects, 2) evaluation of repair techniques for the defects, and 3) implementation of the repair techniques. It was decided that laminates representative of the basic cover and the spare containing voids and delaminations caused by impact damage would be the focus of this development. The chosen repair techniques were resin injection into the damage area and both field and shop type repairs.

The impact damage was created by dropping a 0.454 kg (1.0 lb) impactor with a 25.4 mm (1.0 in) hemispherical head on panels that were clamped over a 152.4 mm (6 in) square opening. The test fixture was designed to measure the impact energy level from the impactor drop height. Tests were conducted with an initial impact energy level of 0.68J (0.5 ft-lb) and incrementally increased at 0.68J (0.5 ft-lb) to a final level of 6.8J (5.0 ft-lb). The panels were visually and ultrasonically inspected and the damage area was defined. The levels of impact damage were established as follows: 1) threshold damage, as defined by ultrasonic inspection, but no visible evidence, 2) visible damage on the back surface, and 3) visible damage on the impacted surface. Both the spar and cover laminates required impact energy levels greater than 6.8J (5.0 ft-lb) to consistently produce visible damage to the impacted surface. It was determined that all repairs would be implemented on panels that showed visible damage to the back surface.

Two patch repair techniques were implemented on the basic cover laminate. The field type repair consisted of an aluminum plate mechanically fastened over the damaged area and the shop repair utilized a cocured graphite tape patch.

The field repair was accomplished using the following procedure:

1. Ultrasonic inspect and map the damage area.

2. Remove the damage area using a diamond router bit.

3. Match drill the graphite panel and a 1.27 mm (0.050 in) thick aluminum plate (2024-T3 clad).

4. Mechanically fasten aluminum plate to graphite panel using 3.969 mm (5/32 in) pan head titanium fasteners and stainless steel Hi-Lok collars. (NAS5202 screws and HL94LP-5 collars were used.) All faying surfaces shall have corrosion resistant sealant applied and fasteners shall be wet installed.

5. Fill the cutout damage area with Epon 934 epoxy filler and cure.

The shop repair was accomplished using the following procedure:

1. Ultrasonic inspect and map the damage area.

2. Remove the damage area using a diamond router bit.

3. Fill the cutout damage area with Epon 934 epoxy filler and cure. Sand the filler level, using care not to damage surface fibers.

4. Preply a four ply graphite tape patch (typical both sides of panel). Orientation for patch on the cover laminate is ($0°/45°/135°/90°$). The 0° and 90° plies are pinked on edges perpendicular to fiber direction and the 45° and 135° plies are pinked on all edges. Plies are increased 6.35 mm (.25 in) from bottom to top (typical all edges).

5. Prepare surface to be bonded by lightly abrading with Scotchbrite then clean and degrease with suitable solvent such as MEK.

6. Apply supplemental layer of film adhesive – FM 400 was used – the same size as top ply of graphite tape patch then apply graphite tape patch.

7. One ply each of peel ply and Armalon are applied and tied to vacuum source. The area is then vacuum bagged and cured.

During the implementation of this repair, it was determined that after mixing, the 934 filler should be placed under vacuum to remove air bubbles prior to filling the damage area.

In order to implement the third type of repair, resin injection into the damaged area, the following activities were completed.

● Resin literature survey.

● Resin evaluation.

● Evaluation of the use of pressure and/or vacuum to fill the damage area.

A literature survey was conducted to evaluate resins for this repair development. Two prime considerations in the selection of a resin were low viscosity and ambient cure. Two resins were chosen for evaluation: EA 956 (Hysol) and CG-1304 (REN Plastics). Both are two-part systems (resin and catalyst). When mixed, the EA 956 system has a viscosity of approximately 45 PA's (450 poises) and the CG-1304 system has a viscosity of 4.5 Pa's (45 poises).

During this development, it was determined that the CG-1304 resin had better flow and wetting characteristics than did the EA 956. The most consistent repairs for the basic cover laminate were accomplished using the following procedure:

106

1. Ultrasonic inspect and map the damage area.

2. Drill a 3.264 mm (#30) hole into the center of the damage area from the front surface. The hole depth should extend through the syntactic ply; however, the drill tip should stop 0.127/0.254 mm (0.005/0.010 in) before exiting through the back side.

3. Two 2.489 mm (#40) holes were drilled into the damage area, approximately as shown in figure 71.

4. On the back side of the damage, apply a piece of Tedlar film approximately 12.7 mm (0.50 in) larger than the visible damage in each direction, held in place by a piece of aluminum tape extending 6.35 mm (0.25 in) past the Tedlar film.

5. Position the vacuum chuck over the damage area. The syringe used is a Biggs #10 disposable type. The vacuum drawn on the vacuum port of the chuck is 254 to 381 mm Hg (10 to 15 in Hg). The resin is injected into the resin port of the chuck using the syringe. When the syringe has been emptied, the damage area is filled. The vacuum source is removed prior to removing the syringe from the resin port. The resin is then allowed to cure. The complete setup for this resin injection repair technique is shown in figure 72.
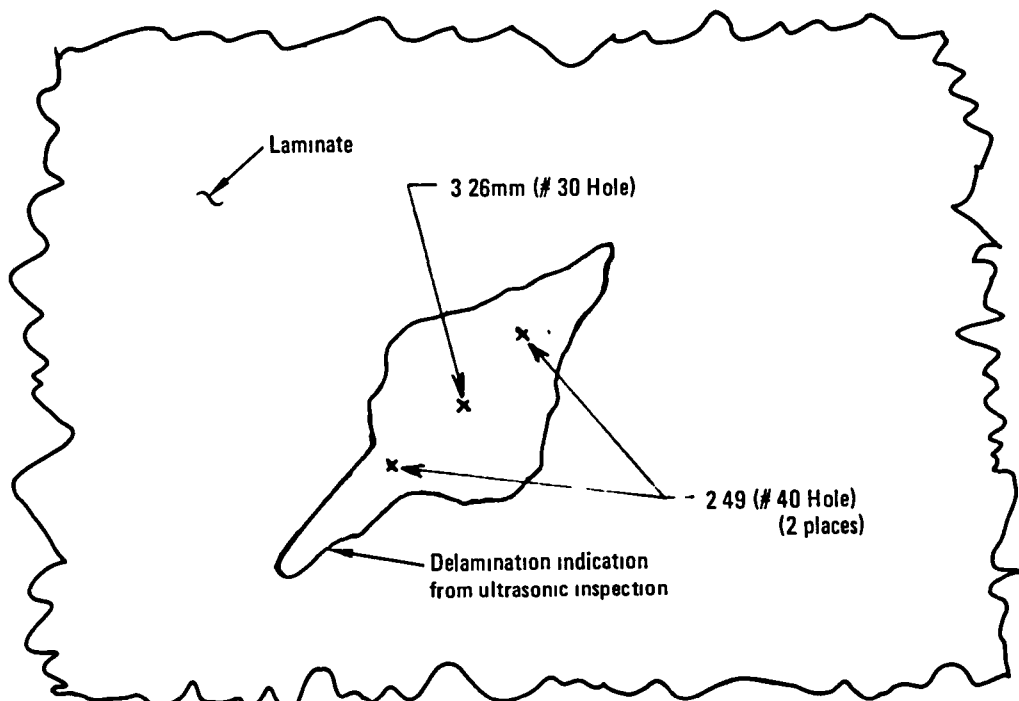
Figure 71. - Typical impact damage area showing holes required for repair.
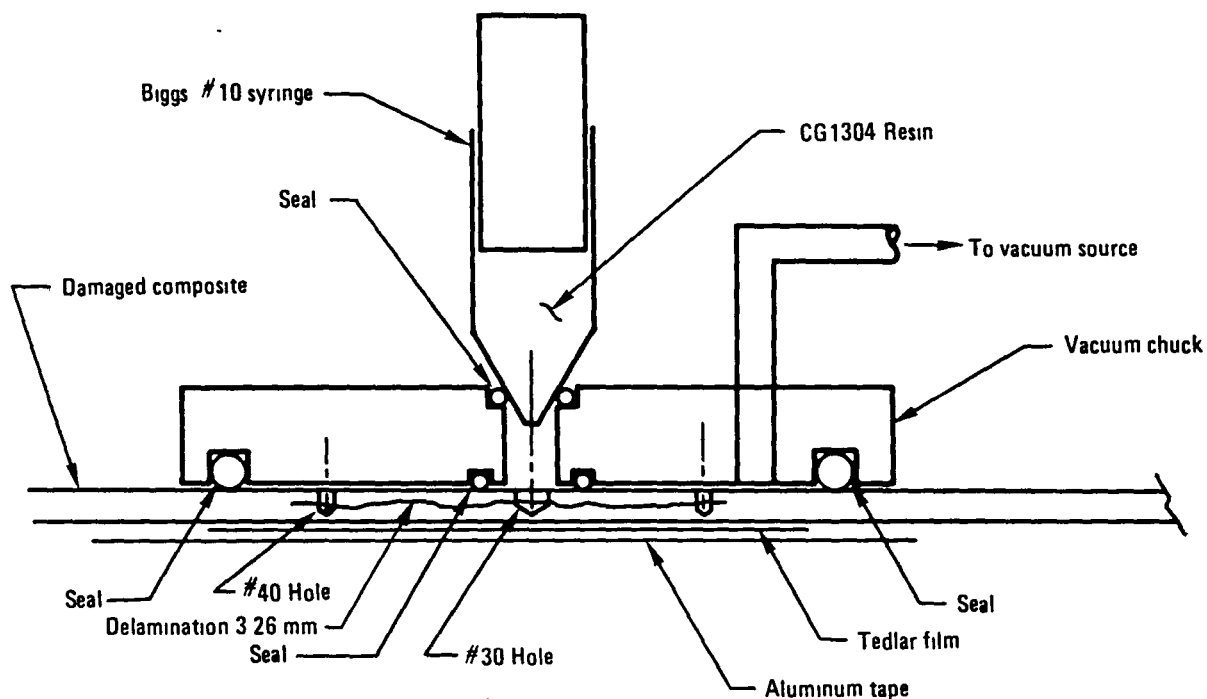
Figure 72. – Resin injection repair setup.

4. CONCEPT VERIFICATION TESTS

The objectives of the concept verification tests were to verify the integrity of critical structural elements or subcomponents and to substantiate the applicable structural analysis. The design details addressed by these tests include the following: static tests of the cover, rib, spar, and rib/spar/fitting; fail-safe tests of the cover and fatigue/residual strength tests of the spar and rib/spar/fitting; a sonic fatigue test of the aileron assembly; and lightning strike tests of the aileron assembly. The lightning tests are discussed in section 1.4.4 of this report. Additional objectives included verifying the shear stiffness of the cover and the buckling behavior of the rib. All tests were conducted under ambient conditions.

4.1 Cover

4.1.1 <u>Test Objectives.</u> - The objectives of this test were to verify the structural integrity of details of the cover design concept, to verify the predicted shear stiffness of the cover, and to verify its fail-safe characteristics

4.1.2 <u>Test specimen.</u> - The test specimen was a 736.6 mm (29 in) by 1016 mm (40 in) section of the lower cover representative of the area at the intersection of the front spar and main ribs.

4.1.3 <u>Test setup and instrumentation.</u> - The panel was installed in a specially designed fixture installed in the Universal Test Frame, which provided the basic reaction to the hydraulic loading actuators, specimen support and flexure support systems. The panel was instrumented with 12 rosette gages in 6 back-to-back locations. These rosette gages are shown schematically in figure 73. Four deflection transducers were installed to measure the shear deflection along the P_A axis of loading, the deflection along P_D axis and the out-of-plane deflection of the panel bay due to buckling.

4.1.4 <u>Test loads and results.</u> - The following loads (with percentage of design loads indicated) were applied to the specimen.

Test 1. Shear Stiffness

P_A = +41.8kN (+9400 lb) (100 percent ultimate)

Test 2. Combined Shear/Spanwise Tension

P_A = +46.0kN (+10,340 lb) (110 percent ultimate)

P_D = +26.9kN (+6050) (110 percent ultimate)

Test 3. Spanwise Compression

P_D = -28.5kN (6400 lb) (100 percent ultimate)

Test 4. Combined Shear/Spanwise Compression

P_A + 41.8kN (+9400 lb) (100 percent ultimate)

P_D = -28.5kN (-6400 lb) (100 percent ultimate)
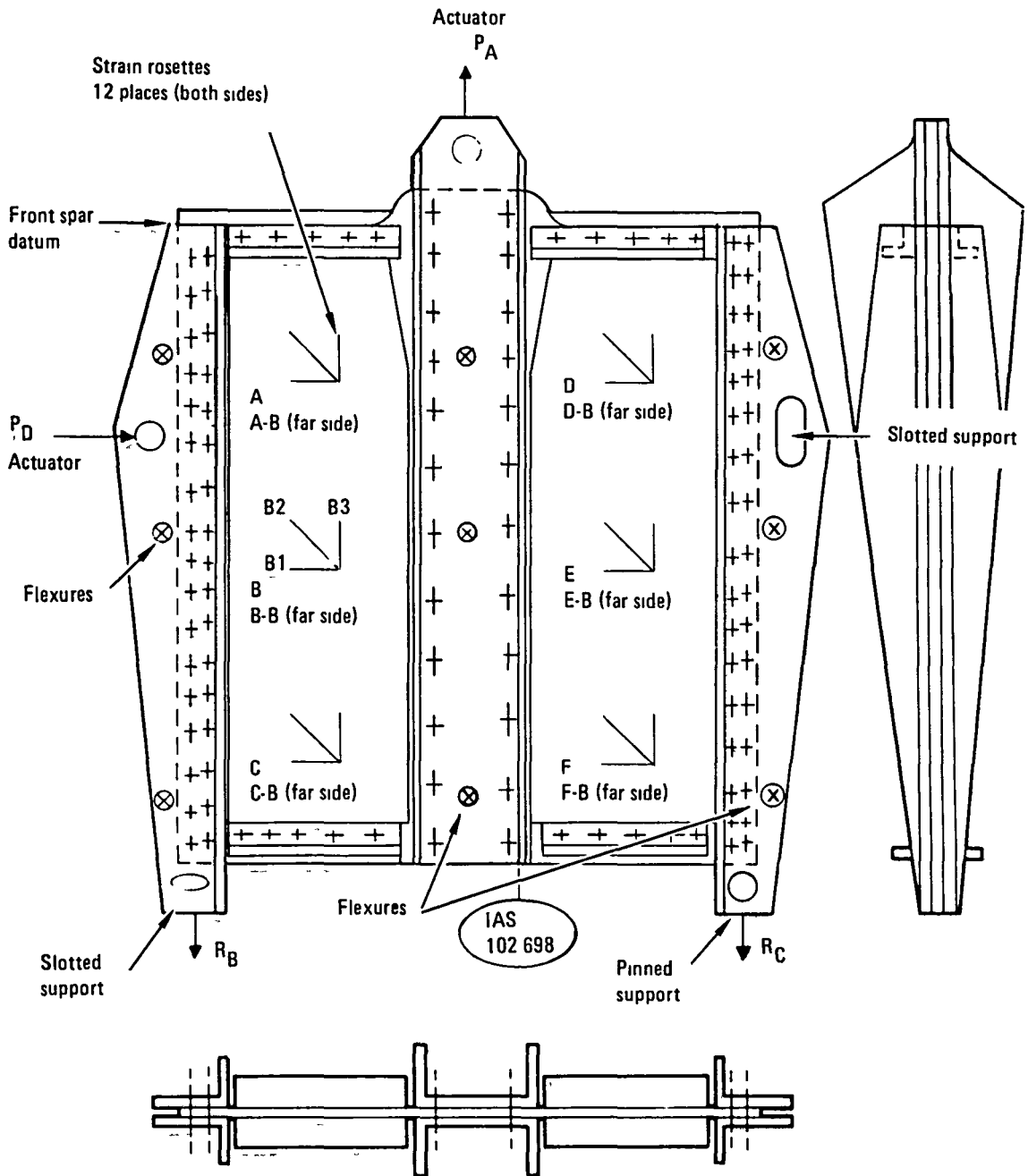
Figure 73. – Cover test configuration and strain gage schematic.

Test 5 Fail-Safe Test

A 305 mm (12 in) long line was drawn on the cover of approximately 45° extending from the intersection of the front spar and main rib doublers at IAS 109 to the IAS 117.4 rib doubler. A 76 mm (3.0 in) cut was made in the middle of this line and the limit loads shown below were applied. The cut was successively lengthened to 152, 229, and 305 mm (6, 9, and 12 in) after each application of limit load. The vector of the loads is approximately normal to the cut causing maximum crack opening displacement.

P_A = 28.0kN (+6300 lb) (100 percent limit)

P_D = 16.5kN (+3700 lb) (100 percent limit)

With the 305 mm (12 in) cut the loads were raised to the following:

P_A = 48.0kN (+10,800 lb) (115 percent ultimate)

P_D = 27.6kN (+6200 lb) (113 percent ultimate)

The results of the shear stiffness test are shown on figures 74 through 77. Figure 74 shows typical element strains for rosette B. Figures 75 through 77 show the maximum shear component of the analysis of the four rosettes at each chordwise location together with the predicted shear strain. The predicted shear strain is based on a finite element analysis of the test configuration. The test panel stiffness averaged 8 percent greater than the predicted stiffness.

Possible environmental effects on the cover strength were accounted for by increasing test loads to approximately 110 percent of design ultimate load. The panel sustained all of these loads without evidence of failure or observable damage.

The fail-safe evaluation consisted of applying limit load to the panel with a cut lengthened successively from 76 to 305 mm (3 to 12 in) in length. The load vector applied crack-opening displacement to the cut. With the 305 mm (12 in) cut the load was increased to 169 percent of design limit load. The panel sustained all of these loads without evidence of failure or observable damage (or damage growth). It is consequently concluded that the design has post damaged strength well beyond design requirements.

This test verified the structural integrity of the details of the design concept, the predicted shear strength, and the fail-safe characteristics.
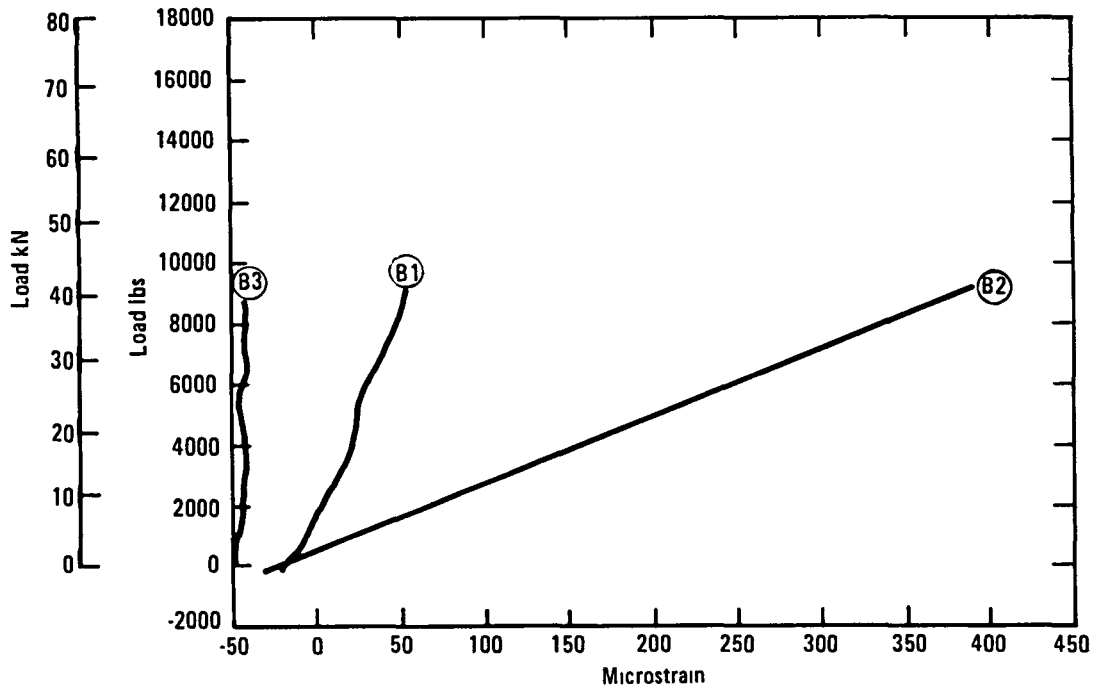
Figure 74. Rosette gage analysis – Typical strains for rosette B (see figure 73).
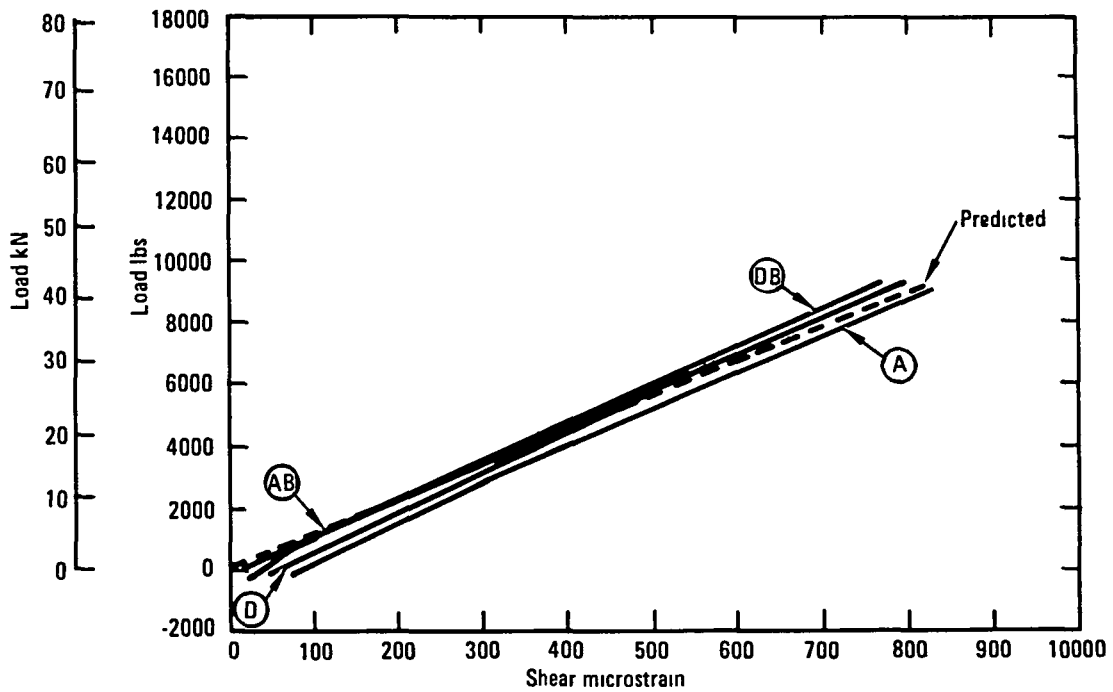
Figure 75   Rosette gage analysis – maximum test and predicted shear strains for rosettes A, A-B, D, and D-B (see figure 73).
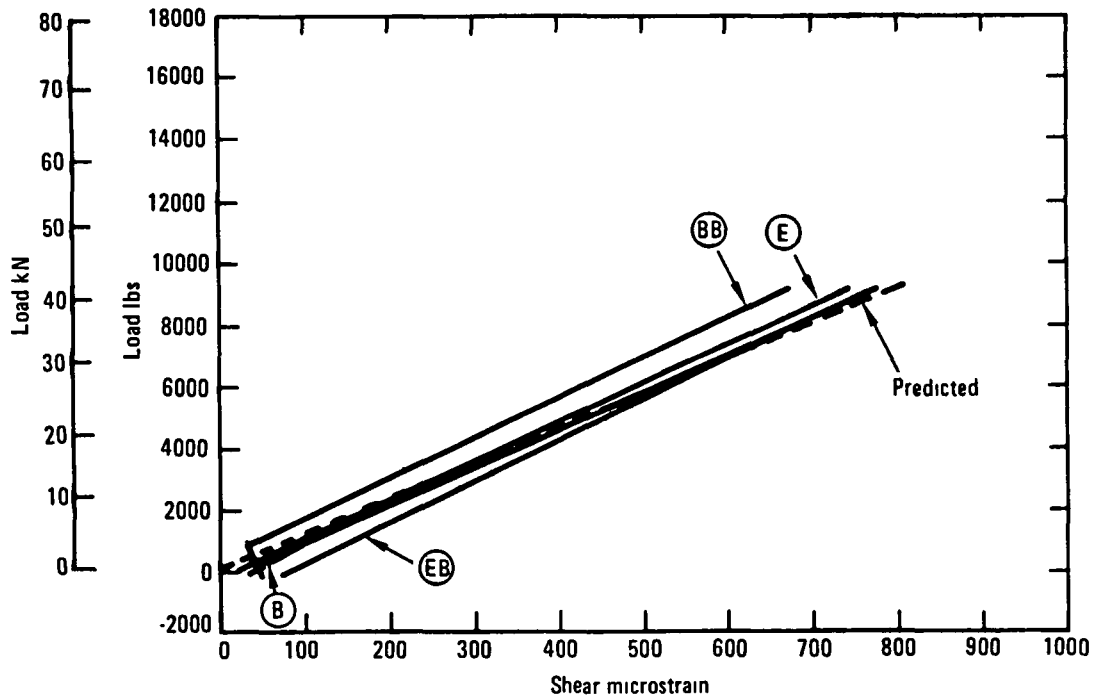
Figure 76. – Rosette gage analysis – maximum test and predicted shear
strains for rosettes B, B-B, E, and E-B (see figure 73).
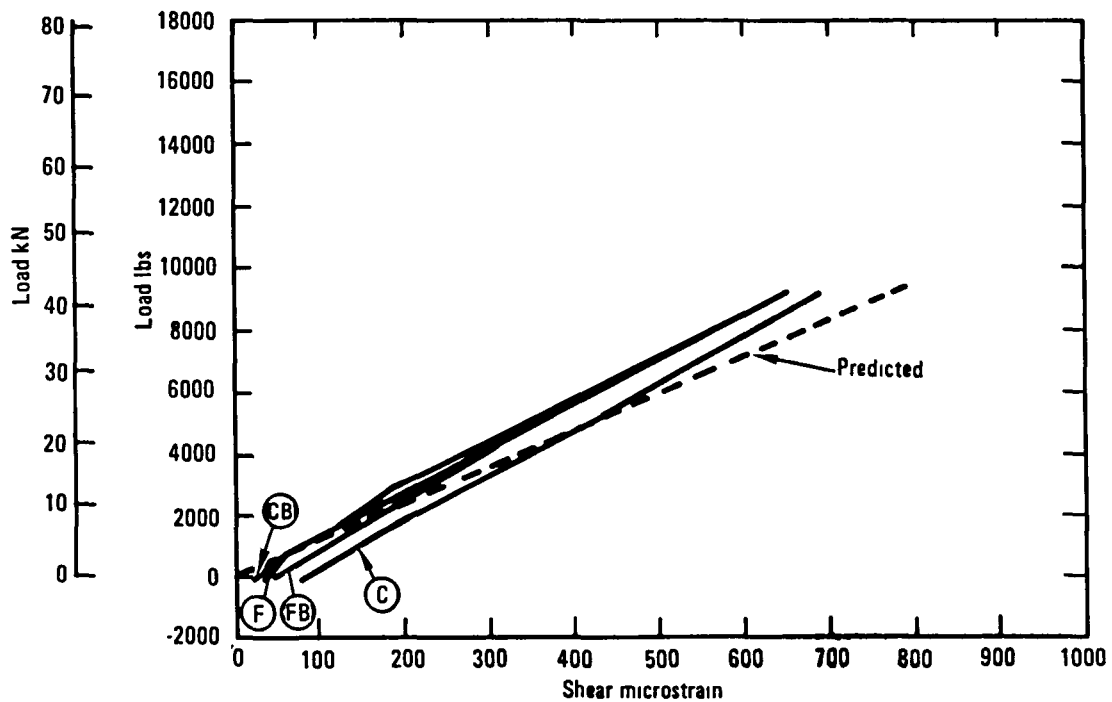
Figure 77. – Rosette gage analysis – maximum test and predicted shear
strains for rosettes C, C-B, F, and F-B (see figure 73).

4.2 Intermediate Rib Web

4.2.1 <u>Test Objectives</u>. - The objectives of this test were to verify the structural integrity of the intermediate rib design concept and to verify its predicted initial buckling and postbuckling strength.

4.2.2 <u>Test specimen</u>. - The test specimen consisted of the forward portion of an intermediate rib web containing a flanged lightening hole.

4.2.3 <u>Test setup and instrumentation</u>. - The test setup is shown in figure 78. The panel was installed in a specially designed shear frame, and this assembly was installed in a Baldwin Static Test Machine. The test rib was instrumented with four (4) rosette gages and eight (8) single axial-type strain gages. The rosette gages were mounted back-to-back to two locations. The 8 axial gages were mounted back-to-back in four places around the periphery of the lightening hole located in the middle of the rib. These gages were installed as shown schematically in figure 79.

4.2.4 <u>Test loads and results</u>. - The design limit and ultimate loads are shown on table 41. The test specimen was installed in a 400K Baldwin Static Test Machine. The specimen was loaded in tension and the axes of loading changed to reproduce the desired shear flows in the specimen. This was accomplished during the first three runs, alternately loading the long axis and the short axis of the rib part.
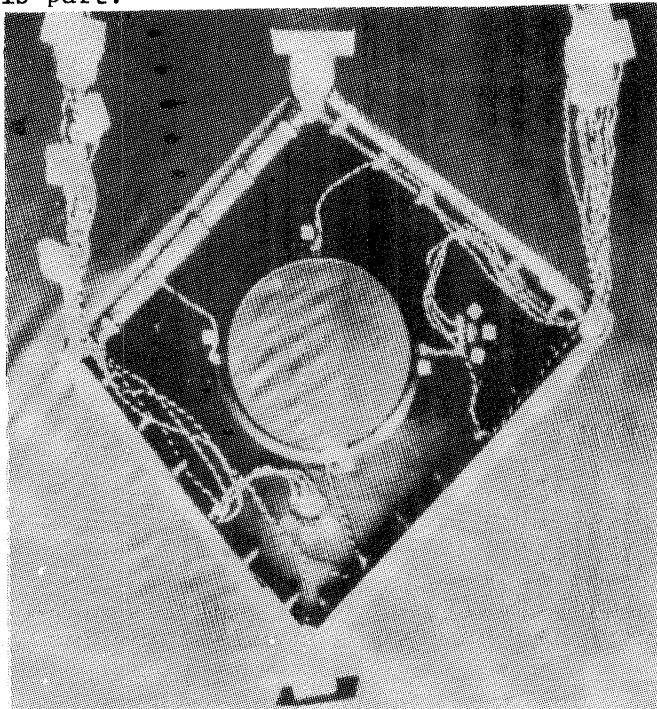
Figure 78. - Rib test specimen.

114
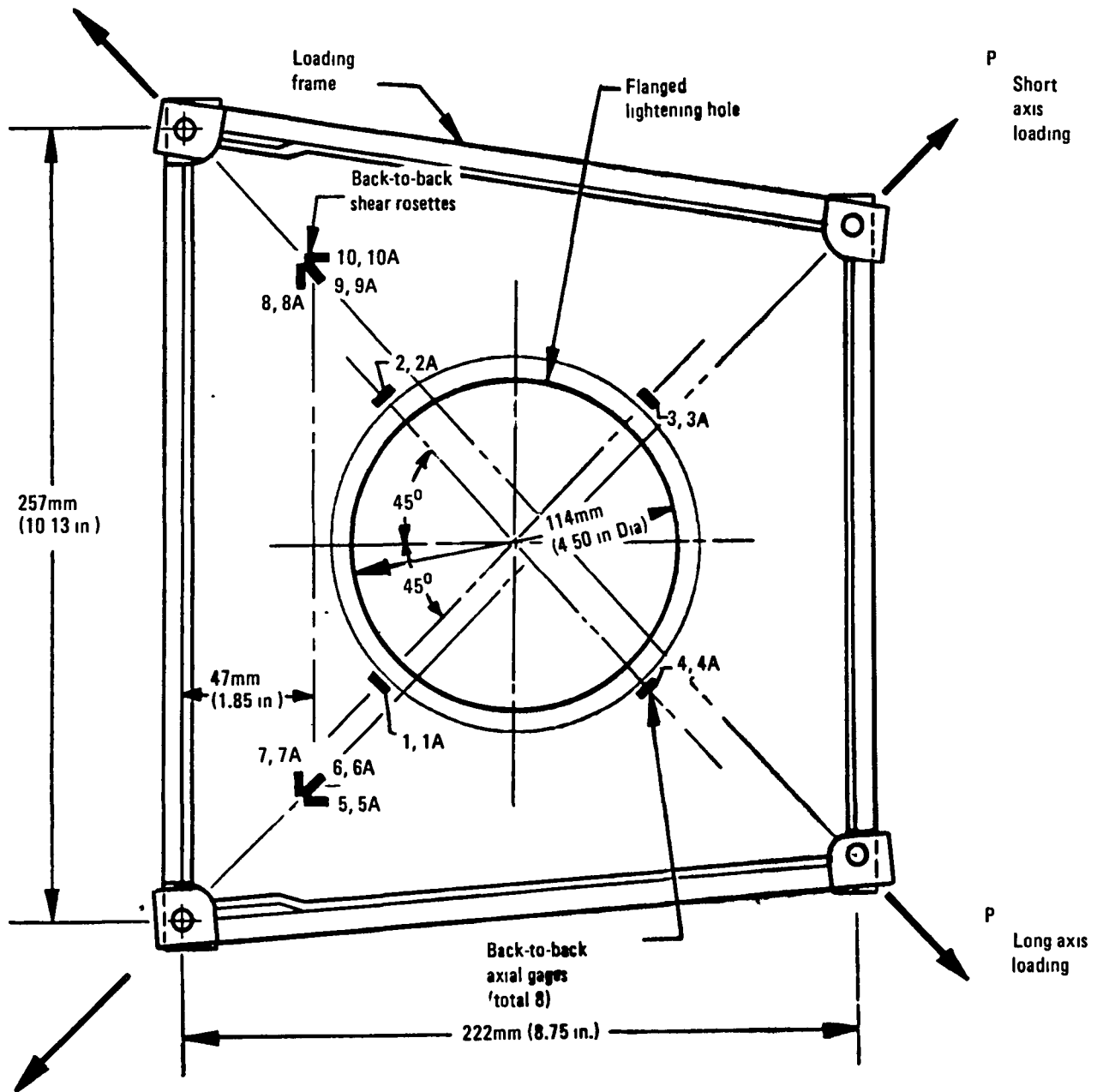
Figure 79. – Rib test configuration and strain gage schematic

TABLE 41. - RIB TEST CONDITIONS AND LOADS

Test or Loading Condition	Max. Load/Remarks	
I. Tension along the long axis, limit load	+4 890 N	+1 100 lbs
II. Tension along the short axis, limit load	+4 890 N	+1 100 lbs
III. Tension along the short axis, ultimate load	+7 340 N	+1 650 lbs
IV. Tension along the short axis, failing load	+20 910 N	+4 700 lbs Specimen failure

The maximum design ultimate shear flow of 22.8kN-m (130 lb/in) on an intermediate rib corresponds to a diagonal load on the specimen of 7340N (1650 lb). The initial buckling was predicted to be 8010N (1800 lb), and collapse was predicted at 20460N (4600 lb).

The final test consisted of loading in tension along the short axis up to design ultimate load and then to failure. Failure occurred at 20910N (4700 lbs). Initial failure occurred at 20020N (4500 lbs) with a drop-off in load. Loading of the specimen continued, and the specimen picked up additional load until the final rupture at 20910N (4700 lb). The rib failure is shown in figure 80. Typical strain gage data are presented in figures 81 through 84.

This test verified the structural integrity of the design concept and the initial buckling and postbuckling strength predictions.
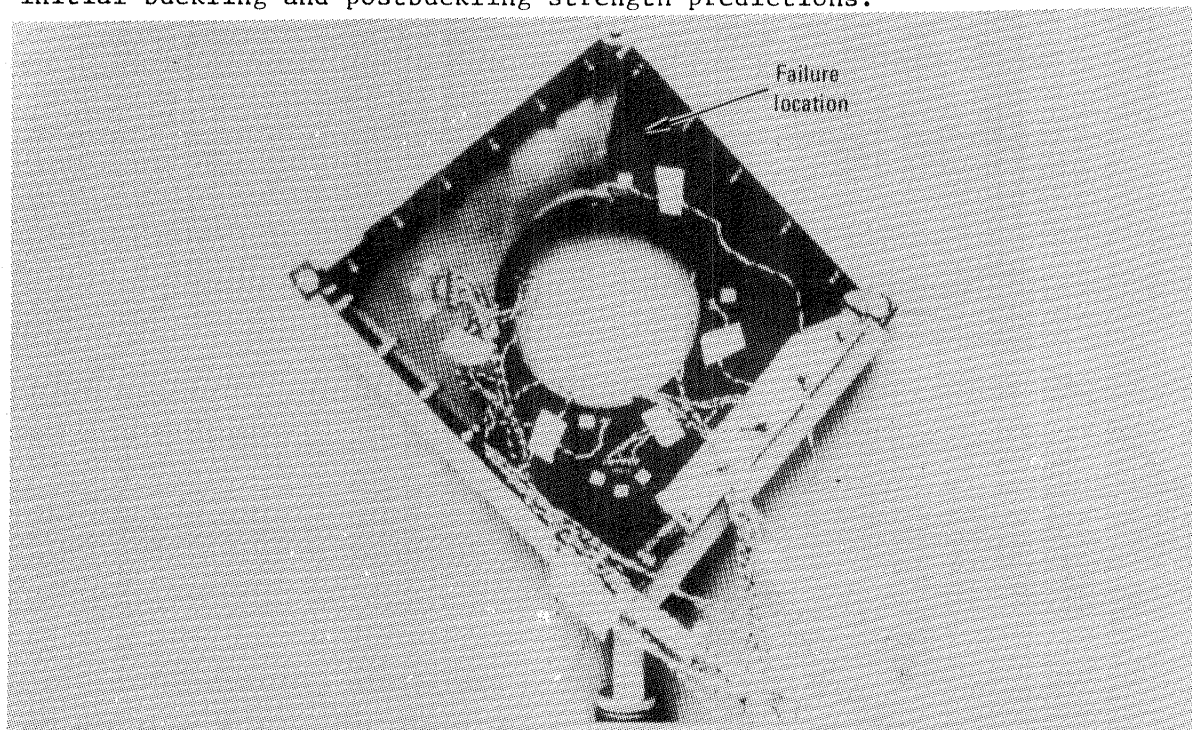
Figure 80. - Compression buckling failure of the rib web.
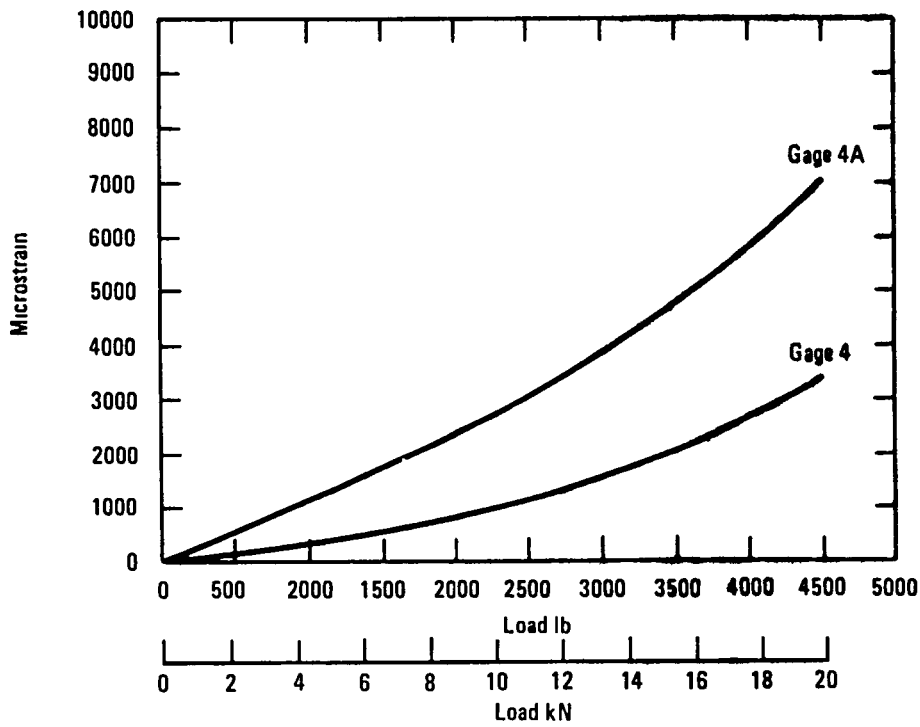
Figure 81. - Test Condition IV (see table 4), strain
gages 4 and 4A (see figure 79).
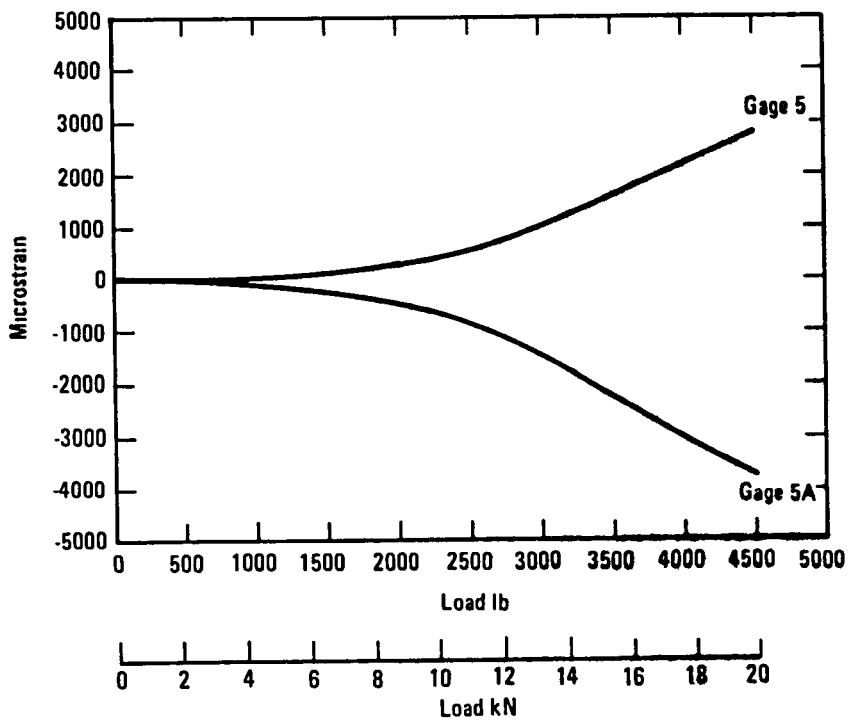
Figure 82. - Test Condition IV (see table 4), strain
gages 5 and 5A (see figure 79).

117
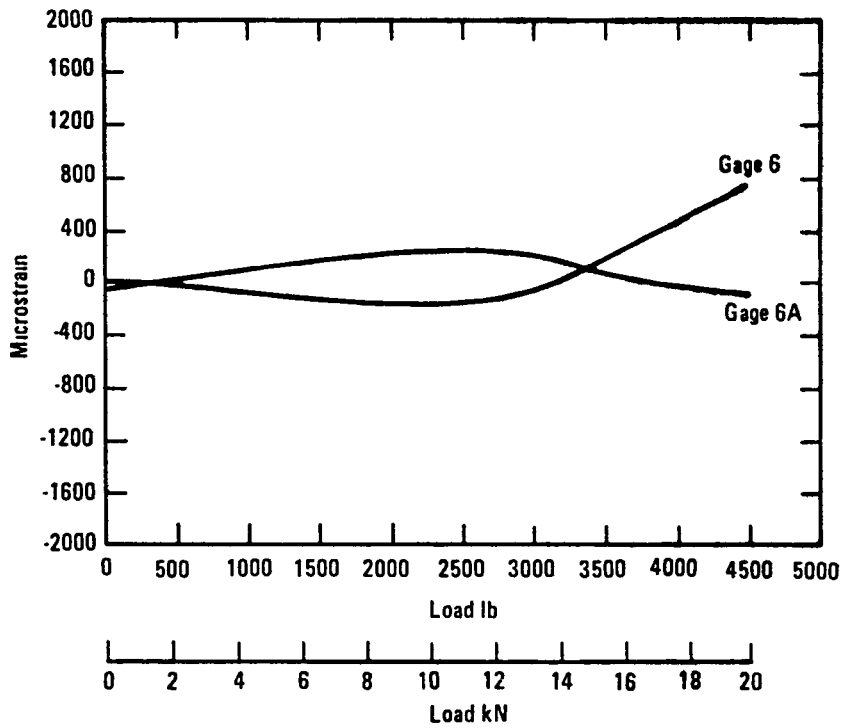
Figure 83. - Test Condition IV (see table 4), strain
gages 6 and 6A (see figure 79).
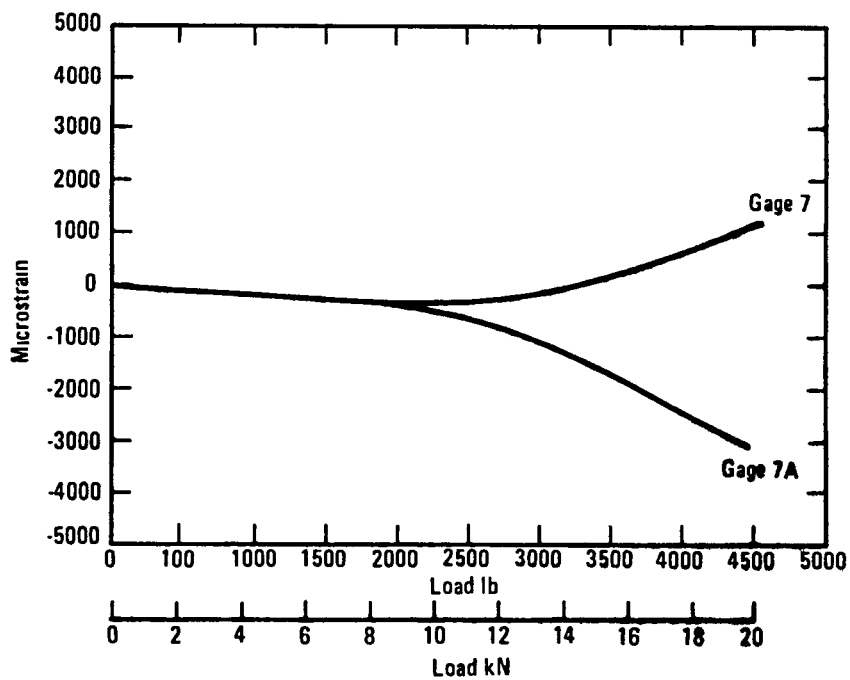
Figure 84. - Test Condition IV (see table 4), strain
gages 7 and 7A (see figure 79).

118

4.3 Front Spar

4.3.1 <u>Test Objectives</u>. - The objectives of this test were to verify the structural integrity of the front spar design concept both statically and in spectrum fatigue loading and to verify the predicted failure strength and failure mode.

4.3.2 <u>Test specimen</u>. - The two front spar test specimens consisted of full scale sections of the spar assembly and sections of the upper and lower covers.

4.3.3 <u>Test setup and instrumentation</u>. - A special loading beam was used to apply the loads to the IAS 102.7 and 107.1 actuator fittings. The loading beam is shown schematically in figure 85. The test specimen was assembled into a test reaction structure shown in figure 86. For the spar cap critical loading condition, a down-loading was applied at IAS 102.98 (Reference Point A). For the spar web shear flow critical condition, the hydraulic actuator was changed over to apply an up-load at IAS 93.81 (Reference Point B).

The test specimen was installed with ten axial type and two rosette type strain gages. These gages were installed as shown schematically in figure 87. In addition, three deflection gages were installed at IAS 80.36, 102.70 and 115.76 to measure front spar deflections during the tests. A load cell placed in series with the hydraulic loading actuator was used to control and monitor the applied loads during the test condition.

4.3.4 <u>Test loads and results</u>. - After completing the installation of the first test specimen, the loading actuator was set up to apply a design ultimate load condition critical for the spar caps at IAS 102.98 (Reference Point A) on the loading beam. The magnitude of the ultimate test download was -18.9kN (-4240 lb) which included a 23 percent environmental factor over design ultimate load. The test was conducted to -19.0kN (-4273 lb) with no evidence of failure. The resultant load/strain rsponses for the spar caps at IAS 97.0 for this test condition are shown on figures 88 through 91. This specimen was inadvertently damaged in a subsequent test as a result of a test fixture deficiency.

For the upload condition, a second specimen was installed in the fixture and the hydraulic loading actuator was changed over to apply a positive loading on the beam at IAS 93.81 (Reference Point B). The loading at Point B on the loading beam produces a reaction couple loading at the IAS 102.7 and 107.1 actuator fittings. This loading condition results in the maximum shear flows in the aileron front spar web between the two fittings. Spectrum fatigue testing was conducted for two lifetimes (72,000 flights) without evidence of structural degradation. Load/strain surveys were conducted after each lifetime of testing.
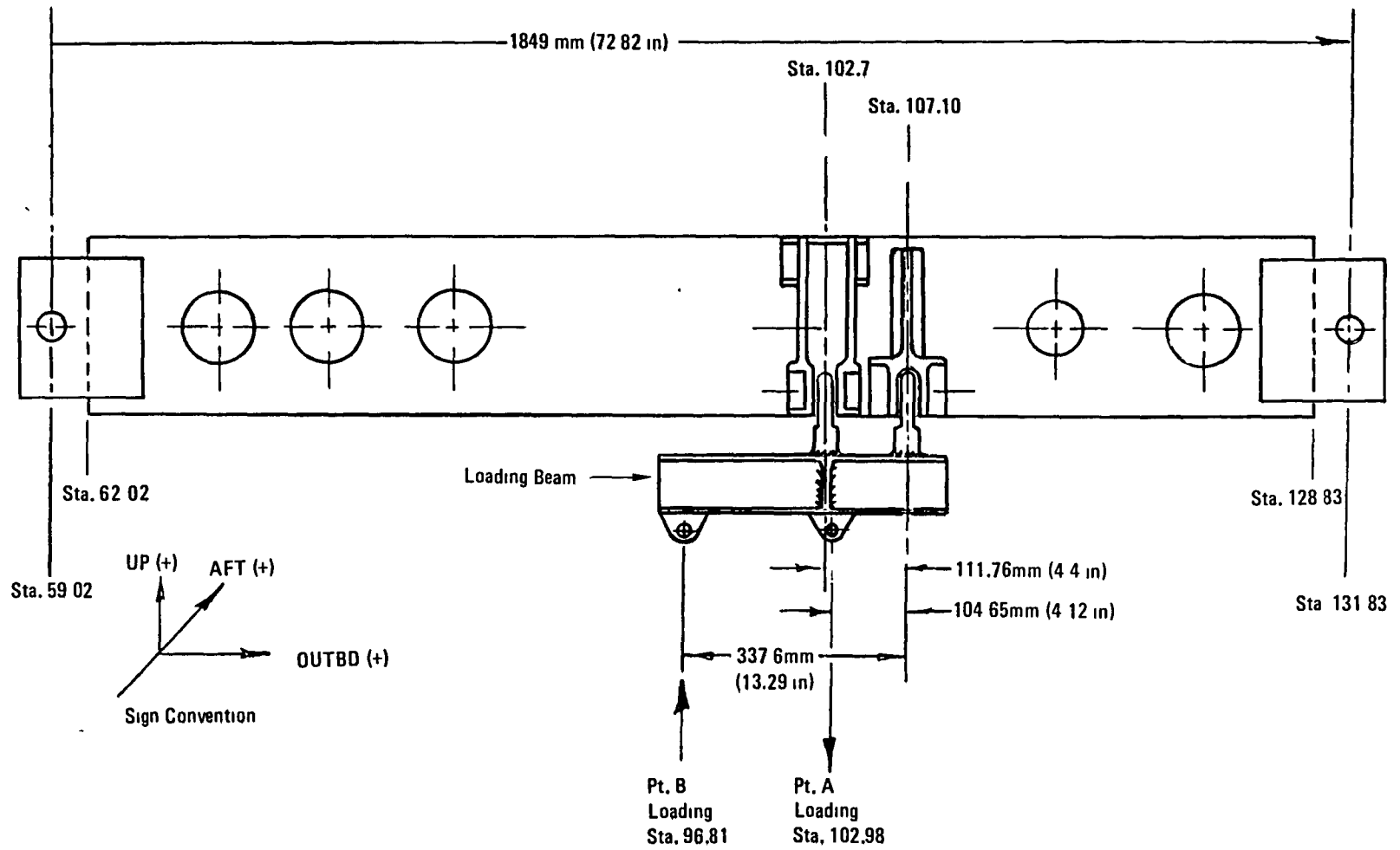
Figure 85. – Front spar loading beam schematic.
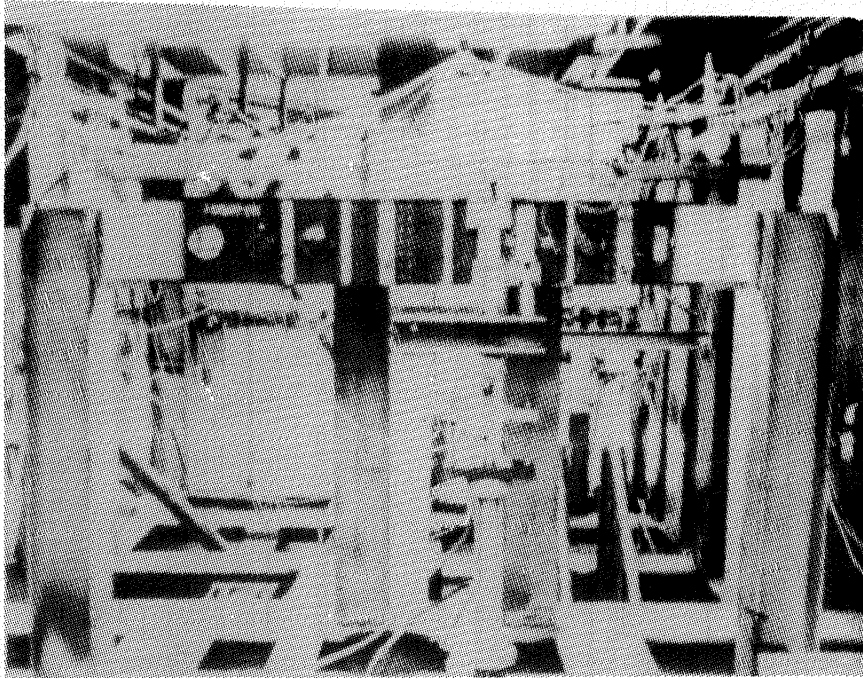
Figure 86. - Aileron front spar test setup.

After completion of the fatigue testing, the test specimen was loaded at Point B on the loading beam until a failure occurred at an upload of 30.9kN (6952 lb). The front spar failed in a buckling mode in the lower beam cap and spar web at approximately IAS 95.0.

The finite element analysis shows that the highest lamina strain occurs in the front spar web at IAS 105. Since the initial estimate of the notched tension strain allowable was 5000 microstrain, failure was predicted at 169% D.U.L. or 28.9kN (6500 lb) for the upload test condition.

The failure load represents 182 percent of design ultimate load (147 percent of ultimate test load) for the critical shear flow and spar bending condition. Figure 92 shows the local web failures from the forward spar web face. Figure 93 shows the lower cover failure.

Initial failure was caused by the local compression buckling instability in the cover/spar cap flanges. Initial buckling occurred at approximately 28.9kN (6500 lb) of loading in Point B as determined by the cover and spar cap strain gages, Numbers 3 and 4, located adjacent to the failure origin (see figure 94). Rosette B at IAS 105.3 (figure 95) showed that in the 45° direction, the strain reached 5460 microstrain which is near the initial estimate of the allowable for this complex loading region.

This test verified the structural integrity of the design concept for both static and fatigue loading. However, the failure strength was higher and the failure mode was different than predicted.

121

7 Outside cover

DEFL ▽

8 Inside cap

DEFL ▽

5 Outside cover

6 Inside cap

DEFL ▽

Ç Fasteners

Inboard aileron stations ⟶

80 36

Web face

110 0   115 76

102 7

Top surface

97 0   105 3

Outboard ⟶

16 15 14 13 12 11

B   A

Lower surface

Rosettes on fwd web face

9 Aft
10 Fwd

9

10

Fwd

Web face

Ç Fasteners

3 Outside cover

1 Outside cover

4 Inside cap

2 Inside cap
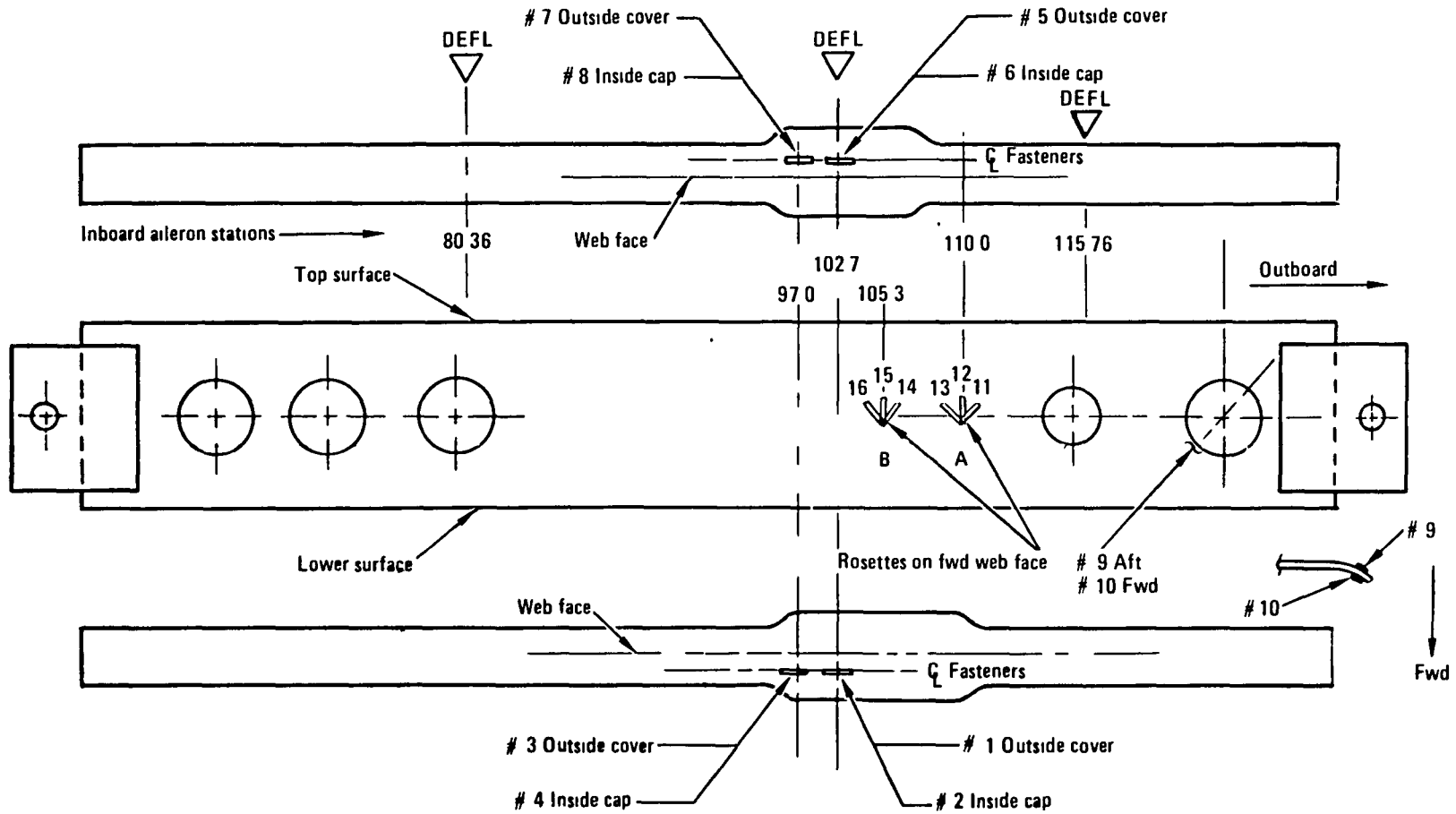
Figure 87. – Spar strain gage locations and identification.
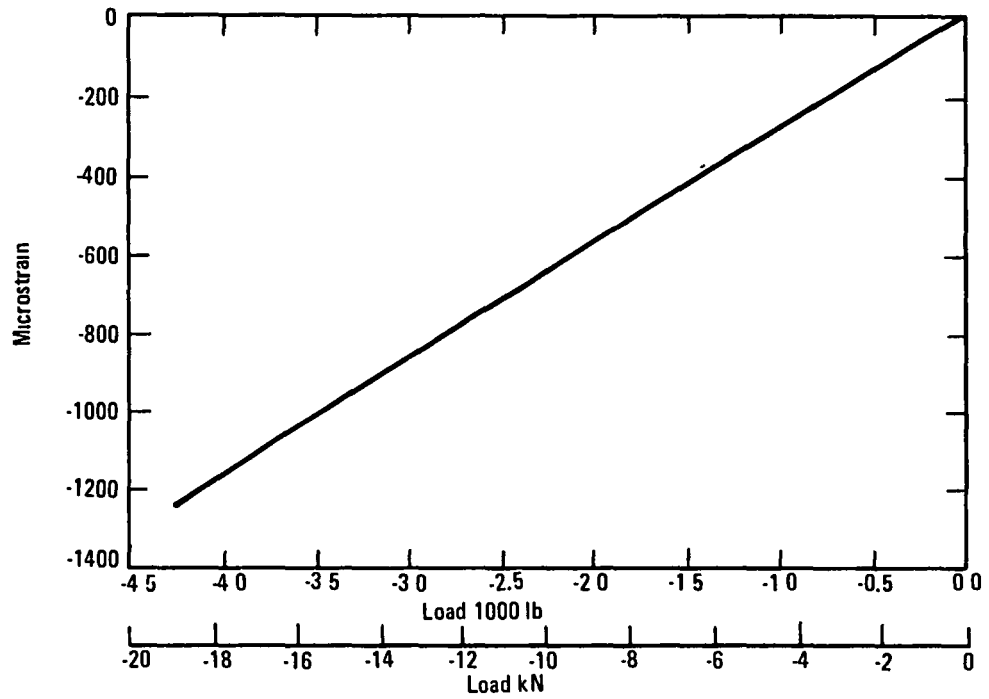
Figure 88. – Load versus strain for spar cap, download, strain gage 8 (see figure 87).
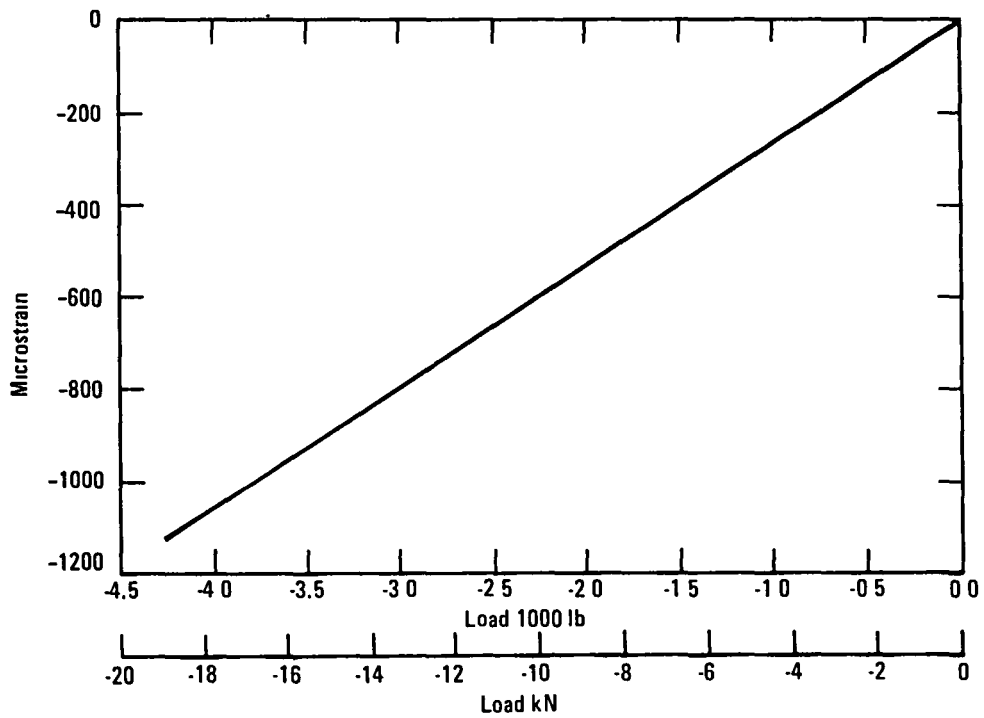
Figure 89. – Load versus strain for spar cap, download, strain gage 7 (see figure 87).
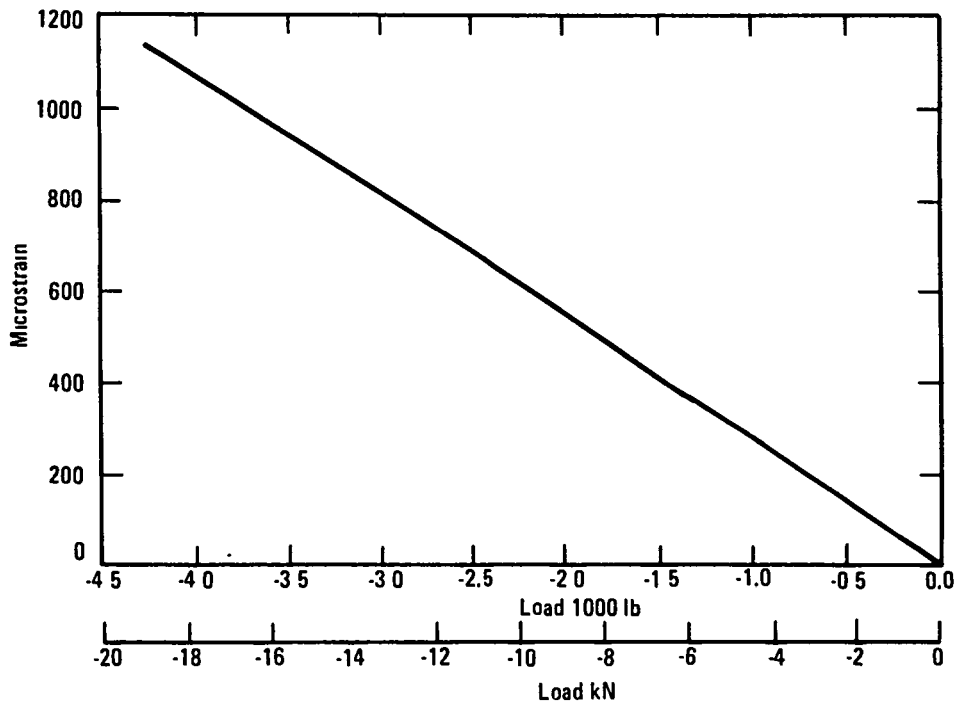
Figure 90. – Load versus strain for spar cap, download, strain gage 4 (see figure 87).
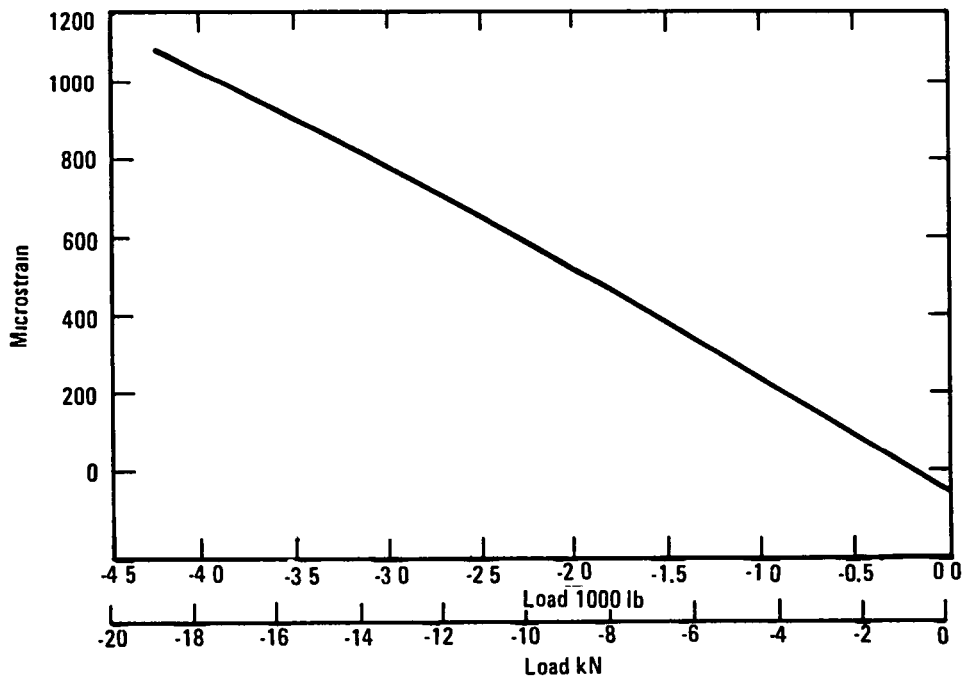
Figure 91. – Load versus strain for spar cap, download, strain gage 3 (see figure 87).
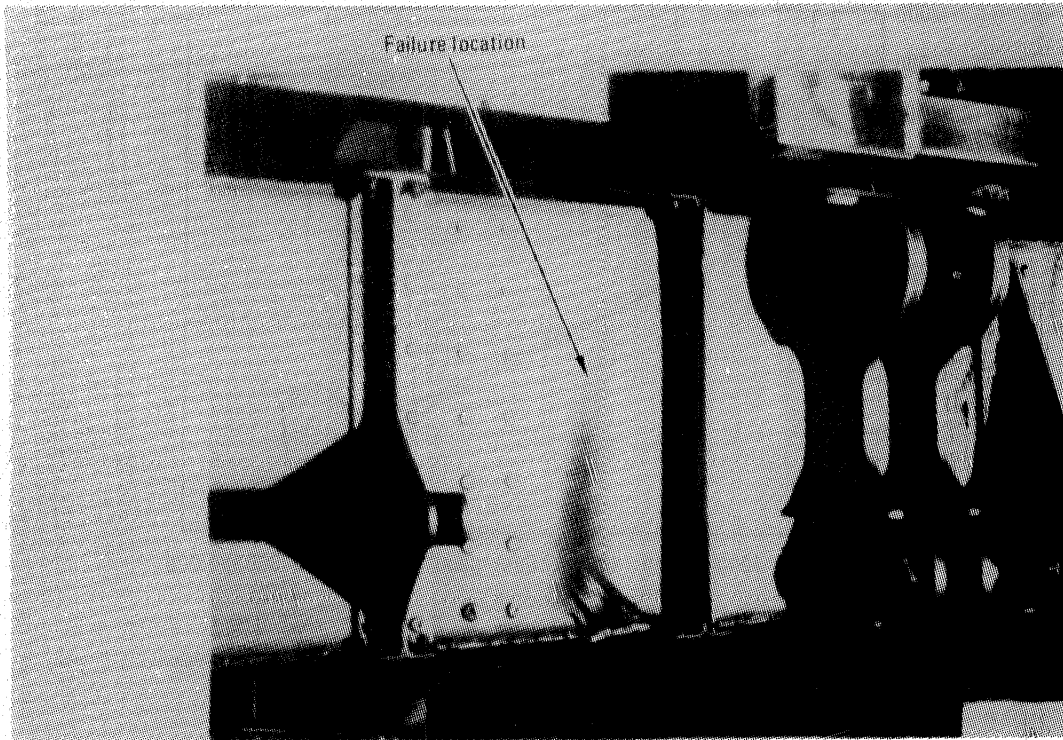
Figure 92. - Forward web face and spar cap/cover failure showing extent of buckling damage.
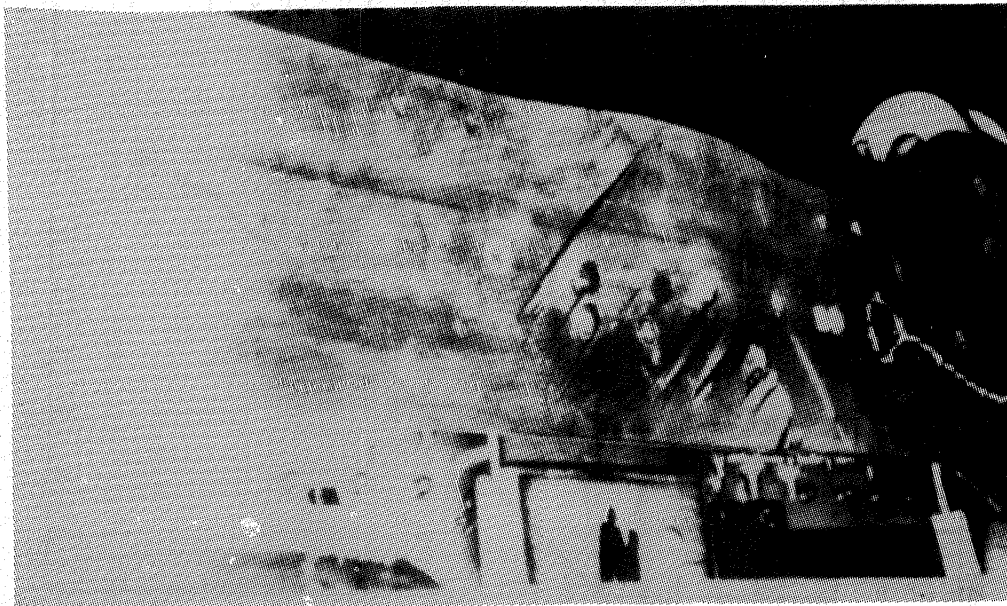
Figure 93. - Cover delamination and ply pulloff from around fastener heads.

125
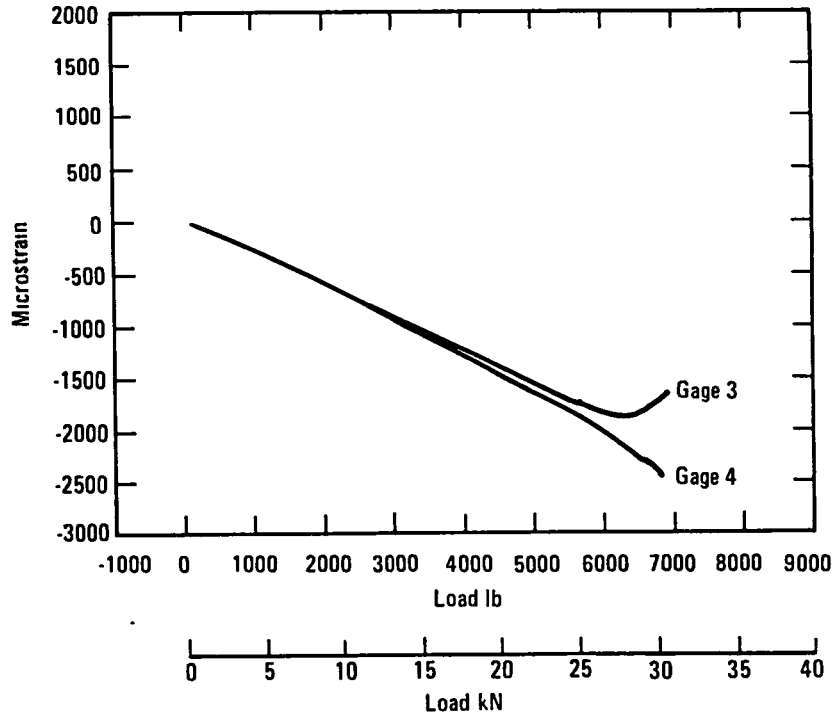
Figure 94. - Back-to-back axial gage data for lower spar cap and cover (see figure 87).
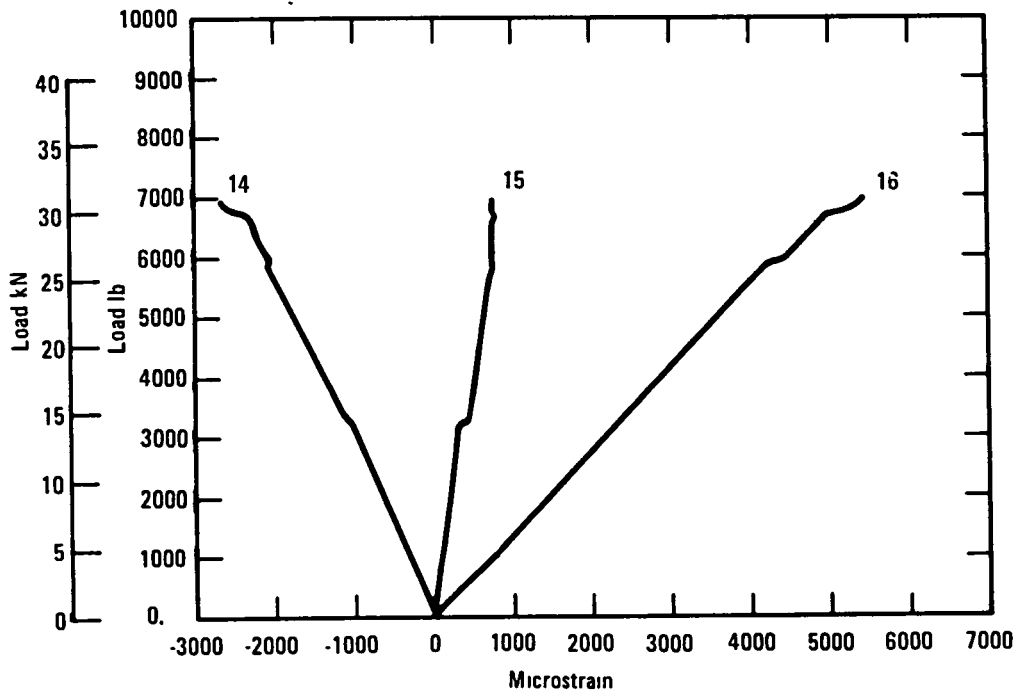
Figure 95. - Rosette gage analysis front spar forward web face (see figure 87).

4.4 Rib/Spar/Fitting

4.4.1 Test Objectives. - The objectives of this test were to verify the structural integrity of the design concept for transfering the hinge/actuator loads into the structure both statically and in spectrum fatigue loading and to verify predicted failure strength and failure modes.

4.4.2 Test specimen. - The rib/spar specimen consisted of the front spar/main rib intersection including sections of the upper and lower covers and the hinge actuator fitting. Two specimens were tested.

4.4.3 Test setup and instrumentation. - The specimen was assembled into a special loading fixture and then installed in the Baldwin 300 Kip Static Test Machine for the loading. This installation is shown in figure 96.
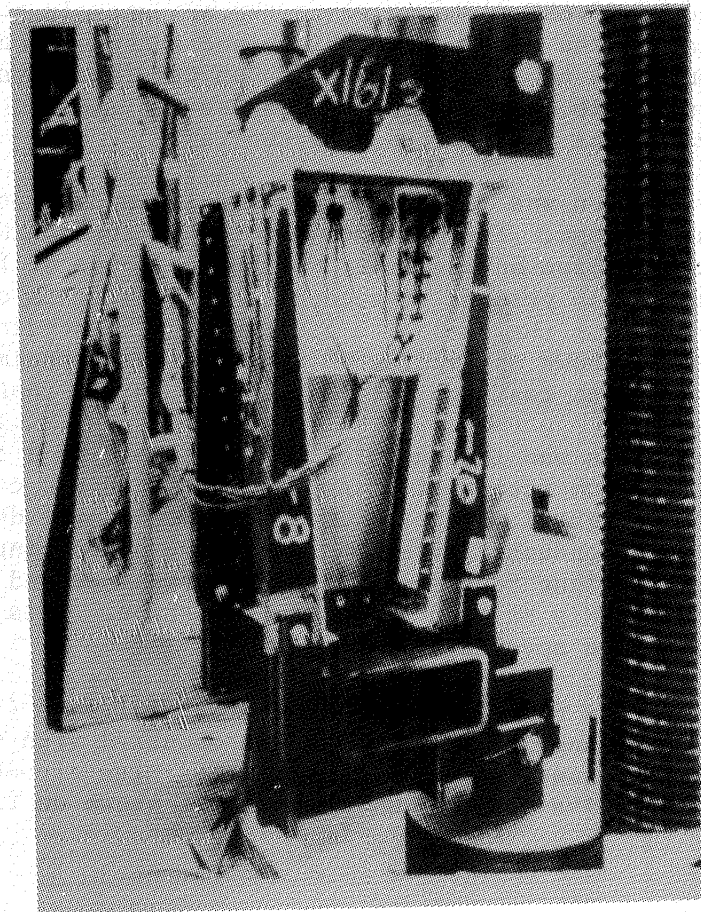
Figure 96. - Rib/spar fitting test setup.

Each test specimen was instrumented with five (5) rosette type strain gages and ten (10) axial-type strain gages. The gage installation is shown schematically in figure 97. A deflection gage was placed in parallel to the loading axis to measure overall travel. A load cell was used in the series with the test specimen to provide the loading reference for the strain gage rosette analysis.

4.4.4 <u>Test loads and results</u>. - The test loads were designed to duplicate the component of load normal to the front spar datum plane from the hinge and actuator loads at IAS 102.7. The loads were introduced to the hinge and actuator lugs through a lever whose length was such as to apply the correct proportion of load to each lug. A compressive load of 61.2kN (13,759 lb) applied to the lever applied the design ultimate compressive load to the hinge lug of 121.2kN (27,256 lb) and the design ultimate tensile load to the actuator lug of 60.0kN (13,487 lb). These loads represented design ultimate Condition 4, 12° down aileron. To simulate the Condition 2, 12° up aileron design ultimate loads, a tensile load of 60.9kN (13,685 lb), applied to the lever was required. This applied a tensile load of 120.5kN (27,089 lb) to the hinge lugs and a compressive load of 59.6kN (13,404 lb) to the actuator lugs. Note that in the aileron installation the component of hinge and actuator loads parallel to the front spar datum tends to relieve the loads on the fasteners attaching the fitting to the spar/rib. Since these loads are not applied in this test, this test is conservative as regards these fasteners.

The first specimen was installed in the Baldwin 300K Static Test Machine for the compression test. The specimen was loaded to 66.9kN (15,047 lb) (load cell reading) compression on the lever without evidence of failure. This load included a factor of 10 percent to account for the effects of adverse environment on the strength of the composite structure. The strain gage records for the upper cover are shown on figures 98 and 99. This specimen was inadvertently damaged in a subsequent test due to deficiencies in the test fixture.

A second specimen was instrumented and installed in a special endurance load fixture. Spectrum fatigue testing was initiated and continued for two lifetimes (72,000 flights) without evidence of structural degradation. Load strain surveys were conducted after each lifetime of testing. After the completion of the fatigue testing, the specimen was removed from the setup and installed in the 300 Kip Baldwin Static Test Machine. This setup was to apply tension loading to the specimen.

This specimen was then loaded to 85.0kN (19,112 lb), (140 percent of DUL) when failure of the inner group of fasteners occurred with subsequent delamination failure of the upper skin cover. These failures are shown in figure 100 and 101. Representative strain gage records are shown on figures 102 through 105.
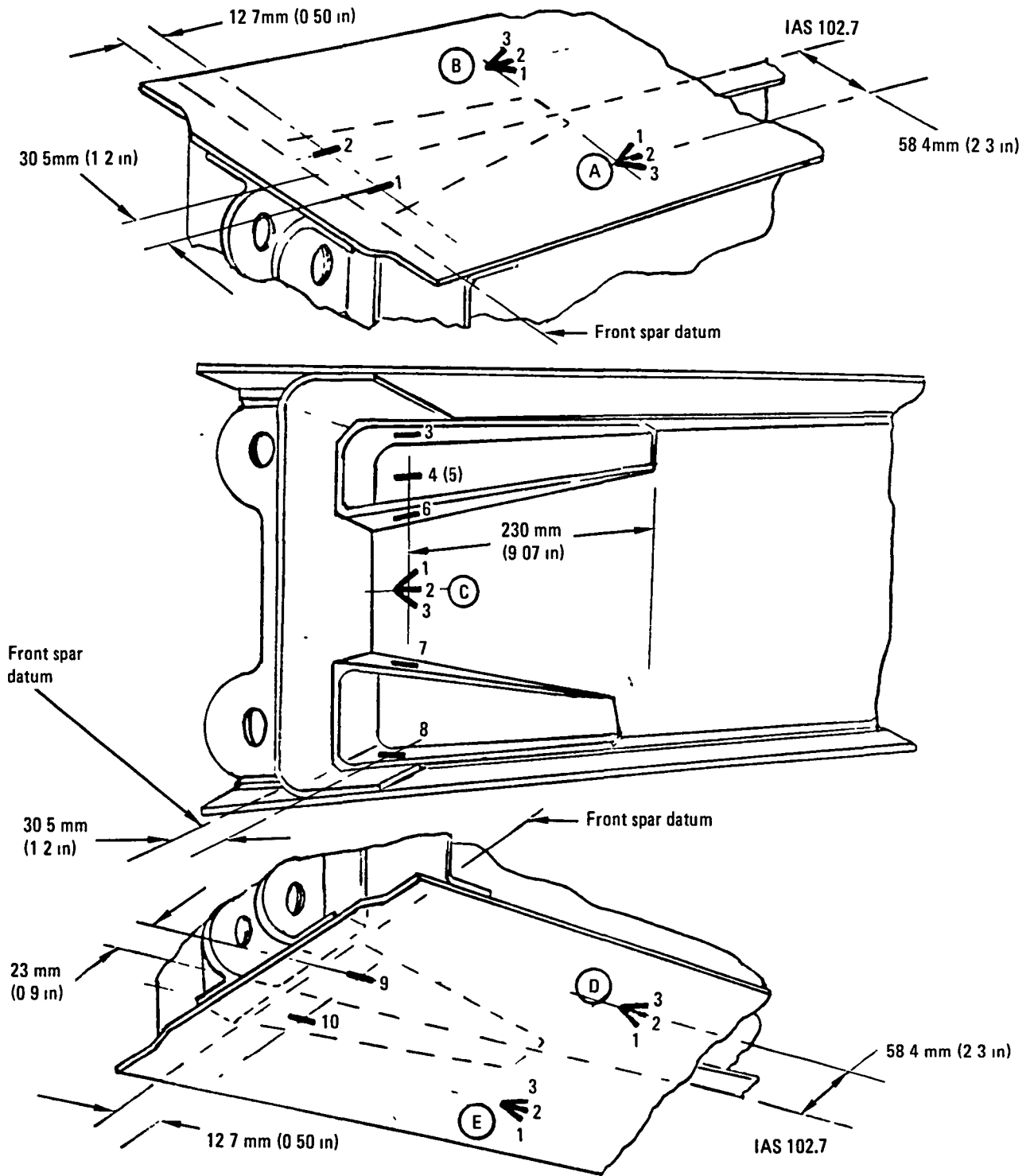
Figure 97. – Strain gage locations and identification for rib/spar specimen.

129
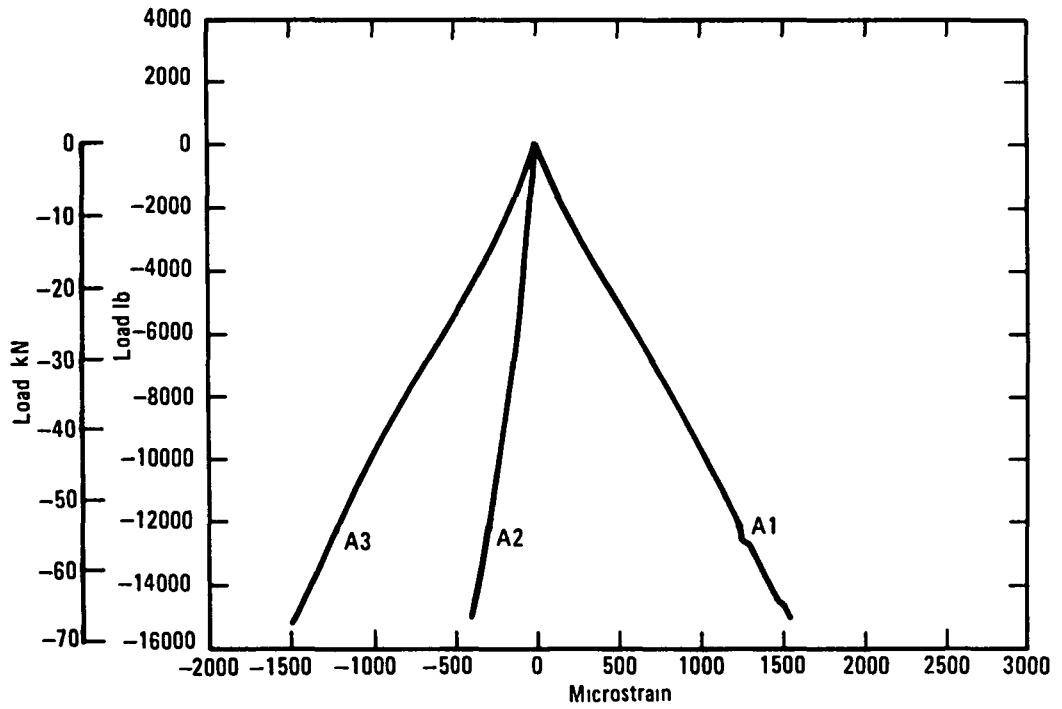
Figure 98. - Rosette gage A analysis - compression
ultimate load (see figure 97).
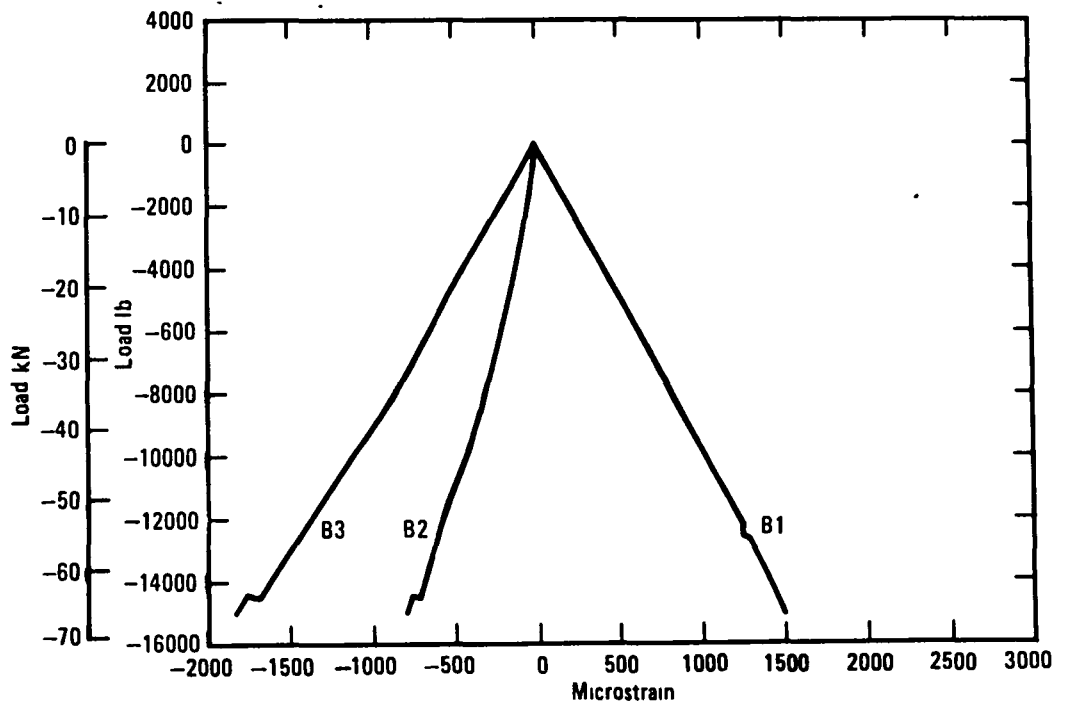
Figure 99. - Rosette gage B analysis - compression
ultimate load (see figure 97).

130
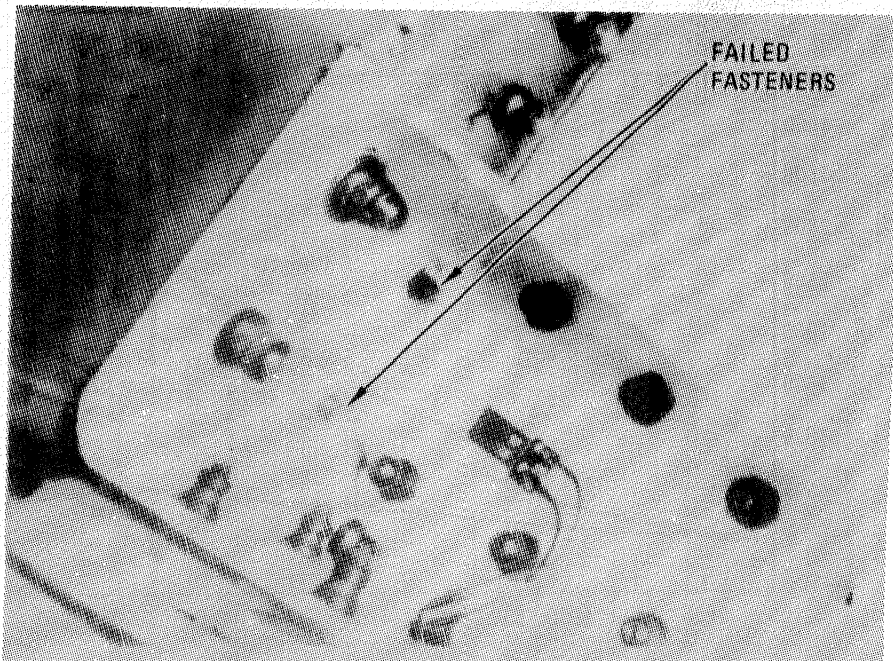
Figure 100. – Failed fasteners in the top
inboard cover fitting.
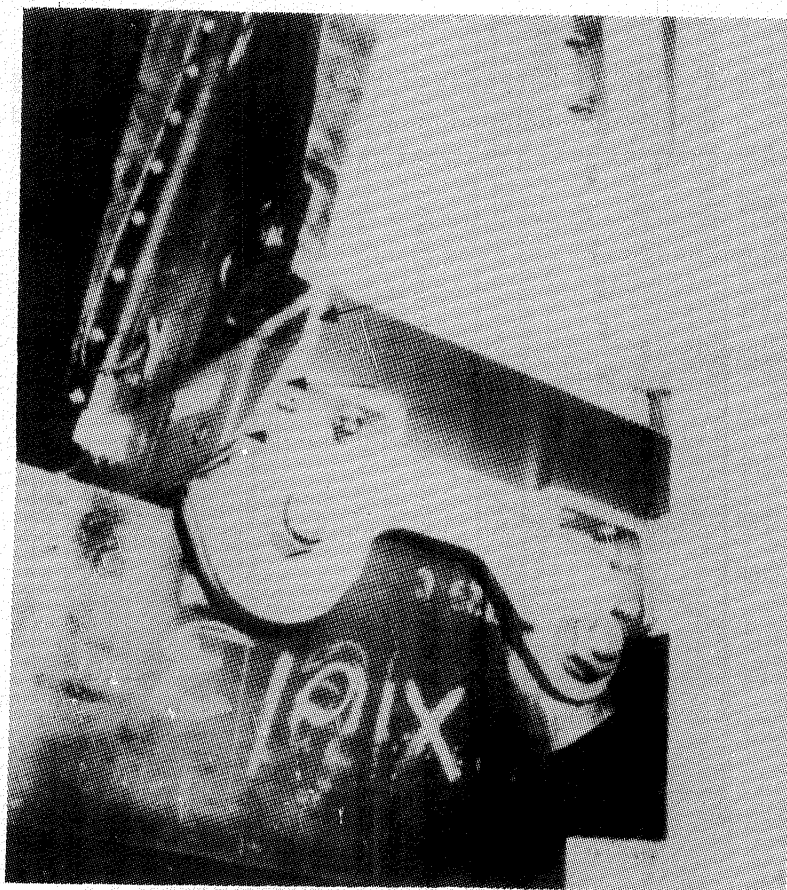
Figure 101. – Upper cover delamination.
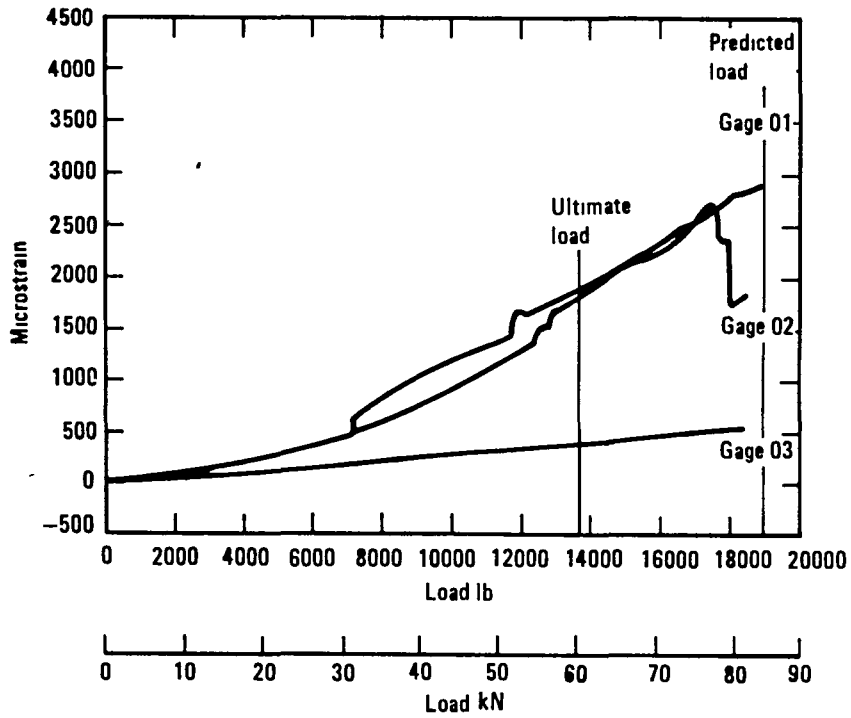
Figure 102. - Rib/spar/fitting strain versus load - gages 1, 2, 3, tensile failure load.
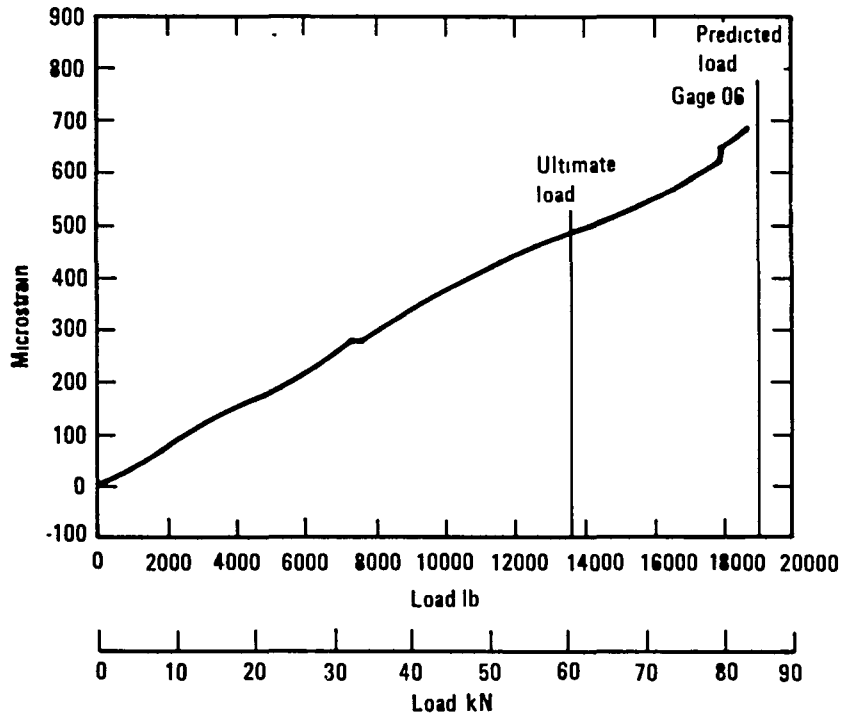
Figure 103. - Rib/spar/fitting strain versus load - gage 6, tensile failure load.
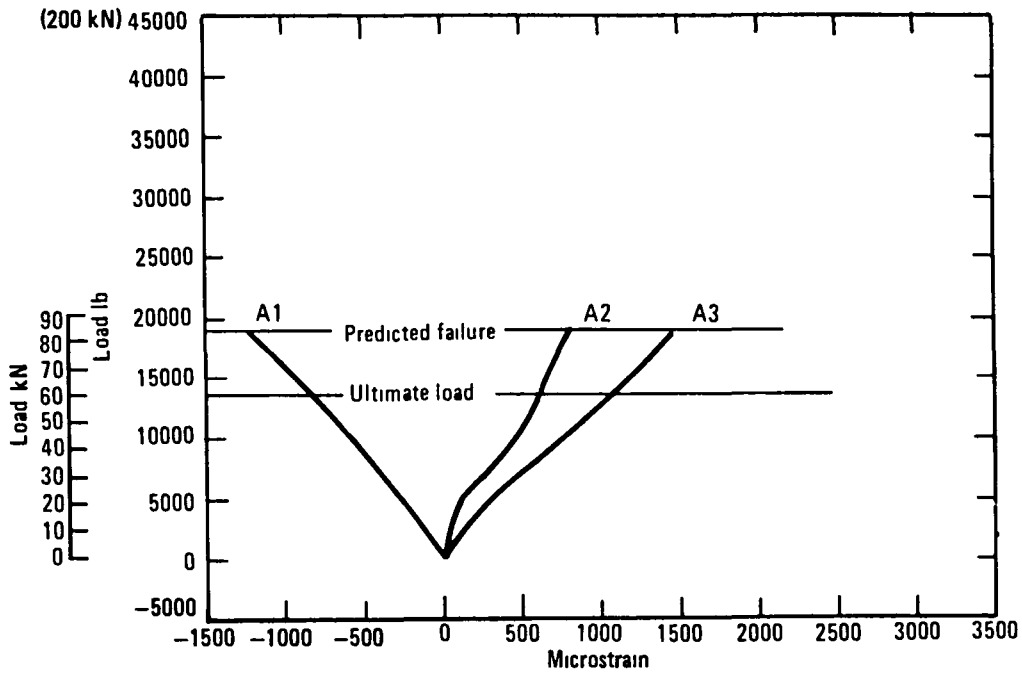
Figure 104. - Rib/spar/fitting strain versus load - rosette A, tensile failure load (see figure 97).
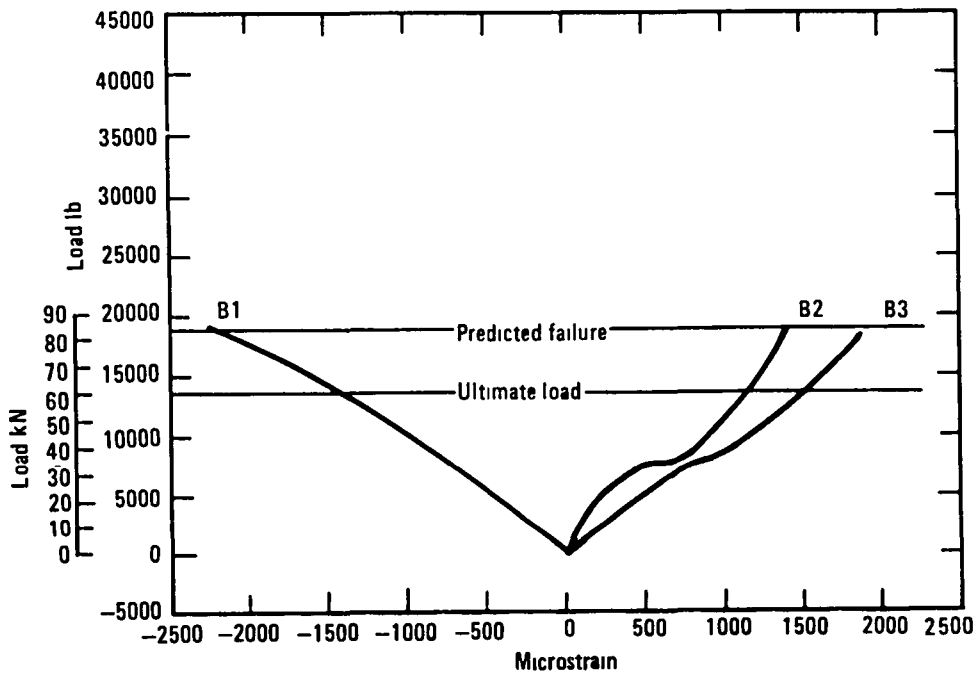
Figure 105. - Rib/spar/fitting strain versus load - rosette B, tensile failure load (see figure 97).

An analysis of the rib/spar specimen indicated the lowest margin of safety occurs in the fasteners attaching the hinge fitting to the bathtub fittings. Failure was predicted at 139% of design ultimate load, or a test load of 84.5kN (19000 lb).

This test verified the structural integrity of the design concept for both static and fatigue loading and verified the predicted failure strength and mode.

4.5 Sonic Fatigue Tests

The L-1011 composite aileron is required to withstand the acoustic loading from the large fan jet engine for the design life of the airplane. The highest noise levels are encountered during takeoff which, therefore, represents the design environment. Since the takeoff noise level falls off rapidly with forward speed, the total takeoff time is compressed into an equivalent time of 360 hours at the maximum takeoff noise level which, therefore, represents the required sonic fatigue design life for the inboard aileron.

A sonic fatigue test program was conducted to demonstrate that the composite aileron meets the design requirements. The program involved the development of random fatigue data, sonic fatigue analysis, and a sonic fatigue proof test on a representative section of the aileron, mounted in an acoustic progressive wave tunnel. The required design life of 360 hours represents a prohibitively long test time. An accelerated 10 hour proof test was conducted in which the test noise level was increased by 5 dB over the takeoff noise level to compensate for the reduction in test time and to account for an anticipated degradation from environmental effects. The time compression procedure required the used random fatigue data for the components in the aileron structure that are potentially critical for sonic fatigue. This included the skin/rib and the skin/spar junctions. Random fatigue data were obtained at room temperature through coupon testing. The coupons were subjected to random reverse bending loads on large electrodynamic shakers, simulating the loading produced by the jet noise.

4.5.1 Assembly sonic fatigue proof testing. - A section of the composite aileron was mounted in the acoustic progressive wave tunnel and proof tested at an accelerated spectrum level (figure 106), 5 dB above the design noise environment for 10 hours. The 10 hours is equivalent to approximately 5 x 10^6 cycles which is approaching the flat portion of the random fatigue curve. The damping in the aileron was generally very low with a viscous damping coefficient of 0.4 percent. Nonlinear panel response was obtained at the higher excitation levels, figure 107. The highest random strain level of 310 μmm/mm (μin/in) RMS was measured at the rib fastener line between the two largest aileron panels. No sonic fatigue failures were obtained in the proof test. Comparing the measured strain with an allowable strain of 600 μmm/mm (μin/in) it is evident that the aileron design has more than an adequate margin. The 5 dB increase in spectrum level is conservative because it included 2 dB to account for anticipated environmental effects.
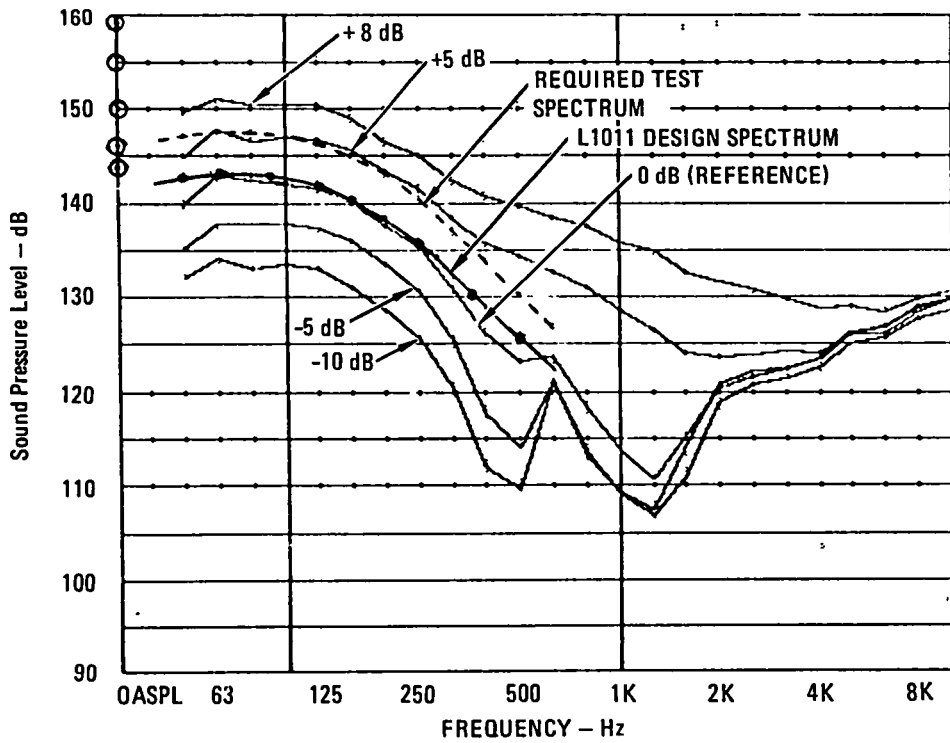
Figure 106. — One-third octave band analysis of shaped acoustic PWT noise.
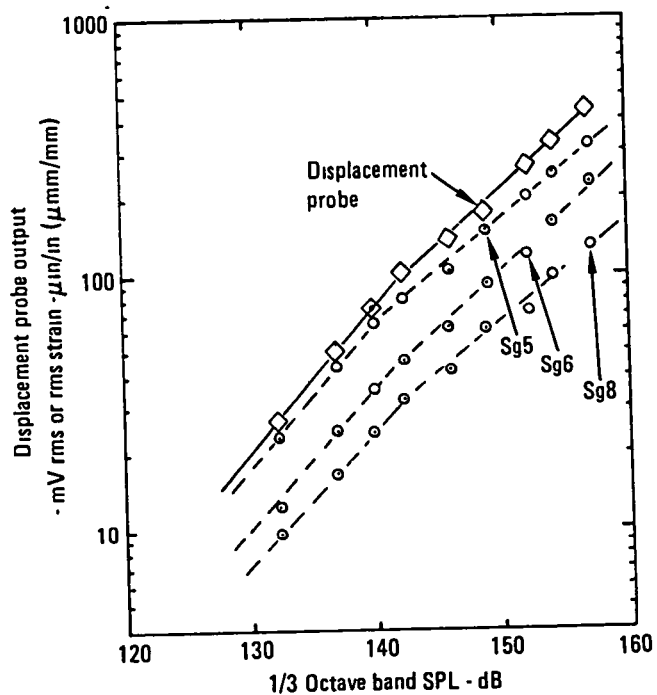
Figure 107. — Displacement probe output and strain as a function of 1/3-octave band SPL centered at 125 Hz

CONCLUSIONS

The simplicity of the composite aileron design and the unique combination of materials utilized have resulted in a very efficient structure which is 23 percent lighter than the metal aileron. Since the composite aileron has 50 percent fewer parts and fasteners than the metal aileron, it is predicted to be cost competitive.

Very simple and practical manufacturing techniques have been developed for the composite aileron. Utilization of male tools, curing to net part size, and use of a single cure cycle for all of the aileron composite parts has resulted in the fabrication of high quality parts. Drilling and machining procedures developed for the composite aileron have been proven to be as simple and reliable as techniques currently employed for aluminum structures.

The structural analysis conducted on the composite aileron in combination with materials tests and concept verification tests have verified that the structural integrity of the aileron meets or exceeds the design requirements. Final substantiation of structural integrity was obtained with the completion of the static and damage growth/fail-safe ground tests.

REFERENCES

1. Griffin, C.F.: Advanced Composite Aileron for L-1011 Transport Aircraft - Task I Final. NASA CR-145370. July 1978.

2. James, A.M.: Design of Advanced Composite Ailerons of Transport Aircraft. NASA CR-132657. May 1975.

3. Gause, L.: Low Speed Hard Object Impact on Thick Graphite/Epoxy Plates. NADC-78051-60. May 1978.

4. Rhodes, M.: Low-Velocity Impact Damage in Graphite-Fiber Reinforced Epoxy Laminates. 34th Conference on Reinforced Plastics/Composites - Society of Plastics Industry. January 29, 1979.

APPENDIX A

MATERIAL PROPERTY TEST DATA

Test data for the tension, compression, and inplane shear tests conducted on tape, fabric, and hybrid laminates are summarized in this Appendix. It contains the backup data for the graphite/epoxy material properties discussed in Section 2, Material Verification. The data summarized include the strength, modulus, failure strain and the normalized values of strength and modulus. Normalization of the data is based on thickness ratios, where the nominal thickness for tape is 0.19mm (7.5 mils)/ply and the thickness for fabric is 0.356mm (14 mils)/ply. Note that while the nominal thickness of the fabric differs slightly from that used for the preliminary design properties the resultant ply properties are not significantly different.

TABLE A1. – TAPE DATA – TENSION (SI UNITS)

Laminate & Condition	t Ave/Ply mm	N	F Ave MPa	CV [3] %	N	E Avg GPa	CV [3] %	N	c Ave 10^{-3} mm/mm	CV [3] %	Normalized F_N MPa	Normalized E_N GPa
$(45/0/-45/0/90)_S$ [1] 40-40-20 [2]												
RTD UN	2022	5	591 31	10 360	5	66 33	1 747	5	9 424	12 270	627 56	70 40
RTD UN	2004	30	362 10	6 345	30	65 74	3 941	30	5 973	12 391	408 10	74 12
219K D UN	2014	5	549 53	10 042	5	66 74	3,197	5	8 866	12 071	581 02	70 53
219K D N	1991	10	326 69	5 667	10	65 10	1 965	10	5 018	6 186	341 50	68 05
355K W UN	2019	5	627 01	8 722	5	69 64	3 501	4	9 357	9 802	664 65	73 84
355K W N	1996	10	379 56	3 792	10	66 624	2 913	9	5 738	4 769	397 76	69 84
$(45/0/-45/90/0)_S$ [1] 40 40-20 [2]												
RTD UN	2083	5	530 69	6 79							580 19	
RTD N	2096	5	339 77	1 47							373 76	
219K D N	2096	5	329 71	4 27							362 66	
$(\pm 45/03/\pm 45/0)_S$ [1] 50-50-0 [2]												
RTD UN	1976	5	887 36	3 46							908 04	
219K D N	.1996	5	399 21	5 14							417 82	
$(45/90/-45/0_2)_S$ [1] 40-40-20 [2]												
RTD UN	2014	5	546 06	3 13							577 78	
219K D N	2027	5	349 56	5 26							372 32	

[1] 0 19 mm/ply nominal thickness

[2] % $0°$, % $\pm 45°$, % $90°$

[3] Coefficient of Variation

TABLE A1A. – TAPE DATA – TENSION (CUSTOMARY UNITS)

Laminate & Condition	t Ave/Ply in	N	F Ave ksi	CV[3] %	N	E Ave Msi	CV[3] %	N	c Ave 10^{-3} in/in	CV[3] %	Normalized F_N ksi	Normalized E_N ksi
$(45/0/-45/0/90)_S$ [1]												
40-40-20 [2]												
RTD UN	00796	5	85 76	10 360	5	9 62	1 747	5	9 424	12 270	91 02	10 21
RTD UN	00789	30	52 52	6 345	30	9 53	3 941	30	5 973	12 391	59 19	10 75
-65D UN	00793	5	79 70	10 042	5	9 68	3 197	5	8 866	12 071	84 27	10 23
-65D N	00784	10	47 38	5 667	10	9 44	1 965	10	5 018	6 186	49 53	9 87
180W UN	00795	5	90 94	8 722	5	10 10	3 501	4	9 357	9 802	96 40	10 71
180W N	00786	10	55 05	3 792	10	9 66	2 913	9	5 738	4 769	57 69	10 13
$(45/0/-45/90/0)_S$ [1]												
40-40-20 [2]												
RTD UN	0082	5	76 97	6 79							84 15	
RTD UN	00825	5	49 28	1 47							54 21	
-65D N	00825	5	47 82	4 27							52 60	
$(\pm45/0_3/+45/0)_S$ [1]												
50-50-0 [2]												
RTD UN	00778	5	128 7	3 46							131 7	
-65D N	00786	5	57 9	5 14							60 6	
$(45/90/-45/0_2)_S$ [1]												
40-40-20 [2]												
RTD UN	00793	5	79 2	2 13							83 8	
-65D N	00798	5	50 7	5 25							54 0	

[1] 7 5 mils/ply nominal thickness

[2] % 0°, % $\pm45^o$, % 90°

[3] Coefficient of Variation

TABLE A2. - TAPE DATA - COMPRESSION (SI UNITS)

Laminate & Condition	t Ave/Ply mm	N	F Ave MPa	CV③ %	N	E Ave GPa	CV③ %	N	ϵ Ave 10^{-3}mm/mm	CV③ %	Normalized F_N MPa	Normalized E_N GPa
(45/0/-45/0/90)$_S$ ① 40-40-20 ②												
RTD UN	2014	5	714 02	7 397	4	62 19	0 941	4		8 510	754 98	65 78
RTD UN	2022	5	478 77	9 682	5	63 13	0 763	5		10 495	508.14	67.02
219K D UN	2012	5	724 91	5 759	4	61 66	4 732	4		6 711	765 52	65 09
355K W UN	2017	5	581 78	13 078	5	62 32	0 826	5		12 800	615 91	65 98
(45/0/-45/90/0)$_S$ ① 40-40-20 ②												
RTD UN	2098	5	636 25	6 13	5	62 19	4 32	5		9 67	700 71	68 46
355K W N	2098	5	409 55	5 21	5	60 12	9 42	5		8 84	451 06	66 19

① 0.19 mm/ply nominal thickness
② % 0°, % ±45°, % 90°
③ Coefficient of Variation

TABLE A2A. - TAPE DATA - COMPRESSION (CUSTOMARY UNITS)

Laminate & Condition	t Avg/Ply in	N	F Ave ksi	CV③ %	N	E Ave Msi	CV③ %	N	ϵ Ave 10^{-3} in/in	CV③ %	Normalized F_N ksi	Normalized E_N Msi
(45/0/-45/0/90)$_S$ ① 40-40-20 ②												
RTD UN	00793	5	103 56	7 397	4	9 02	0 941	4	12 514	8 510	109 50	9 54
RTD UN	00796	5	69 44	9 682	5	9 16	0 763	5	7 853	10 495	73 70	9 72
-65D UN	00792	5	105 14	5 759	4	8 94	4 732	4	12 747	6 711	111 03	9 44
180W UN	00794	5	84 38	13 078	5	9 04	0 826	5	10 071	12 800	89 33	9 57
(45/0/-45/90/0)$_S$ ① 40-40-20 ②												
RTD UN	00826	5	92 28	6 13	5	9 02	4 32	5	11 424	9 67	101 63	9 93
180W N	00826	5	59 40	5 21	5	8 72	9 42	5	7 098	8 84	65 42	9 60

① 7 5 mils/ply nominal thickness
② % 0°, % ±45°, % 90°
③ Coefficient of Variation

A3

TABLE A3. - TAPE DATA - SHEAR (SI UNITS)

Laminate & Condition	t Ave/Ply mm	N	F Ave MPa	CV ③ %	N	G Ave GPa	CV ③ %	N	γ Ave 10⁻³ mm/mm	CV ③ %	Normalized F_N MPa	Normalized G_N GPa
(45/0/-45/0/90)s ① 40-40-20 ②												
RTD UN	19 69	5	297 47	7 169	5	16 92	8 014	5	19 462	6 040	307 37	17 51
RTD N	19 51	5	214 65	4 123	5	14 04	8 777	5	15 936	14 216	219 80	14 34
219K D UN	19 74	5	252 87	11 843	5	16 27	5 748	4	15 605	8 094	262 00	16 82
355K W UN	19 76	5	281 72	2 714	5	15 56	7 802	5	19 704	7 512	292 27	16 13

① 0 19 mm/ply tape, 0 35 mm/ply fabric nominal thickness

② % 0°, % ±45°, % 90°

③ Coefficient of Variation

TABLE A3A. - TAPE DATA - SHEAR (CUSTOMARY UNITS)

Laminate & Condition	t Ave/Ply in	N	F Ave ksi	CV ③ %	N	G Ave Msi	CV ③ %	N	γ Ave 10⁻³ in/in	CV ③ %	Normalized F_N ksi	Normalized G_N Msi
(45/0/-45/0/90)s ① 40-40-20 ②												
RTD UN	00775	5	43 14	7 169	5	2 45	8 014	5	19 462	6 040	44 58	2 54
RTD N	00768	5	31.13	4 123	5	2 04	8 777	5	15 936	14 216	31 88	2 08
-65D UN	00777	5	36 68	11 843	5	2 36	5 748	4	15 605	8 094	38 00	2 44
180W UN	00778	5	40 86	2 714	5	2 26	7 802	5	19 704	7 512	42 39	2 34

① 7 5 mils/ply tape, 14 mils/ply fabric nominal thickness

② %0°, % ± 45°, %90°

③ Coefficient of Variation

TABLE A4. – FABRIC DATA – TENSION (SI UNITS)

Laminate & Condition	t Ave mm	N	F Ave MPa	CV② %	N	E Ave GPa	CV② %	N	ε Ave 10^{-6} mm/mm	CV② %	Normalized F_N MPa	Normalized E_N GPa
0° ①												
RTD UN	2 276	100	554 41	8 67	95	66,534	4 83	94	8 454	8 55	591 36	70 95
RTD UN	2 289	5	294 64	6 316	5	69 251	1 854	5	4 800	5 311	316 06	74 26
219 K D UN	2 266	10	458 64 ·	8 49	5 ·	61,432	3 07	5	7 756	9 20	487 05	65 22
219 K D N	2 263	11	245 04	9 02	8	61,225	5 47	8	4 037	10 50	259 93	64 95
219 K W UN	2 273	5	385 55	13 25	5	54,675	6 70	5	6 936	10 40	410 79	58 26
291 K W N	2 250	11	271 03	6 72	8	70,327	7 62	8	3 887	7 20	285 86	74 19
355 K D UN	2 256	5	535 86	3 40	5	61,777	2 57	4	8 790	5 80	566 47	65 29
355 K W UN	2 258	10	525 93	7 35	5	67 086	4 04	8	7 750	9 30	556 61	71 02
① 355 K W N	2 263	11	302 68	6 38	8	68,327	4 44	8	4 470	6 98	321 09	72 46
90°												
RTD UN	2 263	30	489 67	9 76	20	65,845	4 06	30	7 524	11 20	519 38	69 84
219K D UN	2 271	5	460 09	10 47	5	62,191	4 26	5	7 722	7 20	491 11	66 19
355K D UN	2 263	5	517 04	7 64	5	65,914	1 59	5	7 780	6 70	548 41	69 91
① 355K W UN	2 278	11	463 19	11 95	6	61,019	10 26	11	8 360	12 06	509 32	65 16
±45°												
RTD UN	2 248	52	192 71	9 89	39	18 53	15 262	*	*	*	203 05	19 51
219K D UN	2 256	9	205 60	5 90	4	19 86	10 420	*	*	*	217 32	20 96
219K D N	2 245	11	179 47	8 46	11	19 56	8 26	*	*	*	188 85	20 62
219K W UN	2 253	5	215 12	2 60	5	17 93	13 503	*	*	*	227.18	18 96
219K W N	2 245	11	193 05	4 82	11	21 18	8 94	*	*	*	203 19	22 27
355K D UN	2 250	5	176 78	1 40	5	16 96	4 13	*	*	*	186 43	17 86
355K W UN	2 256	10	165 89	9 50	5	14 96	17 933	*	*	*	175 33	15 79
355K W N	2 238	11	138 86	7 76	11	15 30		*	*	*	145 62	16 06

TABLE A4. – FABRIC DATA – TENSION (SI UNITS) (Continued)

Laminate & Condition	t Ave mm	N	F Ave MPa	CV [2] %	N	E Ave GPa	CV [2] %	N	ϵ Ave 10^{-6}mm/mm	CV [2] %	Normalized F_N MPa	Normalized E_N GPa
(45/0₃/45) [1]												
RT D UN	1 882	27	423 48	5 06	27	50 06	4 501	27	8 505	6 861	448 30	53 02
RT D N	1 925	30	252 28	6 15	20	44 06	2 00	20	5 806	5 30	273 10	47 71
219K D UN	1 923	5	373 70	2 70	5	52 54	2 90	5	7 357	3 40	404 10	56 81
219K D N	1 902	21	225 04	7 98	19	47 88	5 314	19	4 605	8 034	240 76	51 23
219K W N	1 882	11	235 39	12 37	11	52 32	7 647	11	4 527	17 618	249 18	55 36
355K W UN	1 910	5	416 31	4 00	5	47 51	2 50	5	8 702	4 80	447 26	51 02
355K W N	1 905	21	265 93	4 75	20	47 57	6 923	20	5 506	10 755	284 96	50 95
(45/0/135/0/45) [1]												
RT D UN	1 908	27	375 42	7 09	27	40 08	4 671	27	9 429	9 239	402 79	43 02
RT D N	1 935	30	220 63	4 47	20	38 13	3 10	20	5 790	4 72	240 14	41 51
219K D UN	1 928	5	353 36	3 41	5	39 99	1 76	5	9 240	2 71	383 14	43 37
219K D N	1 910	21	203 74	5 80	20	39 36	7 158	20	5 110	9 738	218 91	42 26
219K W N	1 900	11	226 15	4 60	11	42 97	5 850	11	5 425	9 734	241 66	45 92
355K W UN	1 935	5	374 66	2 90	4	38 96	3 40	5	10 068	4 20	407 82	42 40
355K W N	1 913	21	226 42	4 47	21	37 90	10 345	21	5 881	8 713	243 59	40 75

*Failure Strains $\gg$ 10 000 μmm/mm – Data Not Tabulated

[1] 0 35 mm/ply fabric – nominal thickness

[2] Coefficient of variation

TABLE A4A. - FABRIC DATA - TENSION (CUSTOMARY UNITS)

Laminate & Condition	t Ave in	N	F Ave ksi	CV ② %	N	E Ave Msi	CV ② %	N	ε Ave 10^{-6} in/in	CV ② %	Normalized F_N (ksi)	Normalized E_N (Msi)
0° ①												
RTD UN	0896	100	80 41	8 67	95	9 65	4 83	94	8454	8 65	85 77	10 29
RTD N	0901	5	42 73	6 31	5	10 04	1 85	5	4800	5 311	45 84	10 77
-65D UN	0892	10	66 52	8 49	5	8 91	3 07	5	77 56	9 20	70 64	9 46
-65D N	0891	11	35 54	9 02	8	8 88	5 47	8	4037	10 50	37 70	9 42
-65W UN	0895	5	55 92	13 25	5	7 93	6 70	5	6936	10 40	59 58	8 45
-65W N	0886	11	39 31	6 72	8	10 20	7 62	8	38 87	7 20	41 46	10 76
180D UN	0888	5	77 72	3 40	5	8 96	2 57	4	8790	5 80	82 16	9 47
180W UN	0889	10	76 28	7 35	5	9 73	4 04	8	7750	9 30	80 73	10 30
180W N	0891	11	43 90	6 38	8	9 91	4 44	8	4470	6 98	46 57	10 51
90° ①												
RTD UN	0891	30	71 02	9 76	20	9 55	4 06	30	7524	11 20	75 33	10 13
-65D UN	0894	5	66 93	10 47	5	9 02	4 26	5	7722	7 20	71 23	9 60
180D UN	0891	5	74 99	7 64	5	9 56	1 59	5	7780	6 70	79 54	10 14
180W UN	0897	11	69 18	11 95	6	8 85	10 26	11	8360	12 06	73 87	9 45
±45° ①												
RTD UN	0885	52	27 95	9 89	39	2 69	15 262	*	*	*	29 45	2 83
-65D UN	0888	9	29 82	5 90	4	2 88	3 32	*	*	*	31 52	3 04
-65D N	0884	11	26 03	8 46	11	2 84	10 420	*	*	*	27 39	2 99
-65W UN	0887	5	31 20	2 60	5	2 60	8 26	*	*	*	32 95	2 75
-65W N	0884	11	28 00	4 82	11	3 07	13 503	*	*	*	29 47	3 23
180D UN	0886	5	25 64	1 40	5	2 46	8 94	*	*	*	27 04	2 59
180W UN	0888	10	24 06	9 50	5	2 17	4 13	*	*	*	25 43	2 29
180W N	0881	11	20 14	7 76	11	2 22	17 933	*	*	*	21 12	2 33

TABLE A4A. – FABRIC DATA – TENSION (CUSTOMARY UNITS) (Continued)

Laminate & Condition	t Ave in	N	F Ave ksi	CV [2] %	N	E Ave Msi	CV [2] %	N	ϵ Ave 10^{-6} in/in	CV [2] %	Normalized F_N ksi	Normalized E_N Msi
(45/0$_3$/45) [1]												
RTD UN	0741	27	61 42	5 06	27	7 26	4 501	27	8505	6 861	65 02	7 69
RTD N	0758	30	36 58	6 15	20	6 39	7 00	20	5806	5 30	39 61	6 92
-65D UN	0757	5	54 20	2 90	5	7 62	2 90	5	7357	3 40	58 61	8 24
-65D N	0749	21	32 64	7 98	19	6 94	5 314	19	4605	8 034	34 92	7 43
-65W N	0741	11	34 14	12 37	11	7 59	7 647	11	4527	17 618	36 14	8 03
180W UN	0752	5	60 38	4 00	5	6 89	2 50	5	8702	4 80	64 87	7 40
180W N	0750	21	38 57	4 75	20	6 90	6 923	20	5506	10 755	41 33	7 39
(45/0/135/0/45) [1]												
RTD UN	0751	27	54 45	7 09	27	5 81	4 671	27	9429	9 239	58 42	6 24
RTD N	0762	30	32 00	4 47	20	5 53	3 10	20	5790	4 72	34 83	6 02
-65D UN	0759	5	51 25	3 41	5	5 80	1 76	5	9240	2 71	55 57	6 29
-65D N	0752	21	29 55	5 80	20	5 71	7 158	20	5110	9 738	31 75	6 13
6 5W N	0748	11	32 80	4 60	11	6 23	5 850	11	5245	9 734	34 05	6 66
180W UN	0762	5	54 34	2 90	4	5 65	3 40	5	10068	4 20	59 15	6 15
180W N	0753	21	32 84	4 47	21	5 50	10 345	21	5881	8 713	35 33	5 91

*Failure Strains $\gg$ 10 000 μ in/in – Data Not Tabulated

[1] 0 014 in/ply fabric – nominal thickness

[2] Coefficient of variation

TABLE A5. – FABRIC DATA – COMPRESSION (SI UNITS)

Laminate & Condition	t Ave mm	N	F Ave MPa	CV① %	N	E Avg GPa	CV② %	N	ϵ Ave 10^{-6} mm/mm	CV② %	Normalized F_N MPa	Normalized E_N GPa
0° ①												
RTD UN	2 268	52	548 82	9 90	42	59 43	4 65	22	10332	12 94	583 43	63 16
219K D UN	2 250	10	588 54	5 23	5	61 57	6 98	5	10630	5 8	620 73	64 95
219K D N	2 253	8	462 50	10 62	7	62 67	8 85	8	7552	8 20	488 36	66 19
219K W UN	2 256	5	585 85	12 20	5	55 43	9 18	4	11010	19 42	619 36	58 61
219 K W N	2 248	8	440 30	6 89	7	61 16	12 75	8	6956	11 05	463 88	64 47
355K W UN	2 256	10	409 62	10 48	5	59 02	7 04	5	6780	6 2	432 99	62 40
355K W N	2 253	8	259 79	5 85	8	67 36	18 37	8	3919	12 94	274 34	71 15
355K D UN	2 248	5	505 80	12 12	5	59 71	2 25	5	9246	13 7	532 90	62 88
90° ①												
RTD UN	2 266	30	509 73	9 61	25	59 85	3 98	22	9125	9 2	541 31	63 57
219K D UN	2 261	10	566 54	8 62	10	59 36	8 10	10	10718	9 6	600 26	62 88
355K W UN	2 294	10	376 66	12 95	5	56 95	2 11	5	6484	6 3	404 93	61 23
±45° ①												
RTD UN	2 258	22	212 50	4 49	22	16 00	13 32	*	*	*	224 91	16 96
219K D N	2 261	8	221 53	5 83	8	19 44	6 04	*	*	*	234 70	20 62
219 K W N	2 261	8	229 32	5 40	8	17 24	7 98	*	*	*	242 97	18 27
355K W N	2 250	8	121 42	4 62	8	11 03	5 78	*	*	*	128 04	11 65
(45/0₃/45)①												
RTD UN	1 882	27	540 48	11 38	27	44 26	6 29	27	12961	16 06	572 13	46 88
RTD N	1 913	5	350 12	4 30	5	47 02	1 50	5	7784	5 50	376 59	50 61
219K D UN	1 895	5	490 36	14 30	5	48 61	5 20	5	11006	16 70	522 55	51 78
219 K D N	1 885	8	382 93	9 89	8	43 44	14 91	8	8880	10 55	405 89	46 06
219K W N	1 887	8	400 31	3 05	8	43 99	5 84	8	10729	20 44	424 92	46 68
355K W UN	1 900	5	453 12	6 50	5	49 78	6 30	5	9946	8 40	484 22	53 23
355K W N	1 890	8	329 29	10 47	8	45 99	13 05	8	6311	6 62	309 71	48 88

A9

TABLE A5. - FABRIC DATA - COMPRESSION (SI UNITS) (Continued)

Laminate & Condition	t Ave mm	N	F Ave MPa	CV ② %	N	E Ave GPa	CV ② %	N	ϵ Ave 10^{-6}mm/mm	CV ② %	Normalized F_N MPa	Normalized E_N GPa
(45/0/135/0/45) ①												
RTD UN	1 895	27	466 64	7 05	27	37 85	4 84	26	13544	12 13	497 32	40 33
RTD N	1 930	5	292 61	3 70	5	38 36	3 10	5	7811	2 80	317 71	41 64
219K D UN	1 918	5	446 92	5 99	5	39.16	2 40	5	12060	6 60	482 01	42 26
219K D N	1 897	8	341 77	6 91	8	40 96	12 87	8	7969	24 76	364 73	43 71
219K W N	1 897	8	357 70	5 36	7	33 92	6 86	8	12094	19 58	381 69	36 20
355K W UN	1 918	5	337 57	9 20	4	37 44	1 30	4	9993	7 30	364 11	40 40
355K W N	1 902	8	244 83	11 51	7	36 47	9 49	8	6949	9 29	262 00	39 02

① 0 35 mm/ply fabric — nominal thickness

② Coefficient of variation

TABLE A5A. - FABRIC DATA - COMPRESSION (CUSTOMARY UNITS)

Laminate & Condition	t Ave in	N	F Ave ksi	CV [2] %	N	E Ave Msi	CV [2] %	N	ε Ave (μ in/in)	CV [2] %	Normalized F_N ksi	Normalized E_N Msi
0° [1]												
RTD UN	0893	52	79 60	9 90	42	8 62	4 65	22	10332	12 94	8462	9 16
-65D UN	0886	10	85 36	5 23	5	8 93	6 98	5	10680	5 8	90 03	9 42
-65D N	0887	8	67 08	10 62	7	9 09	8 85	8	7552	8 20	70 83	9 60
-65W UN	0888	5	84 97	12 20	5	8 04	9 18	4	11011	19 42	89 83	8 50
-65W N	0885	8	63 86	6 89	7	8 87	12 75	8	69 56	11 05	67 28	9 35
180w un	0888	10	59 41	10 18	5	8 56	7 04	5	6780	6 2	62 80	9 05
180W N	0887	8	37 68	5 85	8	9 77	18 37	8	3919	12 94	39 79	10 32
180D UN	0885	5	73 36	12 92	5	8 66	2 25	5	9246	13 7	77 29	9 12
90° [1]												
RTD UN	0892	30	73 93	9 01	25	8 68	3 98	22	9125	9 2	78 51	9 22
-65D UN	0890	10	82 17	8 62	10	8 61	8 10	10	10718	9 6	87 06	9 12
180W UN	0903	10	54 63	12 95	5	8 26	2 11	5	6484	6 3	58 73	8 88
±45° [1]												
RTD UN	0889	22	30 82	4 49	22	2 32	13 32	*	*	*	32 62	2 46
-65D N	0890	8	32 13	5 83	8	2 82	6 04	*	*	*	34 04	2.99
-65W N	0890	8	33 26	5 40	8	2 50	7 98	*	*	*	35 24	2 65
180W N	0886	8	17 61	4 62	8	1 60	5 78	*	*	*	18 57	1 69
(45/0$_3$/45) [1]												
RTD UN	0741	27	78 39	11 38	27	6 42	6 29	27	12961	16 06	82 98	6 80
RTD UN	0753	5	50 78	4 30	5	6 82	1 50	5	7784	5 50	54 62	7 34
-65D UN	0746	5	71 12	14 30	5	7 05	5 20	5	11006	16 70	75 79	7 51
-65D N	0742	8	55 54	9 89	8	6 30	14 91	8	8880	10 55	58 87	6 68
-65W N	0743	8	58 06	3 05	8	6 38	5 84	8	10729	20 44	561 63	6 77
180W UN	0748	5	65 72	6 50	5	7 22	6 30	5	9946	8 40	70 23	7 72
180W N	0744	8	42 26	10 47	8	6 67	13 05	8	63 11	6 62	44 92	7 09

TABLE A5A. - FABRIC DATA - COMPRESSION (CUSTOMARY UNITS)(Continued)

Laminate & Condition	t Ave in	N	F Ave ksi	CV ② %	N	E Ave Msi	CV ② %	N	ε Ave 10⁻⁶ in/in	CV ② %	Normalized F_N ksi	Normalized E_N Msi
(45/0/135/0/45) ①												
RTD UN	0746	27	67 68	7 05	27	5 49	4 84	26	13541	12 13	72 13	5 85
RTD N	0760	5	42 44	3 70	5	5 56	3 10	5	7811	2 80	46 08	6 04
-65D UN	0755	5	64 82	5 99	5	5 68	2 40	5	12060	6 60	69 91	6 13
-65D N	0747	8	49 57	6 91	8	5 94	12 87	8	7969	24 76	52 90	6 34
-65W N	0747	8	51 88	5 36	7	4 92	6 86	8	12094	19 58	55 36	5 25
180W UN	0755	5	48 96	9 20	4	5 43	1 30	4	9993	7 30	52 81	5 86
180W N	0749	8	35 51	11 51	7	5 29	9 49	8	6949	9 29	38 00	5 66

① 0 014 in/ply fabric — nominal thickness

② Coffficient of variation

TABLE A6. – FABRIC DATA – INPLANE SHEAR (SI UNITS)

Laminate & Condition	t Ave mm	N	F Ave MPa	CV[2] %	N	G Ave GPa	CV[2] %	N	γ Ave 10^{-6}mm/mm	CV[2] %	Normalized F_N MPa	Normalized G_N GPa
±45° [1]												
RT D UN	2 225	6	264 55	8 09	6	31 92	12 23	6	9167	15 32	275 86	33 30
219K D N	2 12	3	246 63	8 14	3	24 99	5 19	3	12083	14 31	255 73	26 96
219K W N	2 240	3	255 80	9 12	3	25 72	9 68	3	11158	6 71	268 62	27 03
355K W N	2 243	3	270 69	1 44	3	28 20	3 42	3	11442	5 85	284 55	29 65
(45/0$_3$/45) [1]												
RT D UN	1 920	6	256 90	3 77	6	13 24	2 86	6	14846	7 30	277 45	14 27
219K D N	1 925	3	173 27	2 66	3	12 62	7 46	3	15900	4 01	187 61	13 65
219K W N	1 935	3	180 64	2 21	3	13 10	2 77	3	16657	7 70	196 64	14 27
355K W N	1 902	3	166 44	90	3	14 20	10 94	3	13767	7 57	178 09	15.17
(45/0/135/0/45) [1]												
RT D UN	1 869	11	244 07	5 66	11	18 41	10 19	11	14567	8 28	256 62	19 37
RT D N	1 829	3	214 98	3 40	3	18 69	10 29	3	12300	7 15	221 11	19 24
219K D UN	1 849	4	219 53	13 19	3	23 72	5 10	1	9600		228 29	24 68
219K D N	1 902	3	217 12	1 69	3	17 44	8 76	3	14742	9 17	232 28	18 68
219K W N	1 908	3	227 04	3 52	3	17 24	4 58	3	15900	4 17	243 59	18 48
355K W UN	1 852	3	191 67	16 75	3	33 92	14 57	3	5980	9 77	199 60	35 30
355K W N	1 895	3	222 01	3 78	3	19 31	2 19	3	14542	6 10	236 63	20 55

[1] 0 35 mm/ply fabric – nominal thickness

[2] Coefficient of variation

TABLE A6A. - FABRIC DATA - INPLANE SHEAR (CUSTOMARY UNITS)

Laminate & Condition	t Ave in	N	F Ave ksi	CV [2] %	N	G Avg Msi	CV [2] %	N	γ Avg 10^-6 in/in	CV [2] %	Normalized F_N ksi	Normalized G_N Msi
±45° [1]												
RTD UN	0876	6	38 37	8 09	6	4 63	12 23	6	9167	15 32	40 01	4 83
65D N	0871	3	35 77	8 14	3	3 77	5 19	3	12083	14 31	37 09	3 91
-65W N	0882	3	37 10	9 12	3	3 73	9 68	3	11158	6 71	38 96	3 92
180W N	0883	3	39 26	1 44	3	4 09	3 42	3	11442	5 85	41 27	4 30
(45/0₃/45) [1]												
RTD UN	0756	6	37 26	3 77	6	1 92	2 86	6	14846	7 30	40 24	2 07
-65D N	0758	3	25 13	2 66	3	1 83	7 46	3	15900	4 01	27 21	1 98
-65W N	0762	3	26 20	2 21	3	1 90	2 77	3	16657	7 70	28 52	2 07
180W N	0749	3	24 14	90	3	2 06	10 94	3	13767	7 57	25 83	2 20
(45/0/135/0/45) [1]												
RTD UN	0736	11	35 40	5 66	11	2 67	10 19	11	14567	8 28	37 22	2 81
RTD N	0720	3	31 18	3 40	3	2 71	10 29	3	12300	7 15	32 07	2 79
-65D UN	0728	4	31 84	13 19	3	3 44	5 10	1	9600		33 11	3 58
-65D N	0749	3	31 49	1 69	3	2 53	8 76	3	14742	9 17	33 69	2 71
-65W N	0751	3	32 93	3 52	3	2 50	4 58	3	15900	4 17	35 33	2 68
180W UN	0729	3	27 80	16 75	3	4 92	14 57	3	5980	9 77	28 95	5 12
180W N	0746	3	32 20	3 78	3	2 80	2 19	3	14542	6 10	34 32	2 98

[1] 0 014 in/ply fabric — nominal thickness

[2] Coefficient of variation

TABLE A7. — HYBRID DATA — TENSION (SI UNITS)

Laminate & Condition	t Ave mm	N	F Ave MPa	CV(2) %	N	E Avg GPa	CV(2) %	N	c Ave 10^{-6} mm/mm	CV(2) %	Normalized F_N MPa	Normalized E_N GPa
ACA Cover (45/0/-45/SYN/-45/0/45)(1)(3)												
RTD UN	2 210	10	302 96	9 49	3	33 10	1 60	3	10154	5 80	319 50	34 89
RTD UN	2 182	30	193 81	4 24	30	32 68	4 40	30	5872	6 51	201 95	34 06
219K D UN	2 184	5	319 09	4 30	5	33 37	2 80	5	9504	6 90	332 60	34 82
219K D N	2 210	18	164 51	9 95	5	32 89	3 30	5	5401	4 00	173 47	34 68
355K W UN	2 192	5	370 11	3 60	5	30 82	2 00	5	11801	4 10	387 14	32 20
355K W N	2 182	10	219 67	9 88	10	28 89	8 54	10	7394	13 39	228 70	30 06
ACA Main Rib Cap ($45_T/90_T/5_T/-5_T/0_T/-5_T/5_T/90_F/45_F$)(1)(3)												
RTD UN	2 662	5	612 94	4 38							687 41	
219K D N	2 659	20	353 01	6 30							395 07	
ACA Cover and Doublers ($45_T/0_T/135_T/95_T/85_T/90_T/85_T/95_T/135_T/0_T/45_T/90_T/135_T/90_F$) Load at 90 (1)(3)												
RTD UN	3 282	5	575 71	6 89							625 35	
219K D N	3 277	19	321 99	4 19							348 87	

(1) 0 19 mm/ply tape, 0 35 mm/ply fabric nominal thickness

(2) Coefficient of Variation

(3) T = Tape, F = Fabric, SYN = Syntactic

TABLE A7A — HYBRID DATA — TENSION (CUSTOMARY UNITS)

Laminate & Condition	t Ave in	N	F Ave ksi	CV(2) %	N	E Ave Msi	CV(2) %	N	ϵ Ave 10^{-6} in/in	CV(2) %	Normalized F_N ksi	Normalized E_N Msi
ACA Cover (45/0/-45/SYN/-45/0/45)(1)(3)												
RTD UN	0870	10	43 94	9 49	3	4 80	1 60	3	10154	5 80	46 34	5 06
RTN N	0859	30	28 11	4 24	30	4 74	4 40	30	5872	6 51	29 29	4 94
-65D UN	0860	5	46 28	4 30	5	4 84	2 80	5	9504	6 90	48 24	5 05
-65D N	0870	18	23 86	9 95	5	4 77	3 30	5	5401	4 00	25 16	5 03
180W UN	0863	5	53 68	3 60	5	4 47	2 00	5	11801	4 10	56 15	4 67
180W N	0859	10	31 86	9 88	10	4 19	8 54	10	7394	13 39	33 17	4 36
ACA Main Rib Cap ($45_F/90_F/5_T/-5_T/0_T/-5_T/-5_T/90_F/45_F$)(1)(3)												
RTD UN	1048	5	88 9	4 38							99 7	
-65D N	1047	20	51 2	6 30							57 3	
ACA Cover & Doublers ($45_T/0_T/135_T/95_T/85_T/90_T/85_T/95_T/135_T/0_T/45_T/90_T/135_T/90_F$)				Load at 90° (1)(3)								
RTD UN	1292	5	83 5	6 89							90 7	
-65D n	1290	19	46 7	4 19							50 6	

(1) 7 5 mils/ply tape, 14 mils/ply fabric, nominal thickness

(2) Coefficient of Variation

(3) T = Tape, F = Fabric, SYN = Syntactic

TABLE A8. – HYBRID DATA – COMPRESSION (SI UNITS)

Laminate & Condition	t Ave mm	N	F Ave MPa	CV ② %	N	E Ave GPa	CV ② %	N	ε Ave 10^{-6} mm/mm	CV ② %	Normalized F_N MPa	Normalized E_N GPa
ACA Cover (45/0/-45/SYN/-45/0/45) ① ③												
RT D UN	2 189	5	351 29	8 81	5	31 10	2 98	5	13608	13 54	367 08	37 41
RT D N	2 174	4	220 63	4 40	4	32 82	8 00	4	7132	3 50	228 91	34 06
219K D UN	2 189	4	317 02	13 28	4	31 44	2 50	4	12533	29 98	330 95	32 82
355K W UN	2 195	5	247 11	11 10	5	32 82	1 80	5	8667	13 50	258 55	34 34
355K W N	2 220	10	198 71	8 25	10	27 86	4 99	10	7698	11 66	210 50	29 51
ACA Main Rib Cap (45$_F$/90$_F$/5$_T$/-5$_T$/0$_T$/ 5$_T$/5$_T$/90$_F$/45$_F$) ① ③												
RT D UN	2 662	5	613 08	4 38							687 20	
355K W N	2 659	20	353 01	6 30							395 28	
ACA Cover and Doublers (45$_T$/0$_T$/135$_T$/95$_T$/85$_T$/90$_T$/85$_T$/95$_T$/135$_T$/0$_T$/45$_T$/90$_T$/135$_T$/90$_F$) Load at 90° ① ③												
RT D UN	3 282	5	575 92	6 89							625 29	
355K W N	3 277	19	321 92	4 19							348 94	

①   0 19 mm/ply tape, 0 35 mm/ply fabric, nominal thickness

②   Coefficient of Variation

③   T = Tape, F = Fabric, SYN = Syntactic

TABLE A8A. – HYBRID DATA – COMPRESSION (CUSTOMARY UNITS)

Laminate & Condition	t Ave in	N	F Ave ksi	CV [2] %	N	E Ave Msi	CV [2] %	N	c Ave 10^{-6} in/in	CV [2] %	Normalized F_N ksi	Normalized E_N Msi
ACA Cover (45/0/-45/SYN/-45/0/45) ①③												
RTD UN	0862	5	50 95	8 81	5	4 51	2 98	5	13608	13 54	53 24	4 71
RTD N	0856	4	32 00	4 40	4	4 76	8 00	4	7132	3 50	33 2	4 94
-65D UN	0862	4	45 98	13 28	4	4 56	2 50	4	12533	29 98	48 0	4 76
180W UN	0864	5	35 84	11 10	5	4 76	1 80	5	8667	13 50	37 5	4 98
180W N	0874	10	28 82	8 25	10	4 04	4 99	10	7698	11 66	30 53	4 28
ACA Main Rib Cap $(45_F/90_F/5_T/-5_T/0_T/-5_T/5_T/90_F/45_F)$ ①③												
RTD UN	1048	5	88 92	4 38							99 67	
180W N	1047	20	51 20	6 30							57 33	
ACA Cover and Doublers $(45_T/0_T/135_T/95_T/85_T/90_T/85_T/95_T/135_T/0_T/45_T/90_T/135_T/90_F)$ ①③												
RTD UN	1292	5	83 53	6 89							90 69	
180W N	1290	19	46 69	4 19							50 61	

① 7 5 mils/ply tape, 14 mils/ply fabric, nominal thickness

② Coefficient of Variation

③ T = Tape, F = Fabric, SYN = Syntactic

APPENDIX B

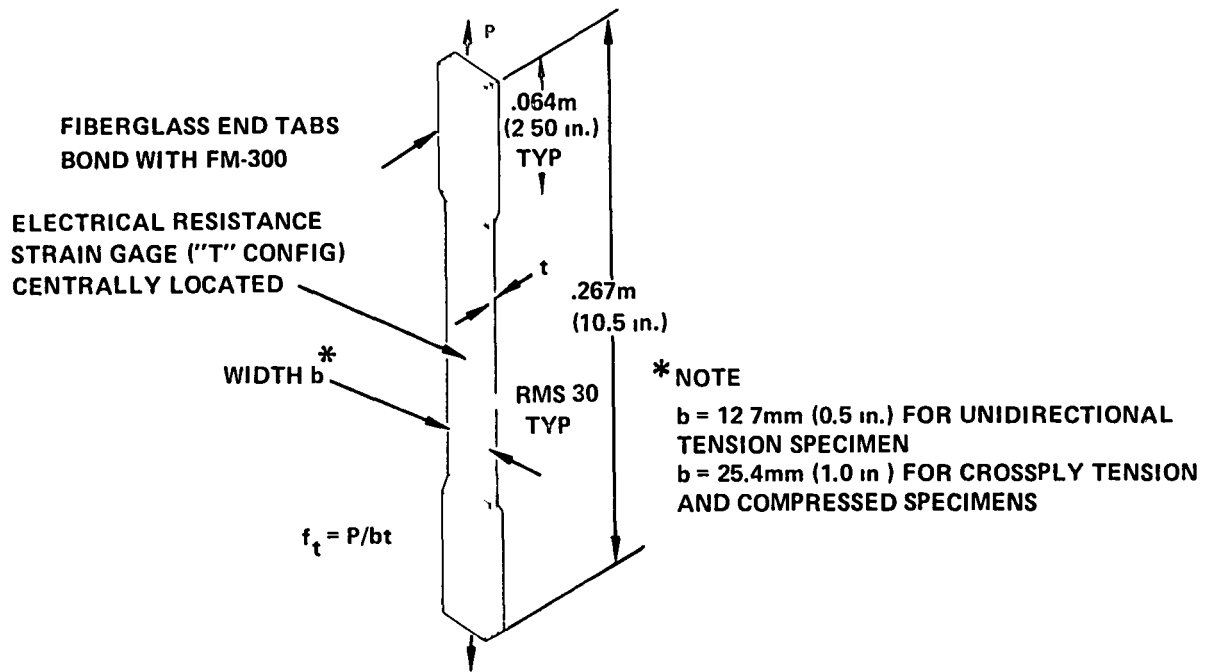COUPON CONFIGURATIONS FOR DESIGN DATA TESTS

FIBERGLASS END TABS
BOND WITH FM-300

ELECTRICAL RESISTANCE
STRAIN GAGE ("T" CONFIG)
CENTRALLY LOCATED

WIDTH b *

$f_t = P/bt$

P

.064m
(2 50 in.)
TYP

t

.267m
(10.5 in.)

RMS 30
TYP

*NOTE

b = 12 7mm (0.5 in.) FOR UNIDIRECTIONAL
TENSION SPECIMEN
b = 25.4mm (1.0 in) FOR CROSSPLY TENSION
AND COMPRESSED SPECIMENS

FIGURE B1 CROSSPLY TENSION AND COMPRESSION AND UNIDIRECTIONAL TENSION COUPON

FIBER ORIENTATION

RMS 30
TYP

16mm
(0.630 in.)   b6 35mm (0 250 in)

t

3mm
(0.12 in.)

p
L/2

L = 4t
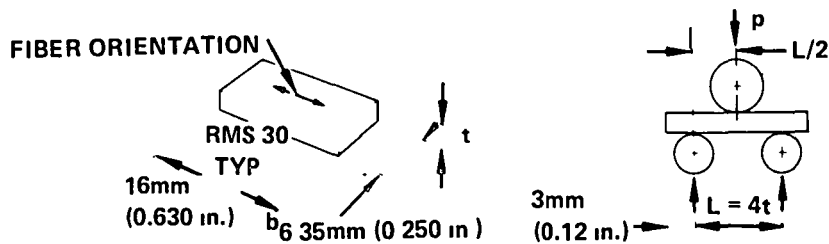
FIGURE B2. 0° INTERLAMINAR SHEAR TEST

SPECIMEN

3.99mm
(0.157 in.)

6.35mm
(1/4 in.)

57.15mm
(2.25 in.)

12.7mm
(0 5 in.)

STRAIN GAGE

EDGE   FRONT

FIBERGLASS TAB

FIXTURE
LOAD

SPECIMEN

COLLET
GRIP

TAPERED
SLEEVE

CYLINDRICAL
SHELL

12.7mm (0.5 in.)
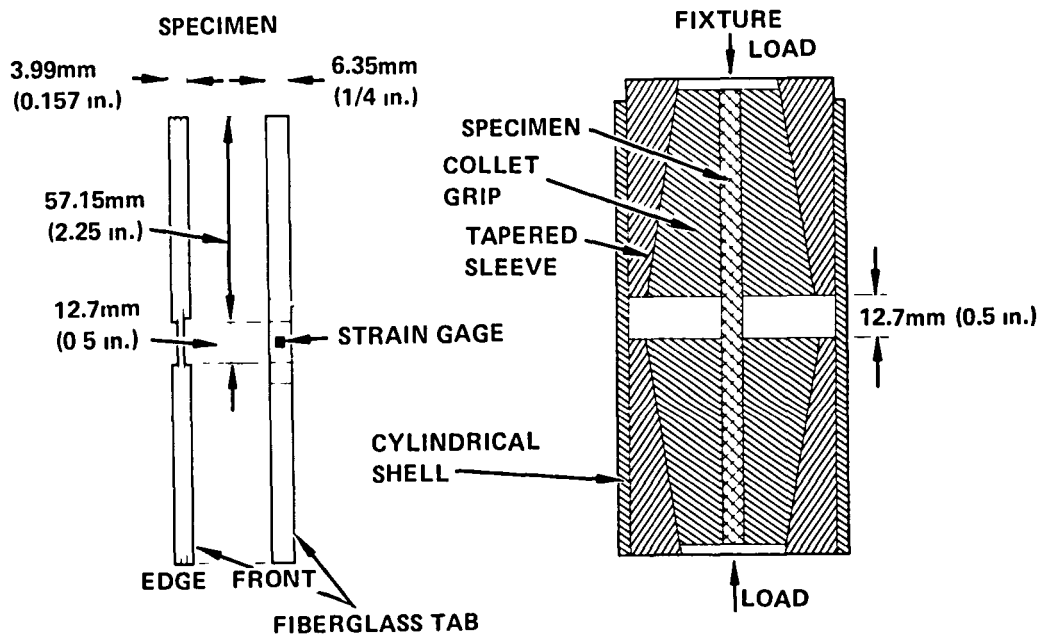
LOAD

FIGURE B3. CELANESE COMPRESSION TEST SPECIMEN AND FIXTURE
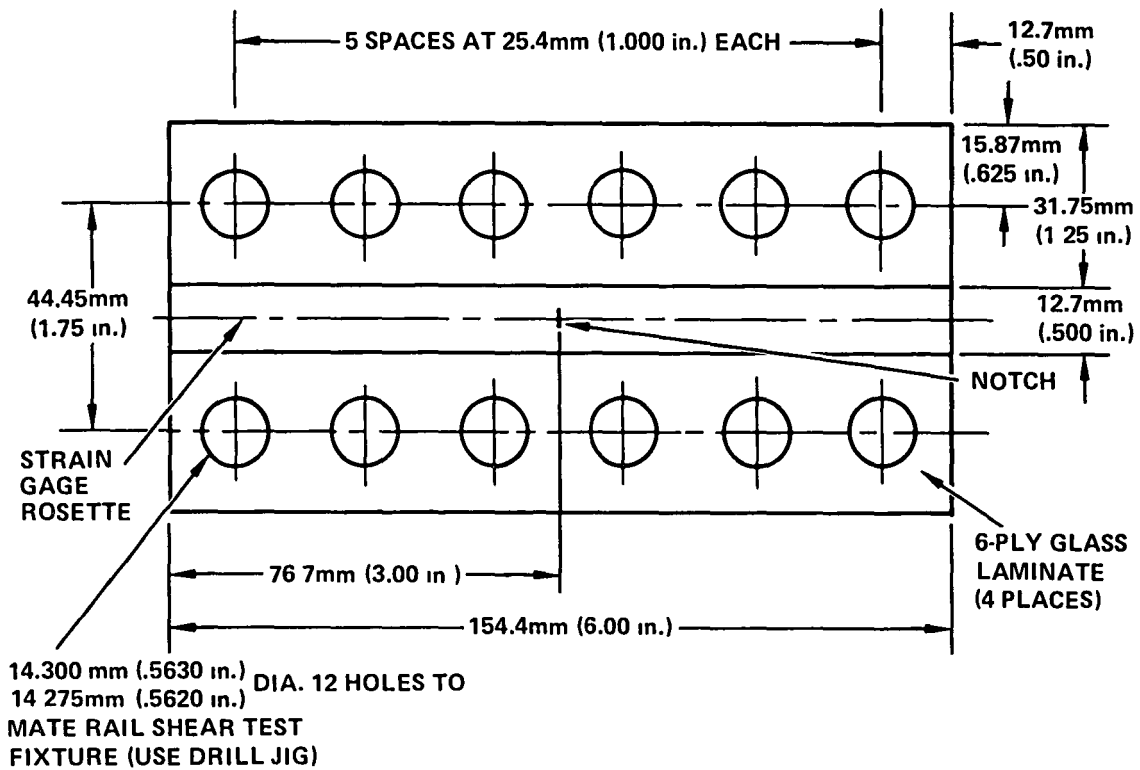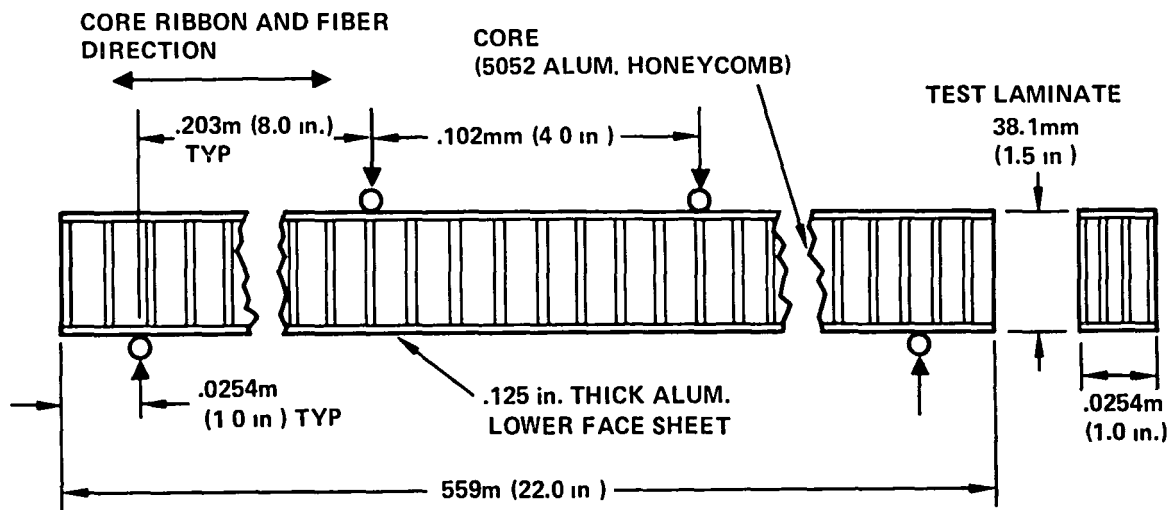
FIGURE B4   IN-PLANE SHEAR SPECIMEN

FIGURE B5   SANDWICH BEAM COMPRESSION TEST

B-2

1 REPORT NO NASA CR-165635	2 GOVERNMENT ACCESSION NO.	3 RECIPIENT'S CATALOG NO
4 TITLE AND SUBTITLE Advanced Composite Aileron For L-1011 Transport Aircraft - Design and Analysis		5 REPORT DATE April 1981
		6 PERFORMING ORG CODE 76-23
7 AUTHOR(S) C. F. Griffin, L. D. Fogg, E. G. Dunning		8 PERFORMING ORG REPORT NO LR 29635
		10 WORK UNIT NO
9 PERFORMING ORGANIZATION NAME AND ADDRESS LOCKHEED-CALIFORNIA COMPANY P O BOX 551 BURBANK, CALIFORNIA 91520		11 CONTRACT OR GRANT NO NAS 1-15069
		13 TYPE OF REPORT AND PERIOD COVERED Contractor Rpt. April 1977 to Oct. 1980
12 SPONSORING AGENCY NAME AND ADDRESS National Aeronautics and Space Administration Washington, DC 20546		14 SPONSORING AGENCY CODE

15 SUPPLEMENTARY NOTES
Langley Technical Monitor   Dr, H.A. Leybold Final Report

16 ABSTRACT

The activities documented in this report are associated with Task II of the Advanced Composite Aileron (ACA) program.

Detail design of the composite aileron has been completed. The aileron design is a multi-rib configuration with single piece upper and lower covers mechanically fastened to the substructure. Covers, front, spar and ribs are fabricated with graphite/epoxy tape or fabric composite material. The design has a weight savings of 23 percent compared to the aluminum aileron. The composite aileron has 50 percent fewer fasteners and parts than the metal aileron and is predicted to be cost competitive.

Structural integrity of the composite aileron was verified by structural analysis and an extensive test program. Static, failsafe, and vibration analyses have been conducted on the composite aileron using finite element models and specialized computer programs for composite material laminates. The fundamental behavior of the composite materials used in the aileron was determined by coupon tests for a variety of environmental conditions. Critical details of the design were interrogated by static and fatigue tests on full-scale subcomponents and subassemblies of the aileron.

17 KEY WORDS (SUGGESTED BY AUTHOR(S)) Composites, Materials, Secondary Structure Design, Testing, Transport Aircraft, Graphite Epoxy	18 DISTRIBUTION STATEMENT FEDD Distribution

19 SECURITY CLASSIF (OF THIS REPORT) Unclassified	20 SECURITY CLASSIF (OF THIS PAGE) Unclassified	21 NO OF PAGES 172	22 PRICE*

Available: NASA's Industrial Applications Center

End of Document